THE UNIVERSITY
of EDINBURGH

Ceramide synthase 4: a novel metabolic regulator of oncogene-induced senescence

Flora Lucy Dix

THE UNIVERSITY *of* EDINBURGH

Thesis submitted for the degree of Doctor of Philosophy (PhD)

The University of Edinburgh

2018

Declaration

This is to certify that the work covered in this thesis is my own work or that where research was carried out in collaboration, or with support from others, I have clearly acknowledged their contribution to the relevant experiments. This thesis has not been previously submitted for any other degree or professional qualification.

Flora Lucy Dix, March 2018

Acknowledgements

First, thank you to Juan Carlos Acosta for his supervision and imparting his endless scientific knowledge. I also thank Andy Finch for all his wise guidance as my second supervisor. I am grateful to Nick Hastie, Phil Whitfield and You-Ying Chau for their useful discussion during my thesis committee meetings. An extra thank you to Phil, and his colleagues Mary and Seshu, for their collaboration and expertise in lipidomics. I am also indebted to Jimi Wills and Joy Edwards-Hicks; thank you for setting up the lipidomics platform at the IGMM and for patiently putting up with my constant mass spec related questions. Finally, on the academic side, I wish to thank Cathy Abbott for being a wonderfully supportive mentor.

Thank you to the Acosta lab ladies: Andrea, Irene, Núria, Priya and Rachel. All of you assisted me during minor and major lab/life disasters, and your friendship really helped me cross the PhD finish line. I am especially thankful to Andrea, Queen of cloning/everything; I (and this project) would be nowhere without your tremendous support. I also appreciate all the helpful advice from our friendly Wilkinson lab neighbours, particularly Alice and Maggie.

To Ailsa, Fiona, Joy, Katy, Louise and Sonia (the 2013-17 ladies!), your friendship and patient ears have been invaluable. I owe apologies to Chloe, Hannah, Garineh, Nat, David and Dan for being an absent friend over the past four years, but thank you for your love and loyalty. A mention is also deserved for St Andrew Boat Club, who have helped me forget about science every so often with a cheeky rowing session.

I wish to thank my wonderful family, who have continually helped me get to this point. Sam and Hettie, I have always respected you for providing impossible academic standards for me to beat but I know I'll always be your silly little sister, PhD or no PhD. Mum and Dad, you are the most supportive and inspiring parents I could wish for; thank you for pushing me to do my best at everything I pursue. And lastly, I would not have finished this adventure without the constant encouragement and love from my boyfriend Andy. I say you're not funny, but you always manage to make me smile and laugh every day and that has been so important for me.

Abstract

Senescence is a cell stress program characterized by a stable cell cycle arrest and thus aims to protect against replication of potentially harmful cells. In oncogene-induced senescence (OIS) the cell cycle arrest is brought about by activation of an oncogene. This in turn initiates a DNA damage response and subsequently, the DDR induces p53-p21 and RB tumour suppressor pathways. The metabolism of senescent cells is highly altered, notably there is increased secretion of proteins and increased functional activity of certain metabolic enzymes. There have been many recent studies investigating the role of specific metabolic pathways in OIS and how they may be targeted for therapeutic benefit. This thesis aims to identify novel metabolic regulators of OIS, by combining high throughput RNAi screening and LC-MS based methods. This thesis has identified and validated 17 essential OIS metabolic genes; in this list, there was enrichment for genes involved in lipid biosynthetic processes. Lipid metabolism was an attractive focus for this thesis as it has not been extensively studied in current literature. Next, ceramide synthase 4 (CERS4) was extensively validated as a key enzyme for both OIS and replicative senescence. Using LC-MS based lipidomics, CERS4-driven rewiring of lipid metabolism in OIS was revealed and this corresponded with an accumulation of ceramides due to increased *de novo* ceramide synthesis. It was then confirmed OIS-related ceramide is mechanistically linked to cell cycle via the PP1-RB-E2F axis. Ceramide activates PP1, which physically binds to RB in a CERS4-dependent manner. PP1 is then able to dephosphorylate and activate RB, which inhibits transcription of E2F targets (cell cycle genes). Overall, this thesis identifies a metabolic checkpoint that links altered lipid metabolism with OIS.

Lay Summary

Senescence is a biological process cells undergo when they encounter stress – cells will stop dividing and undergo numerous physical and chemical changes. In oncogene-induced senescence (OIS), a gene suffers a dangerous change (mutation) in its sequence that will pre-dispose the cell to increased pre-cancerous cell division. This altered gene is termed an oncogene, and OIS will be activated when an oncogene is mutated. When the cell gains an additional oncogenic mutation, it will convert from a pre-cancerous to a cancerous state. OIS is a fail-safe mechanism that attempts to prevent the pre-cancerous cells from replicating and therefore converting to cancer.

Metabolism is the set of chemical reactions that occur in a cell that allows it to function and remain alive. These reactions involve many different metabolites, such as sugars, fats and proteins, and are controlled by proteins called enzymes. Normal cell metabolism has been extensively studied and in recent years there has been increased interest in how metabolism of senescent cells is altered. Due to the involvement of senescence in cancer, it is thought the altered metabolic pathways could be potential targets for new cancer therapies. Therefore, the main aim for this thesis was to identify new metabolic regulators of OIS, that could one day be therapeutic targets for cancer treatment.

In this thesis, large-scale changes in fat content of OIS cells were shown and a role for an enzyme involved in fat metabolism in OIS was identified. This enzyme synthesizes specific fats known as ceramides, that are vital for cell function. It was found OIS causes increased levels of ceramides and this was due to increased activity of a metabolic pathway that makes ceramides from scratch. Further investigation of this pathway demonstrated activation of a cell division protein essential for OIS by ceramide, thus linking the altered fat metabolism to cell division and OIS. In the future, it is vital to confirm these results using a model more relevant to humans so the therapeutic benefit of targeting this metabolic pathway can be established.

Table of Contents

List of Figures and Tables

Figures

Tables

List of Abbreviations

4OHT	4-hydroxytamoxifen
ASAH1	Acid ceramidase 1
ATM	Ataxia-telangiectasia mutated apical kinase
ATP	Adenosine triphosphate
BrdU	Bromodeoxyuridine
BSA	Bovine serum albumin
CDK	Cyclin dependent kinase
CDKN / CDKi	CDK inhibitor
cDNA	Complementary DNA
Cer	Ceramide
CERK	Ceramide kinase
CERS4	Ceramide synthase 4
Ct	Threshold cycle
CV	Crystal violet
Da	Dalton
DAPI	4’,6-diamidino-2-phenylindole
DDR	DNA damage response
DF1	Dharmafect 1 transfection reagent
dH_2O	Distilled water

DMEM	Dulbecco's modified eagle's medium
DMSO	Dimethyl sulfoxide
DNA	Deoxyribonucleic acid
dsRNA	Double-stranded RNA
ECL	Enhanced chemiluminescence
ECM	Extracellular matrix
EtOH	Ethanol
ev	pSUPER.retro.puro empty vector
FBS	Fetal bovine serum
FH	Fumarate hydratase
gDNA	Genomic DNA
GLS	Glutaminases
GLUT1	Glucose transporter 1
GO	Gene ontology
HCS	High content screening
HK	Hexokinases
HPLC	High-performance liquid chromatography
HRP	Horse radish peroxidase
IDH	Isocitrate dehydrogenase
IF	Immunofluorescence

IgG	Immunoglobulin G
IL	Interleukin
IP	Immunoprecipitation
LAA	Linoleamide alkyne
LC-MS	Liquid chromatography mass spectrometry
m/z	Mass to charge ratio
MiDAS	Mitochondrial dysfunction associated senescence
mRNA	Messenger RNA
mTOR	Mechanistic target of rapamycin
NADH	Nicotinamide adenine dinucleotide, reduced
NADPH	Nicotinamide adenine dinucleotide phosphate, reduced
NT	Non-target siRNA
NTP	Non-target pool siRNA
OIS	Oncogene-induced senescence
OXPHOS	Oxidative phosphorylation
PBS	Phosphate-buffered saline
PCA	Principle component analysis
PD	Population doublings
PDH	Pyruvate dehydrogenase
PDK1	PDH-kinase 1

PDP2	PDH-phosphatase 2
PEI	Polyethyleneimine
PKM	Pyruvate kinase, muscle
PP1	Protein phosphatase 1
PPP	Pentose phosphate pathway
pS/TQ	Phosphorylated serine/threonine-glutamine residue
qPCR	Quantitative real-time polymerase chain reaction
RB	Retinoblastoma
RISC	RNA-induced silencing complex
RNA	Ribonucleic acid
RNAi	RNA interference
ROS	Reactive oxygen species
RT	Retention time
S.D.	Standard deviation
S.E.M.	Standard error of the mean
SA β-gal	Senescence-associated β-galactosidase
SAHF	Senescence-associated heterochromatic foci
SASP	Senescence-associated secretory phenotype
SDS-PAGE	Sodium dodecyl sulphate polyacrylamide gel electrophoresis
shC4	shRNA targeting CERS4

shP	shRNA targeting p53
shRNA	Short hairpin RNA
siC4	siRNA targeting CERS4
siRNA	Small interfering RNA
Sph	Sphingosine
SPHK1	Sphingosine kinase 1
TBS	Tris-buffered saline
TCA cycle	Tricarboxylic acid cycle
TIC	Total ion count
TGFβ	Transforming growth factor beta
WB	Western blot
γH2AX	Phosphorylated histone H2AX

Chapter One: Introduction

1.1 Cellular senescence

Senescence, derived from the Latin word *senescere* (meaning 'to grow old'), is typically associated with organismal aging. In concept, cellular senescence (henceforth, 'senescence') is biological aging at a cellular level. However, over the past 20 years, senescence has been implicated in biological situations other than aging, such as cancer and tissue repair. In this section, all concepts of senescence are explored, including: a historical overview of senescence research; markers used to identify senescent cells *in vitro* and *in vivo*; types and triggers of senescence; and the role senescence plays in health and disease.

1.1.1 Discovery of senescence

The concept of senescence was first postulated in 1891. August Weismann suggested in his collection of biological essays "*death takes place because a worn-out tissue cannot forever renew itself and because a capacity for increase by means of cell division is not everlasting but finite*" (Weismann *et al.*, 1891). This view was challenged in 1921 by Alexis Carrel and Albert Ebeling, who reportedly cultured chick heart fibroblasts continuously for 34 years (Carrel and Ebeling, 1921). This work created a dogma in the tissue culture community that cells grown in culture, provided with nutrients, were immortal. However, this work could not be reproduced by anyone and was likely due to experimental error. In 1961, the pioneer of the senescence field Leonard Hayflick, along with Paul Moorhead, published work contradicting the widely-accepted dogma (Hayflick and Moorhead, 1961). They indicated the limited proliferative capacity of primary human cells in culture occurred in three phases (figure 1.1): primary culture (i.e. pre-passaging), phase I; exponential growth, phase II; slowing and arrested growth (i.e. senescence), phase III. Hayflick published work in 1965 further supporting the limited *in vitro* lifetime of primary human cells and concluded this phenomenon "*may be an expression of aging or senescence at the cellular level*" (Hayflick, 1965). These two seminal papers have been collectively citated over 6000 times (as of July 2017), which reflects the significance of Hayflick's work to the senescence field. Hayflick has

been further recognised for his founding work, by naming the point at which cells begin to senesce in his honour: the Hayflick limit. It is important to introduce here that senescence is implicated in cancer biology due to the unique ability of cancer cells to overcome the Hayflick limit and grow indefinitely (figure 1.1).

Senescence is now defined as a failsafe mechanism that initiates a stable cell cycle arrest and halts division of harmful cells. It is driven by multiple different stresses (such as telomere shortening or oncogene activation) and results in a diverse collection of phenotypes (collectively known as senescence markers). Since Hayflick's seminal work, the fundamental mechanisms of senescence and role of senescence in human health and disease have been established and will be reviewed in the rest of this chapter.

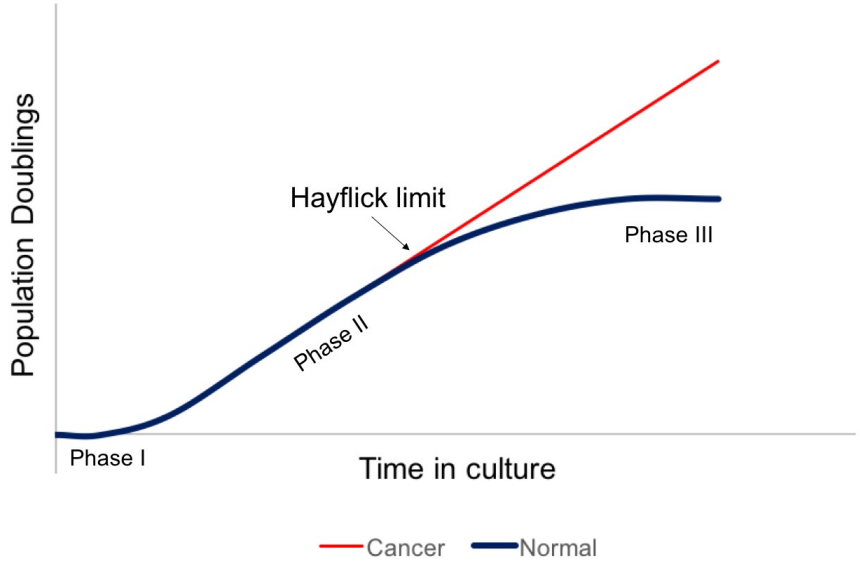

Figure 1.1 Hayflick's three phase phenomenon of primary human cell growth *in vitro*

Hayflick theorised the following three phases of cell growth in culture. Phase I comprised of no growth of cells before passaging started. Phase II was exponential growth of cells during passaging. Phase III was a slowing and eventual arrest of cell growth, even though passaging was continued. Hayflick found these phase III/senescent cells could remain in culture for up to one year before dying (Hayflick, 1965). The point between phases II and III is termed the Hayflick limit. Cancer cells can grow exponentially beyond the Hayflick limit and thus bypass senescence. Adapted from Shay and Wright (2000).

1.1.2 Senescence markers

As described in the previous section, growth arrest is the hallmark feature of senescence and is used for preliminary identification of senescent cells *in vitro* and *in vivo*. However, as stable growth arrest (or G_0 phase of the cell cycle) can be attributed to quiescence or terminal differentiation, cell cycle exit cannot be used alone for the identification of senescence. Senescence results in a heterogeneous phenotype that is unique due to multiple effector programmes (reviewed by Salama *et al.*, 2014). In addition to cell cycle analysis, the senescence markers summarised below can be used to confirm the presence of senescence, phenotypically and molecularly.

1.1.2.1 Cell morphology

Morphological changes due to senescence can be quite prominent and are used as initial identification in cases where senescence is not originally expected. Although morphology depends on the senescence trigger, senescent cells are generally flat and enlarged with vacuoler and nuclear modifications. H-Ras^{V12}-induced senescent fibroblasts have this general phenotype, with increased cytoplasmic vesicles (Serrano *et al.*, 1997). In contrast, BRAF^{V600E}-induced senescent melanocytes have a spindle-shaped morphology (Michaloglou *et al.*, 2005).

1.1.2.2 DNA damage

Senescence can be induced by a variety of different triggers and mostly DNA damage and the activation of DNA damage response (DDR) pathways are an essential post-trigger mechanism of senescence induction and maintenance (Fagagna *et al.*, 2003). First, the DDR is induced by senescence triggers such as: telomere shortening (Harley, Futcher and Greider, 1990), ionising radiation (Di Leonardo *et al.*, 1994), drugs (e.g. etoposide and cisplatin (Chang *et al.*, 1999)) or oncogene-induced hyperproliferation (Gorgoulis *et al.*, 2005). DNA damage, such as double stranded DNA breaks, is sensed by specialised protein complexes. The sensor complex recruits and activates ATM apical kinase, which phosphorylates histone H2AX at Ser139 to form γH2AX (this phosphorylated protein is often used as a DDR marker). γH2AX is a vital component of the DDR signal transduction cascade,

acting in a positive feedback loop to recruit more ATM to the DNA damage lesion (Celeste *et al.*, 2002). The positive feedback loop is enforced by DNA damage mediators MDC1 and 53BP1 (Abraham, 2002; Lou *et al.*, 2003). ATM only phosphorylates serine or threonine residues if they are followed by a negatively charged glutamine (SQ/TQ) (Kim *et al.*, 1999). Another marker commonly used to detect DDR are these phosphorylated S/T Q residues (or pS/TQ) on DNA damage mediators. When the DDR kinase activity reaches a specific threshold, downstream DDR factors, such as checkpoint kinases 1/2 (CHK1/2), are activated by phosphorylation (Buscemi *et al.*, 2004; Bekker-Jensen *et al.*, 2006). Effector proteins, such as p53 and subsequently $p21^{CIP1}$, are activated by CHK1/2 and initiate cell cycle arrest to allow the cell to attempt DNA repair (d'Adda di Fagagna, 2008).

1.1.2.3 Tumour suppressor activation

Tumour suppressors are effector proteins that mediate the stable cell cycle arrest in senescence and are activated by many different pathways. For example, in some types of senescence the DDR is a vital trigger for tumour suppressor expression. See figure 1.2.A for an overview of the most common tumour suppressors activated in senescence. p53 (encoded in humans by *TP53*) is commonly known as the 'guardian of the genome' (Efeyan and Serrano, 2007) and is heavily implicated in senescence signalling. The p53 node specifically modulates the activity and expression of cyclin-dependent kinase inhibitor (CDKi) $p21^{CIP1}$ (encoded by *CDKN1A*). Other commonly measured CDKi for senescence detection in humans include $p16^{INK4a}$ (encoded by *CDKN2A*) and $p15^{INK4b}$ (encoded by *CDKN2B*). Inhibition of CDKs and cyclin complexes results in the critical step of senescence induction: the hypophosphorylation and activation of Retinoblastoma protein (encoded by *RB*), which in turn inhibits E2F-promoted cell cycle gene transcription (Chicas *et al.*, 2010). The regulation of RB phosphorylation is critical for cell cycle progression, which is mediated by protein phosphatases and CDKs (see figure 1.2.B). RB activity can be measured as an indicator of senescence, by analysing E2F target gene expression and RB phosphorylation state.

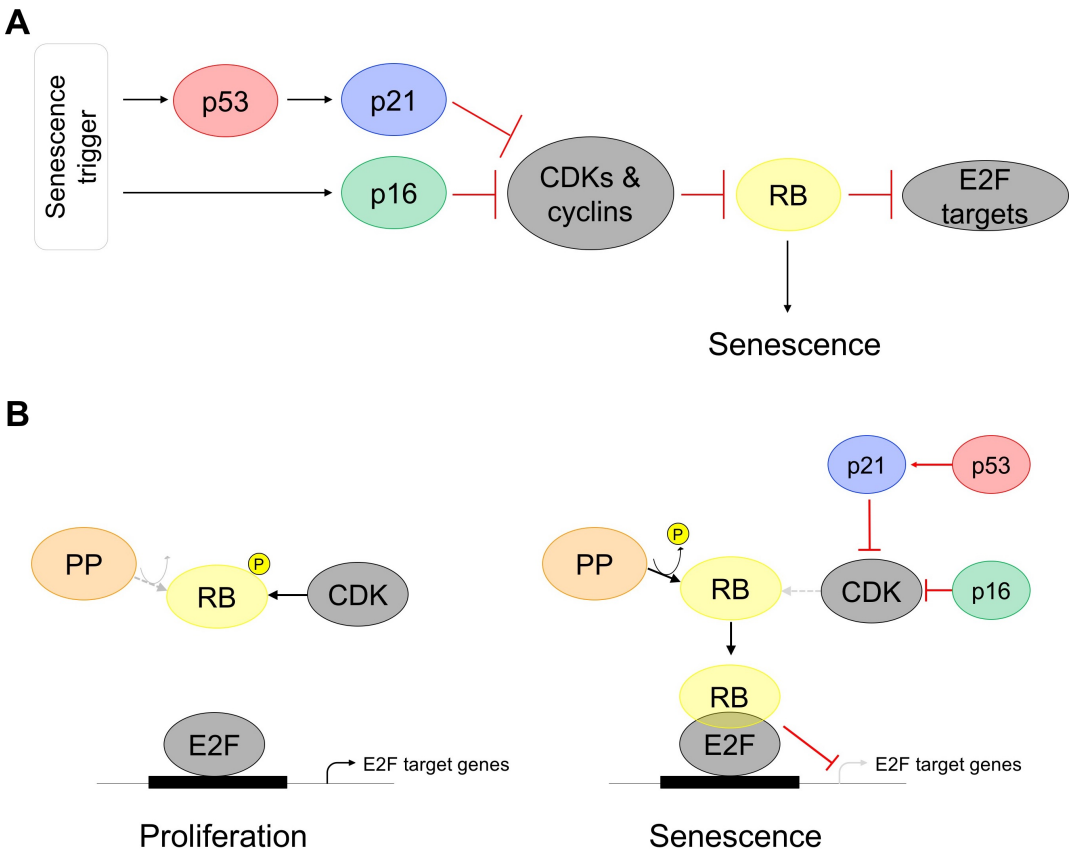

Figure 1.2 Tumour suppressor networks activated during senescence

(A) *Tumour suppressors are essential for senescence signalling. Senescence can have a variety of different triggers; generally, there is activation of p53/p21^{CIP1} and p16^{INK4a}/RB tumour suppressors, with reciprocal regulation between the two pathways. p16^{INK4a} and p21^{CIP1} are CDK inhibitors and result in activation of RB to repress E2F-promoted cell cycle genes.* ***(B)*** *The regulation of RB is essential for cell cycle control. In proliferating cells, RB is phosphorylated by CDKs and inactivated; pRB frees E2F transcription factors to initiate the transcription of genes essential for cell cycle progression (left schematic). In non-proliferating cells, RB is hypophosphorylated by protein phosphatases (PP) and activated; RB prevents transcription of E2F target genes (right schematic).*

Red lines indicate inhibitory functions. Grey lines/arrows indicate inhibited pathways. Black lines/arrows indicate active pathways.

1.1.2.4 Senescence-associated heterochromatic foci

Senescence causes an unusual nuclear phenotype due to gene expression patterns and regulation of senescence markers, ultimately leading to global changes in chromatin structure (reviewed by Adams (2007)). One of the well characterised and unique gene regulation mechanisms in senescence is that of the murine and human *INK4A-ARF* locus (which encodes senescence marker $p16^{INK4a}$). The locus is repressed by H3K27 trimethylation and associated polycomb proteins (Jacobs *et al.*, 1999); this negative regulation is counteracted by Jumonji Domain containing 3 (JMJD3) driven H3K27 demethylation (Agger *et al.*, 2009; Barradas *et al.*, 2009). Although chromatin regulation had been previously postulated (Rogakou and Sekeri–Pataryas, 1999), it was not until 2003 when senescence-associated heterochromatic foci (henceforth, SAHF) were fully characterised. Narita and colleagues found DAPI-stained nuclei of human senescent cells had a punctate staining pattern, differing to the diffuse DNA distribution of proliferating and quiescent cells (Narita *et al.*, 2003). The authors also found SAHF chromatin was more compact and resistant to nuclease digestion. SAHFs are enriched in heterochromatic marks (e.g. H3K9 methylation), chromatin-binding High Mobility Group (HMGA) proteins (Narita *et al.*, 2006) and transcription-silencing histone macroH2A (Zhang *et al.*, 2005); and lack euchromatic marks (e.g. H3K9 acetylation and H3K4 methylation). Formation of a single SAHF is a multi-step process involving the condensation of a single chromosome (Zhang, Chen and Adams, 2007). SAHF formation is driven by chromatin regulators Anti-Silencing Function 1a (ASF1a) and histone cell cycle regulator (HIRA) (Zhang *et al.*, 2005). The function of SAHFs is thought to contribute to the stable transcriptional programme of senescent cells; specifically, stable transcriptional repression of proliferation-associated genes (such as cyclin A). The tumour suppressor RB and HGMA proteins are required for SAHF function by cooperating recruitment of heterochromatic proteins to E2F-driven promoters and resulting in the repression of E2F target gene transcription (Narita *et al.*, 2003, 2006).

1.1.2.5 Senescence-associated β-galactosidase

Senescence-associated β-galactosidase (SA β-gal) was one of the first characterised features of senescence and can be easily measured *in vitro* and *in vivo* (Dimri *et al.*,

1995). The β-gal is encoded by the gene *GLB1* (in humans) and is localised to lysosomes (Lee *et al.*, 2006). Non-senescent β-gal activity occurs at pH 4 but lysosomal expansion during senescence (Kurz *et al.*, 2000) results in increased activity of the β-gal that can be measured specifically at pH 6. It is unknown if SA β-gal has a role for induction and/or maintenance of senescence. In recent years, there have been multiple studies showing senescent cells have highly altered metabolism (see *1.2.3*). Increased activity of lysosomal β-gal, together with its implications in autophagy (Gerland *et al.*, 2003; Narita *et al.*, 2011), may reflect the changing metabolic environment senescence generates. The use of SA β-gal as a marker for senescence may be limited as it is also detected in quiescence induced by confluency and serum withdrawal (Yang and Hu, 2005). Nonetheless, when used in combination with other markers, SA β-gal is a good initial indicator of senescence.

1.1.2.6 Senescence-associated secretory phenotype

Senescent cells have a diverse secretome, used to enforce a complex response on the cellular microenvironment, utilising both autocrine and paracrine pathways. Historically, individual secreted factors were implicated in replicative senescence, including extracellular matrix (ECM) factors such as fibronectin, collagenase and gelatinase (Mann, McKeown-Longo and Millis, 1988; Millis *et al.*, 1989; Sottile *et al.*, 1989; Zeng and Millis, 1994). Microarray analysis was used to identify a strong inflammatory response present in the senescent transcriptome, that mimicked wound repair processes (Shelton *et al.*, 1999). More recently, the composition of the senescence-associated secretory phenotype (SASP) has been characterised using gene expression profiling, antibody arrays and proteomics. The SASP is composed of cytokines (interleukins: IL6, IL1α, IL1β), chemokines (IL8 and immune cell attractants: MCPs and MIPs), growth factors (transforming growth factor beta (TGFβ)), ECM components (matrix metalloproteases) and proteases (Acosta *et al.*, 2013). Expression of the SASP is mediated by transcription factors C/EBPβ and NF-κB (Acosta *et al.*, 2008; Kuilman *et al.*, 2008; Chien *et al.*, 2011; Jing *et al.*, 2011); specifically, chemokine signalling is regulated via these transcription factors and subsequently through the CXCR2 receptor (Acosta *et al.*, 2008). C/EBPβ also has a role for regulating the composition of the SASP. Hoare *et al.* (2016) found NOTCH1

represses C/EBPβ in an 'early' TGFβ SASP response and vice versa in a 'late' and classical NF-κB-C/EBPβ-IL6-IL8 SASP response. In addition, persistent DNA damage is essential for the regulation of some SASP factors, such as IL6 and IL8, in many different types of senescence (Bartkova *et al.*, 2006; Di Micco *et al.*, 2006; Coppé *et al.*, 2008; Rodier *et al.*, 2009). More recently, IL1 signalling activation, via the inflammasome and caspase-1, has been implicated in SASP expression (particularly IL6 and IL8), upstream of C/EBPβ and NF-κB (Acosta *et al.*, 2013). Furthermore, IL1α has been proposed as a master regulator of senescence, through mTOR activity (Laberge *et al.*, 2015). Finally, inflammasome-mediated SASP expression is linked to oxidative stress activation and the DDR (Hubackova *et al.*, 2012).

The SASP can have both autocrine and paracrine functions, which result in complex and paradoxical outcomes. There is debate whether the function of the SASP is beneficial or detrimental for human physiology and pathology. SASP pro-inflammatory factors can threaten neighbouring cells with harmful outcomes, such as cancer and fibrosis. Whereas, SASP factors also have an essential tumour suppressive role for the induction and maintenance of the cell cycle arrest. The roles of senescence and the SASP for human health and disease, good and bad, are further discussed in *1.1.4*.

1.1.2.7 Summary

Senescent markers described here are hallmark features of many different senescence scenarios. They provide a useful tool for identifying senescent cells *in vitro* and *in vivo*, particularly when measured together using High Content Analysis (Acosta *et al.*, 2013). The presence or absence of an individual senescent marker is highly dependent on the context of the cellular senescence, such as genetic background and tissue microenvironment. In the next section, the triggers and mechanisms of the three main types of senescence are described.

1.1.3 Types of senescence

1.1.3.1 Replicative senescence

The senescence Hayflick observed in cultured fibroblasts is now recognised as replicative senescence, typically associated with aging. During the 1970s, work on DNA replication and chromosome structure drastically changed the field's understanding of the causative mechanisms of replicative senescence. First, James Watson described the 'end-replication problem' (Watson, 1972), resulting in the 3' end of the lagging strand not being completely replicated. This occurs because there is no lagging strand priming DNA available for a polymerase to bind and initiate replication of the next Okazaki fragment. Next, Alexey Olovnikov hypothesised the 'marginotomy theory of aging' (Olovnikov, 1973): the end of DNA molecules were composed of 'telogenes', prone to shortening during each division (according to Watson's end-replication problem). Olovnikov realised this could be an explanation for Hayflick's observation of human cells having a finite number of replications when cultured *in vitro*.

Telomeres are sequences of DNA composed of tandem repeats (in mammals: 5'-TTAGGG-3') found at the end of every chromosome. They function to protect the genome from DNA metabolising enzymes and are often referred to as 'molecular clocks' that record the replication of cells (McClintock, 1941; Blackburn, 1991; Muñoz-Espín and Serrano, 2014). Once the telomeric sequence length was determined, many studies proved Watson's and Olovnikov's hypotheses were correct by showing telomere length changed depending on tissue type (Cooke and Smith, 1986) and human telomeres shortened *in vitro* (Harley, Futcher and Greider, 1990) and *in vivo* (Lindsey *et al.*, 1991). Meanwhile, Carol Greider had also used the telomere-enriched protozoan *Tetrahymena thermophila* to identify an enzyme (now known as 'telomerase') that maintains telomere length (Greider and Blackburn, 1985). Telomerase elongates telomeric regions using an innate RNA template and reverse transcriptase activity (Feng *et al.*, 1995). Telomerase research was a turning point in the field, as it allowed definitive demonstration that telomere shortening could specifically induce senescence, rather than it being an effector programme; expression of the telomerase catalytic subunit in primary human cells resulted in

senescence bypass when the cells were passaged (Bodnar *et al.*, 1998). The ectopic expression of telomerase is now often used for cell immortalisation and this discovery has been fundamental for industrial and clinical R&D in recent years.

As stated previously, the DNA damage response (DDR) is a key mechanism for senescence induction and maintenance. Human cells detect telomere shortening as a type of DNA damage, and as telomeres are not easily targeted by DNA repair mechanisms, the DDR eventually occurs. In recent years, the molecular mechanisms of telomere regulation and function relative to the DDR have been examined. Telomere structure was determined in 1999 using electron microscopy; Griffith and colleagues demonstrated the 3' single strand telomeric DNA loops back to form a t-loop (Griffith *et al.*, 1999). Telomeres recruit a multi-protein complex collectively known as shelterin, composed of six proteins: TRF1, TRF2, POT1, TIN2, TPP1 and Rap1, that recognise and protect the telomeres (Palm and de Lange, 2008). Shelterin proteins have been shown to have contradicting functions, depending on an unknown threshold for telomere length and shelterin recruitment. Shelterin proteins contribute to persistent telomeric DDR by inhibition of DNA repair at telomeres but also inhibit DDR kinases ATM/ATR when present at sufficient levels (van Steensel, Smogorzewska and de Lange, 1998; Fumagalli *et al.*, 2012). In addition, telomere shortening can trigger a DDR through ATM to p53 and $p21^{CIP1}$ tumour suppressors but not $p16^{INK4a}$ (Herbig *et al.*, 2004). In conclusion, the molecular mechanism that links telomere shortening to replicative senescence is complex and depends upon a balance of multiple factors, that is disturbed when telomeres shorten below a certain threshold.

1.1.3.2 Oncogene-induced senescence

H-Ras (a member of the Ras superfamily of proteins) was first identified as an oncogene by Jennifer Harvey's work on sarcoma-causing viruses in rats (Harvey, 1964) and subsequently, the human H-Ras gene was identified in cancer cells (Cooper, 1982; Parada *et al.*, 1982). Since their discovery, Ras genes have been extensively studied and shown to be mutated in many different types of cancers (Prior, Lewis and Mattos, 2012).

In 1997, Serrano and colleagues identified a cell cycle arrest in human primary cells with oncogenic H-Ras^{V12} expression, that was phenotypically identical to replicative senescence (Serrano *et al.*, 1997). They characterised oncogene-induced senescence (hereafter, OIS) by an activation of p16^{INK4a}/RB and p53/p21^{CIP1} pathways, in addition to classical senescence markers (such as morphological changes and SA β-gal). This was the first indication that Ras oncogene expression could primarily be involved in cell cycle arrest and not transformation. It was also a pivotal study for the field as it exposed a type of senescence independent of telomere shortening. This was confirmed shortly after by showing telomerase: (1) is not essential for OIS (Wei, Wei and Sedivy, 1999) and (2) is highly expressed in cancer cells (Shay and Wright, 2006). Conversely, recent work has shown that derepression of telomerase can bypass OIS *in vitro* via epigenetic and transcriptional regulation of activity (P. L. Patel *et al.*, 2016). Additional mutations in OIS-essential genes (such as p53 and RB) are required to bypass senescence and allow progression of cancer (Dirac and Bernards, 2003; Sage *et al.*, 2003). Since Serrano's original work, OIS has been established as an 'emergency brake on cancer'; in response to oncogene-induced hyperproliferation, OIS acts to halt division of cells vulnerable to transformation (in-keeping with the classical definition of senescence).

There are approximately 50 oncogenes recognised to induce senescence *in vitro* and *in vivo*, many of which are part of the Ras signalling pathway (reviewed by Gorgoulis and Halazonetis, 2010). In 2005, multiple groups published the first evidence of OIS *in vivo* (mouse and human), using a variety of different oncogenic drivers: K*rasV12*-driven lung adenoma in mice (Collado *et al.*, 2005); BRAF^{E600}-driven melanocytic nevi in humans (Michaloglou *et al.*, 2005); and *Pten*$^{-/-}$-driven prostate intraepithelial neoplasia (PIN) in mice (Chen *et al.*, 2005). OIS was exclusively observed in pre-malignant lesions, along with tumour suppressor expression and SA β-gal activity, and was absent in more advanced cancerous lesions. In addition to *Pten* inactivation (Chen *et al.*, 2005), other tumour suppressors have been implicated in OIS after loss *in vivo* including: neurofibromin-1/NF1 (Courtois-Cox *et al.*, 2006), von Hippel-Lindau/VHL (Young *et al.*, 2008) and Retinoblastoma/RB (Shamma *et al.*, 2009). Oncogenic BRAF and K-Ras have also been implicated in mouse and human serrated colorectal cancers (Bennecke *et al.*,

2010; Carragher *et al.*, 2010). These *in vivo* models have helped establish the role of OIS in cancer biology, and in recent years its use in the development of new cancer therapeutics has been explored (reviewed by Acosta and Gil, 2012). OIS and cancer pathology is further discussed in *1.1.4.1*.

OIS is typified by upregulation of $p16^{INK4a}$ and p53 pathways but expression and function of these pathways vastly depends on genetic context of the OIS. In mice, inactivation of $p19^{ARF}$ is capable of bypassing OIS and allow tumour development driven by Ha-*ras* (Kamijo *et al.*, 1997). This $p19^{ARF}$ tumour suppression is mediated upstream of p53, independently of DNA damage and the DDR (Christophorou *et al.*, 2006). In humans, OIS is more susceptible to bypass by $p16^{INK4a}$ inactivation, upstream of RB, rather than $p14^{ARF}$ (the human ortholog of $p19^{ARF}$) (Wei, Hemmer and Sedivy, 2001; Ben-Porath and Weinberg, 2005). Also, tumour suppressor activity of p53 is essential for OIS induced by *Pten* inactivation in mice. *Pten*$^{-/-}$ mice with p53 knockdown exhibited a lethal invasive prostate cancer, similar to human pathology, due to bypass of OIS at the PIN stage (Chen *et al.*, 2005). Finally, although *Pten*-loss induced cellular senescence (PICS) does not present with DNA damage (Alimonti *et al.*, 2010), the DDR is an established mechanism for OIS-related tumour suppressor activation. For example, $H\text{-}Ras^{V12}$ expression in human cells results in an increased number of prematurely terminated replication forks and double stranded DNA breaks and inhibition of DDR kinase ATM bypasses OIS (Bartkova *et al.*, 2006; Di Micco *et al.*, 2006).

1.1.3.3 Mitochondrial dysfunction-associated senescence

Mitochondria were first implicated in senescence by Denham Harman, who hypothesised reactive oxygen species (ROS), produced as a by-product of mitochondrial redox metabolism, cause the damage to DNA, lipids and proteins typified in aging (Harman, 1972). Since this 'Mitochondrial Theory of Aging', there has been much work done to determine the role of mitochondria in replicative senescence (reviewed by Passos, von Zglinicki and Kirkwood, 2007). In recent years, there has been progress in understanding the mechanistic role mitochondria and ROS play in senescence, coinciding with many studies also implicating rewired mitochondrial metabolism (described in *1.2.3.1*). Dysfunctional mitochondrial

activity and content have been analysed in a variety of models, to determine whether mitochondria can affect senescent features, such as the SASP, and therefore are effectors of senescence.

First, Correia-Melo *et al.* (2016) targeted human fibroblasts for mitochondrial depletion using Parkin-CCCP mediated mitophagy (Narendra *et al.*, 2008) and assessed the senescent response, induced by radiation. The authors found mitochondrial depletion increased glycolysis-generated ATP, indicating senescence is dependent on mitochondrial oxidative metabolism (similar to the essentiality of pyruvate dehydrogenase during OIS (Kaplon *et al.*, 2013)). Mitochondrial depletion also caused a reversal of senescent-specific transcription, particularly pro-inflammatory factors of the SASP. Importantly, the authors also found a mechanism that linked senescent-associated mitochondria accumulation to the DDR via transcriptional activation of mitochondrial biogenesis regulator PGC-1β and upstream regulators ATM, Akt and mTOR. Overall, this study revealed senescent cells increase their mitochondrial content to accumulate ROS and promote a persistent DDR, thus creating a positive feedback loop for reinforcing senescence.

Second, a similar study utilised RNAi (for depleting sirtuins 3/5) and pharmacological inhibition (rotenone and antimycin, electron transport chain inhibitors) in human fibroblasts to disrupt the function of mitochondria. Using these approaches, Wiley *et al.* (2016) characterised a distinct type of senescence called mitochondrial dysfunction-associated senescence (MiDAS). During MiDAS, a decrease in NAD+/NADH ratio activates AMPK-p53 signalling that enforces a growth arrest. In addition, MiDAS is characterised by a lack of IL1R-dependent pro-inflammatory factors of the SASP, indicating the composition of the SASP depends on the context of senescence. The authors also found senescent cells in a mouse with increased mitochondrial DNA mutations had a MiDAS-type SASP, confirming MiDAS is exists *in vivo* and is likely to be physiologically relevant to humans.

Together, these recent studies have revealed mitochondria are central effectors for the maintenance of traditional senescence and the induction of a distinct type of senescence (MiDAS). How these findings are implicated in human health and disease are still being assessed. Finally, the mechanistic effects of altered

mitochondrial metabolism and other rewired metabolic pathways during senescence are discussed further in *1.2.3*; and identifying novel senescent-induced metabolic rewiring is the focus of this thesis (*1.4*).

1.1.3.4 Summary

Senescence can be triggered by a variety of different mechanisms; the best characterised, described above, include telomere shortening, oncogene activation (or tumour suppressor loss) and mitochondrial dysfunction and ROS. In this section, it has been described that the type of senescence and the resulting phenotype vastly depend on the trigger; how these different types of senescence responses positively and negatively affect tissue biology is discussed next.

1.1.4 Role of senescence in health and disease

Senescence has a complex role in human health and disease (reviewed by Muñoz-Espín and Serrano, 2014). Over the years, senescence has been associated with many diseases and current efforts are focussed on delineating the underlying senescence-related pathological mechanisms. In addition, senescence has recently been implicated during embryonic development and normal physiological settings. This section reviews the role of senescence for human health and disease and how it can be therapeutically manipulated.

1.1.4.1 Cancer

Oncogene-induced senescence plays a pivotal role in cancer prevention, as introduced in *1.1.3.2.* OIS is detected in benign stages of both mouse and human tumorigenesis and must be bypassed in subsequent cells to allow progression of malignant lesions. Remaining senescent cells in a tumorigenic lesion are permanently arrested and are cleared by immune cells (some examples of immune clearance mechanisms are further discussed below). A key effector programme of OIS, the SASP, can contribute to both anti- and pro-tumorigenic outcomes. The SASP is a complex signalling network of secreted factors, with both autocrine and paracrine functions (see *1.1.2.6*). Acosta *et al.* (2008) and Kuilman *et al.* (2008) showed SASP factors IL6 and IL8 reinforce both replicative and oncogene-induced senescence by maintaining the cell cycle arrest via tumour suppressor regulation and therefore work

as an autocrine feedback network. As an example of paracrine senescence, vascular endothelial growth factor (VEGF) and other TGFβ ligands were identified to regulate tumour suppressors $p15^{INK4b}$ and $p21^{CIP1}$ during paracrine senescence; via this pathway, the SASP can mediate the paracrine spread of tumour suppressive senescence to normal cells (Hubackova *et al.*, 2012; Acosta *et al.*, 2013). In contrast, murine senescent fibroblasts have been shown to promote tumour vascularisation and tumorigenesis via VEGF (Coppé *et al.*, 2006). Other pro-tumorigenic effects of the SASP include promoting: proliferation and transformation of mammary epithelial cells (Krtolica *et al.*, 2001); motility of cancer cells *in vitro* (Ohuchida *et al.*, 2004; Coppé *et al.*, 2008); differentiation of mammary epithelial cells (Parrinello *et al.*, 2005). In conclusion, some would argue the anti-tumorigenic benefits of senescence outweigh the detrimental pro-tumorigenic effects. However, there is a fine balance between the two outcomes of OIS, depending on the context (e.g. cell types involved) and the effect on the whole tumour microenvironment.

OIS has a vital role for the immune surveillance of murine liver cancer tumorigenesis, specifically hepatocellular carcinomas (HCC). Xue *et al.*, (2007) showed the SASP can signal, in a paracrine-manner, for immune clearance. This activation of the innate immune response was p53-dependent and resulted in natural killer (NK) cell-mediated clearance of senescent cells from pre-malignant liver lesions. This was further supported by work showing NK cell recruitment to p53-induced senescent liver lesions is dependent on the chemokine CCL2 (Iannello et al., 2013). CCL2 is also secreted from senescent pre-malignant hepatocytes to recruit $CCR2^{+}$ myeloid cells (Eggert *et al.*, 2016). When differentiation of immature myeloid cells into macrophages occurs, senescent cells and pre-malignant lesions are cleared; however, when differentiation does not occur, immature myeloid cells promote HCC growth through NK cell inhibition, indicating the protective function of senescence against cancer is context-dependent. In addition, $GR\text{-}1^{+}$ myeloid cells deregulate senescence in prostate lesions by interfering with the SASP, and thus protecting surrounding tumour cells from senescence (Di Mitri *et al.*, 2014). Lastly, $CD4^{+}$ T cells have been implicated in the clearance of senescent cells from pre-malignant liver lesions (Kang *et al.*, 2011). Together, these studies show there is a requirement for immune clearance of senescent cells to prevent development of

cancer, but this largely depends on the correct differentiation and stimulation of immune cells. However, 'senescence surveillance', utilising both innate and adaptive immune systems, can promote a controlled elimination programme of pre-malignant senescent cells. If the appropriate disease context is evident, senescence surveillance could specifically be harnessed to provide an attractive target for cancer therapy.

In recent years, many pro-senescence therapies have been explored experimentally and clinically, with an aim to replace conventional cancer treatment strategies, chemo- and radiotherapy. Historically, cancer drugs and ionizing radiation are both known to cause therapy-induced senescence (TIS), which requires engagement of $p16^{INK4a}$ and p53 tumour suppressor pathways (Schmitt *et al.*, 2002). Genetic depletion of $p16^{INK4a}$ and p53 results in drug resistance, therefore TIS is required for a robust response to chemotherapy. This indicates senescence could be pharmacologically upregulated for therapeutic gain in cancers. However, caution must be used when developing pro-senescence therapies due to its finely balanced anti- and pro-tumorigenic features. In addition, there is risk of DNA damage when inducing senescence, that can cause detrimental genetic abnormalities. Indeed, analysis of human prostate tumour microenvironments identified DDR-NF-κB activated WNT16B (a secreted factor), which attenuated the effects of conventional chemotherapy and promoted tumorigenesis (Suvn *et al.*, 2012). In contrast, *Pten*-loss induced cellular senescence (PICS) in a murine prostate cancer model does not exhibit DNA damage (Alimonti *et al.*, 2010); therefore, inhibition of *Pten* and activation of PICS could be a possible pro-senescence therapy for prostate cancers. Alimonti *et al.* (2010) showed Pten inhibitor VO-OHpic induced PICS specifically in $Pten^{+/-}$ tumours. This further highlights the importance of genetic context when evaluating pro-senescence therapies. Another promising target for pro-senescence therapy is the inhibition of CDKs; particularly, inhibition of CDK4 with PD-00332991 and LEE-011 induces senescence in glioblastoma, neuroblastoma and breast cancer in *in vitro* and *in vivo* models (Michaud *et al.*, 2010; Thangavel *et al.*, 2011; Rader *et al.*, 2013). These proof-of-principle studies have been followed up with clinical trials (Finn *et al.*, 2015), and PD-00332991 is now approved for use in ER-positive breast cancer (Inman, 2015). In addition, senescence markers can be used as a prognostic tool for human cancer; for example, increased p21-positivity,

stabilised by mTORC1/4E-BP1, indicates better survival in head and neck squamous cell carcinomas (Llanos *et al.*, 2016). Overall, development of pro-senescence therapies for cancer will depend on evaluating which mechanistic pathway to target, how this will affect other pathways and assessing the genetic context of individual patient tumours.

1.1.4.2 Aging

It has been proposed senescence and aging are associated since Hayflick's seminal work in the 1960s. However, the causal mechanism linking senescence to aging biology is still a current topic of research, and is discussed below. Many studies have shown aged mammalian cells and tissues have accumulated senescent cells with different markers. For example: DNA damage is progressively accumulated in aged primates (Herbig *et al.*, 2006; Jeyapalan *et al.*, 2007); telomere length and resulting dysfunction is implicated in aged murine stem cells (Flores *et al.*, 2008); and SA β-gal activity is increased in cultured human cells and aged human skin tissue (Dimri *et al.*, 1995). Cell cycle inhibitors such as $p21^{CIP1}$ and $p15^{INK4b}$ are not usually upregulated in aging-related senescence but accumulated $p16^{INK4a}$ is consistently implicated (Krishnamurthy *et al.*, 2004). Furthermore, telomere shortening triggers senescence through ATM, p53 and $p21^{CIP1}$, not $p16^{INK4a}$ (Herbig *et al.*, 2004), suggesting accumulated $p16^{INK4a}$ in aged tissues is triggered by a telomere-independent aspect of aging.

Due to accumulated $p16^{INK4a}$ prevalence in aged senescent cells and tissues, it is believed to be a functional biomarker for aging-related senescence. Indeed, in 2006 three studies were the first to show senescence plays a casual role in aging, via $p16^{INK4a}$ accumulation. These studies showed age-dependent increased $p16^{INK4a}$ in tissue stem cell/progenitor compartments: neural stem cells (Molofsky *et al.*, 2006), haematopoietic stem cells (Janzen *et al.*, 2006), and pancreatic islet cells (Krishnamurthy *et al.*, 2006). In all these cell types, senescence led to decreased regenerative capacity in aged tissues that could be rescued with genetic ablation of $p16^{INK4a}$. $p16^{INK4a}$ is also essential for accelerated aging in a progeroid mouse model with mutated checkpoint protein, BubR1 (Baker *et al.*, 2008). Recently, two other papers from the van Deursen group have presented further evidence for the function

of $p16^{INK4a}$ during aging-related senescence. Baker *et al.* (2011) developed an innovative mouse model, by introducing a transgene, INK-ATTAC, into the mutant *BubR1*$^{H/H}$ background. The INK-ATTAC construct has an AP20187-inducible caspase-8 (apoptosis activator) controlled by a $p16^{INK4a}$ gene promoter, that is only transcriptionally active in senescent cells. Therefore, upon AP20187 treatment, the INK-ATTAC can selectively induce elimination of $p16^{INK4a}$-positive senescent cells by apoptosis. The authors used this model to show lifelong or late-life clearance of $p16^{INK4a}$-positive senescent cells delays the onset of age-related phenotypes, such as eye degeneration, exercise ability and adipose content. However, *BubR1*$^{H/H}$*;INK-ATTAC* mice do not have extended lifespan as the progeroid mice died of $p16^{INK4a}$-independent cardiac failure. This study was repeated in wild-type mice, to analyse the effects on naturally-occurring $p16^{INK4a}$-positive senescent cell clearance. Both male and female INK-ATTAC mice have extended median (not maximum) lifespan, delayed tumorigenesis of age-related cancers and reduced deterioration corresponding with increased functionality of tissues, such as: heart, kidney and fat (Baker *et al.*, 2016). These studies and others (Xu *et al.*, 2015; Hashimoto *et al.*, 2016) highlight the benefit of therapeutically removing senescent cells to extend a healthy lifespan.

As described previously, immune clearance of senescent cells is a vital mechanism to prevent persistent senescence in a tissue, that can lead to detrimental pathology. It is widely known the immune system declines with age, perhaps explaining the presence of persistent and detrimental senescence during aging. Therefore, genetically targeting the clearance of senescent cells is an attractive method to delay aging, and is currently being assessed for therapeutic viability in mouse models (as discussed above). Further, a recent study revealed therapeutically activating senescent cell apoptosis by perturbing FOXO4-p53 interactions can restore tissue homeostasis in aged tissues (Baar *et al.*, 2017). Senescence also has a role in age-related diseases, and there is potential in targeting senescent cells to counteract them (reviewed by Childs *et al.* (2017)). These pathologies include: atherosclerosis (Vasile *et al.*, 2001), type 2 diabetes (Tchkonia *et al.*, 2010), glaucoma (Liton *et al.*, 2005), osteoarthritis (Martin and Buckwalter, 2003) and lung disease (Noureddine *et al.*, 2011). Recent studies have shown the reversal of atherosclerosis and osteoarthritis in mice after

genetically ablating $p16^{INK4a}$ (Childs *et al.*, 2016; Jeon *et al.*, 2017, respectively). Finally, many 'senolytic' therapies have been explored to promote elimination of senescent cells in aging humans, using small molecules. For example, inhibitors of the BCL-2 family, ABT-737 and navitoclax, allow senescence-specific apoptosis in age-related diseases (Childs *et al.*, 2016; Yosef *et al.*, 2016).

Ultimately, aging is not considered a disease, and although it does increase the risk of developing many associated diseases, through a mechanism involving senescence, it is likely aging will never be prevented in humans. Instead, the use of anti-senescent therapies for delaying or maintaining specific age-related diseases is more likely to be clinically assessed in the future.

1.1.4.3 Fibrosis

Senescence has been implicated in fibrosis (the accumulation of fibrotic lesions usually coupled with a loss of tissue function) of many different tissue types. The best characterised is the formation of senescent fibrotic scars in response to chronic liver damage. Hepatic stellate cells (HSCs) are damage-activated to proliferate as myofibroblasts, which eventually form a fibrotic scar with collagen and a unique ECM. In humans, the periphery of the scar stains positive for SA β-gal and founding HSCs express p53, $p21^{CIP1}$ and $p16^{INK4a}$ (Wiemann *et al.*, 2002; Krizhanovsky *et al.*, 2008). The senescent cells within the scar produce a SASP to eliminate the scar and allow tissue repair; particularly, CCN1 is a key mediator of this process and treatment with recombinant CCN1 can promote HSC senescence to reverse liver fibrosis in mice (Kim *et al.*, 2013). In addition, activated HSCs secrete IL22, which mediates senescence through STAT3/SOCS3 p53 activation. IL22 overexpression in mice livers accelerates recovery of fibrosis by inducing HSC senescence (Kong *et al.*, 2012). Together, these studies indicate the efficacy of pro-senescence therapies for the reversal of liver fibrosis. Additionally, fibrosis in response to renal injury has been shown to beneficially induce senescence in mice and human kidneys, with increased $p16^{INK4a}$, $p21^{CIP1}$and SA β-gal (J. Liu *et al.*, 2012; Clements *et al.*, 2013). Furthermore, p53-positive senescent myofibroblasts are present in areas of the heart after myocardial infarction (Zhu *et al.*, 2013). As pro-senescence therapies have had some success with liver fibrosis, there could also be a future use for them in

preventing fibrosis post-renal and -cardiac injury and improving recovery. Finally, senescence can also be detrimental in certain fibrotic environments. For example, in a mouse model of idiopathic pulmonary fibrosis (a chronic disorder affecting lung function), SA β-gal positive cells concomitantly activate NOX4 to generate oxidative stress and inflammation in fibrotic lesions (Hecker *et al.*, 2014). This response can be attenuated and damage reversed using the anti-inflammatory drug rupatadine (Lv *et al.*, 2013) and drug combination dasatinib/quercetin (Schafer *et al.*, 2017).

1.1.4.4 Wound healing

Senescence has also been implicated in the fibrotic response during wound healing. Jun and Lau (2010) found the SASP factor CCN1 can mediate senescence in the granulation tissues of healing wounds and subsequently expression of anti-fibrotic genes (like its implications in liver fibrosis). The authors found senescence is established by CCN1 binding to integrin-$\alpha_6\beta_1$, initiating DDR activated p53 and RAC1-NOX1 activated $p16^{INK4a}$/RB. This process was lost in a CCN1-mutant mouse (with no integrin-$\alpha_6\beta_1$ binding domain) and fibrosis of the wound was exacerbated. Furthermore, topical recombinant CCN1 treatment reversed the harmful effect on wound healing in the CCN1-mutant mouse. Additionally, a more recent study, utilising a model like the INK-ATTAC mouse described in *1.1.4.2*, has shown senescence is involved in tissue remodelling in a healthy *in vivo* context (Demaria *et al.*, 2014). In this study, the p16-3MR mouse was used to specifically eliminate senescent cells by apoptosis. The resulting response to a wound was delayed due to a reduced transient presence of senescence in the early stages of wound healing. Senescence fibroblasts and endothelial cells were found to express platelet-derived growth factor AA (PDGF-AA), and topical treatment of PDGF-AA restores normal wound healing. Finally, senescence has been positively associated with tissue damage, due to the concomitant activation of cellular reprogramming by IL6 secretion (Mosteiro *et al.*, 2016). From studies like these, there is now evidence to support the theory that senescence is a vital and beneficial process for tissue repair. However, senescence is a double-edged sword; as discussed earlier in this section, beneficial outcomes of senescence depend on sufficient clearance of senescent cells from areas of tissue damage (such as pre-malignant lesions). This must be considered

when developing therapies targeting senescence, to ensure tissues return to pre-damage conditions rather than develop chronic damage.

1.1.4.5 Embryonic development

In 2013, seminal papers from the Serrano and Keyes groups described programmed senescence present in developing mouse embryos (Muñoz-Espín *et al.*, 2013; Storer *et al.*, 2013). Observations were similar in chickens and humans, indicating this is a conserved process between vertebrates. Embryonic structures implicated in developmental senescence include, but not limited to: the mesonephros (the temporary embryonic kidney); endolymphatic sac (an inner ear tube); and the apical ectodermal ridge (AER, a transient structure in limb buds). These structures exhibited non-proliferative cells with SA β-gal, tumour suppressor expression and heterochromatic markers. Senescence in the mesonephros and endolymphatic sac is dependent on $p21^{CIP1}$, not p53 or DNA damage, and was regulated by TGFβ-SMAD and PI3K-FOXO pathways (Muñoz-Espín *et al.*, 2013). Senescence in the AER is characterised by a SASP that activates Erk in the mesenchyme proximal to the AER, and instructs the structure to remain senescent. The SASP also feeds back to the AER to mediate immune clearance of senescent cells at the correct development transition (Storer *et al.*, 2013). Apoptosis is generally important for development (Fuchs and Steller, 2011) and from the two previous studies, apoptosis is a known compensatory mechanism if senescence fails during embryonic development. Despite this, morphological defects in adults occur if senescence is absent during development (Muñoz-Espín *et al.*, 2013). It is interesting to note here that senescence has also been observed in two specialised adult cell types, megakaryocytes (Besancenot *et al.*, 2010) and placental syncytiotrophoblasts (Chuprin *et al.*, 2013). These two cell types are the only naturally polyploid mammalian cells known to undergo endoreduplication during differentiation (Ullah *et al.*, 2009), and thus senescence could be underlying cause of this developmental programme.

1.1.4.6 Obesity and diabetes

Senescence has been identified in obese murine and human adipose tissues, associated with type 2 diabetes. Minamino *et al.* (2009) found a vital role for oxidative stress and p53 activation in adipose tissue of diabetic mice on a high fat

diet. The senescent adipocytes presented with SA β-gal, p53 expression and SASP-like pro-inflammatory response. Importantly, targeting p53 expression in the diabetic mice reversed the senescence phenotype and improved insulin resistance. Further to this study, obesity-related protein HMGA2 has been implicated in human adipose tissue senescence characterised by *CDKN2A* expression (Markowski *et al.*, 2013). In addition, when *CDKN2A* expression is ablated in a progeroid mouse, adipose tissue does not senesce (Baker *et al.*, 2008, 2011). Although adipose tissue senescence is detrimentally linked to obesity and diabetes, it is preventable with low fat diet and reversible by introducing exercise (Schafer *et al.*, 2016). This study identifies a novel cellular mechanism that demonstrates exercise is beneficial for disease prevention.

In similar context, a recent study has implicated senescence in age-related resistance to white to beige adipocyte differentiation. This process is induced by cold temperatures and results in beige adipocyte thermogenesis (or 'beiging'). Berry *et al.* (2017) found aged murine and human adipocytes were incapable of beiging due to a SA β-gal-positive senescence phenotype, activated through p38-MAPK-$p16^{INK4a}$ pathways. The authors showed targeting senescent cells with a p38/MAPK inhibitor restored beiging in aged human cells. Therefore, combining senescence inhibition with hypothermia-induced beiging may be a potential strategy for reversing obesity and diabetes in aging humans. In addition, pancreatic β-cells have been implicated in age-related insulin resistance and diabetes pathogenesis (Aguayo-Mazzucato *et al.*, 2017). In response to aging, β-cells exhibited heterogeneous expression of senescent markers SA β-gal, $p16^{INK4a}$ and p53, which correlated with rapid decline in function. These studies suggest targeting senescence in aging-related metabolic dysfunction could be a novel therapy for diabetes.

1.1.4.7 Summary

The basic function of senescence is to clear unwanted and/or harmful cells. This function in normal physiological and pathological environments has revealed a general mechanism for senescence in tissue remodelling, as follows: (1) senescence establishment; (2) clearance (i.e. senescence surveillance); (3) regeneration of tissue. The clearance of senescent cells by innate and adaptive immune systems is vital for the transient nature of protective senescence. When senescent cells persist, tissue

dysfunction occurs in the senescent microenvironment and aggravates pathology of initially protected tissues.

1.1.5 Cellular senescence summary

Senescence is a stable cell cycle arrest that is utilised in environments where cells undergo potentially harmful alterations, such as telomere shortening, oncogene activation and mitochondrial stress. Senescent cells have a distinct phenotype including: morphological changes, DNA damage, tumour suppressor activity, heterochromatic markers, β-galactosidase activity and a distinctive secretome. These changes in cell phenotype can be used to identify senescent cells *in vitro* and *in vivo*, in addition to proliferation readouts. Senescence has a role in both human health and disease; in recent years, mechanisms of how senescence contributes to normal physiology and disease pathology have been revealed. There is promise in targeting senescence for novel disease therapies, however, it is essential to gain understanding of the cellular and molecular mechanisms of senescence to progress further in therapy development.

1.2 Metabolism in cancer and senescence

The seminal work identifying altered metabolism in cancer tissues was performed by Otto Warburg, the pioneer of cancer metabolism, a century ago. However, only in the past decade has there been substantial progress in understanding the functional mechanisms that link metabolites to cancer growth. This is largely due to the development of new technologies that provide accurate readouts of metabolism, such as liquid chromatography mass spectrometry (LC-MS) machines. These technologies coupled with new genetic models for different cancers have vastly expanded the understanding of the consequences of cancer-specific metabolism and how this may be therapeutically targeted (extensively reviewed in a 2016 NRC Focus issue (volume 16.10); foreword by Cairns and Mak (2016)). Although senescent cells are permanently arrested, they are capable of hypertrophy and remain metabolically active. This knowledge, along with the well-established role for senescence in cancer pathologies, has caused recent advances in perturbing specific metabolic pathways

and determining the function in OIS. In this section, there is a brief overview of how metabolism is experimentally investigated using mass spectrometry, followed by the fundamentals of cancer metabolism. Next, seminal studies that have contributed to deconvoluting the complex function of metabolic alterations in OIS are reviewed. Finally, an overview of ceramide metabolism is provided due to this thesis' work implicating ceramides in OIS. Figure 1.3 can be used to aid visualisation of the main metabolic pathways (in purple) and related enzymes (green circles) described in this section.

Figure 1.3 Schematic summary of metabolic pathways implicated in cancer and senescence (next page)

Glucose is transported across the extracellular membrane via glucose transporter 1 (GLUT1). Glucose is metabolised in the cytoplasm through a multiple-step process called glycolysis. The first step of glycolysis is the conversion of glucose to glucose-6-phosphate, catalysed by hexokinases (HK). Glucose-6-phosphate is used in the pentose phosphate pathway to yield ribose-5-phosphate units for nucleotide (i.e. RNA and DNA) metabolism. Four glycolytic steps occur before 3-phosphoglycerate is produced; this metabolite is an essential precursor for serine and glycine metabolism and the synthesis of one-carbon units. The final step of glycolysis is the conversion of phosphoenolpyruvate to pyruvate, catalysed by pyruvate kinases (PKM). Cytoplasmic glycolysis and mitochondrial TCA cycle are linked via a gatekeeper enzyme pyruvate dehydrogenase (PDH), that converts pyruvate to acetyl-coA. PDH activity is stimulated by PDH-phosphatase 2 (PDP2) and inhibited by PDH-kinase 1 (PDK1). Acetyl-coA enters the TCA cycle to synthesise citrate from oxaloacetate. Citrate and acetyl-coA are the main precursors for fatty acid synthesis and downstream lipid metabolism (e.g. triglycerides, cholesterol, and sphingolipids). The reverse reaction of the next step in the TCA cycle (citrate to α-ketoglutarate), catalysed by isocitrate dehydrogenase (IDH), is also important for fatty acid synthesis. Glutamine to glutamate metabolism, catalysed by glutaminases (GLS), is an additional mechanism for α-ketoglutarate production. The penultimate step before oxaloacetate is synthesised to restart the TCA cycle is the hydration of fumarate to malate, catalysed by fumarate hydratase (FH). Energy released from the TCA cycle and subsequent oxidative phosphorylation, as nicotinamide adenine dinucleotide (NADH) and adenosine triphosphate (ATP), is used for cellular processes such as autophagy and protein synthesis (driven by mechanistic target of rapamycin (mTOR)).

Pathways implicated in cancer and/or senescence = purple; specific enzymes implicated in cancer and/or senescence = green circles.

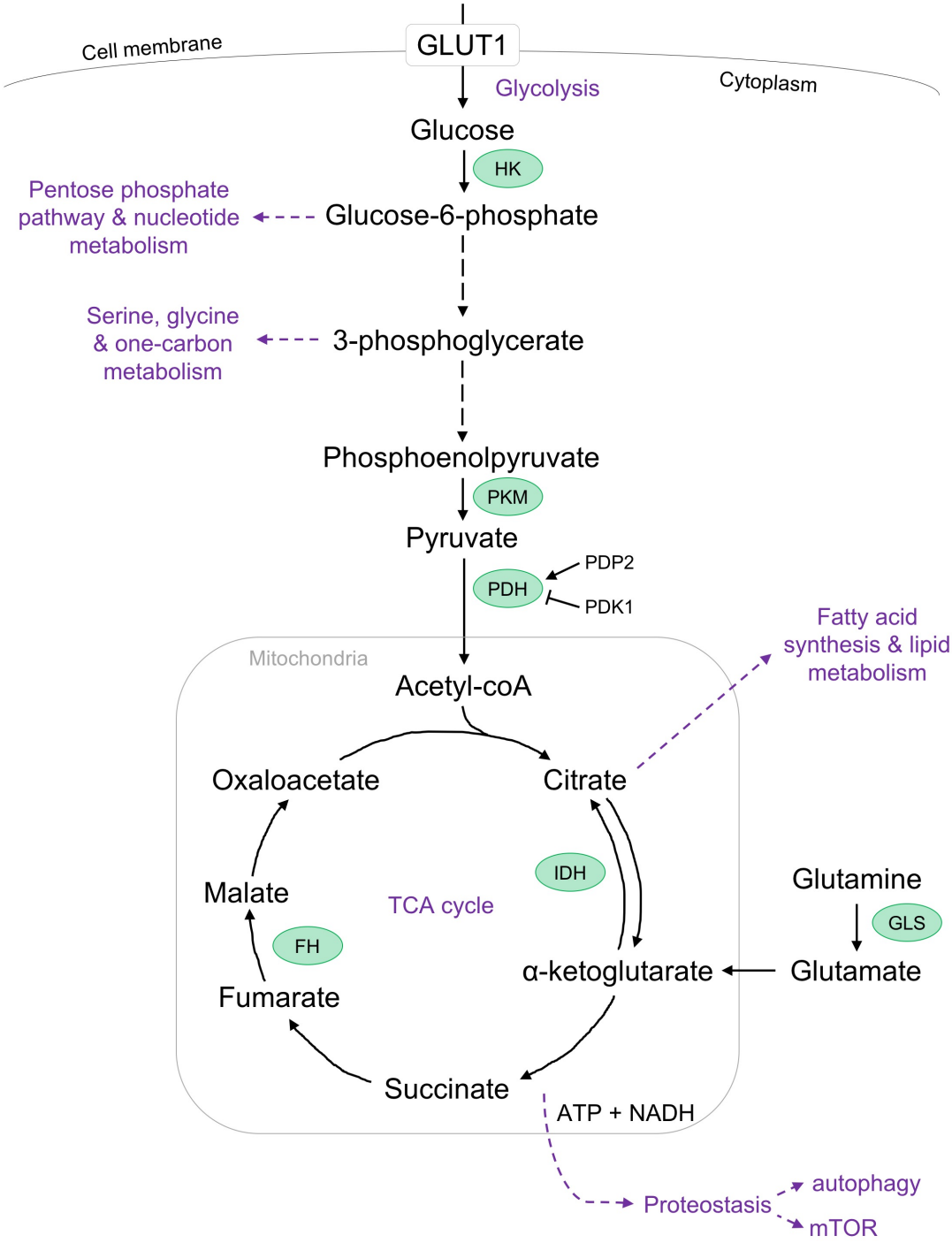

Figure 1.3 Schematic summary of metabolic pathways implicated in cancer and senescence

1.2.1 Measuring metabolism

The metabolome is composed of small molecules (<1500Da) that are the precursors of essential cellular macromolecules, providing the foundation of cellular energy production, in addition to having their own independent functions. The metabolome can be loosely broken down into the following molecules: nucleotides, amino acids, carbohydrates and lipids (Kell and Oliver, 2016). Complex metabolic networks link these molecules, meaning determining the activity and regulation of the intricate pathways has been challenging. In the past decade, there has been huge development in mass spectrometry methods for metabolomics and lipidomics (the specific detection of lipids). Mass spectrometry can be used to analyse a large range of molecules, with high sensitivity and dynamic range. Furthermore, combined methods, such as liquid chromatography mass spectrometry (LC-MS), can provide more accurate platforms for analysing metabolomes/lipidomes and for identifying unknown single molecules (Patti, Yanes and Siuzdak, 2012). First, LC is used for enhanced separation of a liquid phase; this has several benefits for example, providing a 'retention time' to aid identification of similarly sized molecules. Next, separated molecules are injected into the MS component; here, many steps occur to ionise, detect and identify molecules. Ionisation is required to give molecules a charge and allow the MS to detect it using a mass/charge ratio (m/z). Depending on the type of MS, different devices can be used to aid ion detection and identification. The Q-Exactive mass spectrometer (Thermo) used for lipidomics in this thesis uses an 'orbitrap' to detect ions, by applying a voltage and measuring the orbit frequency of ions. In addition, the Q-Exactive has a 'quadrapole' that can be used to filter and isolate ions of a specified m/z, when required. Lastly, tandem-MS (MS/MS) can be used to fragment ions and aid identification of molecules; the Q-Exactive uses a 'HCD cell' to facilitate fragmentation.

Untargeted metabolomics is useful for the large-scale detection of metabolite levels in novel biological contexts (Patti, Yanes and Siuzdak, 2012). However, findings from these untargeted studies always require validation with more targeted analyses, to accurately quantify metabolite levels (Chokkathukalam *et al.*, 2014). In addition, metabolic pathways can be further interrogated using stable heavy-isotope labelling.

This technique uses stable heavy isotopes, such as ^{13}C, to measure the activity of a metabolic pathway. Due to the change in mass with heavy isotopes, mass spectrometry can reliably detect different isotopologs of the same molecule. Generally, the stable heavy isotopes are provided as synthetically made 'tracers', which will be precursor molecules for the targeted metabolic pathway. For example, $^{13}C_2$-glucose can be used to measure glycolysis and the pentose phosphate pathway (Lee *et al.*, 1998) and U-$^{13}C_5$-glutamine can be used to measure the TCA cycle starting with citrate (Metallo and Vander Heiden, 2013). Using this method, heavy isotopes can be traced through a metabolic pathway; so, depending on the activity of that pathway, the heavy isotopes will be incorporated into endogenous molecules at certain rates. Using an unlabelled control, the percentage of heavy-labelled molecules of total levels (i.e. all isotopes) can be calculated to indicate the activity of the metabolic pathway. In the next section, studies relevant to cancer metabolism, using LC-MS and stable heavy-isotope labelling, are examined. These examples demonstrate how powerful this method can be for biological research (also reviewed by Johnson, Ivanisevic and Siuzdak (2016)). However, it is important to note than careful experimental design and optimisation must be implemented to gain the correct information from stable heavy-isotope labelling (Metallo, Walther and Stephanopoulos, 2009).

1.2.2 Cancer metabolism

Cancer cells have high bioenergetic and biosynthetic demands that are met by remodelling of energy-releasing metabolic pathways and increased nutrient acquisition. This fundamental process in malignant transformation of cells was first hypothesised and illustrated by Otto Warburg in the 1920s. Warburg observed tumour slices preferentially metabolise glucose to lactate by glycolysis, which is normally observed as a response to hypoxia in normal tissues (Warburg, Posener and Negelein, 1924). This occurs even though ATP generation from aerobic glycolysis is inefficient compared to oxidative phosphorylation. Warburg postulated this phenomenon (referred to as the 'Warburg Effect', figure 1.4) was due to mitochondrial dysfunction in cancer (Warburg, 1956); however, many studies have subsequently suggested the cause and function of the Warburg Effect is far more

complex. In 2009, Vander Heiden and colleagues hypothesised the Warburg Effect, and related cancer-related metabolic reprogramming, occurs to allow sufficient production of essential cellular macromolecules (nucleic acids, proteins and lipids) that support expansion of cells (Vander Heiden, Cantley and Thompson, 2009). Ultimately, this is the basic principle answering *why* cancer cells require reprogrammed metabolism; but *how* does cancer mechanistically achieve this outcome? Below, this question is explored utilising evidence from studies analysing glucose, glutamine and one-carbon metabolism in cancer; genetic implications and therapeutic opportunities are included where relevant.

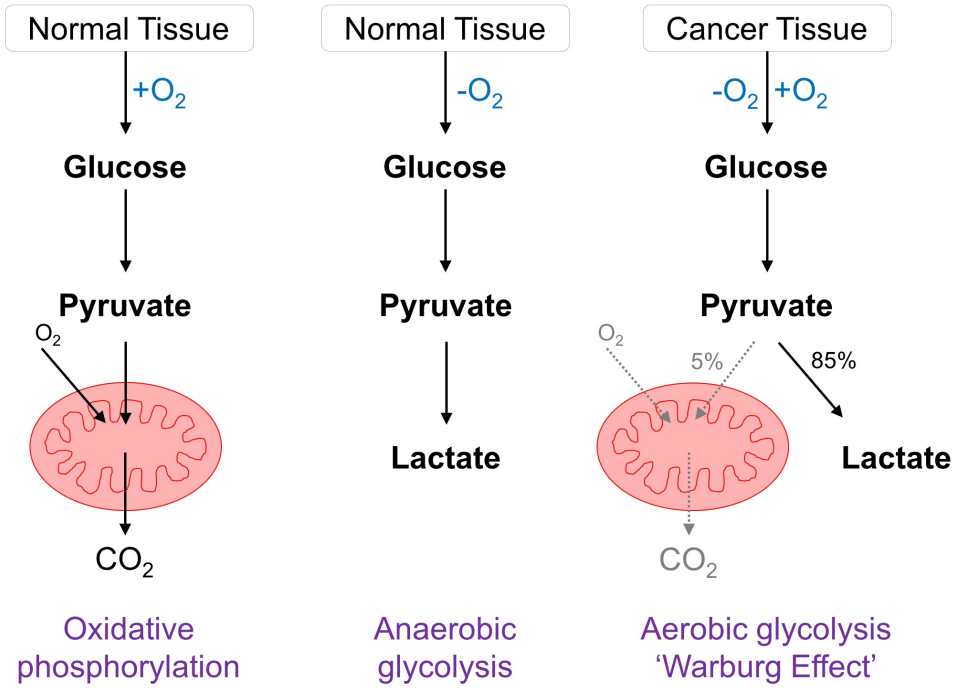

Figure 1.4 Pathways of glucose utilisation and energy production in normal and cancer tissues

Normal tissues can metabolise glucose to synthesise ATP via two pathways, depending on the presence or absence of oxygen: oxidative phosphorylation (yields 36 mol ATP per mol of glucose) and anaerobic glycolysis (yields 2 mol ATP per mol of glucose). Cancer tissues convert glucose to pyruvate and lactate via glycolysis, regardless of the presence or absence of oxygen – this is known as the Warburg Effect. Diagram adapted from (Vander Heiden, Cantley and Thompson, 2009).

1.2.2.1 Glucose metabolism

Since Warburg's original observation of increased aerobic glycolysis, there has been identification of many positive and negative regulatory pathways for glucose metabolism (reviewed by Hay (2016)). There are many mechanisms by which cancer exploits these regulatory pathways to adapt metabolism to their environment, and several key examples are described here. First, glucose transport into cancer cells is accelerated due to the increased expression and activity of glucose transporters, such as GLUT1 in Ras/BRAF mediated cancers (Yun *et al.*, 2009). Small molecule inhibitors of GLUT1 have shown to selectively kill cancer cells *in vitro* (Y. Liu *et al.*, 2012), however homozygous deletion of GLUT1 in mice is embryonic lethal (Wang *et al.*, 2006), suggesting widespread expression of GLUT1 is essential for normal cell function. Interestingly, GLUTs also transport oxidised vitamin C (dehydroascorbic acid, DHA). High dose DHA disrupts glycolysis in Ras/BRAF colorectal cancer cells (Corpe *et al.*, 2013) and high dose vitamin C has some clinical benefit in human cancers (Mikirova *et al.*, 2012).

Second, cancer-induced increased glucose uptake also facilitates the first committed step of glycolysis: the phosphorylation of glucose to glucose-6-phosphate, catalysed by hexokinase 2 (HK2). Cancer cells increase expression of HK2 to ensure high levels of glucose remain in cells and fluxes through downstream metabolic pathway (Patra and Hay, 2013). In adult mice, systemic deletion of HK2 inhibits tumour initiation/maintenance and there is no compensatory expression of hexokinase 1 (Patra *et al.*, 2013). This demonstrates it is possible to perturb a glycolytic enzyme for therapeutic benefit. Additionally, hexokinase activity is an inadvertent readout of cancer diagnostic/prognostic tool FDG-PET imaging. Cells are radiolabelled with glucose analogue [^{18}F] fluoro-2-deoxyglucose (FDG) and using PET imaging, cancer cells can be selectively detected by measuring the increased uptake, trapping (i.e. HK2 activity) and glycolytic metabolism of FDG (Okazumi *et al.*, 1992; Kelloff *et al.*, 2005).

Third, the final step of glycolysis- the conversion of phosphoenolpyruvate to pyruvate, catalysed by pyruvate kinases- is attenuated in cancer. This is mediated by the preferential expression of low-affinity and low-activity pyruvate kinase isoform

M2 (PKM2) (Christofk, Vander Heiden, Harris, *et al.*, 2008; Christofk, Vander Heiden, Wu, *et al.*, 2008). This observation contrasts with the increased flux of upstream glycolytic reactions but functions to support biosynthesis of macromolecules for cell proliferation. At low activity, PKM2 mediates the diversion of glycolytic metabolites from the TCA cycle, into pathways that facilitate the biosynthesis of nucleic acids, amino acids and fatty acids (such as the pentose phosphate pathway for ribose synthesis) (Christofk, Vander Heiden, Wu, *et al.*, 2008). Therefore, PKM2 acts as a gatekeeper, that determines if carbon from glucose is either metabolised for macromolecule biosynthesis or used for ATP generation by oxidative phosphorylation (Vander Heiden, Cantley and Thompson, 2009). Small molecule activators of PKM2 (DASA-58 and TEPP-46) limit the diversion of glucose to the pentose phosphate pathway and interfere with macromolecule biosynthesis in a cancer xenograft model (Anastasiou *et al.*, 2012). This suggests pyruvate kinases are a key regulatory node in cancer-driven glycolysis and outcomes are activity-dependent.

Finally, further to alterations to specific glycolytic enzymes, p53 has a regulatory role in glucose metabolism through the activation of 'TP53-inducible glycolysis and apoptosis regulator' (TIGAR) (Jen and Cheung, 2005; Bensaad *et al.*, 2006). In normal tumour environments, TIGAR upregulates the pentose phosphate pathway, whereas in hypoxic conditions, TIGAR will mediate glycolysis through hexokinase 2 activation (Cheung, Ludwig and Vousden, 2012). As p53 is the most frequently mutated gene in cancers, its role in glucose metabolism regulation is an important feature to understand for therapy development.

1.2.2.2 Glutamine metabolism

Glutamine is a conditionally essential amino acid, meaning in stressed environments, cells have increased glutamine demand which *de novo* synthesis cannot fulfil (Rubin, 1990). Subsequent glutamine depletion can result in cell death and glutamine dependence in cancer cells (Yuneva *et al.*, 2007). Rapidly dividing cells, including cancer cells, have increased glutamine consumption (Windmueller and Spaeth, 1974). Glutamine provides a central carbon and nitrogen source for cancer cells to use for biosynthetic and energetic processes, and support proliferation; how this

function of glutamine is altered in cancer is further explored below. First, it is important to note the main steps of glutamine metabolism. Glutamine is transported into cells via multiple different transporters (Bhutia *et al.*, 2015). In addition, the degradation of macromolecules can supply a cellular pool of glutamine, especially in Ras-driven cancer (Commisso *et al.*, 2013; Kamphorst *et al.*, 2015). Once in the cell, glutamine is converted to glutamate by glutaminases (GLS) (Krebs, 1935). This is followed by the conversion of glutamate to α-ketoglutarate by either glutamate dehydrogenases (GLUD) or aminotransferases, depending on the cell type involved (Moreadith and Lehninger, 1984). The flux of glutamine into the TCA cycle, via α-ketoglutarate, generates ATP and NADH to support biosynthesis of macromolecules.

Glutamine has multiple functions that result directly and indirectly of its flux into the TCA cycle. For example, glutamine mediates the synthesis of aspartate from TCA intermediate oxaloacetate; this regulation is vital for nucleotide biosynthesis and is the mechanism by which glutamine depletion initiates S-phase arrest in KRas-driven cancer cells (D. Patel *et al.*, 2016). Additionally, increased glutamine flux through the TCA cycle stimulates malic enzyme-mediated pyruvate to lactate conversion in glioblastoma cells. This releases NADPH that facilitates the use of glucose-derived carbon for fatty acid synthesis (DeBerardinis *et al.*, 2007). Furthermore, glutamine can be used as an alternative carbon source to support citrate-mediated fatty acid synthesis. Reductive carboxylation is a reverse pathway of part of the TCA cycle: glutamine-derived α-ketoglutarate is converted to citrate, by NADPH-dependent isocitrate dehydrogenases (IDH) (Wise *et al.*, 2011). This process is important for fatty acid synthesis in hypoxic tumours, *in vitro* and *in vivo*, and supports tumorigenesis (Metallo *et al.*, 2012; Mullen *et al.*, 2012; Sun and Denko, 2014).

The reprogramming of glutamine metabolism is highly dependent on the tissue of origin and oncogenic driver (reviewed by Altman, Stine and Dang (2016)). Cells transformed with Myc oncogene are highly dependent on exogenous glutamine (Yuneva *et al.*, 2007), and have increased protein/mRNA expression of glutamine-metabolic enzyme GLS (Wise *et al.*, 2008; Gao *et al.*, 2009). Myc overexpression and increased glutamine metabolism are also implicated in Kaposi's Sarcoma-Associated Herpes Virus (KSHV) infection and subsequent tumorigenesis of

Kaposi's Sarcoma (Sanchez *et al.*, 2015). Moreover, KRas-driven cancers also have glutamine dependence (Weinberg *et al.*, 2010; Gaglio *et al.*, 2011), however this is mutation dependent, with G12V mutations in lung cancer less dependent than G12D and G12C (Brunelli *et al.*, 2014).

The studies above indicate the complexity of glutamine metabolism and its genetic regulators in cancer. Targeting this pathway for therapeutic benefit is challenging, but some clinical progress has been made with allosteric inhibitors of GLS. CB-839 has been shown to have efficacy in humans against triple-negative breast cancer and leukaemia (Gross *et al.*, 2014; Jacque *et al.*, 2015). Targeting glutamine in combination with other therapies provides an attractive prospect of synthetic lethality, with improved outcomes. For example, metformin decreases glucose oxidation, leading to increased glutamine reductive carboxylation. Metformin in combination with a glutamine metabolism inhibitor attenuates the proliferation of prostate cancer cells *in vitro* and *in vivo* (Fendt *et al.*, 2013). The synergistic effects of targeting glutamine in combination with another therapy is yet to be clinically validated in humans. Finally, the use of [^{18}F] fluorinated glutamine has been clinically validated for diagnosis of glioma, instead of FDG-PET (Venneti *et al.*, 2015). This is because the brain has an increased ability to uptake glucose, making FDG-PET not specific enough to detect cancer cells (Kelloff *et al.*, 2005).

1.2.2.3 One-carbon metabolism

In addition to glutamine, non-essential amino acids serine and glycine are vital for cancer cell metabolism. Serine and glycine are the major sources of one-carbon units for pathways that support cancer proliferation (reviewed by Yang and Vousden, 2016 & Newman and Maddocks, 2017). Serine is sourced from: *de novo* synthesis (using glycolysis intermediate 3-phosphoglycerate), extracellular uptake and protein degradation (Commisso *et al.*, 2013; Galluzzi *et al.*, 2015; Kamphorst *et al.*, 2015). Serine is metabolised to glycine and a methyl group (used as a one-carbon source) by serine hydroxymethyltransferase (SHMT). For cancer cell proliferation, SHMT expression and activity is required (Jain *et al.*, 2012; Ye *et al.*, 2014). Additionally, the serine synthesis pathway (SSP) is upregulated in cancer (Pollari *et al.*, 2011; Possemato *et al.*, 2011) and in serine-starved conditions, growth of cancers *in vitro*

and in xenograft models is decreased (Maddocks *et al.*, 2013; Labuschagne *et al.*, 2014). This evidence suggests serine metabolism, synthesis and catabolism, is important for tumorigenesis. Glycine is also another independent source of one-carbon units, through the glycine cleavage system (GCS). The GCS cleaves a methylene group from glycine that is donated to an acceptor molecule, such as tetrahydrofolate. Lung cancer and glioblastoma cells exhibit upregulation and dependency on GCS enzyme glycine decarboxylase (Zhang *et al.*, 2012; Kim *et al.*, 2015). However, high glycine levels can be toxic (Rose *et al.*, 1999), therefore the GCS functions as a regulator of glycine levels, rather than one-carbon generation, to maintain ideal conditions for tumourigenesis.

The folate cycle is the major pathway that processes one-carbon units for use in downstream functions. Dihydrofolate reductase (DHFR) is the central enzyme that generates tetrahydrofolate (THF) from folic acid. THF is subsequently methylated (mTHF) using one-carbon units, which are later used for many pathways such as nucleotide biosynthesis. For example, two one-carbon units are required for the conversion of ribose-6-phosphate to inosine monophosphate (IMP), a precursor for purine nucleotides (Maddocks *et al.*, 2013; Labuschagne *et al.*, 2014; Kim *et al.*, 2015). In cancer, this pathway is important: inhibition of serine metabolism results in accumulated pre-IMP intermediates, as no one-carbon units are available and results in decreased proliferation and purine levels. In addition, one-carbon units can be used for DNA/protein methylation, and are implicated in cancer-related epigenetic modifications (Maddocks *et al.*, 2016). Finally, one-carbon metabolism also provides a pool of reducing co-factors NADH/NADPH, which critically support biosynthetic processes (Ducker *et al.*, 2016; Meiser *et al.*, 2016).

Anti-folates are inhibitors of DHFR and function to prevent THF metabolism and subsequently block one-carbon metabolism. The use of anti-folates as anti-cancer therapeutics has been established since the 1940s (Farber *et al.*, 1948); however, folate metabolism is important for normal cells therefore these drugs, such as methotrexate, have harmful side-effects. More recently, targeting one-carbon metabolic regulators has yielded therapeutic benefit for certain cancers. For example, targeting SSP enzyme phosphoglycerate dehydrogenase can decrease one-carbon

metabolism and inhibit *in vitro* and xenograft cancer cell proliferation (Mullarky *et al.*, 2016; Pacold *et al.*, 2016). However, cells that cannot depend on SSP activity must acquire serine for one-carbon metabolism from external sources. To this end, starving cells of exogenous serine significantly improves survival in different cancer mouse models (Maddocks *et al.*, 2017). This study also found KRas-driven models of pancreatic and intestinal cancers have increased *de novo* synthesis of serine, and therefore were less susceptible to serine starvation. Thus, understanding the dependency of some cancers on exogenous nutrients suggests how diet can contribute to cancer progression, and is an important factor to appreciate when considering cancer therapies.

1.2.2.4 Summary

It is evident from cancer metabolism research discussed here, that metabolism is not a simple homeostatic process but rather, a highly regulated, interconnected and dynamic network of processes programmed to meet the demands of the cellular environment. The reprogramming of metabolism is a vital hallmark of cancer; this arises to generate biomass molecules to support cell proliferation, in addition to generating the energy to fuel these biosynthesis pathways. There are many genetic drivers of cancer metabolism, which could provide novel targets for future cancer therapeutics; although, designing small molecules targeting these genes may be challenging due to structural similarities between functionally-different isoforms. Further, synthetic lethal approaches, combining metabolic inhibition with traditional therapies, are being clinically tested for efficacy in humans. Overall, deconvoluting the causes of reprogrammed cancer metabolism will lead to future development of new cancer therapies.

1.2.3 Senescence-induced metabolic alterations

As alluded by SA β-galactosidase activity and increased lysosomal content (Dimri *et al.*, 1995; Kurz *et al.*, 2000), senescent cells are highly metabolically active. The increased translation and secretion of SASP factors may explain senescence-induced metabolic alterations, as cells must re-balance energy supplies to maintain proteostasis; this hypothesis is further discussed later in this section. In recent years, there have been many studies deconvoluting rewired metabolism in senescence and

have identified this as a fundamental functional mechanism for senescence. Four main metabolic pathways are examined in this section: glycolysis-TCA cycle, proteostasis, nucleotide synthesis and fatty acid metabolism.

1.2.3.1 Glycolysis and TCA cycle

In replicative senescence, cells shift glucose metabolism to glycolysis, yet have low energy levels as they are serially passaged (Bittles and Harper, 1984; Zwerschke *et al.*, 2003). In OIS, cells also have altered activity through glycolytic and TCA cycle pathways (Kondoh *et al.*, 2005). Specifically, increased mitochondrial oxidative metabolism has been characterised in OIS, thought to allow enhanced energy production and meet demand (Dörr *et al.*, 2013; Kaplon *et al.*, 2013). These studies have led an exciting time for senescence research, identifying mechanisms that link rewired metabolism to OIS and revealing therapeutic benefits of targeting metabolism in cancer. Kaplon *et al.* (2013) identified a metabolic switch controlled by pyruvate dehydrogenase (PDH, a gatekeeper linking cytoplasmic glycolysis and mitochondrial TCA cycle) in $BRAF^{V600E}$ and Ras^{G12V} induced senescence. The authors found OIS regulates PDH activity through suppression of PDH-kinase 1 (PDK1) and activation of PDH-phosphatase 2 (PDP2). The resulting activation of PDH increases TCA cycle and oxygen consumption, and maintained OIS state. Importantly, the PDK1-PDP2-PDH axis was identified as a tumour suppressor mechanism against $BRAF^{V600E}$ mediated melanoma and genetic ablation of PDK1 expression caused tumour regression in mice with established melanoma. Therefore, identification of this metabolic switch in OIS yielded a novel pathway that can be beneficially exploited for cancer therapy. Further to this study, Retinoblastoma (RB) had been identified as a central mediator for the activation of glycolysis and mitochondrial oxidative phosphorylation (OXPHOS) in OIS (Takebayashi *et al.*, 2015). RB controls the upregulation of glycolytic and OXPHOS gene expression in OIS, to actively increase energy production. This provides a potential mechanistic link between metabolic remodelling and cell cycle arrest that Kaplon *et al.* (2013) did not ascertain. Finally, senescence induced by chemotherapeutic drug cyclophosphamide in a mouse lymphoma model is typified by increased glucose consumption and ATP generation (Dörr *et al.*, 2013). This is linked to alterations in

proteostasis and renders senescent cells amenable to selective elimination in cancerous lesions by blocking glucose utilisation (further discussed in *1.2.3.1*).

Moving into mitochondrial metabolism, loss of fumarate hydratase (FH) can induce senescence via accumulation of a newly-identified tumour suppressor metabolite fumarate (Zheng *et al.*, 2015). Hereditary mutations in FH can cause a highly malignant renal cancer, characterised by decreased enzyme activity and accumulated fumarate (a TCA cycle metabolite) (Tomlinson *et al.*, 2002; Pollard *et al.*, 2005). The resulting stress from the dysfunctional TCA cycle is overcome by the induction of senescence, via oxidative stress mediated succination of glutathione. Zheng *et al.* (2015) identified the mechanism linking fumarate to senescence by utilising analytical and computational chemistry. An unusual metabolite, succinated glutathione (succinicGSH), is produced from fumarate-induced succination activity, and induces persistent oxidative stress and consequently, senescence characterised by SA β-gal and $p21^{CIP1}$ expression. The authors hypothesise fumarate also induces the succination and inhibition of Keap1, which in turn frees and activates anti-oxidant factor Nrf2 to maintain a viable level of oxidative stress and maintain senescence state. Although this study does not provide comprehensive mechanistic data, it suggests FH is an important mitochondrial tumour suppressor for renal cancer. Senescence driven by FH loss is another example of tumour suppressor gene loss inducing senescence (like *Pten*-loss (Alimonti *et al.*, 2010)); although FH-loss is mediated through a different mechanism, involving altered TCA cycle metabolism.

Malate, another TCA cycle metabolite, has also been implicated in senescence, via interactions with p53 (Jiang *et al.*, 2013). Malate can be decarboxylated by two malic enzymes (cytoplasmic ME1 and mitochondrial ME2), to yield pyruvate (which is fed back into the TCA cycle) and CO_2. This reaction is dependent on the reduction of $NADP^+$ to NADPH, which is also vital for other metabolic activities relevant to senescence, such as lipid biosynthesis and anti-oxidant responses. Jiang *et al.* (2013) found MEs and p53 are reciprocally regulated in senescence: ME expression/activity is suppressed by p53, whereas increased ME delays replicative senescence. The suppression of MEs is mechanistically linked to senescence induction via the concomitant depletion in NADPH, a vital mediator of anti-oxidant responses. This

results in accumulated oxidative stress and AMPK-mediated p53 phosphorylation and activation. This study concluded p53 plays a central role in coordinating metabolic rewiring in response to cellular stress and its mutual metabolic regulation is vital for senescence.

It is important to note here that although these studies represent important progression in the understanding of senescence-related metabolic alterations, the use of different models of senescence makes interpretation more complex because of the sensitive response metabolism has towards stress. It appears metabolic profiles of senescence are model-dependent and the context of senescence induction (e.g. duration and intensity of trigger) must be considered if these studies are translated into clinical settings.

1.2.3.2 Proteostasis: autophagy and mTOR

Proteostasis is a homeostatic process to balance the degradation and synthesis of proteins. In senescence, several different proteostatic mechanisms have been implicated, involving either protein degradation (via autophagy) and synthesis (via mTOR control). Autophagy is the process whereby organelles and macromolecules are isolated in double-membrane autophagosomes and degraded by fusion with lysosomes (autolysosomes). This cellular degradation process is functionally relevant to senescence depending on cell system and trigger (Gamerdinger *et al.*, 2009; Capparelli *et al.*, 2012; Singh *et al.*, 2012). For example, (Patschan *et al.*, 2008) identified autophagy as a cell survival mechanism, determining the fate of stressed cells: senescence or death. Other studies have mechanistically linked both activation and inhibition of autophagy in senescence.

First, autophagy and protein synthesis (via master regulator mTOR) are spatially coupled in OIS. Narita *et al.* (2011) hypothesised senescent cells must have a mechanism to accommodate both anabolism and catabolism of proteins, to ultimately facilitate SASP expression. In Ras^{V12}-induced senescence, a distinct compartment following the Golgi is formed; in the TOR-autophagy spatial coupling compartment (TASSC) autolysosomes and mTOR accumulate. Amino acids and Rag GTPase recruit and activate TASSC-localised mTOR, which is required for IL6 and IL8

synthesis. Cytoplasmic-derived autophagosomes are recruited to allow autophagy by fusing with TASSC-localised lysosomes, and thus providing amino acids to enrich mTOR recruitment to the TASSC. This study highlights the importance of both anabolism and catabolism for senescence and indicates the mechanism by which senescent cells can augment the opposing processes for efficient protein turnover. In addition, autophagy-mediated degradation of nuclear envelope proteins is activated in OIS (Lenain *et al.*, 2015). Specifically, lamin B1 and lamin A were globally targeted for autophagy in $BRAF^{V600E}$ and Ras^{G12V} induced senescence, resulting in aberrant nuclear morphology. The activation of autophagy, as described by Narita *et al.*, (2011) and Lenain *et al.* (2015), is concomitant with increased lysosomal content in senescence; these studies further highlight multiple aspects of cellular metabolism need to cooperate to maintain proteostasis in senescence.

In contrast, senescent cells can also inhibit autophagy, which mechanistically functions to upregulate the SASP. Kang *et al.* (2015) identified transcription factor GATA4 as an essential mediator of SASP activation via NF-κB. Senescence stimuli and DDR kinases ATM/ATR suppress p62-mediated selective autophagy of GATA4. Accumulated GATA4 mediates SASP expression and inflammation through TRAF3IP2 and IL1A induction of NF-κB. Also, GATA4 is accumulated in aged mouse and human tissues, indicating this mechanism could drive age-related detrimental inflammation and inhibition of GATA4 may be of therapeutic benefit. Further to this, inhibition of MDM2, a ubiquitin-conjugating enzyme that targets p53 for proteasomal degradation, can drive senescence (Efeyan *et al.*, 2007). Also, abnormal Ras/ERK signalling can activate senescence-associated protein degradation, that selectively targets assorted groups of proteins for proteasome degradation (Deschênes-Simard *et al.*, 2013). These final two studies indicate other protein degradation pathways, other than autophagy, are implicated in senescence.

To conclude, although autophagy activation occurs during senescence, it appears inhibition of specific autophagy components is required for SASP production. Although there is a balance of activation and inhibition of protein degradation in senescence, there are additional mechanisms to maintain proteostasis through the regulation of protein synthesis, as described next.

Recently, there has been a focus in the field to examine the mechanisms by which senescent cells facilitate the synthesis and secretion of SASP proteins. Two studies have characterised mTOR as a central factor for SASP regulation in senescence. Both studies found rapamycin (the classical mTOR inhibitor) ablated the SASP but did not subsequently affect the cell cycle arrest (Herranz *et al.*, 2015; Laberge *et al.*, 2015). The two studies utilised different techniques to perturb this observation and found different mechanisms by which mTOR regulates the SASP. First, it is important to note that mTOR is a master regulator of protein synthesis that mediates the translation of mRNAs encoding target proteins. Laberge *et al.* found IL1α mRNA transcript was preferentially translated through mTOR control in senescence. Expressed and secreted IL1α then signals through IL1R1 receptor to activate global transcription factor NF-κB, which subsequently initiates the transcription of other inflammatory SASP factors. In contrast, Herranz *et al.* found MAPKAPK2 (a serine/threonine kinase) mRNA transcript was preferentially translated through mTOR and 4EBP1 control in senescence. Using phosphoproteomics, the authors identified MAPKAPK2-mediated phosphorylation of RNA-binding protein ZFP36L1; in turn, this inhibits ZFP36L1-mediated degradation of SASP transcripts. As discussed previously, it has been proposed targeting senescent cells is a novel approach to treat a variety of different diseases (reviewed by Childs *et al.* (2017)). These two studies provide essential evidence that specifically targeting only the SASP, via mTOR inhibition, could achieve similar therapeutic benefit, especially for pathological scenarios with inflammation.

Similarly, there are additional links to the SASP, proteostasis and therapeutic targeting of senescence-related metabolic alterations in cancer. Dörr *et al.* (2013) found therapy-induced senescence (TIS) in a lymphoma mouse model upregulates metabolic pathways, including glucose utilisation and SASP production. In this model of senescence, the higher energetic demands cause the activation of a proteoxic response through an ER stress-UPR-ubiquitination-autophagy cascade and consequently tumour development. TIS cells subjected to pharmacological inhibition of glucose utilisation and autophagy are targeted for selective elimination through caspase-mediated apoptosis. After metabolic elimination of TIS cells, lymphomas regress and following treatment outcomes are improved. The authors considered a

synthetic lethal-like metabolic targeting of senescent cells for treatment of primary lymphoma cancer. First, senescence is induced with chemotoxic drugs. Subsequently, senescent cells are selectively removed by targeting their aberrant metabolism. This presents a novel and intuitive approach for cancer therapy; it exploits first the beneficial effects of senescence in halting cancer and then prioritises the removal of senescent cells before the detrimental effects develop.

1.2.3.3 Nucleotide metabolism

Another essential metabolic rewiring process for OIS is the suppression of deoxyribonucleotide triphosphates (dNTPs) (Aird *et al.*, 2013). Ras-induced senescence results in the repression of rate-limiting dNTP synthesis enzyme, ribonucleotide reductase subunit M2 (RRM2), through E2F7 transcriptional repressor recruitment. Decreased dNTP levels are associated with aberrant DNA replication and the DDR in OIS. Furthermore, RRM2 expression is repressed in senescent melanocytic nevi and activated in tumorigenic melanoma, and high RRM2 expression correlates with poor survival in human melanoma patients. In addition, further perturbation of this mechanism also implicated deregulation of the pentose phosphate pathway (PPP) via G6PD activity in OIS (Aird *et al.*, 2015). As the PPP is vital for the synthesis of dNTP precursors and senescence induces TCA cycle glucose consumption (Kaplon *et al.*, 2013), together this provides further explanation for decreased dNTP levels in senescence. The key mediator of this phenotype was DDR kinase ATM; in response to replication stress, ATM coordinates the downstream upregulation of p53 and suppression of c-MYC, which initiates metabolic reprogramming to repress dNTP synthesis and initiate and maintain cell cycle arrest. This presents a novel mechanism that links DNA damage and replication stress to metabolic rewiring.

1.2.3.4 Fatty acid metabolism

Quijano *et al.* (2012) uncovered altered lipid metabolism in OIS, using comprehensive metabolomics analysis. First, they observed increased levels of intracellular long chain fatty acids and fatty acid oxidation in Ras-induced senescence. Senescent cells exhibited higher basal rate of oxygen consumption mediated by carnitine palmitoyltransferase 1 (CPT1A). This rate-limiting protein

allows the transfer of lipids from cytoplasm to mitochondria for oxidation. Interestingly, CPT1A depletion negatively affects the pro-inflammatory SASP, again indicating metabolic rewiring is essential for proper SASP function. This study also revealed OIS and replicative senescent cells have different and unique metabolic signatures, suggesting metabolic rewiring is context dependent and requires full understanding before pursuing clinical benefits. Further to this, 5-lipoxygenase (5LO) has been implicated in senescence, by promoting oxidative stress-mediated p53 activation (Catalano *et al.*, 2004). 5LO is an enzyme that metabolises arachidonic acid (a fatty acid) to produce lipids such as leukotrienes; these are particularly interesting in terms of senescence due to their well-studied role in inflammation. 5LO activity is increased in Ras-induced senescence of human fibroblasts and mediates the stimulation of oxidative stress. This stimulated phosphorylation of p53 at serine 15 and subsequent activation of p53-target $p21^{CIP1}$. In summary, this study identified 5LO as a key intermediate factor for metabolic alterations and the activation in senescence. Although no data has been shown to implicate leukotrienes in senescence, it is likely leukotrienes provide crosstalk with altered lipid oxidation and the SASP, considering the role 5LO has in leukotriene synthesis and their role in inflammation.

1.2.3.5 Summary

Overviewed here are key studies assessing senescence-related alterations in four pathways of metabolism and the downstream mechanisms identifying metabolic checkpoints for cell cycle arrest. Senescence can activate glucose and oxygen consumption through the TCA cycle and OXPHOS, which are genetically regulated by metabolic enzymes. Also, senescence-induced proteostasis is balanced intricately between protein degradation (autophagy and proteasome activity) and protein synthesis (mTOR activity). Finally, decreased nucleotide synthesis and increased fatty acid oxidation are also essential aberrant metabolic pathways for senescence. In conclusion, senescence requires a different homeostatic state to replicating cells which results in rewiring of glucose, protein, nucleotide and lipid metabolic pathways. Together, these studies suggest altered metabolism is an essential program for senescence induction and maintenance.

1.2.4 Ceramides

1.2.4.1 Ceramide biosynthesis

Ceramides are a subtype of sphingolipids and are characterised by an 18-carbon monounsaturated backbone (known as '18:1-sphingosine') coupled with a fatty acid, via an amide bond. Ceramides are neutral moieties and provide the backbone of complex sphingolipids, such as glyco- and galacto-sphingolipids. Ceramides can be of varying sizes; in humans, the 18:1-sphingosine backbone is bonded to fatty acids with chain lengths of 14-32 carbons (Hannun and Obeid, 2011; Morad and Cabot, 2013). The synthesis of ceramides occurs by three main pathways: *de novo*, recycling and sphingomyelinase. This section focusses on the *de novo* and recycling pathways (figure 1.5) as the sphingomyelinase pathway can be considered as part of the recycling. *De novo* synthesis of ceramide is initiated by rate-limiting enzyme serine palmitoyltransferase (SPT), which catalyses the condensation of serine and palmitoyl-CoA (Linn *et al.*, 2001). This produces the sphingoid backbone of ceramides, which is reduced from 3-ketodihydrosphingosine to dihydrosphingosine by 3-ketodihydrosphingosine reductase (KDSR) (Kihara and Igarashi, 2004). Next, dihydrosphingosine is coupled with a fatty acid (e.g. 16:0 palmitic acid) to produce dihydroceramide, by one of six ceramide synthases (CERS). The preferred activity of specific CERS determines the length and saturation state of the fatty acid (Riebeling *et al.*, 2003; Levy and Futerman, 2010). The final step in *de novo* ceramide synthesis adds a 4,5-*trans* double bond to the sphingoid base, catalysed by dihydroceramide desaturase (DEGS) (Causeret *et al.*, 2000). The recycling pathway of ceramide synthesis involves the breakdown of ceramides to release sphingosine backbone. Ceramide synthases regenerate ceramides using the released sphingosine substrate and free fatty acids (Kitatani, Idkowiak-Baldys and Hannun, 2008). There are several enzymes capable of degrading ceramide for recycling purposes, such as ceramidases, which have pH-dependent activities (Galadari *et al.*, 2006; Xu *et al.*, 2006). In addition, there is compartmentalisation of ceramide metabolism (Hannun and Obeid, 2008); the *de novo* synthesis pathway occurs in the endoplasmic reticulum whereas the recycling synthesis pathway occurs in the lysosome, cytoplasm and endoplasmic reticulum.

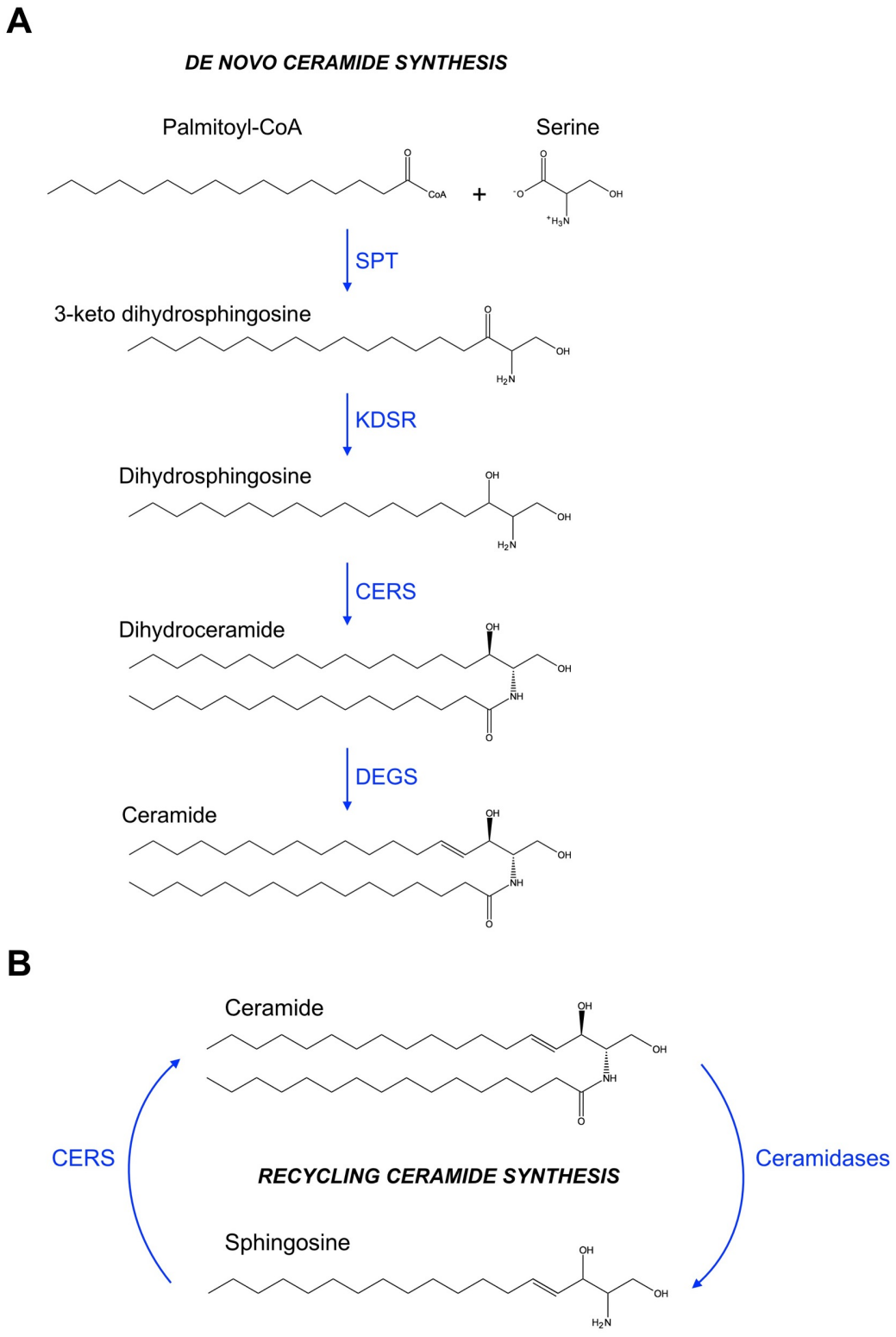

Figure 1.5 Ceramide biosynthesis

(A) *The de novo synthesis of ceramides occurs in the endoplasmic reticulum. The process starts with the condensation of palmitoyl-CoA and serine, catalysed by serine palmitoyltransferase*

(SPT), to produce the sphingoid backbone of ceramides. The next step is a reduction catalysed by 3-ketodihydrosphingosine reductase (KDSR). The product from this step, dihydrosphingosine, is coupled with a fatty acid (on the above diagram the fatty acid donor is 16:0 palmitic acid) to produce dihydroceramide. This step is catalysed by one of six ceramide synthases (CERS). The final step is the addition of a 4,5-trans double bond to the sphingoid backbone, catalysed by dihydroceramide desaturase (DEGS). ***(B)*** *The recycling pathway of ceramide synthesis relies on ceramide degrading enzymes, such as ceramidases, to release the sphingosine backbone. Ceramide synthases then convert the free sphingosine back into ceramides and free fatty acids.*

1.2.4.2 Ceramide metabolism

Ceramides have individual functions, as discussed in *1.2.4.3*, or can be further modified through ceramide metabolism (figure 1.6). Metabolism of ceramide that releases sphingosine has the potential to enter the recycling ceramide synthesis pathway (figure 1.5.B). Otherwise, sphingosine is phosphorylated to sphingosine-1-phosphate by sphingosine kinase (SPHK1). Sphingosine-1-phosphate is a signalling molecule involved in intracellular, extracellular and nuclear regulatory pathways (Fyrst and Saba, 2010). Ceramide-1-phosphate is synthesised by ceramide kinase (CERK) and regulates immune cell processes such as mast cell degranulation (Mitsutake *et al.*, 2004). Ceramide is also modified by addition of phosphocholine catalysed by sphingomyelin synthase (SMS), to form sphingomyelin. The reverse reaction is catalysed by sphingomyelinase and is part of the recycling pathway of ceramide synthesis. Sphingomyelin is a sphingophospholipid present in plasma membranes and is especially found in myelin sheaths of nerve cell axons (Ramstedt and Slotte, 2002). It is proposed sphingomyelin is an essential component of membrane 'lipid rafts' that function to mediate cellular trafficking and signal transduction (Simons and Ikonen, 1997). Glycosylceramides are complex molecules synthesised by the glycosylation of ceramide using mono- and polysaccharides, catalysed by ceramide glycosyltransferases (CGT). Glucosylceramide (ceramide+glucose) is the major lipid component of skin, contributing to water barrier properties of skin (Messner and Cabot, 2010). Galactosylceramide (ceramide+galactose) is a major component of nervous tissue (Coet *et al.*, 1998). Mutations in genes involved in the breakdown glucosyl- and galactosylceramide

cause Gaucher and Krabbe disease, respectively. These diseases are known as lysosomal storage disorders as they are characterised by tissue-specific accumulation of unmetabolised glycosylceramides in lysosomes (Parenti, Andria and Ballabio, 2015).

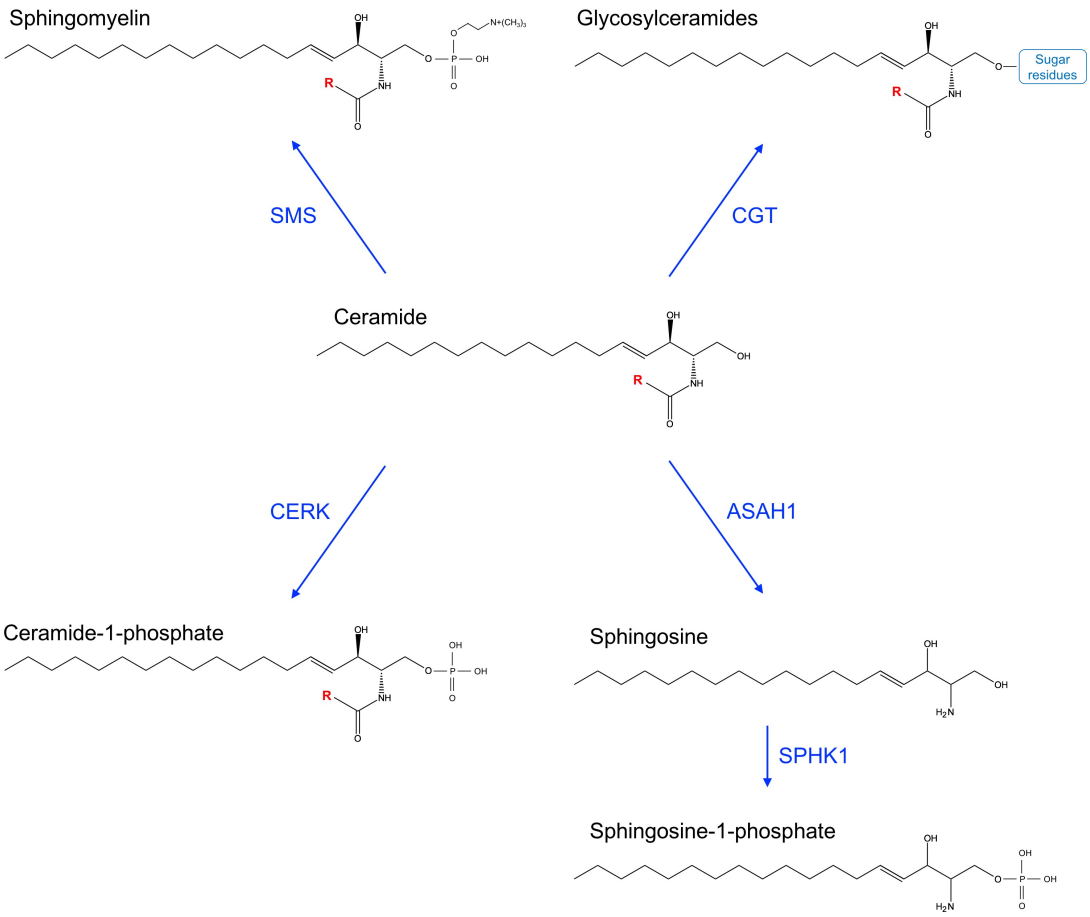

Figure 1.6 Ceramide metabolism

There are four main metabolic fates for ceramide (clockwise from top left): conversion to sphingomyelin, catalysed by sphingomyelinase (SMS); addition of mono and poly sugar residues to synthesise glycosylceramides, catalysed by ceramide glycosyltransferases (CGT); breakdown to sphingosine, catalysed by ceramidase (ASAH1) and phosphorylation to sphingosine-1-phosphate, catalysed by sphingosine kinase (SPHK1); and phosphorylation to ceramide-1-phosphate, catalysed by ceramide kinase (CERK). R = R-group present depends on the length and saturation state of fatty acid added to sphingosine backbone during ceramide biosynthesis (see figure 1.5).

1.2.4.3 Functions of ceramide

More sphingolipid species (~200) are present in human plasma than any other lipid class (Gonzalez-Covarrubias, 2013). This observation correlates with the large list of cellular and molecular functions of sphingolipids, alluded to in the previous sections. These functions of ceramide are also determined by the distinct sub-cellular localisation of the different pathways of ceramide synthesis, making it difficult to define the context of ceramide functions. This section overviews the role ceramides play in cellular membranes and cell cycle and death signalling.

Sphingolipids are amphipathic molecules, containing both hydrophobic and hydrophilic regions. Amphipathic lipids form bilayer membranes typical of the plasma membrane of cells; however, sphingolipids generally have saturated tails which allow them to pack more tightly into ordered regions (van Meer, Voelker and Feigenson, 2008). These sphingolipid-rich regions form dynamic microdomains, known as 'lipid rafts' (Thomas *et al.*, 2004). The rafts are fluid and can float in the normal membrane bilayer due to the association of cholesterol with the sphingolipids. The rafts act as platforms that mediate assembly of proteins involved in cell signalling (Futerman and Hannun, 2004). Ceramide metabolism can promote raft formation in specific cellular locations and thus ceramides have a role in regulating cell signalling (Gulbins and Kolesnick, 2003).

Apoptosis is a series of regulated processes that lead to programmed cell death and is a physiological response to cellular stress. Apoptosis can be induced by a number of factors, such as ionising radiation and tumour necrosis factor alpha (TNFα), and correlates with increased ceramide levels (Haimovitz-Friedman *et al.*, 1994; Dbaibo *et al.*, 2001). There are two major apoptotic pathways, extrinsic and intrinsic, and ceramides have been implicated in both. The extrinsic pathway occurs extracellularly and involves the arrangement of pro-apoptotic receptors and corresponding ligands (such as TNFα) on the cell surface (Morad and Cabot, 2013). Ceramides form platforms on the cell membrane to mediate this receptor clustering (Stancevic and Kolesnick, 2010). The intrinsic pathway is the intracellular signal transduction mediated by the mitochondria, resulting in the release of pro-apoptotic proteins (such as cytochrome c) (Morad and Cabot, 2013). Ceramide induces pore formation in the

mitochondrial outer membrane (Siskind, Kolesnick and Colombini, 2002), increasing the permeability and therefore regulating release of pro-apoptotic proteins. Cancer cells are resistant to apoptosis and there is some work indicating ceramides can be used to induce apoptosis for cancer therapy; this is described in further detail in *1.2.4.4*.

Ceramides also have a regulatory role in cell cycle arrest, with research focussing on replicative senescence. Ceramides were first implicated in senescence by Venable *et al.* (1995); in this study, it was found replicative senescent cells have a 4-fold increase in ceramide content. Furthermore, exogenous ceramide treatment induces senescence in a dose-dependent manner and is mechanistically linked to cell cycle arrest by hypophosphorylated RB (Dbaibo *et al.*, 1995). Ceramide can activate protein phosphatases (Wolff *et al.*, 1994), and although this appears to link ceramide to RB-mediated cell cycle arrest (Castro *et al.*, 2008), the exact mechanism of RB regulation in senescence is unknown. Ceramide-mediated senescence is characterised by p21 activation and resulting CDK2 inhibition (Lee, Bielawska and Obeid, 2000); however, there is contrasting evidence for whether this process is p53-dependent (Pruschy *et al.*, 1999; Struckhoff, Patel and Beckman, 2010) or p53-independent (Kim *et al.*, 2000). Finally, ceramide can inhibit telomerase, identifying it as an upstream regulator of telomere shortening (Ogretmen *et al.*, 2001). Interestingly, most of these studies were performed in replicative senescence models yet it was concluded ceramide has an essential tumour suppressive role.

In the early 2000s, there were many publications implicating ceramides in cell cycle arrest and although ceramides have been identified as a tumour suppressor, no additional characterisation of functional mechanisms concerning ceramides has been performed. This complicates making conclusions of how ceramide mediates cell fate; it is unknown how it is decided in what anti-proliferative way ceramide responds to cellular stress. Balancing ceramide metabolism likely plays a deciding role in cell fate, with a threshold of ceramide levels that will mediate either apoptosis or cell cycle arrest.

1.2.4.4 Ceramide in senescence-related pathologies

Ceramides have a function in cell cycle arrest, albeit this function is mechanistically unclear; therefore, there have been numerous studies alluding altered ceramide metabolism in senescence-related pathologies, discussed here. Recently, there has been an influx of ceramide-containing anti-aging products that increase skin hydration and reduce wrinkles (Guillou *et al.*, 2011). These products boost naturally-occurring ceramide present in the stratum corneum epidermis layer of human skin, which creates a barrier impermeable to water. Furthermore, ceramide synthesis enzymes sphingomyelinase and CERS have decreased activity in the inner epidermal skin layer of aged mice, suggesting a mechanism for decreased ceramide content in aged skin (Jensen *et al.*, 2005). Finally, altered levels of ceramide and glycosylceramides have been observed in aged oocytes (Kujjo *et al.*, 2013) and neurodegenerative tissues (Mencarelli and Martinez–Martinez, 2013). These studies suggest aged cells/tissues have aberrant ceramide synthesis and metabolism, opposing with the senescence-inducing molecular function of ceramide (outlined in the previous section). This discrepancy could be explained by timing-specific functions of ceramide or lack of correlation between expression and activity of ceramides in the aging process.

The genes that encode the six ceramide synthases present in humans were implicated in longevity before the function of the gene products was known. CERS1 was first identified in a screen of longevity-related genes in *Saccharomyces cerevisiae* (D'mello *et al.*, 1994). Gene deletion resulted in a 50% increase in yeast lifespan and thus, the gene was assigned the name Longevity Assurance Gene 1 (LAG1). LAG homologs have been identified in human, mouse and *Caenorhabditis elegans*, indicating conservation of the gene in eukaryotes (Jiang *et al.*, 1998). Human LAGs are assigned the name: LASS (longevity assurance), however since the function of LAG/LASS genes has been identified they are commonly referred to as CERS (ceramide synthase) (Pewzner-Jung *et al.*, 2006). Mammalian CERSs have homolog-specific functions, as outlined in table 1.1. It is unknown why mammalians have six CERS with individual activities, however it implies the importance of specific lengths of ceramides for system and cell biology. Pewzner-Jung *et al.* (2006)

hypothesised the role of CERSs in longevity is independent from their ceramide synthase activity, however work discussed in the previous section and from this thesis suggests that ceramide synthesis does have a role for the biology of aging through cell cycle control.

Gene	Length of ceramide product	Reference
CERS1	C18-ceramide	Venkataraman *et al.*, 2002
CERS2	C20-/C22-/C24-/C26-ceramide	Laviad *et al.*, 2008
CERS3	C18-/C24-ceramide	Mizutani *et al.*, 2006
CERS4	C18-/C20-ceramide	Riebeling *et al.*, 2003
CERS5	C16-ceramide	Riebeling *et al.*, 2003
CERS6	C14-/C16-ceramide	Mizutani *et al.,* 2005

Table 1.1 Ceramide synthase activity of the 6 mammalian CERS homologs

Cancer cells have altered levels of ceramide, suggesting a role in cancer pathogenesis (Ogretmen and Hannun, 2004). For example, ceramide levels are inversely proportional to the severity of malignant glial tumours in humans (Riboni *et al.*, 2002) and ceramide levels are decreased in ovarian tumours (Knapp *et al.*, 2017) and breast tumours (Schiffmann *et al.*, 2009) compared to normal tissues in humans. Decreased levels of ceramide in cancer correlate with increased expression of ceramide metabolic enzymes in certain cancers. SPHK1 expression is required for intestinal adenoma cell proliferation in mice (Kohno *et al.*, 2006), whilst acid ceramidase is overexpressed in human prostate cancers (Seelan *et al.*, 2000). In addition, *de novo* synthesised C16-ceramide is essential for B-cell receptor induced apoptosis of human lymphoma cells (Kroesen *et al.*, 2001). Finally, recent work has provided more detailed insight into the mechanism of altered ceramide metabolism in cancer. CERS4-synthesised ceramide inhibits TGFβ receptor trafficking and

signalling in cancer cells and attenuates tumour metastasis through inhibition of cell migration *in vivo* (Gencer *et al.*, 2017). This suggests the regulation of specific ceramide metabolic pathways can determine the fate of cancer cells and provides a novel mechanism for targeting cancer in humans.

There has been some research into establishing the benefit of increasing intracellular levels of ceramide in combination with traditional chemotherapies for cancer (reviewed by (Li and Zhang, 2015)). There are three ways of increasing intracellular ceramide content: activate synthesis enzymes, inhibit metabolism enzymes or provide exogenous ceramide. SPT activator PSC-833 increases the sensitivity of human carcinoma cells to vinblastine-induced apoptosis (Cabot *et al.*, 1999). CERK inhibitor NVP-231 inhibits proliferation of lung cancer cells and subsequently induces apoptosis. This effect was more evident when combined with staurosporine treatment (Pastukhov *et al.*, 2014). Finally, exogenous ceramide synergistically enhances the anti-proliferation effects of docetaxel in murine and human cancer cells (Feng *et al.*, 2014). The majority of this research was performed *in vitro*, therefore further work is required to determine the therapeutic benefit of targeting ceramides *in vivo*. Ceramides have decreased bioavailability due to hydrophobic chemical properties. There has been development of novel approaches to deliver hydrophobic ceramides to human cells, such as nanoliposomes (Watters *et al.*, 2012). These approaches have provided a platform to test the effects of exogenous ceramides in *in vivo* cancer models. Indeed, exogenous ceramides delivered in nanoliposomes halt leukaemia progression in rats (Liu *et al.*, 2010) and hepatocellular carcinoma growth in mice (Tagaram *et al.*, 2011).

1.2.4.5 Summary

Ceramides are a sphingolipid species synthesised by *de novo* or recycling pathways and can be further metabolised to create modified ceramide with distinctive functions. Ceramides have a variety of different biological functions, mainly as a physical component of cellular membranes and as a signalling regulatory molecule for cell cycle and cell death processes. Ceramides have been implicated in a number of pathological environments, including aging and cancer. Although it is clear

ceramides function in senescence, the specific mechanisms and importance of them is currently unclear.

1.2.5 Metabolism in cancer and senescence summary

Recent improvement in mass spectrometry techniques and accompanying labelling methods has facilitated the vast expansion of knowledge in cancer metabolism. Yet, the Warburg Effect – the preferential usage of aerobic glycolysis in cancer – was first postulated in 1924 and is now believed to be implemented by cancer to drive energy and biomass generation. Due to the dynamic nature of metabolism, the mechanisms driving the Warburg Effect are complex; they include alterations in glucose, glutamine and one-carbon metabolism, in addition to aspects not discussed here, such as acetate metabolism (Mashimo *et al.*, 2014; Schug *et al.*, 2016). OIS results in metabolic reprogramming of glucose, protein, nucleotide and lipid biosynthesis pathways; genes implicated in these pathways provide novel metabolic checkpoints to prevent cancer progression and initiate senescence. In addition, it appears ceramides are implicated in cancer, due to unbalanced ceramide metabolism initiating cellular outcomes: senescence and apoptosis. Finally, alterations in metabolic genes and associated metabolites, in both cancer and OIS, have provided new avenues for cancer therapeutics that are being assessed for clinical efficacy in humans.

1.3 RNA interference and high content screening

The discovery of RNA interference (RNAi) in 1998, and subsequent technical implications for gene silencing, rocketed biological research into the future. In the two decades since, RNAi has been used to make fundamental advances in understanding how genes regulate biological processes. Although in very recent years CRISPR-Cas9 has taken the trendy gene editing top spot, RNAi is still a powerful method for perturbing gene expression. Specifically, CRISPR-Cas9 techniques result in deletion of genes and in the case of essential genes this is incompatible with life. Whereas RNAi can be harnessed to specifically regulate the expression levels of genes, to retain essential gene function and thus allow cellular

readouts. In this section, the molecular mechanisms for RNAi-mediated gene silencing and different types of RNAi are described. In addition, the use of high content screening (HCS) coupled with RNAi for discovering new genetic regulators of physiological and pathological scenarios is overviewed. Finally, examples of how RNAi-HCS methods can be used to identify novel OIS regulators are explored.

1.3.1 RNA interference (RNAi)

1.3.1.1 Overview of RNAi

RNAi is an evolutionary-conserved endogenous biological process first discovered in *C. elegans* worms (Fire *et al.*, 1998). The discovery of RNAi and its function has revolutionized biological research due to its application for post-transcriptional gene silencing. In basic terms, RNAi harnesses gene-specific RNA reagents to initiate the degradation of target gene mRNA, resulting in decreased expression of that gene. In molecular terms, RNAi is a complex multi-step process that employs many different factors (reviewed by Wilson and Doudna (2013)). Briefly, precursor double-stranded RNAs (dsRNA) are processed by RNase III protein Dicer to form small dsRNAs (19-23 nucleotides (nt) in length) with phosphorylated 5' sites and 2-nt unphosphorylated 3' overhangs (Bernstein *et al.*, 2001). The small dsRNAs are also known as small interfering RNAs (siRNA), and their use as synthetic reagents for gene silencing is described in the next section. The siRNA has a guide strand that associates with RNA-induced silencing complex (RISC), and acts as a template to bind target mRNA (Hammond *et al.*, 2000; Nykänen, Haley and Zamore, 2001; Haley and Zamore, 2004). There can be several outcomes of this process, but the post-transcriptional gene silencing is the most characterised; the RISC protein Argonaute-2 is activated upon siRNA association and cleaves the complementary mRNA sequence, and thus effectively silencing the expression of the encoded gene (Hammond *et al.*, 2001; Caudy *et al.*, 2003).

dsRNA mediators of RNAi can activate a non-specific interferon response in mammalian cells (Sledz *et al.*, 2003), therefore there has been careful evaluation of the suitability of using RNAi *in vitro* and *in vivo*. The interferon response is an innate immune process that is usually triggered by viral dsRNAs and can initiate sequence-independent mRNA degradation (Manche *et al.*, 1992; Sledz *et al.*, 2003; Kim *et al.*,

2005). To overcome these non-specific effects of RNAi gene silencing, it has been determined dsRNAs of less than 23 base pairs (bp) in length are able to bypass the interferon response by imitating Dicer-processed siRNAs and enter RNAi downstream of the processing events (Elbashir *et al.*, 2001; Reynolds *et al.*, 2006). In addition to the length of dsRNAs, the system used to introduce RNAi mediators and the targeted cell type must also be evaluated. Overall, there are many obstacles to overcome to establish a specific and efficient RNAi method for gene silencing.

RNAi can be harnessed in multiple different combinations for use in *in vitro* and *in vivo* systems. Use of individual RNAi sequences can play a vital role in the identification of gene function in health and disease states. Whereas, using RNAi technology in combination with high-throughput screening can yield systemic analysis of many genes at once; it is also possible to screen genome-wide RNAi (Ashrafi *et al.*, 2003; Berns *et al.*, 2004; Boutros *et al.*, 2004; Paddison *et al.*, 2004). High-throughput RNAi greatly shortens the time it takes to identify genetic regulators of a biological process or disease. The rest of this section will examine the different types of RNAi that can be used for gene silencing, and how they can be combined with high-throughput screening approaches to yield answers to biological problems.

1.3.1.2 Small interfering RNA (siRNA)

siRNAs were first discovered in plants (Hamilton and Baulcombe, 1999) and soon after, synthetically recapitulated in mammalian cells (Elbashir *et al.*, 2001). To experimentally target gene expression, siRNA sequences are synthesised following optimised design criteria (Leung and Whittaker, 2005), including ensuring the length is between 21-23bp, due to issues with long dsRNAs described previously. In addition, the introduction of siRNA must be evaluated for individual cell systems. There are three main methods of siRNA delivery: lipid-mediated transfection (Malone, Felgner and Verma, 1989), electroporation (Neumann *et al.*, 1982) or virus-mediated infection (Brummelkamp, Bernards and Agami, 2002b). In all cases, siRNA-mediated gene silencing in mammalian cells is transient due to their long-term instability and dilution with every population doubling. So, siRNA delivery must be optimised to allow a certain number of siRNA molecules to be introduced

resulting in transient gene silencing without toxic effects. Finally, off-target effects are common issues with siRNAs due to non-target genes having partially complementary sequences to the target gene, and thus are inadvertently targeted. For example, 3' untranslated region similarity has been implicated as the trigger for off-targeted genes in siRNA-treated human cells (Birmingham *et al.*, 2006). Off-target effects can be combated with algorithm-assisted design of siRNA sequences. In addition, there are commercially available siRNAs (e.g. Dharmacon ON-TARGET*plus* siRNA) that have a patented dual-strand modification that is proven to reduce off-target effects. Specifically, a 2'-*O*-methyl ribosyl modification at position 2 of the siRNA guide strand reduces the silencing of off-targeted genes and enhances specificity to target genes (Jackson *et al.*, 2006). The properties of siRNAs make them amenable to high-throughput screening, for example: under optimised transfection conditions knockdown is highly efficient and off-target effects can be reduced using chemical modifications. However, there are some disadvantages to using siRNAs for screening, for example: their transient effects limits assaying for short-term phenotypes only and they can be stored for limited amounts of time. Nonetheless, if siRNA transfection conditions are optimised for cell type and reagents are handled and stored correctly, screening with siRNAs can be a robust and reliable technique for identifying genetic regulators of the screened biological process.

1.3.1.3 Short hairpin RNA (shRNA)

shRNAs are artificial RNAi molecules used to induce stable gene silencing. They are generally around 60-70bp in length with complementary sequences at 5' and 3' ends; once transcribed, these sequences loop back to create a structure defined as the 'hairpin'. The shRNAs enter the RNAi pathway via Dicer cleavage of the hairpin, which forms siRNAs that associate with the RISC (McManus *et al.*, 2002; Paddison *et al.*, 2002). shRNAs can also be designed to stable express siRNA sequences, that are normally transiently delivered, in mammalian cells (Brummelkamp, Bernards and Agami, 2002a). shRNAs can be introduced to cells by transfection in a plasmid with a RNA polymerase III promoter, which initiates the transcription of the shRNA sequence once in the cell (McManus *et al.*, 2002). However, this delivery method can

have limited uses, depending on the amenability of the target cell to transfection (reviewed by Dykxhoorn, Novina and Sharp (2003)); for example, primary cells are notoriously difficult to stably transfect. Therefore, shRNAs are often cloned into retro- and lenti-viral vector systems, which can be introduced to cells using a virus packaging cell line (such as 293T) to create the shRNA-expressing virus. Cells are infected with the virus and co-expressed shRNA and drug-selection marker sequences are incorporated into host DNA. This allows stably infected cells to be selected and expanded, for long periods with continual provision of the selection drug (Rubinson *et al.*, 2003; Stewart *et al.*, 2003). One of the first functional studies to use viral-mediated shRNA revealed oncogenic K-Ras^{V12} could be specifically repressed in human pancreatic tumours cells. This shRNA-mediated silencing decreased tumorigenicity whilst wild type K-Ras remained intact (Brummelkamp, Bernards and Agami, 2002b). This was one of the first indications that RNAi could be therapeutically manipulated for diseases, such as cancer, and in recent years this concept has been making progress in the clinic (reviewed by Bobbin and Rossi (2016)).

1.3.2 High content screening (HCS)

To gain as much information as possible from RNAi screening, the subsequent phenotype must be measured using an appropriate assay. With siRNA, this phenotype must be short-lived (the 72 hour period subsequent to siRNA transfection yields the best knockdown efficiency). With shRNA, this phenotype can be repeatedly measured over an indefinite period. In the past 10 years, there has been development of the complex technologies that can be coupled with RNAi for high-throughput experiments, such as high content screening (HCS). Image-based HCS provides an excellent automatic platform for multi-parametric image acquisition and analysis. There are many assays that can be measured by image-based HCS; these include: simple immunofluorescence stains, such as measuring BrdU incorporation as a proliferation readout (Gasparri *et al.*, 2004) and complex live cell assays with fluorescently labelled chromosomes to report cell cycle progress (Neumann *et al.*, 2006). In these techniques, DNA can be co-stained using 4',6-diamidino-2-

phenylindole (DAPI). This allows assay quantification by using thresholds to determine if a cell is negative or positive for the measured phenotype.

One of the major issues with RNAi coupled with HCS is the generation of large amounts of data to be analysed. This has become easier to overcome recently with the availability of online software packages, developed for specific types of assays (such as 'web cellHTS2', (Pelz, Gilsdorf and Boutros, 2010)). Screen analysis aids hit identification and classification; generally, hits can be determined using a Z-score analysis. Further, it is vital to perform statistics on HCS datasets, to determine how the distribution and quality of data is affected, such as the Z' factor (Zhang, Chung and Oldenburg, 1999). The Z' factor considers the separation between internal negative and positive controls to attain data variability and quality metrics. After threshold and statistic driven hit identification, hits must be reassessed in an independent validation screen; for primary screens using pooled RNAi (usually at least 3 different sequences for the same target), validation can be performed using deconvoluted RNAs. Overall, if an appropriate assay is used to measure phenotypes after RNAi perturbation of cells, quantitative data can be obtained quickly and easily using HCS.

1.3.3 Using RNAi/microscopy approaches to identify regulators of OIS

Senescence has proven to be very amenable to RNAi experimental approaches; there has been great progression in the understanding of senescence regulatory pathways using shRNA and siRNA mediated methods. Generally, screens targeting senescence employ an assay that identifies a 'bypass of senescence' caused by RNAi knockdown of a gene essential for senescence. Bypass of senescence can be initially analysed in a variety of ways, including: colony formation, proliferation, tumour suppressor expression. As discussed earlier, senescence is not defined by a singular phenotype, so subsequent validation of screen hits using other senescence markers is required.

One of the first large-scale RNAi screens to be reported had implications in senescence biology and introduced a new method to stably express siRNAs as shRNA constructs (Berns *et al.*, 2004). The authors using their RNAi library, targeting 7914 genes in mammalian cells, to identify new components of the p53

pathway implicated in DNA-damage induced senescence. In 2008, a genome-wide shRNA screen was used to identify 17 genes essential for human $BRAF^{V600E}$-induced senescence (Wajapeyee *et al.*, 2008). This screen involved stable transduction of shRNA using retrovirus delivery, followed by colony formation and confirmation of shRNAs by gDNA sequencing. Robust validation was performed using proliferation/apoptosis assays and $p16^{INK4a}$ expression. Subsequently, a role for secreted protein IGFBP7 (one of the top screen hits) was identified for the regulation of senescence in benign nevi and apoptosis in malignant melanoma. Following, a smaller shRNA screen was used to identify regulators of senescence in human fibroblasts, utilising retroviral delivery of pooled shRNA in 96-well plate format (Acosta *et al.*, 2008). This screen identified CXCR2 as a regulator of replicative senescence and OIS; later validation revealed a role for CXCR2 in the regulation of SASP chemokine expression through transcription factors C/EBPβ and NF-κB. More recently, the combination of RNAi screening with other genomics approaches have been utilised to identify novel tumour suppressors vital for $BRAF^{V600E}$-induced senescence (Kaplon *et al.*, 2014). This study performed a near-genome-wide shRNA screen to identify RASEF as essential for senescent nevi. Genome-wide DNA methylation analysis using next-generation sequencing confirmed hypermethylation of RASEF was required for senescence bypass and melanoma progression. Furthermore, a genome-wide siRNA screen was used to associate regulators of $p16^{INK4a}$ with primary cilium (PC) biology, in a replicative senescence *in vitro* model. Bishop *et al.* (2010) identified Hedgehog signalling component SUFU promotes cell cycle via the suppression of $p16^{INK4a}$ and this was both primary cilium-dependent and -independent. Together, these studies highlight the effectiveness of using RNAi to identify potential regulators of senescence and assist the development of new areas of research for the senescence and cancer fields.

1.3.4 RNAi and HCS summary

The original Nobel prize winning discovery of RNA interference in 1998 prompted the development of a new field for biological techniques to target gene expression. RNAi has since been used to extensively examine processes on a genome-wide scale. There are some pitfalls to RNAi but these can generally be overcome if delivery

technique and assay platform are optimised. Using RNAi to modulate gene expression levels instead of gene deletion techniques is advantageous when studying essential genes, such as metabolic enzymes. When coupled with high-content screening, RNAi is a powerful approach to identify novel regulators of cancer associated processes, including oncogene-induced senescence. RNAi is a main method exploited for this thesis; methods, results and discussion involving RNAi can be found throughout subsequent chapters.

1.4 Thesis aims

Although senescent cells are stably arrested they maintain active but rewired metabolism. From recent studies, it is evident OIS-specific metabolic alterations can be targeted for disease therapeutics. In addition, as there are already clinically approved drugs implicated in metabolism, metabolic factors provide an attractive target for novel disease therapeutics in humans. The main aim for this thesis was to identify novel metabolic regulators in OIS, using RNAi and HCS methods combined with *in vitro* cell culture. The next focus was to thoroughly validate screen hits, using senescence marker assays and two senescence models. The next aim was to identify the function of the top screen hit in OIS, utilising accurate mass LC-MS to quantitatively measure metabolism. Lastly, delineating the downstream mechanism that links the identified metabolic regulator to OIS cell cycle arrest was the final aim, using a combination of rescue and binding experiments.

Chapter Two: Materials and Methods

2.1 Chemicals and Solutions

All chemicals and solutions used for this work have been appropriately referenced within the text (information includes supplier and product code). All the solutions in table 2.1 were obtained from the MRC Human Genetics Unit Technical Services.

Product	Composition
Phosphate-buffered saline (PBS)	Dulbeccos tablets + dH_2O
Tris-buffered saline (TBS)	25 mM Tris-HCl + 137mM NaCl + 2.7mM KCl, pH7.4
TBS-tween	TBS + 0.05% Tween 20
IF blocking buffer	PBS + 1% Bovine Serum Albumin + 0.2% Fish Gelatin

Table 2.1 Regularly used solutions

2.2 Cell culture

2.2.1 Cell lines and maintenance

IMR90 and 293T cell lines were obtained from ATCC. All cell lines were maintained in Dulbecco's Modified Eagle's Medium – high glucose (DMEM; Sigma, D5796), supplemented with 10% HyClone Fetal Bovine Serum (Thermo Fisher, SV30180.03) and 1% antibiotic-antimycotic (Thermo Fisher, 15240062); henceforth referred to as 'normal media'. All cell lines were incubated at 37°C with 5% CO_2. Incubators were decontaminated and cultures tested for mycoplasma on a regular basis. For passaging, cells were washed once with PBS and detached using trypsin (Thermo Fisher, 25300-054). Plates were placed in a 37°C incubator for up to 5 minutes, to allow full detachment of cells. Detached cells were pelleted using a centrifuge at 1000rpm for 5 minutes. Cells were resuspended in fresh media and

counted or split 1:4 of the original density. For passaging, cells were cultured in 10cm plates and for experiments, 6- and 96-well plates were used.

2.2.2 Freezing and thawing cells

Confluent plates were trypsinised as described in *2.2.1* and resuspended in 1ml of normal media supplemented with 10% DMSO, and aliquoted in cryotubes. Tubes were stored at -80°C and stocks of each passage were transferred to liquid nitrogen.

Cells were thawed by removal from -80°C and 1-2 minutes in a 37°C water bath. Thawed cells were diluted 1:10 in fresh media and pelleted using a centrifuge at 1000rpm for 5 minutes to remove the DMSO. Cells were resuspended in fresh media (5ml per tube) and added to 10cm plate pre-aliquoted with 10ml media, being careful to distribute the cells across the whole plate. Generally, thawed cells required 2 days to recover and then were split as described in *2.2.1*.

2.2.3 Production of stable cell lines

293T were routinely used as packaging cells to produce retroviruses or lentiviruses for infection in IMR90. Figure 2.1 shows a summary timeline for these experiments.

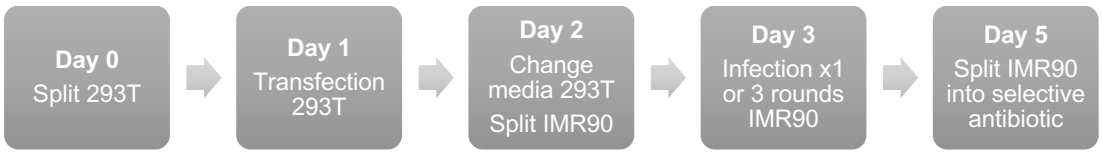

Figure 2.1 Protocol for making stable cell lines

2.2.3.1 293T transfection – production of retroviruses

The day before transfection, 293T were split 1:4 into 10cm dishes and the next day transfections were performed late afternoon. For each dish, 7.5µg GagPol, 2.5µg VSVG and 20µg of midi-prepped plasmid was combined with 500µl unsupplemented DMEM, vortexed and incubated at room temperature for 10 minutes. In a separate tube, a mastermix of polyethyleneimine (PEI; Alfa Aesar, 43896) was prepared and incubated for 10 minutes – for each dish 75µl 1µg/ml PEI was mixed with 500µl

unsupplemented DMEM. 500µl of PEI mastermix was added to each DNA preparation, vortexed and incubated at room temperature for 10 minutes. The transfection mix was then added dropwise over 293T and carefully mixed. Transfected cells were incubated overnight and the media changed the next morning (approximately 16-20 hours after transfection) to avoid toxicity from VSVG and PEI. Transfected cells were incubated for a further 24 hours to allow retrovirus production. GFP was used as a visual control for transfection efficiency.

2.2.3.2 Retroviral infection of IMR90

The day before infection (i.e. the day after 293T transfection), IMR90 were split 1:4 into 10cm dishes. Retroviruses were collected from 293T and filtered through a 0.45µm membrane into a falcon pre-aliquoted with 4µg/ml polybrene (Sigma, H9268). Fresh media was added to 293T and the time noted to start the next round of infection after 2½ hours. Media was aspirated from IMR90 and retrovirus-polybrene mix was added, and dishes placed back in the incubator. This process was repeated twice more. After the third round, 293T were discarded and retrovirus replaced with supplemented DMEM on the IMR90. Infection efficiency was assessed 48 hours post infection, using GFP, and IMR90 split 1:2 or 1:3 into selective antibiotic – 400µg/ml geneticin (G418 sulphate; Thermo Fisher 10131/027), 1µg/ml puromycin (Thermo Fisher, A11138) or 2µg/ml blasticidin (Thermo Fisher, A11139). Selection media was changed every 48 hours as the uninfected cells died, and cells expanded for experiments.

2.2.4 An inducible cell model for OIS

OIS was modelled using human diploid fibroblast primary cells line IMR90 with expression of 4-hydroxytamoxifen inducible ER:Ras^{G12V} or ER:Stop chimaeric fusion proteins. The cell lines are referred to throughout this thesis as: IMR90-ER:Stop (or iStop) and IMR90-ER:Ras (or iRas). An illustration and explanation of this model is shown in figure 2.2. To produce these cells, passage 4 IMR90s were infected with the ER:Stop and ER:Ras constructs as described in *2.2.4.2* (performed by Juan-Carlos Acosta) and expanded to passages 8-15. For expansion of these lines, cells were grown in 400µg/ml geneticin. Cells were frozen down at various passages or used for experiments. Further infections of shRNAs and overexpression constructs

were performed at passage 10-12. To activate Ras^{G12V} and induce senescence in IMR90, 100nM 4-hydroxytamoxifen (4OHT; Sigma, H7904) was administered (the start day of 4OHT treatment is referred to as 'day 0'). For 4OHT treatment, a 100µM stock was diluted 1:1000 in media, added to cells and refreshed every 2-3 days.

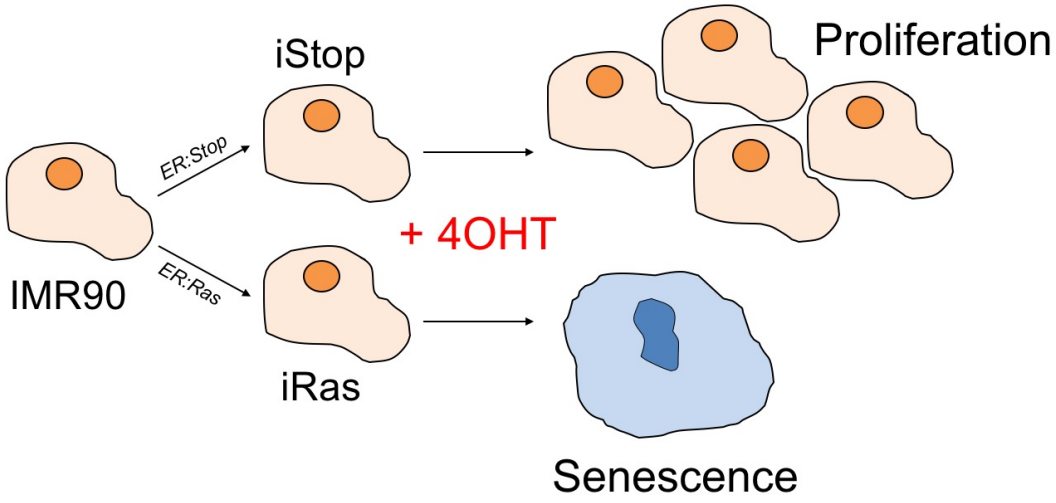

Figure 2.2 The ER:Ras system to model OIS in IMR90 cells

The estrogen receptor (ER) has a hormone-binding domain which, in the absence of estrogen, is bound to chaperones. 4-hydroxytamoxifen (4OHT) is an ER antagonist; this means 4OHT will bind to the ER similarly to estrogen and displace the chaperones. This system is exploited to model OIS, by fusing an oncogenic Ras protein (Ras^{G12V}) to the hormone-binding domain of the ER (iRas cells). In normal conditions, the ER:Ras fusion protein will remain inactive due to chaperone binding. Upon 4OHT treatment, the chaperones dissociate and the ER:Ras fusion protein is constitutively activated; Ras^{G12V} will exert its downstream oncogenic effects, inducing cell cycle arrest and accumulation of senescence markers. For control cells (iStop), the ER is fused with a stop codon, meaning there is no protein bound to hormone-binding domain. The presence of 4OHT has no effect on the proliferation of iStop cells.

2.2.5 Measuring population doublings

Population doublings (PD) were used to measure the growth rate of cells over numerous passages. The Muse Cell Analyser (Merck Millipore) and Muse Cell Count and Viability kit (Merck Millipore, MCH100102) was used to count cells. The

Count and Viability reagent contains two DNA binding dyes that were used to stain viable and non-viable cells, depending on the permeability and nucleated state of a cell. Cells were pelleted as described in *2.2.1* and resuspended in an appropriate volume of normal media. A 1:4 or 1:8 mix of cells and Count & Viability reagent was prepared and incubated at room temperature for up to 5 minutes. One sample was used to set the two gates for the reagent dyes – each dye plot allowed the user to set thresholds to eliminate non-viable and non-nucleated cells. The 'number of cells/ml' value was used to calculate how much volume of the cell resuspension was required to re-seed the sample at 500,000 cells per 10cm dish. The 'total number of cells' (x) value was used to calculate the population doublings using the formula: *PD=LOG(x/500,2).* The PD over numerous passages were added together to evaluate the cumulative PD.

2.2.6 Treatments

IMR90 were treated with a variety of drugs and compounds as listed here. All ceramides and sphingosine were acquired from Avanti Polar Lipids, Inc., and used at final concentrations of 1-2μM. Absolute filtered ethanol was used as a vehicle for all sphingolipids. NVP-231, a ceramide kinase inhibitor, was acquired from Calbiochem (219493) and used at a final concentration of 5μM. SKI-1, a sphingosine kinase inhibitor, was acquired from Abcam (142209) and used at a final concentration of 2μM. Ceranib-1, a ceramidase inhibitor, was acquired from Tocris Bioscience (4448) and used at a final concentration of 2μM. DMSO was used as a vehicle for NVP-231, SKI-1 and ceranib-1.

2.3 Cloning

2.3.1 OligoEngine: pSUPER.retro.puro vector system

The pSUPER RNAi system from OligoEngine allows the stable expression of siRNA sequences and long-term suppression of gene expression. This vector system contains a polymerase-III H1-RNA gene promoter and a 19-nucleotide target sequence (N-19) designed specifically to target mRNA of the target gene, by using siRNA sequences known to transiently knockdown the target gene

(pSUPER.retro.puro, OligoEngine VEC-PRT-0002). Oligonucleotides pairs are designed to contain the N-19 in sense and anti-sense directions, which are separated by a 9-nucleotide spacer. These oligos are annealed and cloned into pSUPER.retro.puro between unique BglII (5' end) and HindIII (3' end) enzyme sites (see figure 2.3 for vector map). When the final cloned vector is introduced to cells, the two N-19 are predicted to fold back to form a stem-loop structure, which is cleaved to produce a functional siRNA.

2.3.2 Oligonucleotide design

The oligonucleotide pairs for CERS4 and TP53 are shown in table 2.2. Andrea Quintanilla designed the CERS4 oligonucleotides using Serial Cloner 2.6.1 'Make shRNA' function. The TP53 oligonucleotides were designed and validated by Brummelkamp et al. 2002.

2.3.3 pSUPER cloning

The OligoEngine manual for pSUPER.retro.puro cloning was followed and is briefly summarised here. The oligonucleotide pairs were annealed using the following programme on an Agilent SureCycler 8800:

4 min @ 90°C --> 10 min @ 70°C --> step-cool to 37°C --> step-cool to 10°C

Next, 1µg pSUPER vector was linearized by sequential digestion at 37°C: first HindIII for 1 hour followed by BglII for a further 2 hours, and heat inactivation at 80°C for 20 minutes. Next the ligation was prepared: 2µl annealed oligos + 1µl T4 ligase buffer + 1µl linear pSUPER vector + 5µl dH_2O + 1µl T4 ligase. The reaction was incubated at 16°C for 3 hours. The ligated vector was transformed into competent bacteria (NEB, C2987) and ampicillin resistant colonies grown overnight at 37°C. Multiple colonies were picked and mini-prepped (using QIAprep mini kit; Qiagen, 27104). To check for positive clones, DNA was digested with EcoRI and HindIII as described above and ran on an agarose gel. Positive clones were identified by the presence of a 281bp band and were further validated by sequencing. Ligated vector DNA was prepared for transfection/ infection by midi-prep (Qiagen, 12945).

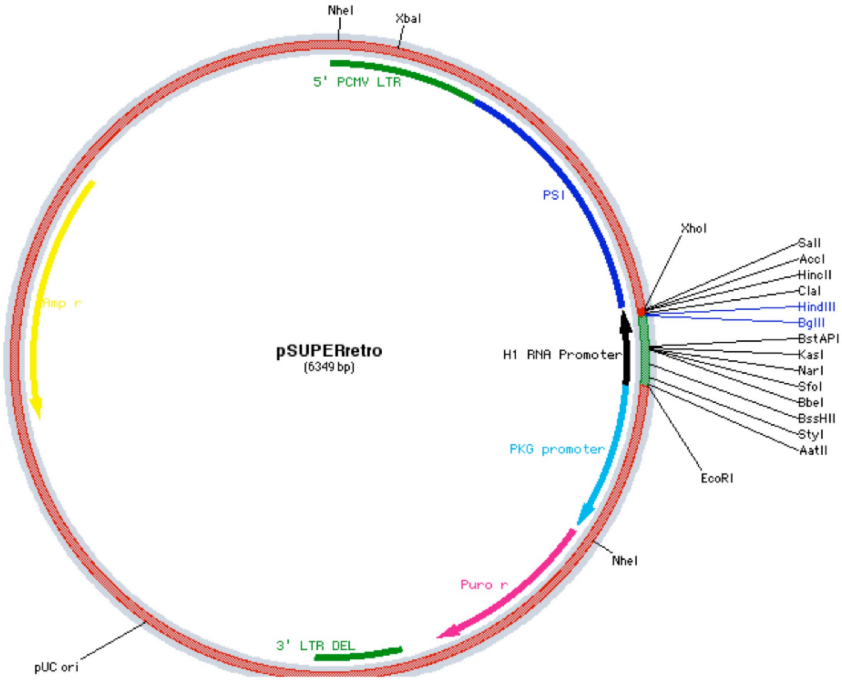

Figure 2.3 Vector map of pSUPER.retro.puro (OligoEngine VEC-PRT-0002)

Target gene [*species*]	**Abbreviation**	**Oligonucleotide sequence**
CERS4 [*Homo sapiens*]	pRS-shCERS4 or shC4	sense: GTGCCAACCTGCTGCGCAT anti-sense: ATGCGCAGCAGGTTGGCAC
TP53 [*Homo sapiens*]	pRS-shP53 or shP53	sense: GACTCCAGTGGTAATCTAC anti-sense: GTAGATTACCACTGGAGTC

Table 2.2 Oligonucleotides for ligation into pSUPER.retro.puro vector

2.4 RNA interference

2.4.1 shRNA (short hairpin RNA)

shRNA sequences were cloned into the pSUPER.retro.puro vector (shortened hereafter as pRS) as described in *2.3*. Retrovirus containing pRS-shRNA sequences was produced by 293T transfection and IMR90s infected with three rounds of virus, as described in *2.2.4*. Knockdown was routinely measured by qPCR and western blot.

2.4.2 siRNA (small interfering RNA)

2.4.2.1 siRNA sequences

All siRNAs were ON-TARGETplus reagents purchased from Dharmacon (see table 2.3 for individual information for commonly used siRNAs). A custom-made pooled siRNA library and deconvoluted siRNA libraries were purchased from Dharmacon for screening purposes. The custom-made library was designed and shared with Andy Finch and Joy Edwards-Hicks, and included a full set of siRNAs targeting lipid metabolism listed by Atilla-Gokcumen et al (2014). For full information on the genes targeted in the siRNA library, refer to Appendix 1.

2.4.2.2 siRNA resuspension

Commonly used siRNAs were routinely purchased as 5nmol in tubes and libraries were purchased as 1nmol in 96 well plates. For resuspension, tubes or plates were spun at 1000rpm for 5 minutes, in a pre-chilled (4°C) centrifuge, to collect dried siRNA in the bottom. 1X siRNA resuspension buffer was prepared by diluting 5X buffer (Dharmacon, B-002000) 1:5 with UltraPure RNase-free distilled water (Life Technologies, 10977035). Routinely, siRNAs were resuspended to a stock concentration of 100μM and incubated for 30-60 minutes at room temperature on an orbital shaker and further diluted with 1X buffer to a working concentration of 1μM. See table 2.4 for 1X buffer volume required for stock and working concentrations. Both 100μM and 1μM siRNA stocks were stored at -20°C.

Target gene [*species*]	Supplier	Sequence
CERS4 [*Homo sapiens*] **BOLD** denotes individual siRNA used for validation experiments	Dharmacon (L-014364-00)	Pool x4 siRNA sequences: **GUGCCAACCUGCUGCGCAU** GGAGAAGGACAUUCGUAGU AGUAUCAGCAAGUGUGCGA GAGGCCAGCUGGAGGUUUC
TP53 [*Homo sapiens*]	Dharmacon (L-0003329-00)	Pool x4 siRNA sequences: GAAAUUUGCGUGUGGAGUA GUGCAGCUGUGGGUUGAUU GCAGUCAGAUCCUAGCGUC GGAGAAUAUUUCACCCUUC
CDKN1A (p21) [*Homo sapiens*]	Dharmacon (L-003471-00)	Pool x4 siRNA sequences: CGACUGUGAUGCGCUAAUG CCUAAUCCGCCCACAGGAA CGUCAGAACCCAUGCGGCA AGACCAGCAUGACAGAUUU
CDKN2A (p16) [*Homo sapiens*]	Dharmacon (L-011007-00)	Pool x4 siRNA sequences: GAUCAUCAGUCACCGAAGG AAACACCGCUUCUGCCUUU UAACGUAGAUAUAUGCCUU CAGAACCAAAGCUCAAAUA
Non-Target control [*N/A*]	Dharmacon (D-001810-10)	Pool x4 siRNA sequences: UAGCGACUAAACACAUCAA UAAGGCUAUGAAGAGAUAC AUGUAUUGGCCUGUAUUAG AUGAACGUGAAUUGCUCAA

Table 2.3 siRNA sequences

nmol siRNA	Volume (µl) 1X buffer required for:	
	100µM (stock conc)	1µM (working conc)
1	10	100
5	50	500

Table 2.4 Recommended dilution for siRNAs

2.4.2.3 siRNA reverse transfection

30nM siRNA were aliquoted into 96 well plates or 6 well plates. Dharmafect 1 transfection reagent (DF1; Dharmacon, T-2001) was diluted in unsupplemented DMEM and added on top of siRNA (see table 2.5 for volumes). The siRNA-DF1-DMEM mix was incubated at room temperature for 30-60 minutes, whilst IMR90 were trypsinised and counted. IMR90 were seeded on top of the siRNA-DF1-DMEM mix – 1-6x10^3 cells per well for 96 well plates and 2x10^5 cells per well for 6 well plates. 72 hours post-transfection cells were collected for protein and mRNA analysis or fixed for immunofluorescence. On occasion, a repeat transfection was performed for a second 72-hour period. For the mid-throughput siRNA library (described in *2.4.2.1*), various automated instruments, including multi-channel electronic pipettes and cell plater, were used to aid efficient and consistent siRNA transfection. Knockdown was routinely measured by qPCR and western blot.

Plate format	Volume (µl) of transfection reagent per well			30nM siRNA (µl)
	DF1	Unsup. DMEM	Total	
96 wells	0.1	17.4	17.5	3.6
6 wells	2	348	350	72

Table 2.5 Transfection conditions

2.4.2.4 siRNA transfection during OIS timecourse

A routine experiment was to reverse transfect siRNAs during a 4OHT timecourse in the ER:Ras system. Figure 2.4 shows a summary timeline for this experiment.

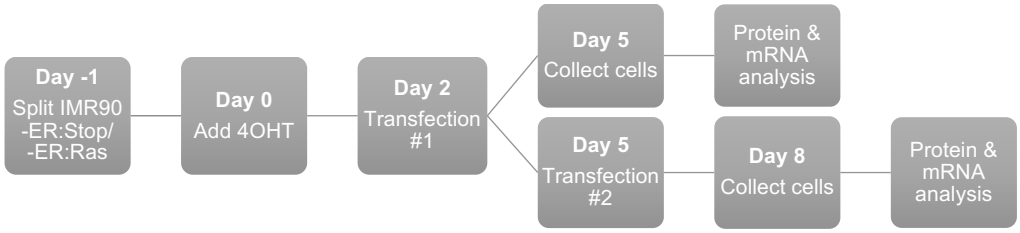

Figure 2.4 Protocol for siRNA reverse transfection during a typical OIS timecourse experiment

2.5 Immunofluorescence and high content analysis

2.5.1 Antibodies

Primary and secondary antibodies used for immunofluorescence are listed in tables 2.8 and 2.9. All antibodies had been previously validated by RNAi knockdown or overexpression analysis. Typically, stains were performed in triplicate wells of a 96 well plate.

2.5.2 BrdU labelling

Bromodeoxyuridine (BrdU) incorporation measured by immunofluorescence was used as a proliferation readout. 500µM BrdU intermediate stock in unsupplemented DMEM was diluted 1:10 in 96 well plates, previously seeded at 1-6x10^3 cells per well. Cells were placed back in the incubator for 17 hours to allow incorporation of the synthetic BrdU into the cell DNA. For detection of BrdU incorporation, a primary antibody (BD Biosciences, 555627) was diluted 1:2000 with 0.5U/µl DNase (Sigma, D4527) and1mM $MgCl_2$. DNase and magnesium co-factor are required to unwind DNA and allow the BrdU antibody easier access to the nucleotide.

2.5.3 Staining protocol

All steps in this staining protocol were performed at room temperature on an orbital shaker and all washing steps were performed using a hand-operated liquidator (Mettler Toledo). Cells seeded in 96 well plates were washed once with PBS to wash the media away. In a fume cabinet, cells were fixed in 30µl 4% paraformaldehyde (FD NeuroTech, PF101) for 1 hour, and washed three times with PBS. Cells were permeabilised with 30µl 0.2% Triton-X100/PBS for 10 minutes and washed three times with PBS. Following permeabilisation, cells were blocked in 30µl IF blocking buffer (composition in table 2.1) for 1 hour. During blocking, primary and secondary antibodies were prepared in IF blocking buffer and stored on ice (dilutions found in tables 2.8 & 2.9). Immediately after blocking, 30µl of diluted primary antibody was added to cells and incubated for 30 minutes. After three PBS washes, 30µl of diluted secondary antibody was added to cells and incubated for 45 minutes. From this step, plates were wrapped in foil to prevent bleaching of the light sensitive Alexa Fluor antibodies. After three PBS washes, 30µl of 1µg/ml 4',6-diamidino-2-phenylindole/PBS (DAPI; Molecular Probes, D1306) was used to stain for nuclei and was incubated for 20-30 minutes. Cells were washed three times in PBS and exactly 100µl PBS was added to each well.

2.5.4 High Content Analysis using the ImageXpress (Molecular Devices)

Image acquisition was performed at 10X magnification with a fixed number of sites per well (between 4-9, depending on cell density). Exposure time and focus were optimised for each experiment and was consistent for all wells/plates. Image analysis was performed using the Meta Xpress <Multi Wavelength Cell Scoring> analysis. Using positive/negative controls, a positive-stain threshold was set and all images subjected to positive-stain scoring using the same threshold. Cell number was calculated by counting DAPI-positive nuclei. The raw image data was exported and further data analysis performed using Excel. Raw images were visualised and merged using Image J software.

2.5.4.1 Screen image analysis using web cellHTS2

For robust hit identification the online software package 'web cellHTS2' was used (Pelz, Gilsdorf and Boutros, 2010). This software provided comprehensive data visualization and offers quality control and normalization metrics for the siRNA screen. Raw data files were formatted and uploaded as previously described by Pelz et al. (2010) and underwent statistical evaluation.

2.6 Western blotting

2.6.1 Lysate preparation

Cells were pelleted as described in *2.2.1*, resuspended in 1ml PBS and aliquoted in 1.5ml eppendorfs. Cells were washed in PBS using a bench top centrifuge at 4000rpm for 5 minutes. The PBS supernatant was removed by aspiration and pellets were either lysed or, on occasion, stored at -80°C and thawed on ice for 5 minute before lysis. Lysis buffer was prepared by diluting Cell Lysis Buffer (Cell Signalling, 9803) and cOmplete EDTA-free Protease Inhibitor Cocktail (Roche, 04693159001) 1:10 with dH_2O (i.e. 100µl of each + 800µl dH_2O). The composition of the lysis buffer is found in table 2.6. Depending on the pellet size, cells were resuspended in 20-250µl lysis buffer and incubated on ice for 5-10 minutes. Samples were spun at 14,000rpm for 10 minutes, in a pre-chilled (4°C) centrifuge. The supernatant was collected into a fresh tube and protein concentration determined.

2.6.2 Bradford assay for determination of protein concentration

Bradford reagent (Biorad, 500-0006) was removed from the fridge 30 minutes before use and diluted 1:5 in dH_2O. This dilution was stored at room temperature for up to one week. A 96 well plate format was used and a standard curve performed for each plate, using Pierce BSA Standard Pre-diluted Set (Thermo Fisher, 23208). Before aliquoting samples, various dilutions were tested with Bradford in 0.5ml tubes to ensure readings were within the standard curve. 2µl of standards and diluted samples were mixed with 198µl of 1X Bradford reagent using a multi-channel manual pipette. A Biorad iMark microplate reader was used to measure the absorbance at 595nm.

Each sample was measured in triplicate and compared to the BSA standard curve with known concentrations of protein. Using Excel, the standard curve values were plotted and resulting regression formula was used to calculate the sample protein concentration. This Bradford assay was shown to be detergent compatible and it was not necessary to dilute standards in cell lysis buffer.

2.6.3 Preparation of samples for SDS-PAGE

The volume of lysate with desired protein quantity (10-20µg) was calculated. Lysates were mixed with 6X Laemmli SDS sample buffer (reducing) (Alfa Aesar, J61337) and dH_2O to make a final volume of 15-30µl and boiled at 95°C for 5 minutes. Generally, samples were prepared fresh and on occasion samples were stored at -20°C for up to 3 months.

2.6.4 SDS-polyacrylamide gel electrophoresis (SDS-PAGE)

SDS-PAGE was used to separate proteins, exploiting the XCell SureLock Mini-Cell electrophoresis system (Invitrogen). The composition and percentage of the gel was chosen depending on the molecular weight of the protein of interest (see table 2.7). When multiple proteins were of interest, gradient gels were used to achieve the best separation. Samples were carefully loaded and subjected to electrophoresis at 100-150V for 1-2 hours, until the blue loading dye reached the bottom of the gel. A broad range (11-245kDa) colour prestained protein standard (NEB, P7712) was used to determine protein size.

2.6.5 iBlot dry transfer

An iBlot dry blotting system (Invitrogen) was used to transfer proteins from SDS-PAGE gels onto nitrocellulose membrane. Gels were carefully removed from the plastic cassette and trimmed using a gel knife. The bottom anode component of an iBlot nitrocellulose transfer stack (Invitrogen, IB301002) was placed in the iBlot, and gels placed on top of the membrane – with a maximum of two mini gels per transfer stack. Filter paper was soaked in dH_2O and placed on top of the gels, followed by the top cathode component of the transfer stack (electrode side up). After each layer a blotting roller was used to remove any bubbles within the transfer stack. The sponge was placed in the lid of the iBlot and the lid was shut, ensuring a connection by the

red light indicator. Program P3 (20V for 7 minutes) was used to transfer all proteins of interest within a range of 11-120kDa. When the program was finished the transfer stack was disassembled and cut membranes were blocked in TBS + 5% non-fat milk (Marvel) for 1 hour at room temperature. Gels were routinely stained with Coomassie Brilliant Blue Staining Solution (Biorad, 1610436), for 30 minutes at room temperature and washed in tap water overnight until bands were visible. On occasion, when an appropriate loading control was not performed, stained gels were imaged using a LiCor Odyssey-SA.

2.6.6 Antibodies

Where necessary, membranes were cut to blot using multiple antibodies. Membranes were incubated in primary antibody overnight at 4°C on a rocker (see table 2.8 for details of primary antibody conditions). After three 10 minute washes with TBS-tween (0.05% tween), the membranes were incubated with a horse radish peroxidase (HRP)-conjugated secondary antibody for 1 hour at room temperature (see table 2.9 for details of secondary antibody conditions). After another three 10 minute washes with TBS-tween (0.1% tween), ECL was used to visualise bands.

2.6.7 Enhanced chemiluminescence (ECL)

Equal volumes of ECL solution A and solution B (GE Healthcare, RPN2209) were mixed. Where necessary, ECL Prime (GE Healthcare, RPN2232) was used for more sensitive visualisation. Membranes were placed on a clean surface, typically smoothed out cling film on a normal lab bench. ECL was added to the membrane (typically 1.5ml for each full size membrane) and incubated for 5 minutes at room temperature. As the HRP is conjugated directly to the secondary antibody, the light emitted from the oxidation reaction with the ECL substrate will only occur if the protein the antibody detects is present. Membranes were placed in a suitable cassette and exposed to X-ray film, normal or sensitive (SLS, MOL7016 and GE Healthcare, 28906837), for an appropriate time and developed using an X-ray processor.

Component	Concentration in 1X
Tris-HCl pH7.5	20mM
NaCl	150mM
Na2EDTA	1mM
EGTA	1mM
Triton	1%
Sodium pyrophosphate	2.5mM
β-glycerophosphate	1mM
Sodium orthovanadate	1mM
Leupeptin	1µg/ml

Table 2.6 Composition of Cell Lysis Buffer (Cell Signalling, 9803)

Gel type	Num. of wells	Running buffer	Used for
NuPAGE Novex 4-12% Bis-Tris	10 / 12 / 15	NuPAGE MOPS SDS buffer (NP0001)	All proteins (11-245kDa)
Novex WedgeWell 6% Tris-Glycine	10 / 12 / 15	Novex Tris-Glycine SDS buffer (LC2675)	Large proteins (80-245kDa)
Novex WedgeWell 10-20% Tris-Glycine	10 / 12 / 15	Novex Tris-Glycine SDS buffer (LC2675)	Small – medium proteins (11-100kDa)

Table 2.7 Gels used for SDS-PAGE (all Thermo Fisher Scientific)

Target	Molecular Weight (kDa)	Species	Supplier	Dilution
$p16^{INK4a}$	16	Mouse	Santa Cruz 56330	**WB**- 1:5000 (5% milk) **IF**- 1:500
$p21^{CIP1}$	21	Mouse	Sigma P1484	**WB**- 1:3000 (5% milk) **IF**- 1:200
p53	53	Mouse	Santa Cruz 126	**WB**- 1:2000 (5% milk) **IF**- 1:100
IL6	25	Goat	R&D AF206NA	**WB**- 1:1000 (1% BSA) **IF**- 1:100
IL8	11	Mouse	R&D MAB208	**WB**- 1:1000 (1% BSA) **IF**- 1:100
IL1β	15-30	Mouse	R&D MAB201	**WB**- 1:5000 (1% BSA) **IF**- 1:100
RB-total	110-116	Mouse	BD Bio 554136	**WB**- 1:1000 (5% milk)
PP1	38	Goat	Santa Cruz 6108	**WB**- 1:1000 (1% BSA)
pST/Q	-	Rabbit	Cell Signalling 2851	**IF**- 1:100
YH2AX	-	Mouse	Millipore 05636	**IF**- 1:2000

Table 2.8 Primary antibodies used for western blotting (WB) and immunofluorescence (IF)

Target	Supplier	Dilution	Diluent
Mouse-HRP	Sigma A2554	**WB**- 1:10,000-40,000	Same as primary
Rabbit-HRP	Sigma A0545	**WB**- 1:10,000-40,000	Same as primary
Goat-HRP	Santa Cruz 2020	**WB**- 1:5000-10,000	Same as primary
Actin-HRP	Sigma A3854	**WB**- 1:500,000	Same as primary
Mouse-Alexa fluor 488	Life Technologies A11029	**IF**- 1:1000	IF blocking buffer
Mouse-Alexa fluor 594	Life Technologies A11032	**IF**- 1:1000	IF blocking buffer
Rabbit-Alexa fluor 488	Life Technologies A11034	**IF**- 1:1000	IF blocking buffer
Rabbit-Alexa fluor 594	Life Technologies A11037	**IF**- 1:1000	IF blocking buffer

Table 2.9 Secondary antibodies used for western blotting (WB) and immunofluorescence (IF)

2.6.8 Testing CERS4 antibodies

To analyse the expression of CERS4 protein in IMR90 cells several primary antibodies detecting human CERS4 were tested, summarised in table 2.10. Optimisation was attempted by changing antibody concentrations, loading excessive amounts of cell lysates (up to 100µg) and using long exposure times (>1 hour). Despite this, CERS4 protein could only be detected in IMR90 cells cloned for CERS4 overexpression (figure 2.5). In addition, the antibodies listed below were tested using an immunofluorescence protocol (as described in *2.5*). However, no fluorescence signals were detected in any cells, including the CERS4-overexpression cells (data not shown). From this it was concluded CERS4 protein levels are below the threshold of detection by western blotting in the inducible OIS model. This data relates to the results in *4.1* and is further discussed in *7.4.1*.

Antibody (supplier code)	Species	Dilution
Santa Cruz C-19 (65112)	Goat	1:1000 (5% milk)
Santa Cruz D-6 (376497)	Mouse	1:100 (5% milk)
Sigma (SAB4301210)	Rabbit	1:500 (5% milk)

Table 2.10 Primary antibodies tested for detecting CERS4 by western blot

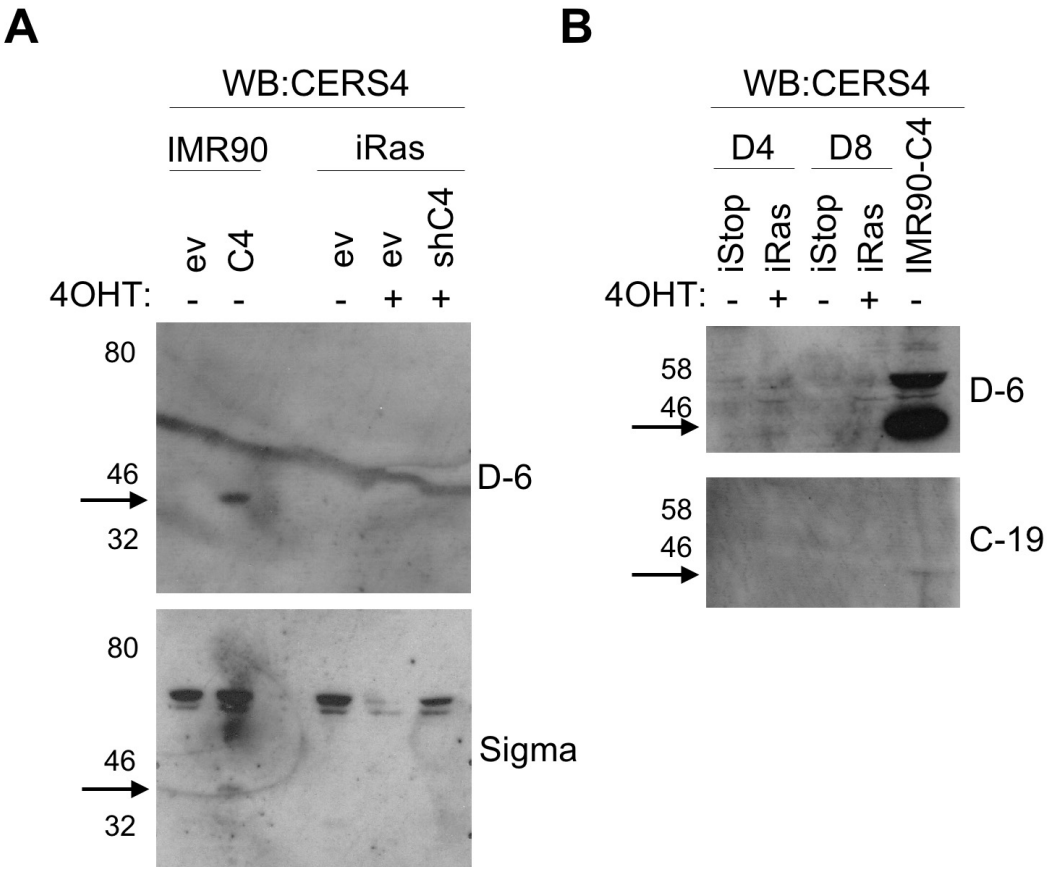

Figure 2.5 CERS4 protein levels detected in IMR90 cells by western blotting

Three CERS4 antibodies (Santa Cruz C-19, D-6 and Sigma) were tested for western blot detection of CERS4 in the following cell lysates: ***(A)*** *IMR90 with CERS4 overexpression (lanes 1-2) and iRas with shCERS4 knockdown (Day 10 of 4OHT) (lanes 3-5). Empty vector controls were used where appropriate (labeled 'ev'). 20µg lysate was separated by SDS-PAGE, using a 4-12% Bis-Tris gel.* ***(B)*** *iStop and iRas at day 4 and 8 of 4OHT (lanes 1-4) and IMR90 with CERS4 overexpression (lane 5). 60µg lysate was separated by SDS-PAGE, using a 4-12% Tris-Glycine gel.* ***Both****: numbers on left represent ladder bands (kDa); representative of 1 experiment; gels were stained with Coomassie to use as a loading control (images not shown).*

4OHT = 4-hydroxytamoxifen, ev = empty vector, shC4 = pRS-shCERS4 (knockdown), C4 = MSCV-CERS4 (overexpression), WB = western blot, arrows = CERS4 bands.

2.7 RB-PP1 co-immunoprecipitation

Cells seeded in 10cm dishes were washed three times with cold PBS, on ice. The following lysis buffer was prepared: 25mM HEPES pH 7.5, 0.5% NP40, 150mM NaCl, 1.5mM $MgCl_2$, 1mM EDTA and 1mM BME. Protease and phosphatase inhibitors were added fresh for every preparation. Depending on confluency, 400-1000µl lysis buffer was used to lyse cells directly on dishes for 10-20 minutes, on ice. Lysates were spun at 14,000rpm for 10 minutes, in a pre-chilled (4°C) centrifuge. The pellet was discarded and 5-10% supernatant was collected for an input control. Immunoprecipitation Dynabeads Protein G (Invitrogen, 10003) were washed three times with lysis buffer without protease and phosphatase inhibitors. For equilibration, 10µl washed beads (per IP) were incubated with RB antibody or IgG control (table 2.10 for information), and rotated for 1-2 hours at 4°C. The remaining lysate was added to the to the equilibrated beads and rotated for 4-6 hours at 4°C. The beads were pelleted by magnetism and 5-10% supernatant was collected to test efficiency of the IP. The remaining supernatant was discarded. The pelleted beads were washed three times with lysis buffer without protease and phosphatase inhibitors. After the final wash, as much supernatant as possible was removed and proteins eluted from beads using SDS loading buffer. All collected samples were boiled and subjected to western blotting of RB and PP1 as described from *2.3.4*.

Target	Application	Species	Supplier	Dilution
RB	IP	Rabbit	Santa Cruz 50	**IP**- 5µg per IP
IgG control	IP	Rabbit	Santa Cruz 2027	**IP**- 5µg per IP
PP1	WB	Goat	Santa Cruz 6108	**WB**- 1:1000
RB-total	WB	Mouse	BD Bio 554136	**WB**- 1:1000

Table 2.11 Antibodies used for RB-PP1 co-immunoprecipitation (IP)

2.8 Quantitative real-time polymerase chain reaction (qPCR)

All steps for this qPCR protocol were performed on a clean surface and sterile filter tips (Rainin) were used for all pipetting steps.

2.8.1 RNA extraction

Cells were pelleted as described in *2.2.1* and washed once with PBS. Cells were lysed using the QIAshredder (Qiagen, 79654) and RNA extracted using RNeasy Plus Mini Kit (Qiagen, 74134), both as per manufacturer's instructions. DNA contamination was prevented by using the gDNA Eliminator Spin Columns. Extracted RNA was eluted in RNase-free dH_2O and quantified using a NanoDrop 2000C.

2.8.2 cDNA synthesis using reverse transcriptase

A 50ng/µl intermediate stock of each RNA sample was prepared. For each set of reactions, an RNA pool (total concentration = 50ng/µl) was made to use as a no-RT control. qScript cDNA SuperMix (QuantaBio, 95048) was used as the reaction buffer and was composed of dNTPs, RNase inhibitor and a qScript reverse transcriptase. For each 40µl reaction, 8µl 5X qScript was mixed with 20µl RNA intermediate stock and 12µl RNase-free dH_2O. For the no-RT control, qScript was replaced with RNase-free dH_2O. Reactions were briefly centrifuged and underwent cDNA synthesis in an Agilent SureCycler 8800. The programme for cDNA synthesis was as follows:

5 min @ 25°C --> 30 min @ 42°C --> 5 min @ 85°C --> ∞ @ 4°C

2.8.3 qPCR

qPCR primers were designed by myself, Andrea Quintanilla and Juan-Carlos Acosta using the NCBI 'Pick primers' tool (see table 2.10 for sequences). It was selected that primers span an exon-exon junction to ensure only the coding region was amplified. Primers were synthesised by Sigma and resuspended in RNase-free dH_2O to make 100µM stocks. For each set of triplicate wells, a 50µl mastermix was prepared (the value in brackets indicates the final reaction concentration): 25µl SYBR Select (1X; Thermo Fisher, 4472908) + 0.5µl forward primer (100nM) + 0.5µl reverse primer (100nM) + 21µl RNase-free dH_2O + 3µl cDNA (75ng). 15µl of

each reaction was carefully aliquoted into triplicate wells of RNase-free 96 well plates (Star Lab, E1403-7700) and briefly centrifuged to ensure all the reaction was pooled at the bottom. qPCR was performed on the Applied Biosystems StepOne Plus Real-Time PCR System, using the following programme:

10 min @ 95°C --> x40 cycles (15s @ 95°C --> 30s @ 60°C --> 15s @ 72°C) --> 15s @ 95°C.

After the cycling stage, a melt curve for each primer set was generated by heating from 60-95°C in 0.3°C increments. Using the StepOne software, a threshold cycle (Ct) was manually defined in the mid-linear phase of the amplification and Excel used for data analysis. The relative expression of target genes was calculated by normalising to housekeeping gene β-actin using the formula $2^{-\Delta Ct}$.

Target	**Forward & Reverse primers**
β-actin (housekeeping gene)	F: CATGTACGTTGCTATCCAGGC R: CTCCTTAATGTCACGCACGAT
ASAH1	F: TGGGAAAGAAAGATGTCATGTG R: CACACAACCTTCCCCAGACT
CDC6	F: GTTCAATTCTGTGCCCGCAA R: TAGCTCTCCTGCAAACATCCAG
CDC7	F: CTCGGTAGGTGGGGATCTCT R: GAGATGCAAAATGCCAGGGTT
CDK1	F: CTTGGCTTCAAAGCTGGCTC R: GGGTATGGTAGATCCCGGCT
CDK2	F: CGAGCTCCTGAAATCCTCCTG R: GGCGAGTCACCATCTCAGCAA
CDKN1A (p21)	F: CCTGTCACTGTCTTGTACCCT R: GCGTTTGGAGTGGTAGAAATCT

Table 2.12 qPCR primers used to quantify human mRNA expression

(continued next page)

Target	Forward & Reverse primers
CDKN2A (p16)	F: CGGTCGGAGGCCGATCCAG R: GCGCCGTGGAGCAGCAGCAGCT
CDKN2B (p15)	F: AATGCGCGAGGAGAACAAG R: CCATCATCATGACCTGGATCG
CERK	F: ATCGTTGTTGGGGACTCGCT R: GGGACACGGAGTAGCGAAGG
CERS4	F: ATCAGACCAGGAGGCAAGTG R: GGCCTCACAGAACTTCTTGGT
GBA	F: TTGCAGGGCTAACCTAGTGC R: GGCTTGGGACATTCCTCTCT
IL6	F: CCAGGAGCCCAGCTATGAAC R: CCCAGGGAGAAGGCAACTG
IL8	F: GAGTGGACCACACTGCGCCA R: TCCACAACCCTCTGCACCCAGT
MCM2	F: GTGGATAAGGCTCGTCAGAT R: GTCGTGGCTGAACTTGTT
ORC1	F: ACATACCCTCACGAAGGTGC R: GCAGAAACATGCAGCCTCAG
PCNA	F: GGTTACTGAGGGCGAGAAGC R: GACCGGCTGAGACTTGCGTA
SMPD2	F: CCGAATACAATCGACAGAAGG R: CCTGTCCACTCCTTCAGCA
SPHK1	F: TTGCAGCTCTTCCGGAGT R: CTCCAGACATGACCACCAGA

2.9 Transcriptomics

2.9.1 AmpliSeq targeted RNA sequencing

Edinburgh Clinical Research Facility Genetics department performed AmpliSeq transcriptomics sequencing of RNA (extracted as described in *2.8.1*). A protocol provided by the CRF is briefly summarised here. All products used were supplied by Thermo Fisher. RNA samples were assessed for quality and were quantified. cDNA was prepared by reverse transcription of RNA samples and then target genes were amplified for 12 cycles of PCR using the Ion AmpliSeq Human Gene Expression Core Panel (A26325). This panel contains 20,802 amplicons (41,604 primers) of approximately 150 bases in length in a single pool. Ion Torrent sequencing adapters and barcodes (4474517) were ligated to the amplicons and adapter-ligated libraries were purified using AMPure XP beads. Libraries were quantified by qPCR. Libraries were then diluted to 100pM and combined in 3 equimolar pools of 8 for template preparation. The Ion PI Hi-Q OT2 200 Kit (A26434) was used for template preparation, followed by sequencing with the Ion PI Hi-Q Sequencing 200 Kit (A26433) and Ion PI Chip Kit v3 (A26771). The Ion Proton (#2456290-0449) platform was used for sequencing; and coupled with the AmpliSeqRNA plugin, was used for analysis of the sequencing output. Summary reports for each sequencing run provided a large amount of data including sequencing run summary, reference alignment statistics, plug-in summary and a detailed list of software version numbers used in each analysis step.

2.9.2 Babelomics 5 RNAseq data analysis

The sequencing output from AmpliSeq transcriptomics was subjected to analysis using the Babelomics 5 'RNA-seq class comparison' tool (Alonso et al., 2015). For this analysis, the normalization method used was TMM and Benjamini and Hochberg multiple-test correction was used to calculate the False Discovery Rate and adjusted p-value (<0.05). The resulting statistic values were further interrogated to indicate differential gene expression compared to the OIS control. Gene Set Enrichment Analysis was used to assign Gene Ontology (GO) to the dataset and gain information on the pathways significantly changing between compared conditions.

2.10 Senescence Associated β-galactosidase activity assay

Cells were seeded at $5x10^4$ cells per well in 6 well plates and cultured for 48-72 hours. Prior to fixation, a solution of PBS with 1mM $MgCl_2$ was prepared and adjusted to pH 5.6-6.0. Media was aspirated, cells washed twice in PBS and fixed with 0.5% glutaraldehyde/PBS (Sigma, G5882) for 10-15 minutes in a fume cabinet. During fixation, the X-gal solution was prepared as shown in table 2.12 and incubated in a 37°C water bath for up to 30 minutes to avoid crystal formation and precipitation. The fixed cells were washed three times in PBS/$MgCl_2$. The pre-warmed X-gal solution was added to the cells and incubated at 37°C for 6-24 hours, depending on the development of the blue precipitate.

	Stock (20X)	Final (1X)	Supplier
$K_3Fe(CN)_6$	100mM	5mM	Sigma 60299
$K_4Fe(CN)_6 \bullet 3H_2O$	100mM	5mM	Sigma 60279
X-gal solution	20mg/ml	1mg/ml	Thermo Fisher R0941

Table 2.13 Composition of X-gal solution, diluted in PBS/$MgCl_2$ pH5.6-6.0

2.11 Crystal Violet colony formation assay

Cells were seeded at $5x10^4$ or $1x10^5$ cells per 10cm dish and cultured for 7-20 days. Colony formation was monitored and growing controls compared to senescent cells were used to determine when to fix cells. For fixation, cells were washed twice in PBS and fixed with 0.5% glutaraldehyde/PBS (Sigma, G5882) for 1 hour in a fume cabinet. The fixed cells were washed three times in PBS and left to dry at room temperature for at least 24 hours. Dried dishes were stained with 0.2% crystal violet/water solution at room temperature for 3-4 hours. The crystal violet was collected (to be re-used) and dishes washed with tap water, and left to dry overnight. Images of the dried dishes were taken using a normal scanner. For quantification, stained dishes were dissolved in 1% acetic acid at room temperature for 4 hours. The 595nm absorbance of the dissolved crystal violet was measured using a spectrophotometer.

2.12 Lipidomics

2.12.1 Compounds used to measure sphingolipid metabolism

For metabolic flux analysis of sphingolipid metabolism, IMR90 were treated with several compounds listed here. Typically, IMR90 were seeded in 10cm dishes or 6 well plates and starved with DMEM+1% FBS. Starvation was used to keep the basal level of metabolism low. To analyse *de novo* sphingolipid biosynthesis, IMR90 were treated with 0.8mM 2,3-$^{13}C_2$-serine (Sigma, 605174) for 6 hours. dH_2O was used as a vehicle for 2,3-$^{13}C_2$-serine. For analysis of sphingolipid recycling pathway, IMR90 were treated with 2µM 17:1/8:0-ceramide (Avanti, 860645) for 3 hours. Absolute filtered ethanol was used as a vehicle for 17:1/8:0-ceramide.

2.12.2 Lipid extraction

To extract lipids from cells a biphasic method based on the Bligh and Dyer method (Bligh and Dyer, 1959) was performed and is briefly summarised here. All solvents were HPLC grade: water (VWR, 83645), propan-2-ol (VWR, 84881), chloroform (Alfa Aesar, 22920) and methanol (Fisher, M/4000/14). Cells were scraped in 1ml PBS and pelleted in a pre-chilled bench top centrifuge (4°C) at 800g for 10 minutes. Cell pellets were washed with 1ml fresh PBS and centrifuged for 2 minutes. The cells were resuspended in 100µl PBS and transferred to a glass test tube. A chloroform/methanol (1:2) solution was prepared and 375µl added to the cells and vortexed. The tubes were agitated vigorously for 30-45 minutes at 4°C. Next, 125µl of each chloroform and water were sequentially added. Tubes were vortexed after each addition. The two phases were separated using a centrifuge at 1000rpm for 5 minutes (room temperature). Using a glass Pasteur pipette, the lower phase was transferred into a flat-bottomed 2ml glass vial (Supelco, 29651) and dried under nitrogen. Dried lipid extracts were stored at 4°C.

To prepare samples for LC-MS, the following reconstitution buffer was used: acetonitrile/propan-2-ol/water (60:30:5). For extracts from 10cm dishes, 100µl reconstitution buffer was added and mixed/vortexed well before aliquoting 30µl into a total recovery 1.2ml glass vial (Supelco, 29658). For extracts from 6 well plates, 50µl reconstitution buffer was added and mixed/vortexed well before aliquoting 25µl

into a total recovery 1.2ml glass vial. The remaining lipid extracts were dried under nitrogen and stored at 4°C in case another sample was later required.

2.12.3 Liquid Chromatography Mass Spectrometry (LC-MS)

Reconstituted lipid extracts were separated on a Kinetex 1.7u C18 100Å column (Phenomenex) using a Thermo Ultimate BioRS HPLC maintained at 45°C. Mobile phases were: [A] acetonitrile/water (60:40) + 10mM ammonium formate and [B] propan-2-ol/acetonitrile (90:10) + 10mM ammonium formate. A flow rate of 0.3ml/min was used and the following multi-step gradient established:

20-97%B gradient for 8 min --> 97%B 2 min --> 20%B 2 min [12 min total]

Separated lipids were eluted into a Thermo Q-exactive mass spectrometrer and acquired in positive ion mode with an ion range of 400-1000m/z or 250-1000m/z.

2.12.4 Data analysis

Raw LC-MS data was analysed using Thermo Xcalibur Qual/Quan Browser software. Sphingolipid ion peaks were confirmed by fragmentation and standards (with Joy Edwards-Hicks). Quan Processing methods were created for quantitative data analysis: peak areas of defined sphingolipids were extracted from raw data files. Peak areas were normalised to Total Ion Count (TIC) or internally normalised by calculating % label for labelling experiments.

2.12.5 University of Highlands & Islands (UHI) Lipidomics

Global lipidomics and quantitative analysis of ceramides were initially performed at the Lipidomics Research Facility at the UHI. Prof Phil Whitfield, Dr Mary Doherty and Seshu Tamireddy performed the extractions, LC-MS and data analysis. UHI are acknowledged throughout the relevant results sections. For all analyses, cells were solvent extracted according to Folch's method (Folch et al, 1957).

2.12.5.1 Global lipidomics

The extracted lipids were analysed by LC-MS in positive and negative ion modes using a C18 column and acetonitrile/water/propan-2-ol gradient. All analyses were performed on a Thermo Exactive Orbitrap mass spectrometer coupled to a Thermo

Accela 1250 UHPLC system. The raw LC-MS data were processed with Progenesis CoMet v2.0 software (Non-linear Dynamics) and searched against HMDB (http://www.hmdb.ca/) and LIPID MAPS (www.lipidmaps.org/) for identifications. The processed data were then subjected to multivariate statistical analysis using SIMCA-P v13.0.2 (Umetrics).

2.12.5.2 Quantitative ceramide analysis

The extracted ceramides were isolated by silica solid phase extraction chromatography. C17:0 ceramide and C12:0 dihydroceramide (Avanti Polar Lipids) were included in the experimental system as internal standards. LC-MS/MS analyses were performed in positive ion mode on a Thermo TSQ Quantum Ultra triple quadrupole mass spectrometer equipped with a heated electrospray source and coupled to a Thermo Accela 1250 UHPLC system. The ceramides were separated on a Kinetex 2.6µm C8 column (100 x 2.1 mm) (Phenomenex), maintained at 40°C. Mobile phases were: [A] 10% acetonitrile + 90% water + 0.1% formic acid and [B] acetonitrile + 0.1% formic acid. A flow rate of 500µl/min was used and the following multi-step gradient established:

80%B gradient for 1 min --> 80-100%B gradient for 15 min --> 100%B 1 min --> re-equilibration to starting conditions [20 min total]

The data were acquired and processed using Thermo Xcalibur software v2.1. The concentration of the ceramide molecular species was determined by comparison to calibration curves generated with C16:0 and C24:1 standards (Avanti Polar Lipids). Total ceramide concentrations were calculated from the summed concentrations of all the monitored molecular species. The values were normalised to cellular protein content determined using the Coomassie Plus Protein Assay (Pierce Biotechnology).

2.13 Metabolic Assays

Protocols for these assays were optimised for 96 well plate format with image acquisition and analysis performed on the ImageXpress (*2.5.4*).

2.13.1 Click-iT Lipid Peroxidation Assay (Molecular Probes, C10446)

25μM Linoleamide Alkyne (LAA) reagent was added to cells previously seeded at 1-6x10^3 cells per well, and incubated at 37°C for 2 hours. Cells were fixed, permeabilised and blocked as described in *2.5.3*, and protected from light throughout this staining protocol. During 1 hour blocking, the LAA reaction cocktail was prepared as described by the manufacturer's instructions. After three PBS washes, 125μl of the prepared LAA reaction cocktail was added per well and incubated for 30 minutes at room temperature on an orbital shaker. After three PBS washes, cells were stained for DAPI, followed by a final PBS wash before image acquisition.

2.13.2 LipidTox Phospholipidosis and Steatosis Detection Assay (Molecular Probes, H34158)

LipidTox Red Reagent was diluted 1:3000 in supplemented DMEM and 100μl added to cells previously seeded at 1-6x10^3 cells per well, and incubated at 37°C for 24 hours. Cells were fixed as described in *2.5.3*, and protected from light throughout this staining protocol. Immediately after fixation, cells were stained for DAPI as described in *2.5.3*. During the DAPI incubation, LipidTox Green Reagent was prepared 1:1000 in PBS. After three PBS washes, 100μl of the diluted LipidTox Green Reagent was added per well and incubated for 30 minutes at room temperature on an orbital shaker. The LipidTox Green Reagent was not washed off before image acquisition. FITC and TxRED filters were used for acquiring the green steatosis stain and red phospholipidosis stain, respectively.

2.14 Statistics

For all experiments with 3 biological replicates (indicated in figure legends), significance calculations were performed using two-tailed Student's t-test or one-way ordinary ANOVA. These calculations were done using Microsoft Excel and GraphPad Prism 7 software.

Chapter Three: Identification of novel metabolic regulators of OIS by siRNA screening

As described in *1.2*, altered cellular metabolism provides an attractive target for cancer therapies. In addition, it has been argued OIS can be specifically targeted to promote its anti-cancer features (reviewed by Acosta and Gil (2012)). The first aim for this thesis was to identify new metabolic regulators of OIS, by utilising a high-content screening platform coupled with an siRNA library targeting 553 genes, encoding metabolic enzymes and transcription factors. Essential metabolic genes for OIS were identified by siRNA knockdown causing a 'bypass of OIS', measured by BrdU incorporation as a proliferation readout. In this chapter, the results from the primary siRNA screen and subsequent validation are described.

3.1 Primary siRNA screen

3.1.1 Screen design and workflow

The primary siRNA library was custom-made from Dharmacon and was designed and shared with Andy Finch and Joy Edwards-Hicks. The library was composed of pooled siRNA sequences – four different sequences per gene. A total of 553 genes involved in a variety of metabolic pathways were targeted in this primary screen (figure 3.1.A). Appendix 1 provides a list of genes targeted in the primary screen. The workflow of the siRNA screen was optimised by Priya Hari for a different project and is overviewed in figure 3.1.B. Briefly, the cells used throughout were IMR90-ER:Ras and IMR90-ER:Stop (or iRas and iStop, see figure 2.2 for details on the 'ER' system used to model OIS in IMR90). For the primary screen, IMR90-ER:Ras were administered 4OHT and subjected to reverse transfection onto siRNAs after 2 and 7 days of 4OHT. Plates were fixed and stained for BrdU incorporation by immunofluorescence 72 hours post-transfection. Images were acquired and analysed using the ImageXpress High Content Analysis microscope. Raw data underwent normalization metrics and were converted to Z-scores for robust hit identification using online software package Web CellHTS2 (Pelz, Gilsdorf and Boutros, 2010).

IMR90s are amenable to BrdU incorporation as a proliferation readout and as cell cycle arrest is a major hallmark of OIS, it was decided BrdU incorporation was a good initial readout for OIS in the siRNA screen. siRNA targeting TP53 was used as a positive control of bypass of OIS (figure 3.1.C, right panel).

3.1.2 Screen results for day 5 time point

Control (Non-Target and siTP53) raw data was checked to ensure the cells were behaving as expected with the addition of 4OHT. Figure 3.1.C indicates the images and raw percentages of BrdU incorporation. Next, the raw data for 'plates as replicates' were processed through Web CellHTS2. Normalisation (using the 'median' method) and quality control metrics indicated a robust screen output for the day 5 time point. Box plots showed the distribution of raw data (pink) and after normalisation (blue) for the three replicates (figure 3.2.A). For plate 6 there were only two replicates due to a practical issue with the experimental procedure. Z' Factor plots indicated good separation between negative (red) and positive (blue) controls and all replicates had a Z' Factor of >0.2, which is of reasonable quality for an siRNA screen (figure 3.2.B). Heatmaps for each plate, except 6, indicated good correlation (>0.8) between the three replicates (figure 3.2.C). The scatter graph comparing the two replicates of plate 6 showed minimal variation (figure 3.2.D).

Next, the Z-scores for each siRNA were extracted from the Web CellHTS2 analysis. Initially, a Q-Q plot showed most data within the theoretical normal distribution (dotted line) and hits were identified by the data deviating from the dotted line at <-2 sample quantile (figure 3.3.A). The red circles indicated all the positive controls (i.e. siTP53) within the screen. Z-scores were converted to positive numbers to better represent the positive effect siRNAs have on OIS state. Significant hits were identified as having a Z-score of >2.0, corresponding to an approximate p-value <0.05 (figure 3.3.B). The higher the Z-score the more likely the siRNA was truly causing a bypass of senescence. TP53 was the top hit at day 5 followed by ceramide synthase 4 (CERS4); a further 13 genes were identified as possibly essential for OIS (figure 3.3.C).

A

Pathway targeted	Number of genes
Glucose metabolism	59
Nucleotide biosynthesis	22
Amino acid biosynthesis	16
Transporters	17
Transcription Factors	18
Lipid biosynthesis	244
Detoxification	62
Other	115
Total	553

B

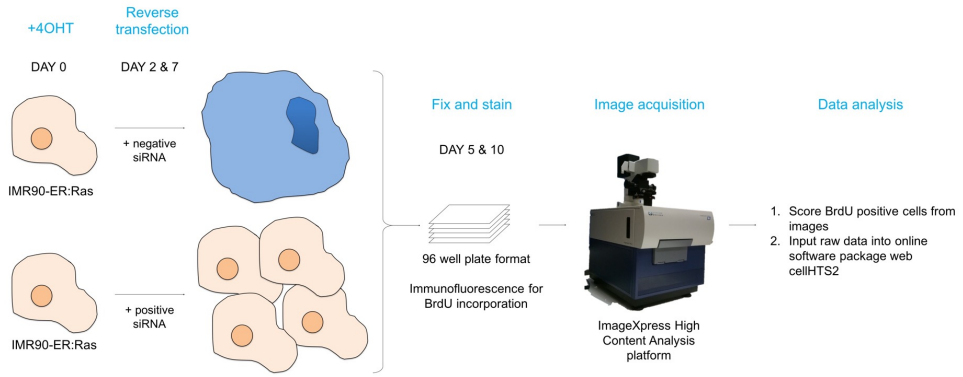

C

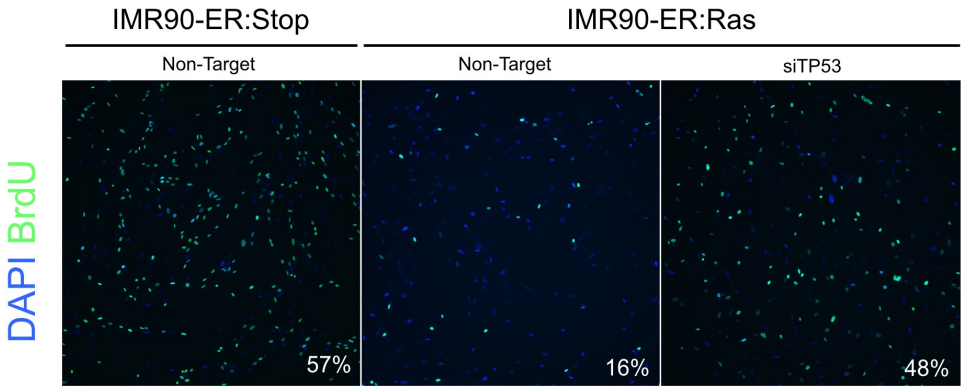

Figure 3.1 Primary siRNA screen design and workflow

(A) Table summarising the metabolic pathways targeted by Dharmacon ON-TARGETplus siRNAs in the custom-design library. ***(B)*** *An overview of the workflow for siRNA screening. See main text for further detail.* ***(C)*** *Representative immunofluorescence images and quantification (% positive cells, bottom right) of BrdU incorporation in IMR90-ER:Stop and IMR90-ER:Ras transfected with indicated siRNA.*

4OHT = 4-hydroxytamoxifen; BrdU = bromodeoxyuridine

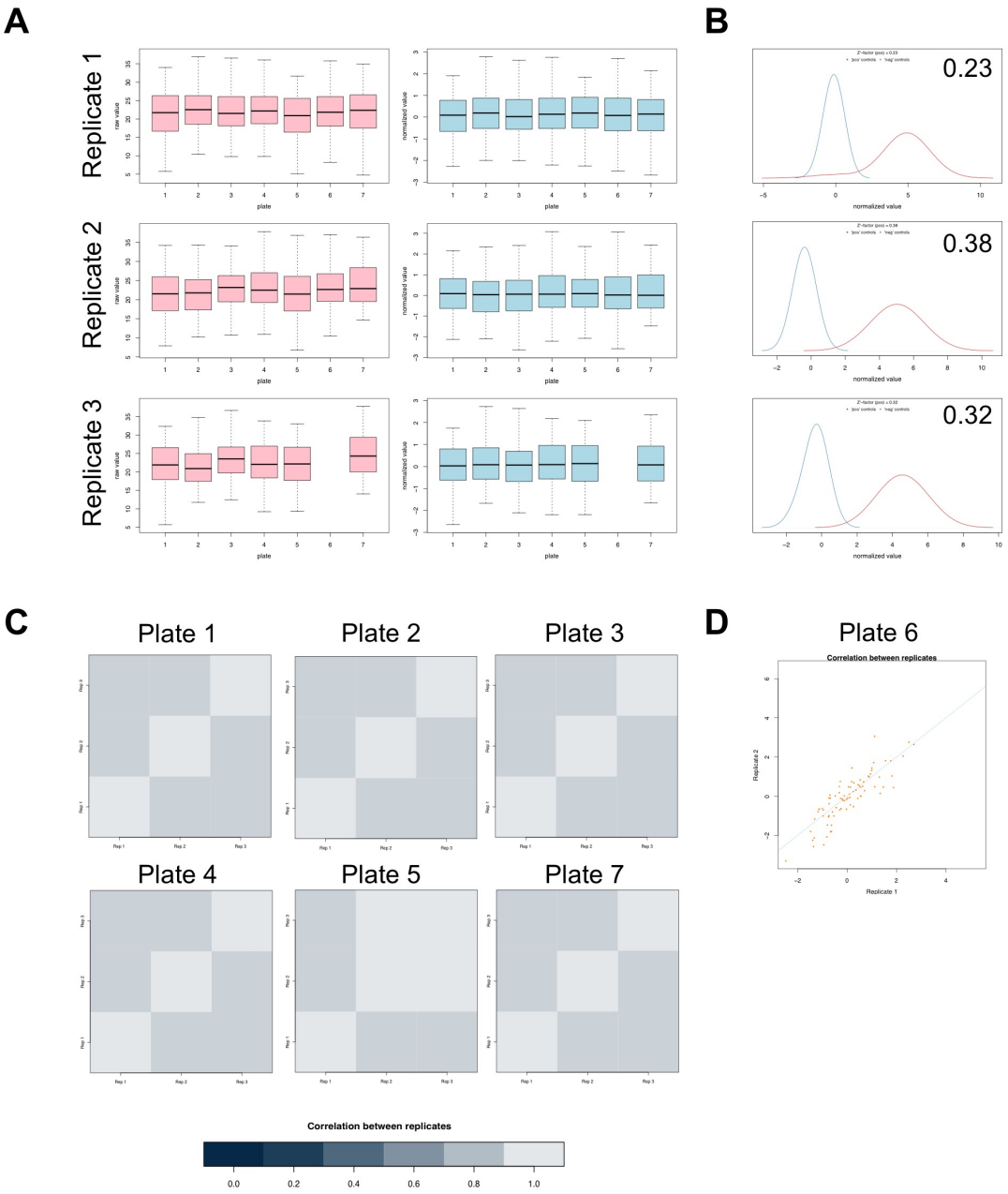

Figure 3.2 Normalisation and quality control metrics for day 5 screen data

(A) *Distribution box plots for raw (pink) and normalised (blue) data. Note: there were only two replicates for plate 6.* ***(B)*** *Z' Factor plots and values (top right) for negative (red) and positive (blue) controls.* ***(C)*** *Heatmaps showing correlation between the three replicates of each plate (except 6).* ***(D)*** *Scatter graph showing variation between the 2 replicates for plate 6 (a correlation heatmap could not be generated for two replicates).*

A

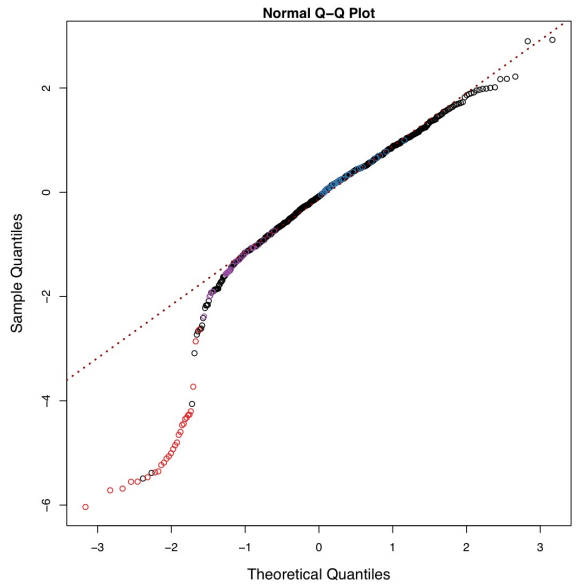

C

	Gene ID	Z-score
	TP53	5.49
1	CERS4	5.38
2	DLST	4.06
3	GCLC	3.09
4	GBA	2.73
5	PTDSS1	2.67
6	SIRT5	2.63
7	BID	2.61
8	KEAP1	2.55
9	LPCAT4	2.41
10	UMPS	2.22
11	SLC7A11	2.17
12	NAMPT	2.17
13	RPS6KB2	2.16
14	SGK1	2.08

B

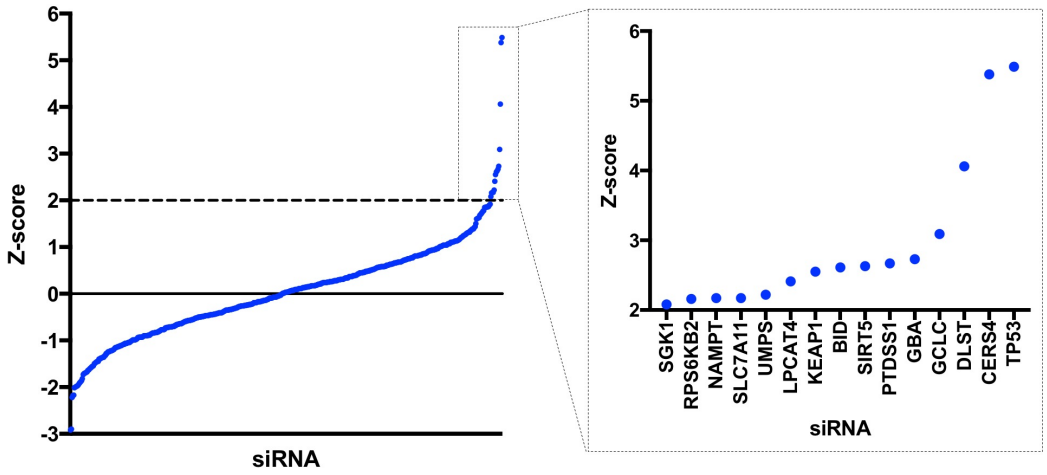

Figure 3.3 Identification of 14 genes possibly essential for OIS

(A) Q-Q plot comparing sample quantiles and theoretical normal distribution quantiles (dotted line = normal distribution). ***(B)*** *Z-scores plot (converted from the Q-Q data) with a zoom on the positive hits with a Z-score of >2.0 (right panel).* ***(C)*** *Table summarising the 14 positive hits with a Z-score of >2.0. Note the top hit is the positive control TP53.*

3.1.3 Screen results for day 10 time point

The raw data for 'plates as replicates' were processed through Web CellHTS2 to gain normalisation and quality control metrics, as with day 5. Box plots showed the distribution of raw data (pink) and after normalisation (blue) for the three replicates (figure 3.4.A). For this time point all plates had three replicates. Z' Factor plots indicated poor separation between negative (red) and positive (blue) controls and all replicates had a Z' Factor of <-0.1 (figure 3.4.B). This could be due to the robust nature of established OIS, resulting in the positive control siRNA against TP53 not bypassing senescence as well as at day 5. Heatmaps for each plate indicated correlation of >0.4 between the three replicates (figure 3.4.C), signifying poor reproducibility between plates. Only two significant hits were identified as having a Z-score of >2.0, TP53 and CERS4 (data not shown).

To overcome this replication issue, the Web CellHTS2 analysis was repeated with 21 'individual plates', rather than 'plates as replicates'. This was to ensure hits were not missed due to one replicate being variable; hits were identified when two or more individual plates had Z-scores >2.0. Distribution box plots of 21 individual plates showed raw (pink) and normalised (blue) data with similar patterns to the first analysis (figure 3.4.D). The Z' Factor was not improved when plates are considered individual rather than replicates (-0.36, figure 3.4.E). Z-scores were converted to positive numbers and significant hits were identified as having a Z-score of >2.0 for two or three of the individual plates, corresponding to an approximate p-value <0.05 (figure 3.5.B-C). Like day 5, TP53 was the top hit followed by CERS4; a further 4 genes were identified as possibly essential for OIS (figure 3.5.D). There were more siRNAs with a Z-score 1.5-2.0, which is indicative of essentiality but not statistically significant (data not shown); however, these were not included in further analysis due to increased variation between the replicates.

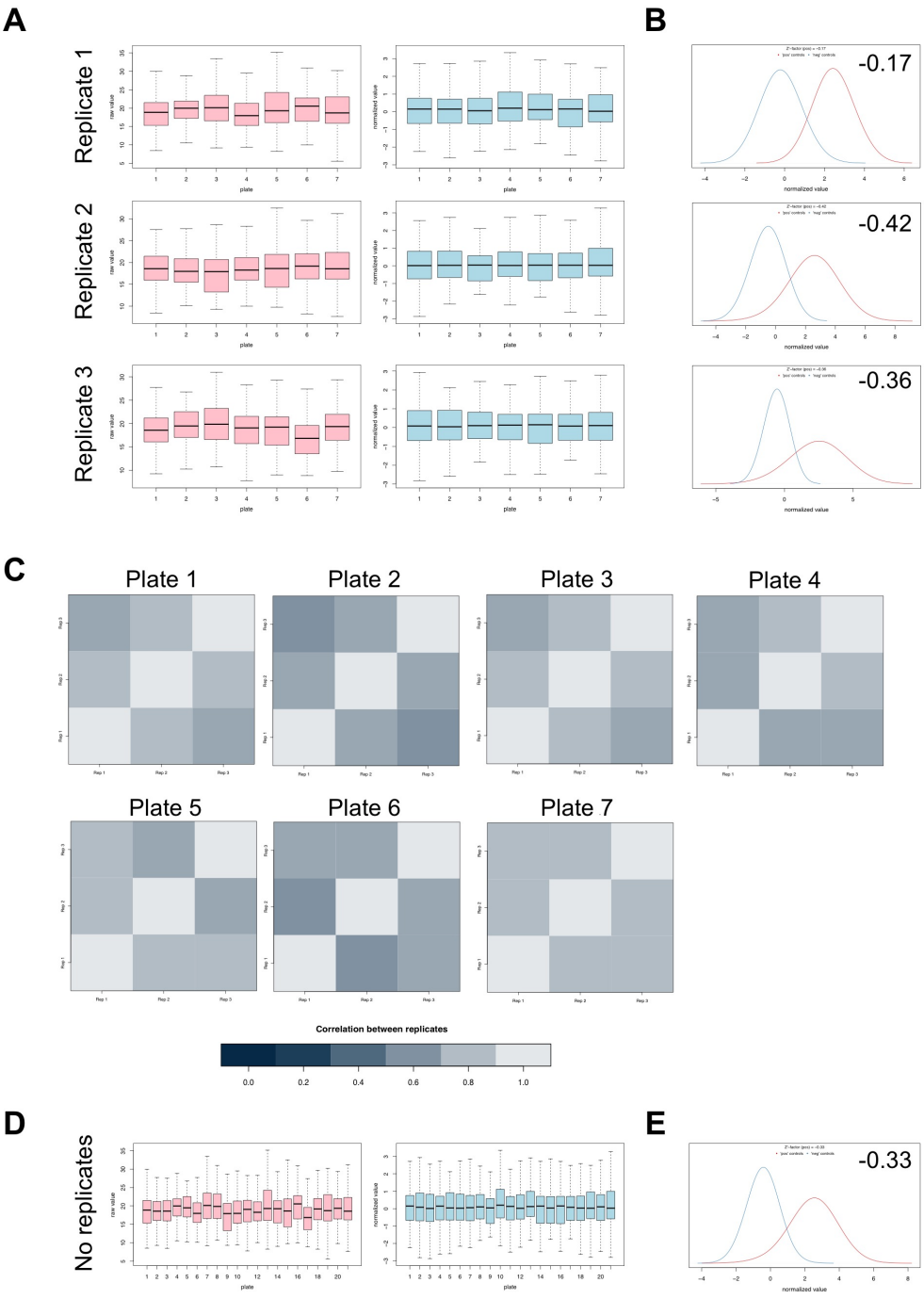

Figure 3.4 Normalisation and quality control metrics for day 10 screen data

(A) *Distribution box plots for raw (pink) and normalised (blue) data.* ***(B)*** *Z' Factor plots and values (top right) for negative (red) and positive (blue) controls.* ***(C)*** *Heatmaps showing correlation between the three replicates of each plate.* ***(D)*** *Distribution box plots of 21 individual plates show raw (pink) and normalised (blue) data.* ***(E)*** *'Individual plates' Z' Factor plots and values (top right) for negative (red) and positive (blue) control*

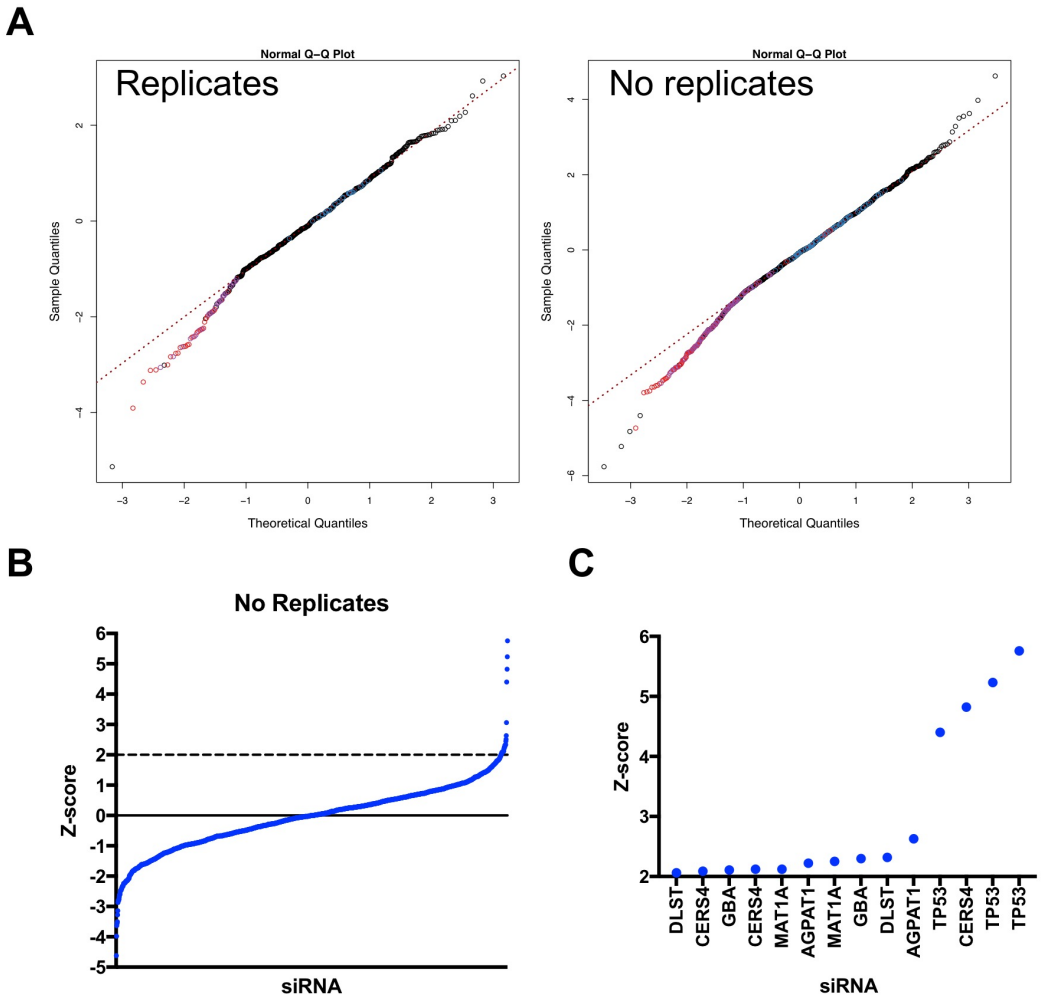

D

	Gene ID	Max. Z-score	Plates with >2.0 Z-score
	TP53	5.70	3
1	CERS4	4.82	3
2	AGPAT1	2.63	2
3	DLST	2.32	2
4	GBA	2.30	2
5	MAT1A	2.25	2

Figure 3.5 Identification of 5 genes possibly essential for OIS – using no replicates normalisation

*(**A**) Q-Q plot comparing sample quantiles and theoretical normal distribution quantiles of analyses with replicates (left) and no replicates (right) (dotted line = normal distribution). **(B)** Z-scores plot (converted from the 'no replicates' Q-Q data). **(C)** Zoom on the positive hits with a Z-score of >2.0, for 2 or 3 replicates. **(D)** Table summarising the 5 positive hits with a Z-score of >2.0, for 2 or 3 replicates.*

3.1.4 Summary

This section has shown it is possible to identify metabolic regulators of OIS using siRNA loss-of-function screening. Using data analysis platforms, 16 genes encoding metabolic enzymes have been identified that, when targeted for knockdown by siRNA, bypass OIS. This indicates these 16 genes are possibly essential for OIS, listed in figure 3.6. 14 genes were identified at day 5 (middle and purple sections, figure 3.6), 5 at day 10 (middle and yellow sections, figure 3.6) and 3 were common at both day 5 and 10 (middle section, figure 3.6). A summary of the gene IDs, function and day 5/10 Z-scores is represented in table 3.1. The next step was to validate these significant hits in a secondary siRNA screen.

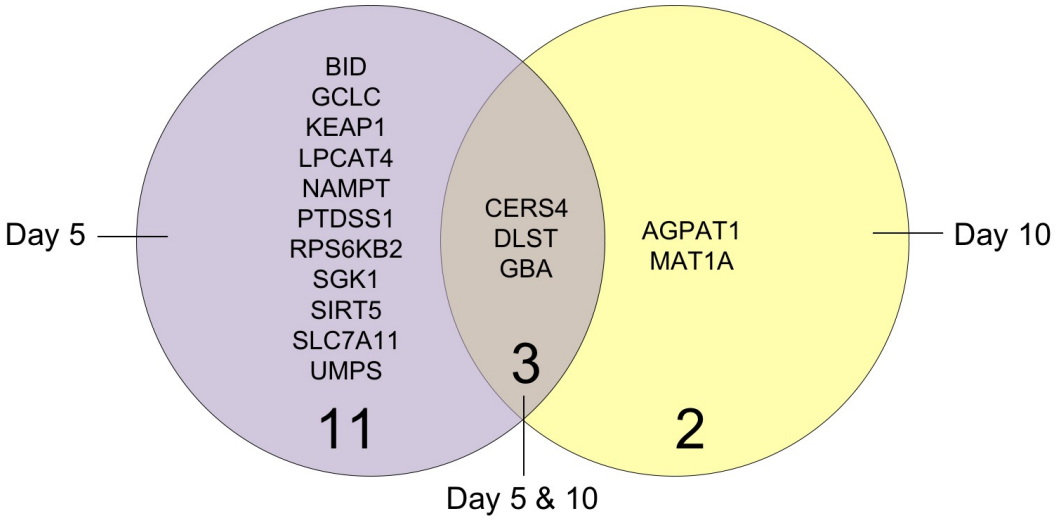

Figure 3.6 Summary of genes identified as possible regulators of OIS from the primary siRNA screen

Gene ID	Gene function	Z-score			
		Day 5	Day 10		
		Average	Rep 1	Rep 2	Rep 3
AGPAT1	Converts lysophosphatidic acid (LPA) → phosphatidic acid (PA)		0.53	2.63	2.22
BID	Death agonist that mediates mitochondrial damage induced by caspase-8	2.61			
CERS4	Ceramide synthase	5.38	2.09	2.12	4.82
DLST	Converts 2-oxoglutarate → succinyl-CoA + CO_2 (TCA cycle)	4.06	2.32	1.42	2.06
GBA	Cleaves the beta-glucosidic linkage of glycosylceramide	2.73	2.30	1.70	2.11
GCLC	First rate-limiting enzyme of glutathione synthesis	3.09			
KEAP1	Promotes proteasome-dependent degradation of NRF2	2.55			
LPCAT4	Converts lysophosphatidic acid (LPA) → phosphatidic acid (PA)	2.41			
MAT1A	Adenosyl moiety of ATP + methionine → SAM + tripolyphosphate		2.25	0.82	2.12
NAMPT	Nicotinamide + 5-PP-1-PP → nicotinamide mononucleotide	2.17			
PTDSS1	Catalyzes the formation of phosphatidylserine from either PC or PE	2.67			
RPS6KB2	Phosphorylates the S6 ribosomal protein and EIF4b	2.16			
SGK1	Kinase activation of potassium, sodium, and chloride channels	2.08			
SIRT5	Mono-ADP-ribosyltransferase activity	2.63			
SLC7A11	Transports cystine into cells in exchange for glutamate	2.17			
UMPS	Catalyzes the final two steps of the *de novo* pyrimidine biosynthesis	2.22			

Table 3.1 Summary of primary screen results, including the function of genes identified as possible regulators of OIS

3.2 Secondary siRNA screen

3.2.1 Screen design and workflow

Pooled siRNAs targeting the 16 genes identified from the primary siRNA screen were deconvoluted and custom-made in two 96-well plates from Dharmacon. Deconvolution meant the four different siRNAs in the primary screen pool were placed in individual wells. The experimental workflow of the secondary screen was identical to the primary screen and is overviewed in figure 3.7. For the data analysis, the following criterion for hit selection was used: only those genes with two or more siRNAs bypassing senescence were validated. In addition to BrdU incorporation, $p16^{INK4a}$ and $p21^{CIP1}$ immunofluorescence staining was included for further validation of bypass of OIS.

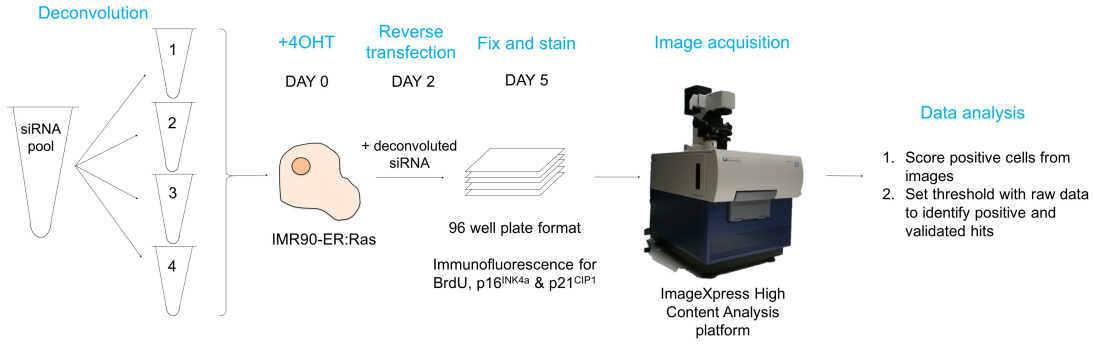

Figure 3.7 Secondary siRNA screen design and workflow

siRNA pools were deconvoluted into four individual siRNAs with different sequences targeting the same gene. iRas were administered 4OHT and subjected to reverse transfection onto siRNAs after 2 days. Plates were fixed and stained for BrdU incorporation, $p16^{INK4a}$ and $p21^{CIP1}$ expression by immunofluorescence 72 hours post-transfection. Images were acquired and analysed using the ImageXpress High Content Analysis microscope. For data analysis and hit identification, a validation criterion for each stain was selected. See main text for further detail.

3.2.2 Screen results

3.2.2.1 BrdU

First, deconvoluted Non-Target siRNA controls were tested to check for any differences compared to the pooled Non-Target (figure 3.8). The raw data indicated that the four NT individual controls performed similarly, and NT4 was selected as a control for the main secondary screen. siRNAs targeting p53 (siTP53) and p21 (siCDKN1A) were also tested in iRas cells to confirm their suitability as positive controls.

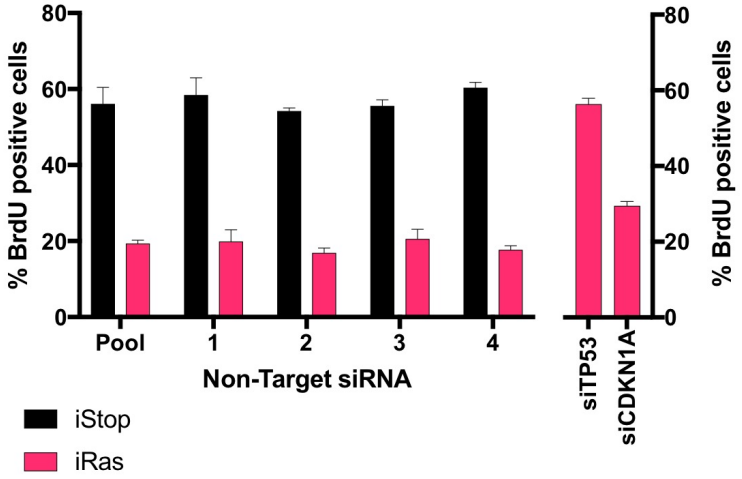

Figure 3.8 Deconvoluted Non-Target siRNA effect on BrdU incorporation compared to the siRNA pool

At day 2 of 4OHT, iStop and iRas cells were transfected with siRNA controls (negative = Non-Target; positive = siTP53 and siCDKN1A) for 72h. At day 4, cells were subjected to a 17h BrdU pulse, and then fixed and stained for BrdU incorporation using immunofluorescence. BrdU positive cells were quantified and % positive cells calculated (n=1, ±S.D).

4OHT = 4-hydroxytamoxifen, BrdU = bromodeoxyuridine.

Next, to evaluate the whole secondary screen, a summary heatmap was created for the three replicates of each plate (figure 3.9). It was clear the reproducibility between replicates was good for both plates. Compared to the siTP53 positive control there were three strong hits: CERS4, KEAP1 and LPCAT4. For robust validation of

significant hits, one-way ANOVA for both plates were calculated using the senescent control as the comparison parameter (i.e. iRas+NT). The criterion to validate hits was: genes with two or more individual siRNAs with significant senescent rescue. All the siRNAs causing a significant ($p<0.05$) bypass of senescence are shown in figure 3.10. 14 of the original 16 genes identified in the primary screen matched the validation criteria, further indicating siRNA screening is a robust technique for use in this system. It was striking to see two siRNAs close to siTP53 efficiency at bypassing OIS (siCERS4_1 and siKEAP1_3). CERS4 was the only gene with all four siRNAs significantly bypassing OIS; this highlights CERS4 as the top hit and was further validated in a variety of OIS assays (data in Chapter 4).

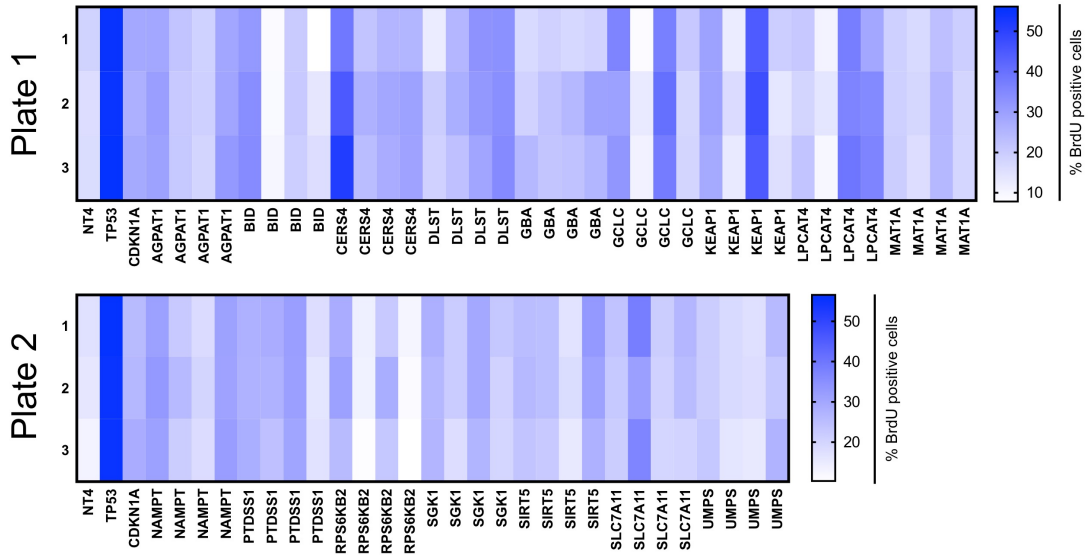

Figure 3.9 Heatmap representing a summary of the raw data for three replicates of each plate

After following the siRNA screening protocol (summarised in figure 3.7), % BrdU positive cells were calculated for each deconvoluted siRNA. A heatmap was generated to show the variability between replicates for each siRNA. Negative (NT4) and positive (siTP53 and siCDKN1A) controls are shown in the first three columns. The darker blue indicates higher BrdU positivity (scale bar on right).

BrdU = bromodeoxyuridine, NT = Non-Target.

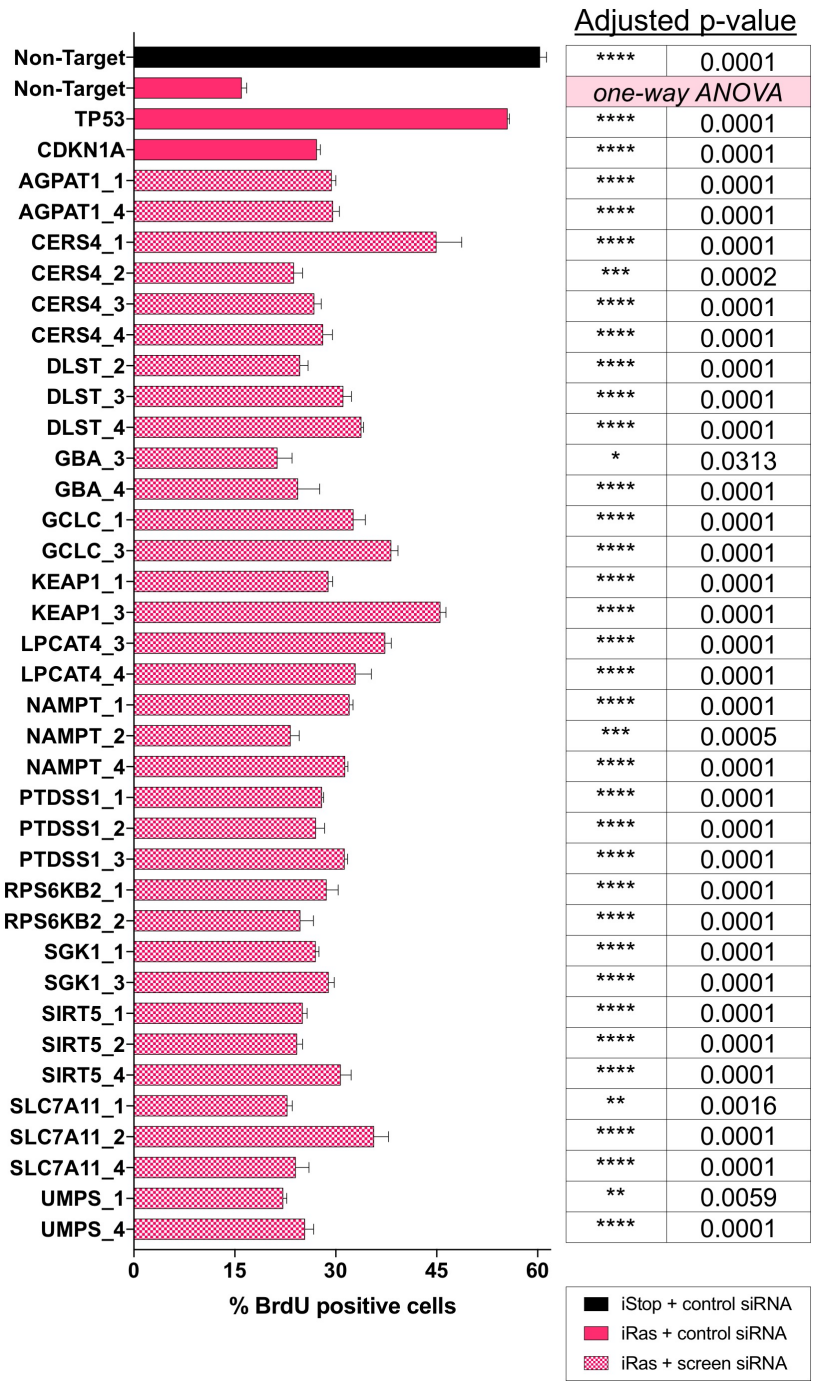

Figure 3.10 Validated hits with significant bypass of senescence

Hits were validated if they matched the following criteria: genes with two or more individual siRNAs with significant senescent rescue, measured as BrdU incorporation. Significance was calculated using the one-way ANOVA function in GraphPad. The legend, bottom right, specifies the cell conditions (n=3, ±S.E.M., ordinary one-way ANOVA (GraphPad)).

BrdU = bromodeoxyuridine.

3.2.2.2 p16 & p21

To further validate the hits, the secondary screen was independently repeated and siRNA-transfected cells stained with $p16^{INK4a}$ and $p21^{CIP1}$ antibodies. In a control plate, knockdown of $p16^{INK4a}$ and $p21^{CIP1}$ proteins was assessed (figure 3.11.A-B, note: siRNAs targeting $p16^{INK4a}$ and $p21^{CIP1}$ are annotated as their gene names, CDKN2A and CDKN1A respectively). The effect of CDKN2A and CDKN1A knockdown on BrdU incorporation was marginal (figure 3.11.B). This suggested there were discrepancies with the experimental system, possibly due to low efficiency siRNA transfection or inadequate 4OHT treatment. Still, the experimental plates were stained and analysed to further validate hits confirmed in *3.2.2.1*.

For both $p16^{INK4a}$ and $p21^{CIP1}$ staining, there was an experimental issue with one replicate of plate 2 (figure 3.12.A/3.13.A, yellow boxes). This further indicated this experiment was not consistent or conclusive. However, there were several genes with significant decreases in both $p16^{INK4a}$ and $p21^{CIP1}$ expression after siRNA knockdown, and most of these genes correlated with those validated by BrdU incorporation (figure 3.12.B/3.13.B). For example, the top hit from the BrdU screen siCERS4_1 resulted in a highly significant bypass in $p16^{INK4a}$ and $p21^{CIP1}$ expression. The second hit from the BrdU screen siKEAP1_3 and a second siKEAP1 also significantly bypassed $p21^{CIP1}$ expression. Additionally, two siRNAs targeting LPCAT4 significantly bypassed both BrdU incorporation and $p16^{INK4a}$ expression.

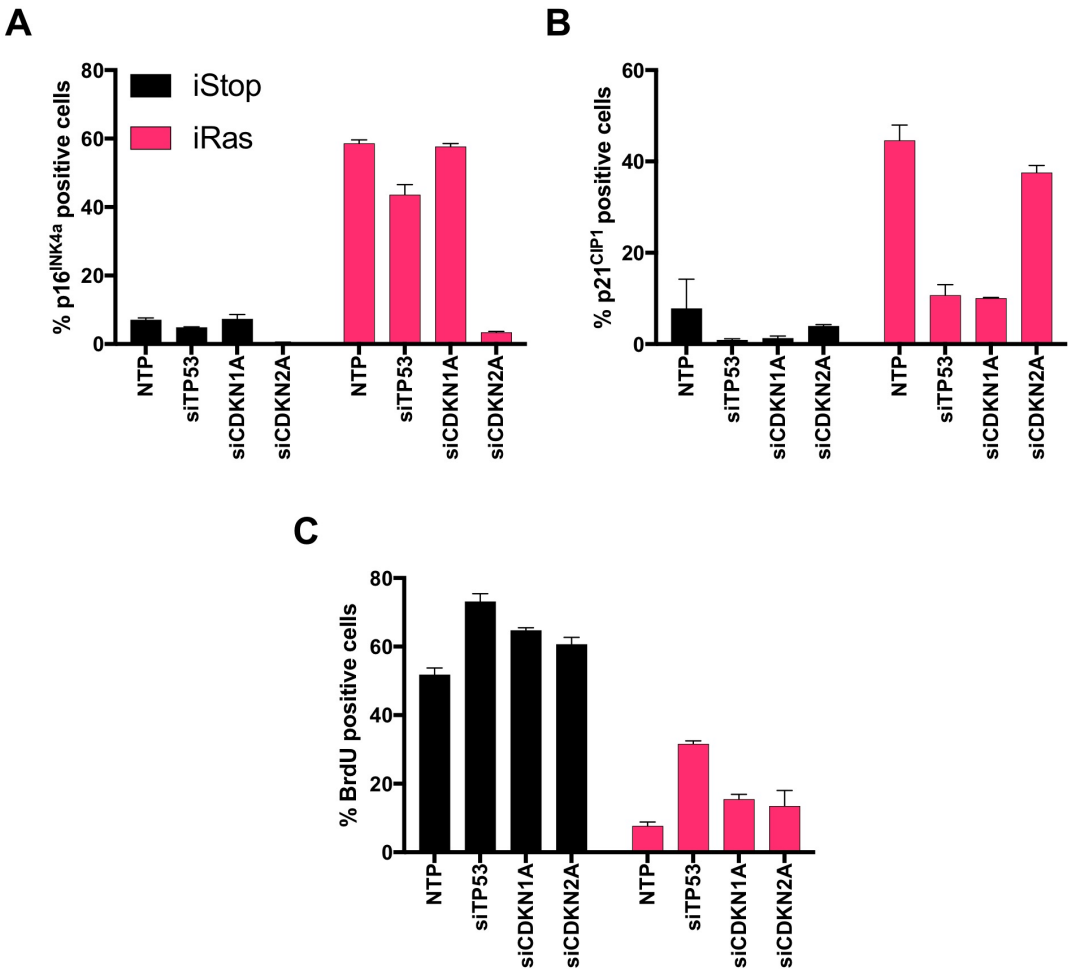

Figure 3.11 Knockdown of CDKN1A and CDKN2A diminished $p21^{CIP1}$ and $p16^{INK4a}$ protein expression and marginally bypassed senescence

At day 2 of 4OHT, iStop and iRas cells were transfected with specified siRNA for 72h. At day 5, cells were fixed and subjected to immunofluorescence staining for ***(A)*** *$p16^{INK4a}$ expression,* ***(B)*** *$p21^{CIP1}$ expression and* ***(C)*** *BrdU incorporation (after a 17h pulse of BrdU). Positive cells for each stain were quantified and % positivity calculated (n=1, ±S.D.)*

4OHT = 4-hydroxytamoxifen, BrdU = bromodeoxyuridine, NTP = Non-Target pool.

A

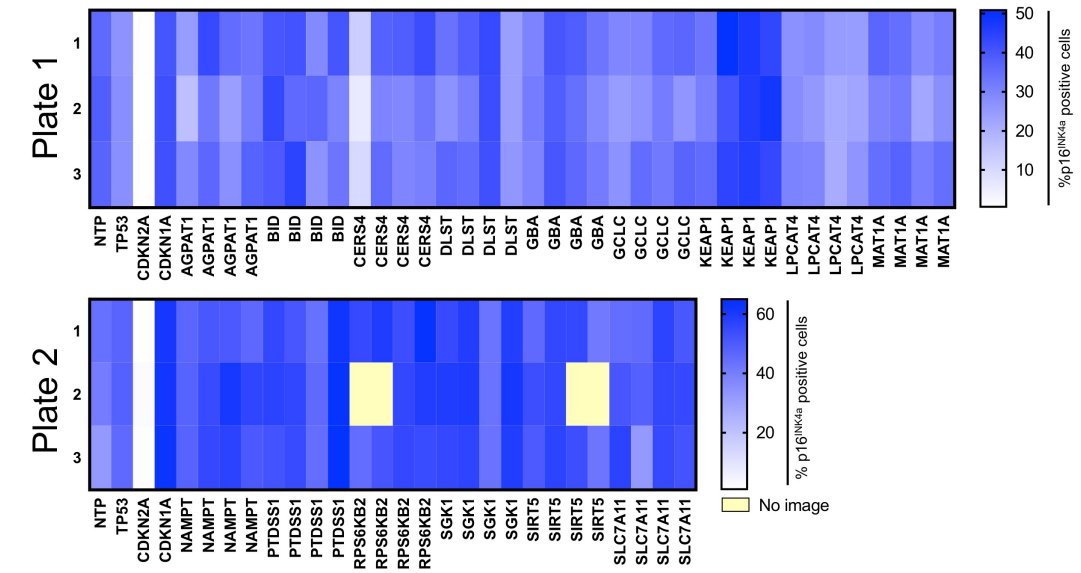

B

Gene ID	Average %p16+ cells	p-value (ANOVA)	No. significant siRNAs	BrdU validated?
AGPAT1	23	0.0029	1	✓
CERS4	10	0.0001	1	✓
DLST	25	0.0111	1	✓
LPCAT4	22/24	0.001/0.0097	2	✓

	Plate 1	Plate 2
NTP	37	39

Figure 3.12 p16 screen further validated 4 hits as bypassing senescence

(A) *After following the siRNA screening protocol (summarised in figure 3.7), % $p16^{INK4a}$ positive cells were calculated for each deconvoluted siRNA. A heatmap for each plate was generated to show the variability between replicates for each siRNA. Negative (NTP) and positive (siTP53, siCDKN2A and siCDKN1A) controls are shown in the first three columns. The lighter blue indicates lower $p16^{INK4a}$ positivity and likely a non-senescent state (scale bar on right). An experimental issue with replicate 2 meant some data from plate 2 were lost (indicated by the yellow boxes).* ***(B)*** *Hits were further validated if they caused a significant rescue in $p16^{INK4a}$ expression, in addition to increased BrdU incorporation. Significance was calculated using the ordinary one-way ANOVA function in GraphPad. The table summarises the significant hits from the p16 screen.*

A

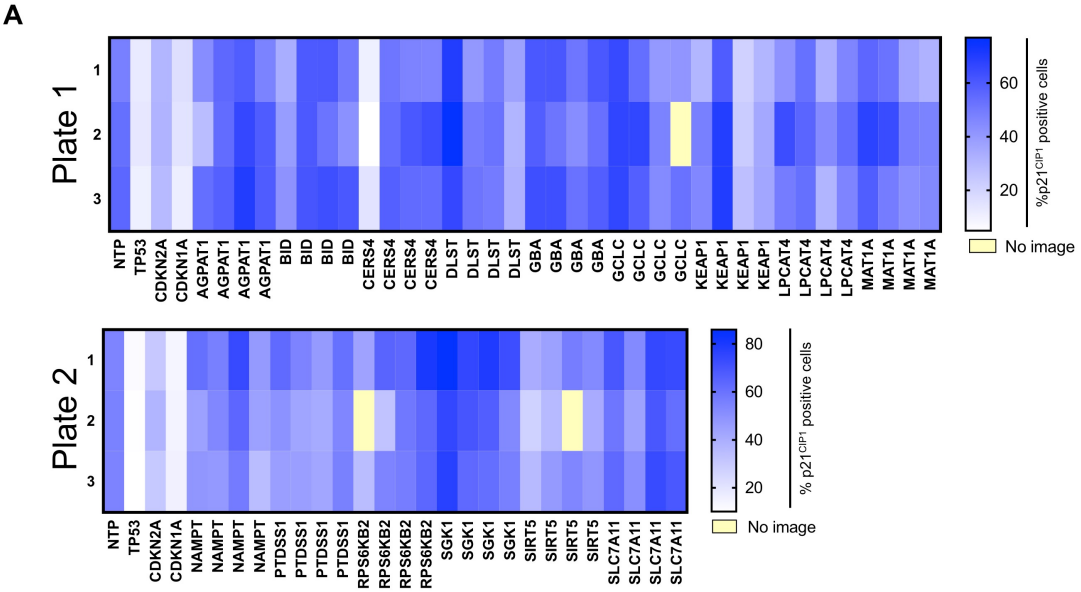

B

Gene ID	Average % p21+ cells	p-value (ANOVA)	No. significant siRNAs	BrdU validated?
CERS4	10	0.0001	1	✓
DLST	34	0.0001	1	✓
KEAP1	24/34	0.0001	2	✓
LPCAT4	36	0.0011	1	✓
SIRT5	34	0.0002	1	✓

	Plate 1	Plate 2
NTP	53	55

Figure 3.13 p21 screen further validated 5 hits as bypassing senescence

(A) *After following the siRNA screening protocol (summarised in figure 3.7), % $p21^{CIP1}$ positive cells were calculated for each deconvoluted siRNA. A heatmap for each plate was generated to show the variability between replicates for each siRNA. Negative (NTP) and positive (siTP53, siCDKN2A and siCDKN1A) controls are shown in the first three columns. The lighter blue indicates lower $p21^{CIP1}$ positivity and likely a non-senescent state (scale bar on right). An experimental issue with replicate 2 meant some data on both plates were lost (indicated by the yellow boxes).* ***(B)*** *Hits were further validated if they caused a significant rescue in $p21^{CIP1}$ expression, in addition to increased BrdU incorporation. Significance was calculated using the ordinary one-way ANOVA function in GraphPad. The table summarises the significant hits from the p21 screen.*

3.2.3 Functional annotation of screen hits

The 14 validated screen hits were functionally annotated and grouped based on similarity using the DAVID Bioinformatics Resource 6.8 'Functional Annotation' tool (Huang, Sherman and Lempicki, 2008). The list of validated genes was inputted as *Homo sapiens* 'Official Gene Symbols' and analysed for enriched GO terms and KEGG pathway maps. There was significant enrichment of genes involved in lipid biosynthetic processes, such as phospholipid and ceramide biosynthesis (table 3.2). Although this was a small group of genes, this analysis still indicated that lipid metabolism is implicated in OIS and warrants further interrogation. Furthermore, there was enrichment for genes involved in oxidative stress response; this group also included KEAP1, a regulator of NRF2-mediated response to oxidative stress, but this did not group with the 3 genes annotated in GO:0006979 by DAVID (table 3.2).

GO term	Process	Count	Genes	p-value
GO:0008610	Lipid biosynthesis	5	CERS4, PTDSS1, LPCAT4, AGPAT1, GBA	0.002
GO:0008654	Phospholipid biosynthesis	3	PTDSS1, LPCAT4, AGPAT1,	0.016
GO:0046513	Ceramide biosynthesis	2	CERS4, GBA	0.050
GO:0006979	Oxidative stress response	3	GBA, GCLC, SLC7A11	0.047

Table 3.2 GO terms enriched in the validated gene list

3.2.4 Summary

In this section, 14 of the 16 hits identified in the primary screen were validated, by deconvoluting pooled siRNAs and staining for BrdU incorporation and $p16^{INK4a}$/$p21^{CIP1}$ expression. This suggested the 14 genes have a vital role in OIS metabolism (table 3.3 for overview). When analysed by functional annotation, it was found 5/14 genes were mapped to lipid metabolism and 4/14 genes were mapped to the oxidative stress response.

Gene ID	KEGG Pathway Classification	Validation		
		BrdU	p16	p21
AGPAT1	Glycerolipid metabolism	✓	✓	✗
CERS4	Sphingolipid metabolism	✓	✓	✓
DLST	Citrate cycle (TCA cycle)	✓	✗	✗
GBA	Sphingolipid metabolism	✓	✗	✗
GCLC	Glutathione metabolism	✓	✓	✓
KEAP1	Ubiquitin mediated proteolysis	✓	✗	✓
LPCAT4	Glycerophospholipid metabolism	✓	✓	✓
NAMPT	Nicotinate and nicotinamide metabolism	✓	✗	✗
PTDSS1	Glycerophospholipid metabolism	✓	✗	✗
RPS6KB2	Signalling pathways	✓	✗	✗
SGK1	Signalling pathways	✓	✗	✓
SIRT5	Sirtuins	✓	✗	✗
SLC7A11	Amino acid transport	✓	✗	✗
UMPS	Pyrimidine metabolism	✓	not tested	

Table 3.3 Summary of secondary screen results, including the top KEGG pathway classification for each gene

3.3 Chapter summary

In this chapter, the aim was to identify novel metabolic regulators of OIS using high-content siRNA screening. 16 genes were found bypassing OIS after pooled siRNA knockdown and 14 were validated by deconvoluting siRNAs. Additional screening for $p16^{INK4a}$/$p21^{CIP1}$ expression was used to further characterise some of the hits. Of these 14 essential OIS genes, there was a significant enrichment of genes involved in lipid biosynthetic processes, such as the top hit ceramide synthase 4 (CERS4). siRNA targeting CERS4 caused a significant bypass in BrdU incorporation (with 4 siRNAs) and $p16^{INK4a}$/$p21^{CIP1}$ expression (with 1 siRNA).

From this data, it can be concluded lipid metabolism has an important role regulating OIS that has not been extensively studied in current literature. In the following chapters investigations are directed to further validate CERS4 during OIS and examine how lipid metabolism may be altered.

Chapter Four: Validation of CERS4 as an essential lipid metabolic regulator for OIS

In chapter 3, lipid metabolism was identified as an important process for OIS and CERS4 as a key enzyme for this association. Results from the siRNA screen requires thorough validation, therefore the next aim for this thesis was to extensively validate CERS4 as a regulator of OIS. As described in *1.1.2*, OIS has a heterogeneous phenotype, thus there are many assays to measure the senescent state of a cell. Here, readouts for proliferation, SA β-galactosidase activity and tumour suppressor and SASP activation (by western blotting and qPCR) were measured. In addition, the effect of CERS4 knockdown was tested in a replicative senescence model. Lastly, pharmacological inhibition of ceramide metabolism was tested to see if targeting ceramides can induce senescence in normal cells. This chapter describes the results from these experiments utilising RNAi genetic knockdowns of CERS4, pharmacological manipulation of ceramide metabolism and senescence assays.

4.1 Knockdown of CERS4 robustly bypasses OIS

4.1.1 Transient CERS4 knockdown rescues proliferation and SA β-galactosidase activity

To investigate the correlation between knockdown efficiency and effect on senescence, mRNA expression of CERS4 in OIS, after targeting expression with siRNA, was analysed. Knockdown efficiency of four siRNAs (i.e. those deconvoluted from the pooled siRNA used in the primary screen) was measured by qPCR 72 hours post transfection. At the mRNA level, CERS4 expression was approximately 50% downregulated in iRas compared to iStop (figure 4.1.A, compare first two bars); although this suggested a decrease in CERS4 activity in OIS, this was not the case, as described in Chapter 5. The discrepancy between CERS4 mRNA expression and activity is discussed in *7.4.1*. siRNA no.1 had the best mRNA knockdown efficiency followed by no.3 and 4 (figure 4.1.A). siRNA no.2 did not knockdown CERS4 mRNA (figure 4.1.A, compare bar 2 and 4). Unfortunately,

protein levels of CERS4 could not be detected with the antibodies tested (figure 2.5). Importantly, all four siRNAs targeting CERS4 significantly increased BrdU incorporation (figure 3.10), correlating with the efficiency of siRNA knockdown (figure 4.1.A). Therefore, for further experiments, just siRNA no.1 and pooled siRNA were used to keep experiments resourceful and practical. IMR90 were targeted for siRNA knockdown of CERS4 at day 5 and day 8 (see figure 2.3 for experimental outline) and proliferation, as measured by BrdU incorporation, was significantly restored at both time points (figure 4.1.B). In addition, targeting CERS4 with siRNA strongly reduced SA β-galactosidase activity (figure 4.1.C).

4.1.2 Generation of an shRNA targeting CERS4 that recapitulates siRNA knockdown

To support data from transient RNAi, stable RNAi was tested by producing a retroviral vector (pSUPER.retro.puro, hereafter referred to as pRS) that allows the long-term expression of siRNA sequences. The cloning method from OligoEngine is described in *2.3*, and was performed with Dr Andrea Quintanilla. When vectors were cloned, IMR90 were infected as described in *2.2.4* and experiments to test the effectiveness of the stable knockdown were performed. Firstly, the knockdown efficiency of the cloned shRNA was extremely good (figure 4.2.A). Corresponding to the siRNA experiments, CERS4 mRNA expression was ~50% downregulated in iRas compared to iStop (figure 4.1.A, compare first two bars). As with the siRNA knockdowns, proliferation was significantly rescued when measuring the cell content by crystal violet staining (figure 4.2.B) and BrdU incorporation (figure 4.2.C). The activation of senescence marker SA β-galactosidase activity was also decreased at day 8 of OIS when the expression of CERS4 was depleted (figure 4.2.D).

4.1.3 Summary

In this section, confirmation that knockdown of CERS4 expression robustly bypasses OIS is shown. This was measured using proliferation readouts and SA β-galactosidase activity. The next objective for this section was to establish the importance of CERS4 for OIS by analysing tumour suppressor pathways and the SASP. As discussed in *1.1.2*, the expression of these components is essential for OIS progression.

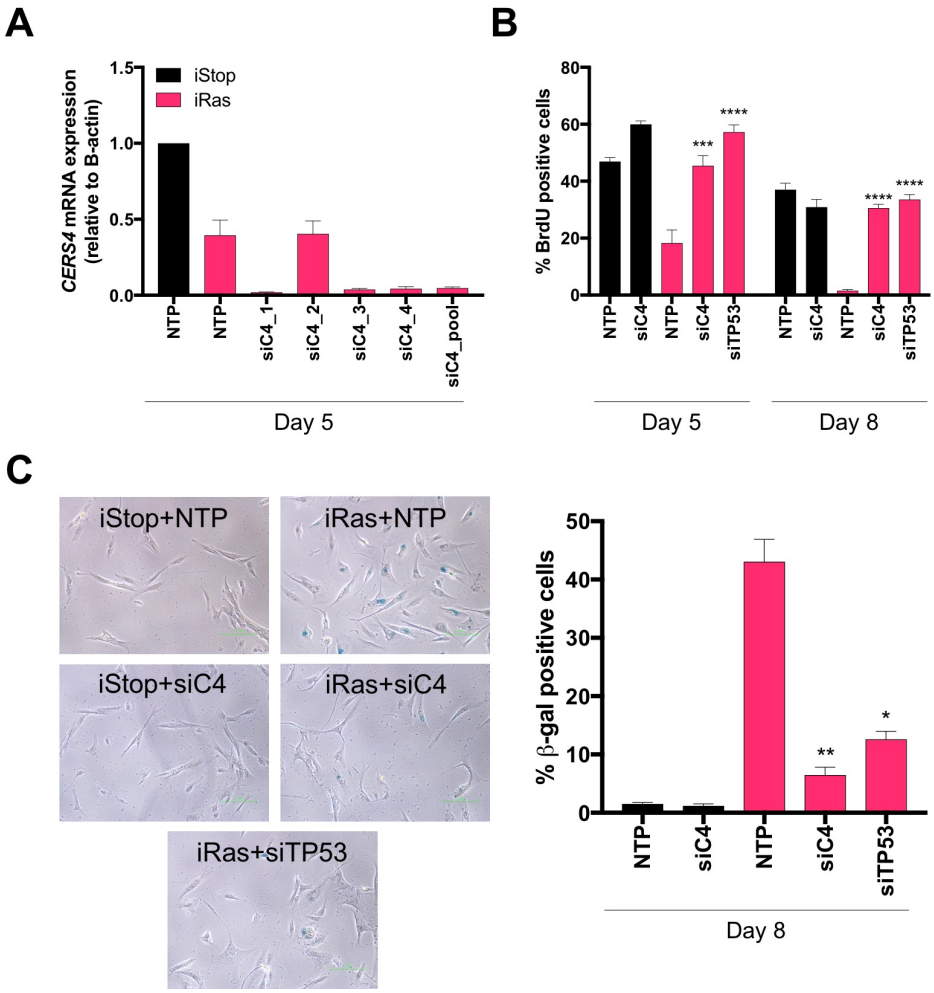

Figure 4.1 Targeting CERS4 with siRNA depleted CERS4 mRNA levels, increased proliferation and decreased SA β-galactosidase activity

(A) *4OHT-treated iStop and iRas were transfected with control (NTP) and deconvoluted siRNAs targeting CERS4 for 72h. RNA was extracted, cDNA synthesised and qPCR used to detect mRNA levels of CERS4. β-actin was used as a housekeeping gene (n=1, ±S.D.). Next, 4OHT-treated iStop and iRas were transfected with siCERS4 no.1 and controls; Day 8 cells were transfected twice as described in figure 2.3. These cells were:* ***(B)*** *subjected to a 17h BrdU pulse, fixed and stained for BrdU incorporation using immunofluorescence. BrdU positive cells were quantified and % positive cells calculated (n=3, ±S.E.M., two-tailed Student's t-test).* ***(C)*** *fixed and stained for SA β-galactosidase activity. SA β-gal positive cells were quantified from images and % positive cells calculated (right graph) (n=3, ±S.E.M., two-tailed Student's t-test, representative images).*

*4OHT = 4-hydroxytamoxifen, BrdU = bromodeoxyuridine, NTP = Non-Target pool, siC4 = siCERS4. * = p≤0.05, ** = p≤0.01, *** = p≤0.001, **** = p≤0.0001.*

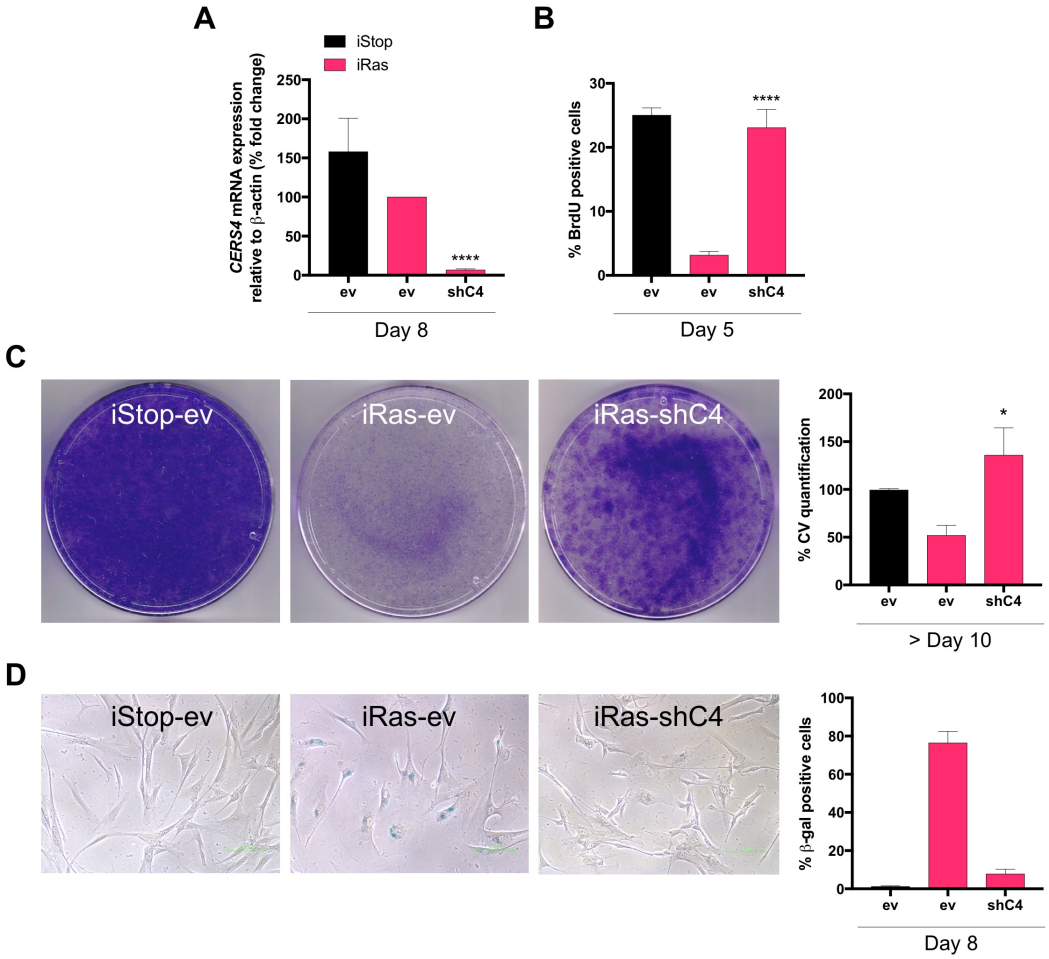

Figure 4.2 Stable mRNA knockdown of CERS4 rescued proliferation and SA β-galactosidase activity

iStop and iRas infected with ev and shC4 were plated into 4OHT at day 0 for OIS analysis at various time points (indicated on figures). ***(A)*** *mRNA expression levels of CERS4 were measured by qPCR. β-actin was used as a housekeeping gene (n=3, ±S.E.M., two-tailed Student's t-test).* ***(B)*** *Cells were subjected to a 17h BrdU pulse, fixed and stained for BrdU incorporation using immunofluorescence. BrdU positive cells were quantified and % positive cells calculated (n=3, ±S.E.M., two-tailed Student's t-test).* ***(C)*** *Cell content over long-term OIS (>10 days 4OHT) was measured using crystal violet staining and quantified by measuring the absorbance of dissolved CV at 595nm (right graph) (n=3, ±S.E.M., two-tailed Student's t-test, representative images).* ***(D)*** *Cells were fixed and stained for SA β-galactosidase activity. SA β-gal positive cells were quantified from images and % positive cells calculated (right graph) (n=1, ±S.D.).*

*4OHT = 4-hydroxytamoxifen, BrdU = bromodeoxyuridine, ev = pRS-empty vector, shC4 = pRS-shCERS4, CV = crystal violet. * = p≤0.05, **** = p≤0.0001.*

4.2 CERS4 regulates p53 and p16 tumour suppressor pathways

To investigate if CERS4 has a role in the regulation of essential tumour suppressor pathways in OIS, protein levels of p53 and $p16^{INK4a}$ pathways were assessed after genetic targeting of CERS4 expression. First, protein expression of p53, $p21^{CIP1}$ (a tumour suppressor downstream of p53) and $p16^{INK4a}$ was measured by immunofluorescence and western blot. shRNA knockdown of CERS4 resulted in significant ($p \leq 0.0001$) decrease in p53, $p21^{CIP1}$ and $p16^{INK4a}$ levels as measured by immunofluorescence (figure 4.3.A, images; 4.3.B, quantification). siRNA knockdown of CERS4 resulted in decreased p53 and $p21^{CIP1}$ expression at day 5 and 8 as measured by western blot (figure 4.3.C, compare lanes 3-4 and 8-9).

Next, to determine if CERS4 is required for the transcription of essential tumour suppressor pathways in OIS, qPCR was used to measure to mRNA levels of *CDKN2A* (p16), *CDKN2B* (p15, a tumour suppressor analogous to p16) and *CDKN1A* (p21). At day 8 of 4OHT, mRNA expression of *CDKN2A*, *CDKN2B* and *CDKN1A* were significantly ($p \leq 0.001$) decreased when CERS4 was depleted by shRNA (figure 4.4). This expression data for tumour suppressors suggests that CERS4 is an essential mechanistic component of OIS induction and/or maintenance.

Here, CERS4 has been confirmed fundamental for the expression of tumour suppressor pathways in OIS, by perturbing CERS4 expression and measuring the protein and mRNA levels of p53/p21 and p16/p15. Next, the involvement of CERS4 in another essential OIS effector programme, the SASP, was examined.

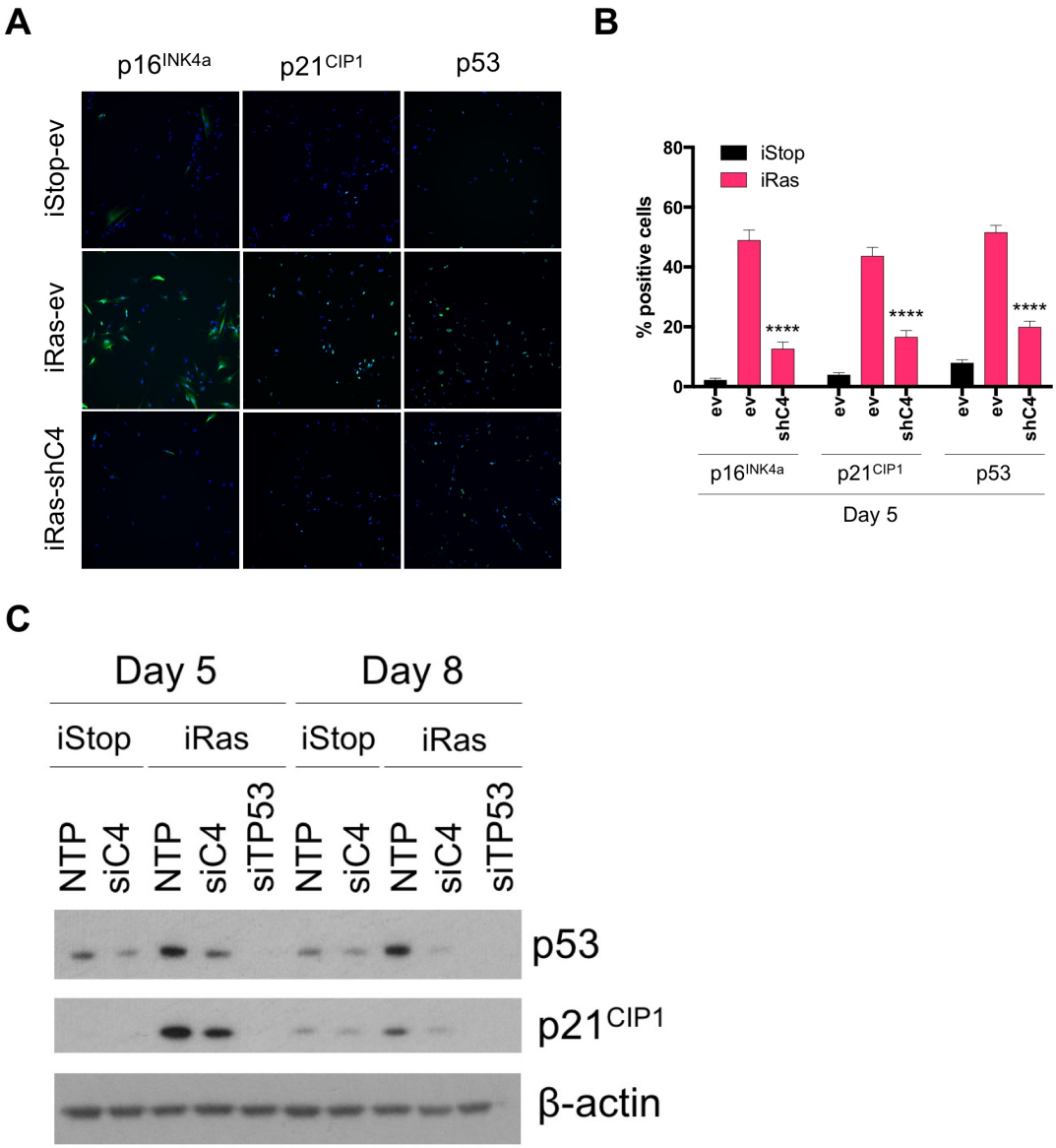

Figure 4.3 CERS4 knockdown significantly reduced expression of tumour suppressors

iStop and iRas were infected with empty vector (ev) and a stable shRNA targeting CERS4 expression (shC4). Cells were selected with puromycin and plated into 4OHT at day 0 for tumour suppressor expression analysis at day 5. ***(A)*** *Images of immunofluorescent staining for $p16^{INK4a}$, $p21^{CIP1}$ and p53 proteins.* ***(B)*** *Quantification of images in (A) using the HCS software MetaXpress (n=3, ±S.E.M., two-tailed Student's t-test).* ***(C)*** *iStop and iRas were subjected to reverse transfection with Non-Target and siCERS4 at day 2 of 4OHT. Cell pellets were collected and lysed on day 5, and subjected to western blotting to detect $p21^{CIP1}$ and p53. Briefly, 20µg lysate was separated by SDS-PAGE, using a 4-12% Bis-Tris gel. Proteins were transferred onto*

a nitrocellulose membrane and blocked with 5% milk. Antibodies for blotted proteins were incubated on the membranes and ECL used to visualize the bands (representative of 3 independent experiments). β-actin was used as a loading control (NOTE: the western blot for β-actin in figure 4.3.C was the same for the β-actin in figure 4.5).

*4OHT = 4-hydroxytamoxifen, BrdU = bromodeoxyuridine, ev = empty vector (pRS), shC4 = pRS-shCERS4, NTP = Non-Target pool, siC4 = siCERS4. **** = p≤0.0001.*

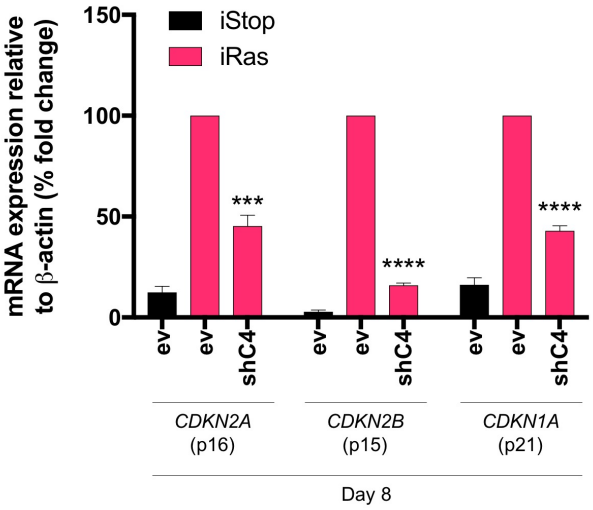

Figure 4.4 CERS4 knockdown significantly reduced transcription of tumour suppressors

iStop and iRas infected with ev and shC4 were analysed for tumour suppressor transcription at day 8 of 4OHT. RNA was extracted, cDNA synthesised and qPCR used to detect mRNA levels of genes encoding p16, p15 and p21. β-actin was used as a housekeeping gene (n=3, ±S.E.M., two-tailed Student's t-test).

*4OHT = 4-hydroxytamoxifen, ev = empty vector (pRS), shC4 = pRS-shCERS4 *** = p≤0.001, **** = p≤0.0001.*

4.3 CERS4 regulates the SASP

As described previously, the expression of the SASP is a vital program for OIS. To examine the role for CERS4 in SASP regulation, the expression of well-known SASP proteins IL1β, IL6 and IL8 was analysed by western blot. It is important to note here SASP expression is a phenotype of established OIS and can only be seen from ~day 5 of 4OHT treatment. CERS4 knockdown strongly ablated the expression of SASP proteins IL1β, IL6 and IL8 at day 8 (figure 4.5, compare lanes 8-9). Targeting CERS4 expression also prevented the initial accumulation of IL1β and IL6 at day 5 (figure 4.5, compare lanes 3-4), further suggesting CERS4 is essential for OIS progression. p53 knockdown did not regulate the expression of SASP factors (figure 4.5, lanes 5&10, as previously hypothesised by Coppé *et al.* (2008).

To investigate the role of CERS4 in the regulation of additional SASP factors, transcriptomic analysis was performed. Biological triplicate RNA samples were extracted from iStop/iRas with Non-Target and iRas with CERS4 siRNA, at day 5 and 8 of 4OHT. RNA samples were analysed using targeted RNA sequencing: AmpliSeq transcriptomics, performed by Edinburgh Clinical Research Facility (see *2.9* for methods). Firstly, table 4.1 shows mapped reads and % valid reads per sample were above-expected for the analysis (~8million and ≥90%, respectively). Next, gene expression analysis was performed using the Babelomics 5 'RNA-seq class comparison' tool (Alonso et al., 2015), and comparisons were made related to the OIS control (i.e. iRas with Non-Target). The statistic values for 57 SASP factors are plotted as % fold change compared to iRas (figure 4.6.A). CERS4 knockdown resulted in a strong bypass of SASP transcriptional activation. mRNA expression levels of SASP factors *IL6* and *IL8* were validated by qPCR and again CERS4 knockdown caused a significant ($p<0.0001$) ablation of SASP transcription (figure 4.6.B).

In this section, by perturbing expression, CERS4 has been identified as essential for transcription and protein expression of the SASP in OIS. In the next section, CERS4 was targeted in a different model of senescence to determine if this metabolic enzyme is ubiquitously vital for senescence mechanisms.

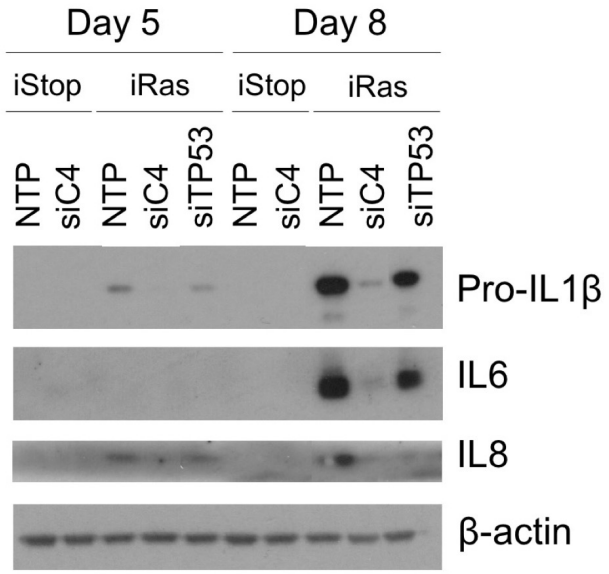

Figure 4.5 CERS4 knockdown ablated expression of SASP proteins IL1β, IL6 and IL8

iStop and iRas were subjected to reverse transfection with Non-Target and siCERS4 at day 2 and 5 of 4OHT. Cell pellets were collected and lysed on day 8, and subjected to western blotting to detect IL1β, IL6 and IL8. Briefly, 20μg lysate was separated by SDS-PAGE, using a 4-12% Bis-Tris gel. Proteins were transferred onto a nitrocellulose membrane and blocked with 5% milk. Antibodies for blotted proteins were incubated on the membranes and ECL used to visualize the bands (representative of 3 independent experiments). β-actin was used as a loading control (NOTE: the western blot for β-actin in figure 4.3.C was the same for the β-actin in figure 4.5).

4OHT = 4-hydroxytamoxifen, NTP = Non-Target pool, siC4 = siCERS4.

Time point	Sample	Replicate	Chip	Mapped reads	Valid reads
Day 5	Stop+NTP	1	1	11,070,707	95.75%
		2	2	12,592,855	96.31%
		3	2	10,862,693	95.87%
	Ras+NTP	1	2	11,162,864	96.57%
		2	2	11,632,930	96.67%
		3	2	11,260,321	96.41%
	Ras+siC4	1	2	12,291,981	95.91%
		2	2	10,876,947	95.82%
		3	2	11,447,104	95.51%
Day 8	Stop+NTP	1	1	10,820,372	95.63%
		2	3	9,788,997	96.21%
		3	3	11,925,605	96.33%
	Ras+NTP	1	3	10,915,829	96.60%
		2	3	12,836,493	96.41%
		3	3	11,072,589	96.65%
	Ras+siC4	1	3	7,421,699	95.76%
		2	3	12,489,109	96.04%
		3	3	9,790,041	95.74%

Table 4.1 Overview of the transcriptomics statistics

AmpliSeq transcriptomics was performed by Edinburgh Clinical Research Facility on the above samples. Briefly, cDNA was prepared by reverse transcription of RNA samples. Target genes were amplified and ligated to sequencing adapters to create libraries for next-generation sequencing. Sequencing outputs were analysed using the AmpliSeqRNA plugin; the run statistics summarised in this table were specified from this analysis. See 2.8 for further details on the methods. NTP = Non-Target pool, siC4 = siCERS4.

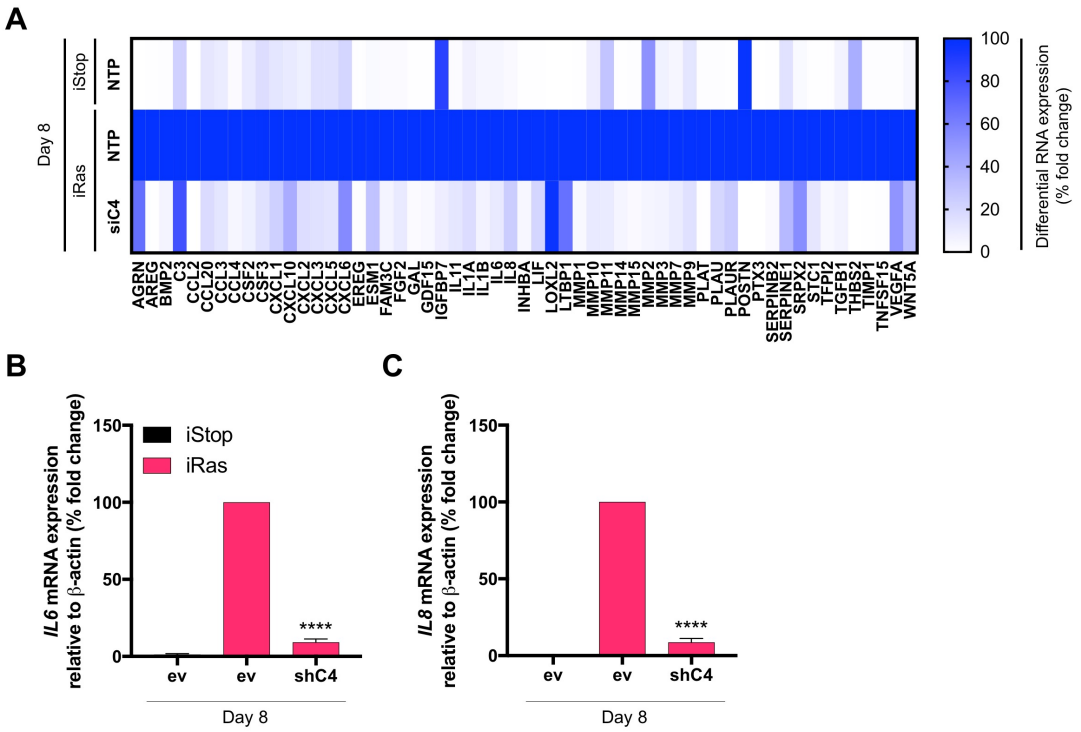

Figure 4.6 Transcriptomics and qPCR confirmed decreased transcription of SASP factors after CERS4 knockdown

(A) *Transcriptomic data analysed using AmpliSeqRNA plugin was subjected to gene expression analysis (see table 4.1 for sample info). The Babelomics 5 'RNA-seq class comparison' tool (Alonso et al., 2015) was used. For this analysis, the normalization method used was TMM and Benjamini and Hochberg multiple-test correction was used to calculate the False Discovery Rate and adjusted p-value (<0.05). Here, the statistic values for 57 SASP factors are plotted as % fold change compared to the OIS control (i.e. iRas with Non-Target). Next, iStop and iRas infected with ev and shC4 were analysed for SASP transcription at day 8 of 4OHT. RNA was extracted, cDNA synthesised and qPCR used to detect mRNA levels of:* ***(B)*** *IL6* ***(C)*** *IL8. β-actin was used as a housekeeping gene (n=3, ±S.E.M., two-tailed Student's t-test).*

ev = empty vector (pRS), shC4 = pRS-shCERS4, NTP = Non-Target pool, siC4 = siCERS4,
***** = p≤0.0001*

4.4 CERS4 knockdown delays replicative senescence

To determine if CERS4 is required for senescence triggered by a different mechanism to OIS, CERS4 was targeted for stable knockdown in parental IMR90 and repeatedly passaged. Population doublings were measured until they reached a cell cycle arrest typified by replicative senescence. First, CERS4 mRNA expression was decreased throughout the early, mid and late passages, indicating the shRNA was active throughout the experiment (figure 4.7.A). Next, the population doublings indicated CERS4 knockdown resulted in a partial increase in lifespan compared to control throughout the experiment. However, replicative senescence eventually overcomes the CERS4 knockdown and cells start to arrest at passage 27 (figure 4.7.B). In addition, SA β-galactosidase activity was significantly decreased with CERS4 knockdown at passage 25, when the control cells were starting to senesce (figure 4.7.C).

As described previously, replicative senescence can have different senescent markers due to DNA damage resulting from telomere shortening rather than oncogene activation. To analyse this, the expression of tumour suppressors p53, $p21^{CIP1}$ and $p16^{INK4a}$ was measured by western blot (figure 4.8). At passage 24 there was no regulation of p53 or $p21^{CIP}$, suggesting CERS4 has no effect on p53 activation by telomere shortening rather than oncogene-induced. Interestingly, $p16^{INK4a}$ expression was repressed in CERS4 knockdown as the experiment progressed (figure 4.8.B). Together, this data suggests CERS4 is not required for telomere shortening and subsequent p53 activation, but is independently required for the activation of the INK4a-ARF locus in replicative senescence (concurring with observations made by Herbig *et al.* (2004)).

Overall, this data suggests CERS4 is essential for replicative senescence, as well as oncogene-induced senescence, and may play a role for the activation of the INK4a-ARF locus in replicative senescence. Next, pharmacological inhibitors of ceramide metabolic enzymes were used to target ceramide and the resulting effect on senescence was analysed.

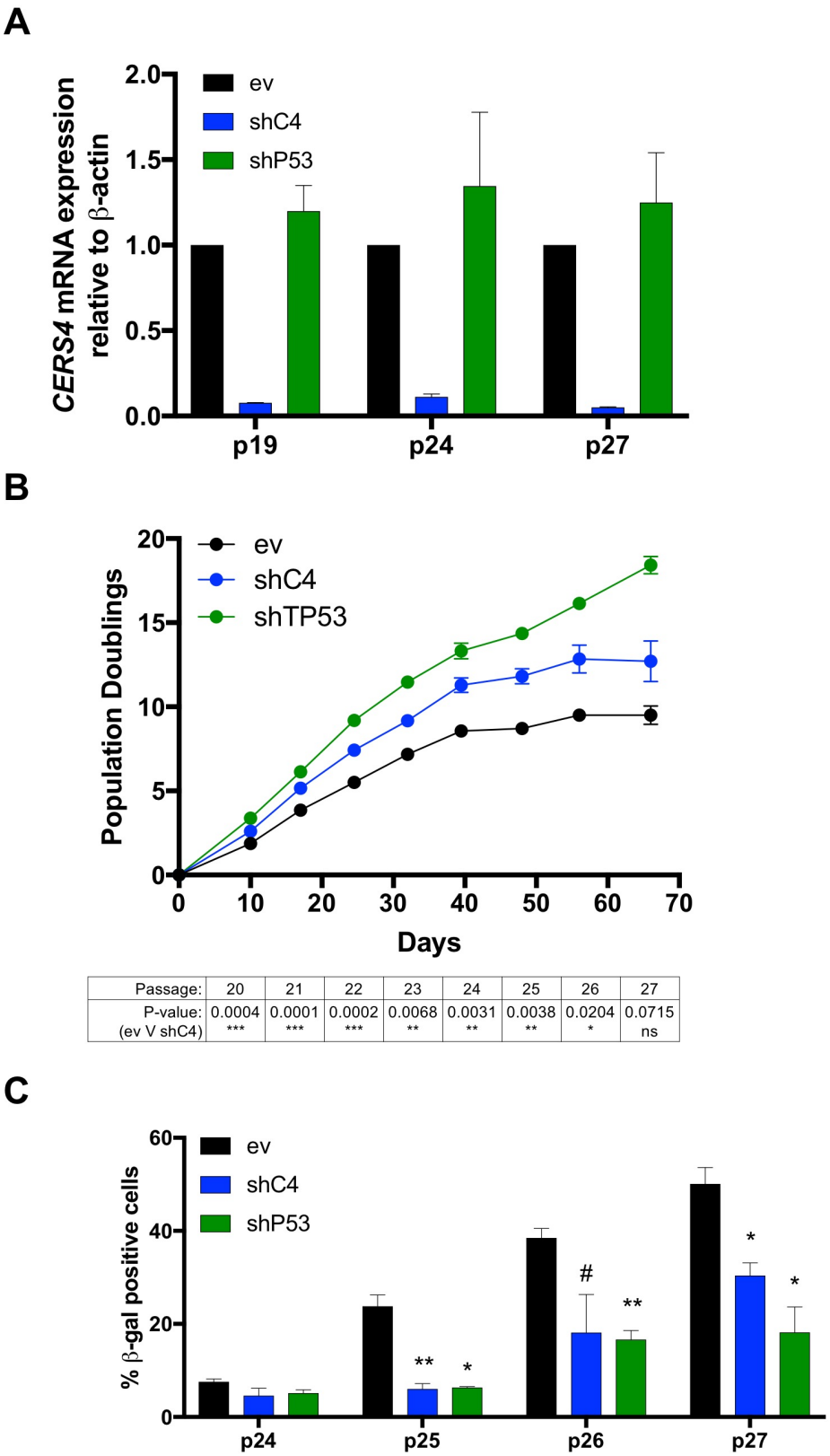

Passage:	20	21	22	23	24	25	26	27
P-value: (ev V shC4)	0.0004 ***	0.0001 ***	0.0002 ***	0.0068 **	0.0031 **	0.0038 **	0.0204 *	0.0715 ns

Figure 4.7 Persistent CERS4 knockdown enforces increased growth in IMR90 and delays replicative senescence (legend next page)

Figure 4.7 *IMR90 were infected with empty vector (ev) and stable shRNAs targeting CERS4 (shC4) and TP53 (shTP53) expression. Throughout, cells were selected with puromycin and pellets collected at each passage for further analysis.* ***(A)*** *mRNA expression levels of CERS4 were measured by qPCR. β-actin was used as a housekeeping gene (n=2, ±S.D.).* ***(B)*** *Population doublings of the three cell types were measured. Briefly, at each passage cells were counted and re-seeded at 500,000 cells per 10cm dishes. A formula was used to calculate the P.D. (see methods 2.2.5) (n=3, ±S.E.M., two-tailed Student's t-test).* ***(C)*** *Cells were fixed and stained for SA β-galactosidase activity. SA β-gal positive cells were quantified from images (not shown) and % positive cells calculated (n=3, ±S.E.M., two-tailed Student's t-test, # = n=2 ±S.D.).*

*ev = empty vector (pRS), shC4 = pRS-shCERS4, * = p≤0.05, ** = p≤0.01, *** = p≤0.001, ns = not significant.*

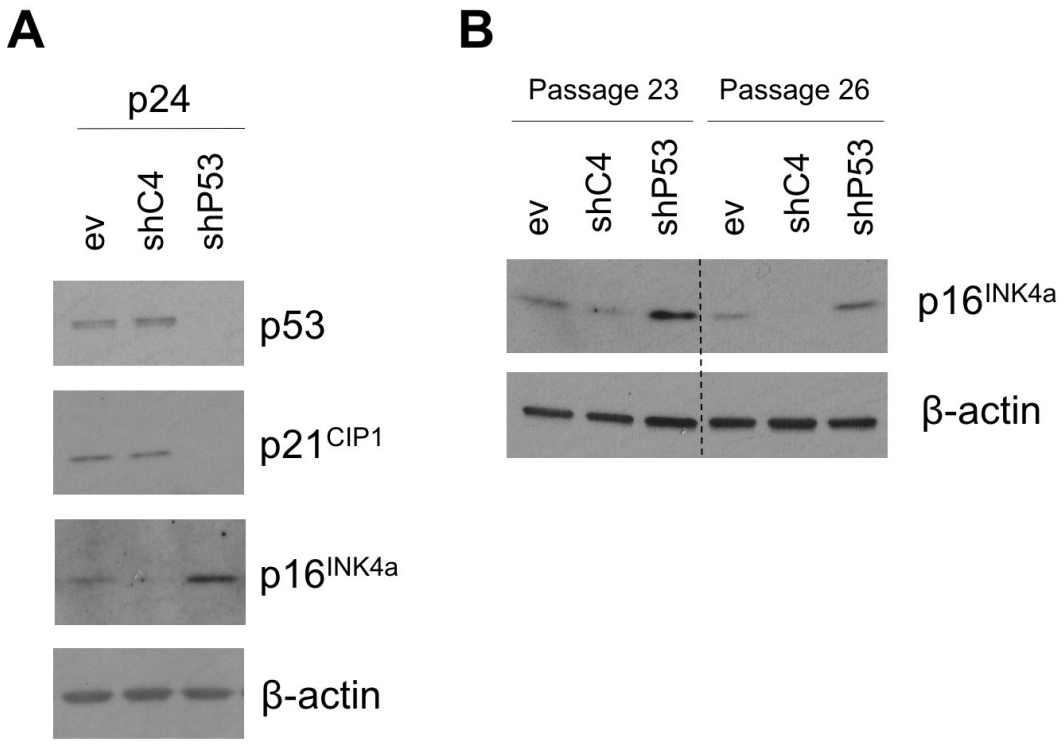

Figure 4.8 CERS4 regulated the activation of $p16^{INK4a}$ in replicative senescence but not the activation of p53

IMR90 were infected with empty vector (ev) and stable shRNAs targeting CERS4 (shC4) and TP53 (shTP53) expression. Throughout, cells were selected with puromycin and pellets collected at each passage for western blot analysis of tumour suppressors $p16^{INK4a}$, $p21^{CIP1}$ and p53. 15μg

cell lysate was separated on 10-20% Tris-Glycine gels and subjected to western blotting of stated proteins. β-actin was used as a loading control. ***(A)*** *Western blots for passage 24 (representative of two independent experiments).* ***(B)*** *Western blot of $p16^{INK4a}$ for different mid and late passages. Dotted line indicates a cropped membrane (representative of two independent experiments).*

ev = empty vector (pRS), shC4 = pRS-shCERS4.

4.5 Pharmacological inhibition of ceramide metabolic enzymes induces a senescence-like cell cycle arrest

CERS4 is a metabolic enzyme involved in the synthesis of ceramides and as shown in this chapter, CERS4 is essential for senescence. Therefore, it can be hypothesised ceramides are also vital for senescence, and increased cellular ceramide content may be able to induce a stable cell cycle arrest. As summarised by Morad and Cabot (2013), sphingosine kinase, ceramidase and ceramide kinase are enzymes that degrade or modify ceramide. Inhibiting post-synthesis modification or degradation of ceramide theoretically results in accumulated ceramide content and thus a similar environment hypothesised for OIS. To ascertain if this hypothesis was correct, inhibitors of these three enzymes were tested for their ability to induce senescence (figure 4.9.A). For this experiment, parental IMR90s were treated with the inhibitors and vehicle controls for 48 hours, and analysed for various senescent markers. Firstly, the inhibitor of sphingosine kinase, SKI-1, caused a potent reduction in proliferation (figure 4.9.B). There was increased expression of $p21^{CIP1}$, p53, pST/Q and ϒH2AX (figure 4.9.B); and ~5-fold increase in SA β-gal activity (bars 1-2, figure 4.9.E). Second, the inhibitor of acidic ceramidase, ceranib-1, caused a 2-fold reduction in proliferation and increased expression of $p21^{CIP1}$and pST/Q (figure 4.9.C); and a minimal increase in SA β-gal activity (bars 3-4, figure 4.9.E). Finally, the inhibitor of ceramide kinase, NVP-231, caused a 6-fold reduction in proliferation and increased expression of $p21^{CIP1}$, p53 and pST/Q (figure 4.9.D); and ~4-fold increase in SA β-gal activity (bars 5-6, figure 4.9.E).

In summary, this data shows pharmacological manipulation of ceramide metabolism, leading to accumulation of ceramides, results in a proliferation arrest in IMR90. This coincides with expression of tumour suppressors, DNA damage markers and slightly increased SA β-gal activity; overall suggesting a senescence-like stable cell cycle arrest. However, this data is not conclusive because the inhibitors were not tested for functional activity. Therefore, mass spectrometry is required to confirm levels of ceramide after inhibition of these enzymes.

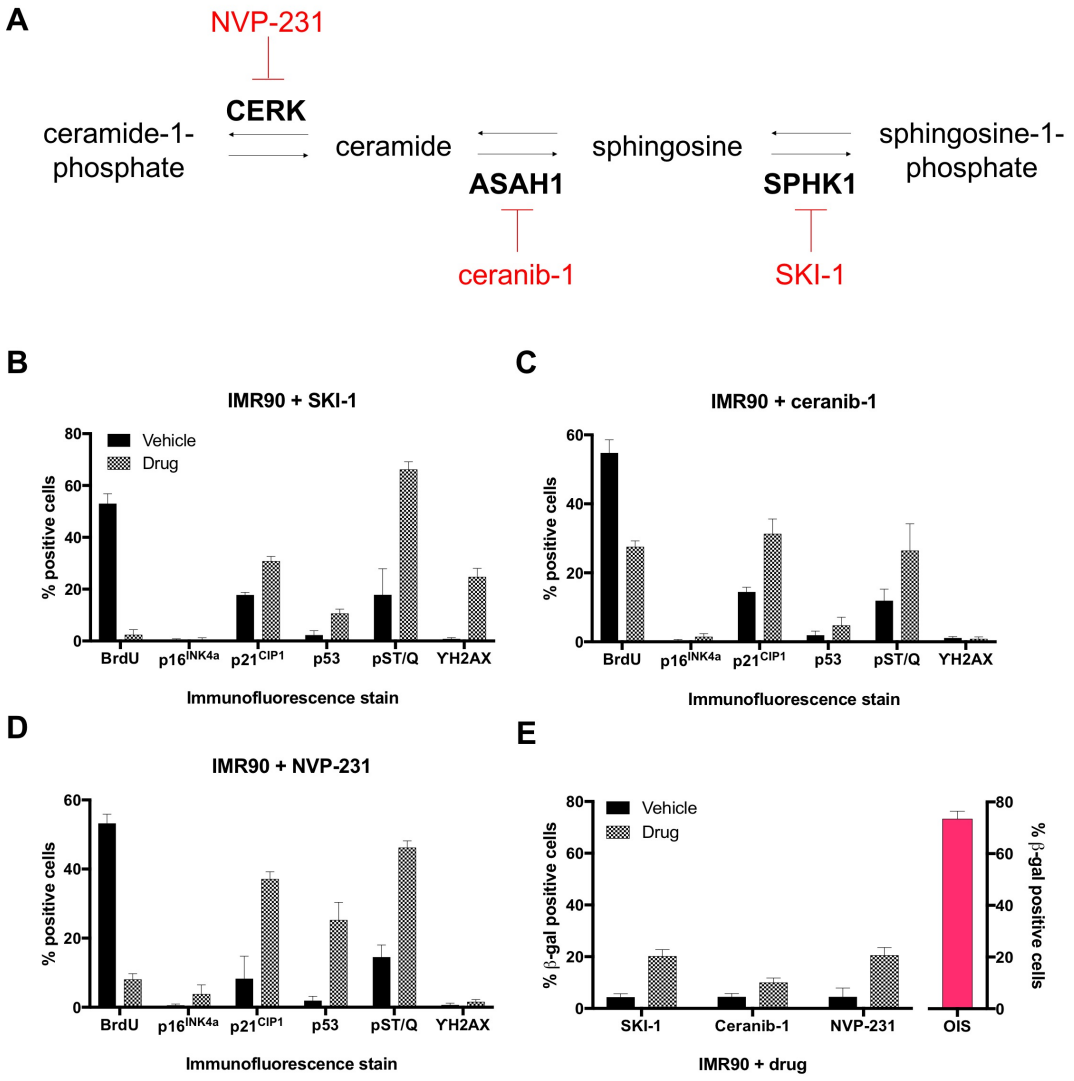

Figure 4.9 Drugs targeting ceramide metabolic enzymes cause proliferation arrest and expression of senescence markers (legend next page)

Figure 4.9 (A) *Pathway schematic indicating ceramide metabolic enzymes inhibited by SKI-1, ceranib-1 and NVP-231. IMR90 were treated with vehicle (DMSO) and* ***(B)*** *2μM SKI-1 or* ***(C)*** *2μM ceranib-1 or* ***(D)*** *5μM NVP-231. 48 hours after treatment, cells were fixed for immunofluorescence staining of BrdU incorporation (17h BrdU pulse), $p16^{INK4a}$, $p21^{CIP1}$, p53 and DNA damage markers: pST/Q and ϒH2AX. Positive cells were quantified from images (not shown) and % positive cells calculated (n=2, ±S.D.).* ***(E)*** *Treated cells were also stained for SA β-galactosidase activity. SA β-gal positive cells were quantified from images (not shown) and % positive cells calculated. OIS cells (day 10 of 4OHT) were used as a positive control (pink bar) (n=1, ±S.D.).*

4OHT = 4-hydroxytamoxifen, BrdU = bromodeoxyuridine.

4.6 Chapter summary

In this chapter, CERS4 has been extensively validated as a key enzyme for both OIS and replicative senescence. CERS4 knockdown by siRNA and shRNA robustly bypasses OIS and rescues the following phenotypes: proliferation, SA β-galactosidase activity and the expression of tumour suppressors and the SASP. Also, targeting CERS4 can delay replicative senescence and affects $p16^{INK4a}$ expression but not p53/$p21^{CIP1}$ expression. Finally, pharmacological manipulation of ceramide metabolism that, theoretically, accumulates ceramides, resulted in a senescence-like cell cycle arrest in IMR90.

When CERS4 is not present in IMR90, due to genetic knockdown, OIS is bypassed and all the typical OIS markers are significantly reduced to control levels. This suggests CERS4 function (ceramide synthesis) is mechanistically linked to OIS. In the next chapter, the main aim was to probe ceramide metabolism in OIS, using LC-MS based techniques, to establish the functional relationship between OIS and CERS4.

Chapter Five: Altered ceramide metabolism in OIS is regulated by CERS4

In the previous chapter CERS4 was thoroughly validated as an essential enzyme for OIS progression. The next aim was to gain understanding of the metabolic function of CERS4 and how this may be implicated during OIS. As described in *1.2.4*, ceramides can be synthesized by six ceramide synthases and by two main pathways: *de novo* and recycling. CERS4 preferentially synthesizes ceramides with 18/20/22 carbon fatty acids, in the *de novo* pathway (Riebeling *et al.*, 2003). For a comprehensive analysis of lipid metabolism in OIS, LC-MS-based lipidomics and labelling studies were utilised. In addition, the transcriptomics dataset, described in chapter four, was used for pathway expression analysis. In this chapter, data is described that indicates OIS results in altered lipid metabolism and CERS4 is implicated in these changes.

The quantitative ceramide analysis was performed in collaboration with Prof Phil Whitfield and colleagues at the University of Highlands & Islands (UHI). The labelling experiments were performed in collaboration with Dr Andy Finch, Joy Edwards-Hicks and Dr Jimi Wills at the Institute of Genetics and Molecular Medicine (IGMM).

5.1 Induction of OIS results in a global rewiring of the lipidome and increase in ceramide content

5.1.1 Transcriptomics confirms transcriptional regulation of lipid metabolism in OIS

For initial analysis of lipid metabolism during OIS, the transcriptomic dataset (described in *4.3.*) was utilised, to determine global mRNA expression of lipid metabolic pathways. Gene Set Enrichment Analysis was implemented to identify enrichment for lipid metabolism gene sets in OIS, and if gene sets are regulated by CERS4. Indeed, for day 8 there were many lipid metabolic pathways upregulated in

OIS (figure 5.1), suggesting a transcriptional program regulating lipid metabolism in OIS. CERS4 knockdown resulted in strongly significant downregulation of three sphingolipid pathways, compared to OIS (figure 5.1, bottom three bars), suggesting enzymatic activity is regulated by genetically targeting CERS4 expression. To further interrogate the expression of lipid metabolic genes in OIS, the statistic values of 8 ceramide metabolic genes were extracted and plotted as % fold change compared to iRas (figure 5.2.A). All, apart from GALC and SMPD1/2, showed increased expression in OIS and this was dependent on CERS4 expression. These results were validated by qPCR and significant increases in expression of GBA, ASAH1 and SPHK1 in OIS were shown (figure 5.2.B). Overall, this data suggests OIS has altered expression of lipid metabolism gene sets and CERS4 is implicated in this transcriptional regulatory program.

5.1.2 Lipid toxicity is accumulated during OIS

Lipid toxicity is the abnormal accumulation of cellular lipids, such as fatty acids, ceramides and phospholipids, and can be measured as an indicator of altered lipid metabolism. As revealed from the bypass-of-senescence siRNA screen, several genes in lipid metabolism are implicated in OIS. As a marker for altered lipid metabolism and to complement the transcriptomic data, lipid toxicity was measured in OIS and cells with CERS4 expression targeted in OIS. Three markers of lipid toxicity were used: lipid peroxidation, the oxidative breakdown of lipids; steatosis, the accumulation of neutral lipids; and phospholipidosis, the accumulation of phospholipids. First, to measure lipid peroxidation a Click-iT reaction was used, briefly described here. In the presence of lipid peroxidation, a linoleamide alkyne (LAA) substrate oxidises to form reactive aldehyde that binds protein or DNA. The aldehyde-protein/DNA adducts are incubated with a fluorescent azide in the presence of copper; the alkyne-containing adducts bind azide to form a stable product that is visualised with a fluorescent microscope. Next, phospholipidosis and steatosis are co-stained using fluorescent dyes with high affinity for phospho- and neutral lipids. Figure 5.3 shows the activation of OIS strongly induced lipid peroxidation, steatosis and phospholipidosis, and knockdown of CERS4 reduced this response. This data

suggests CERS4 contributes to the lipotoxic response in OIS. Next, LC-MS-based lipidomics was used to gain metabolic evidence for altered lipid metabolism in OIS.

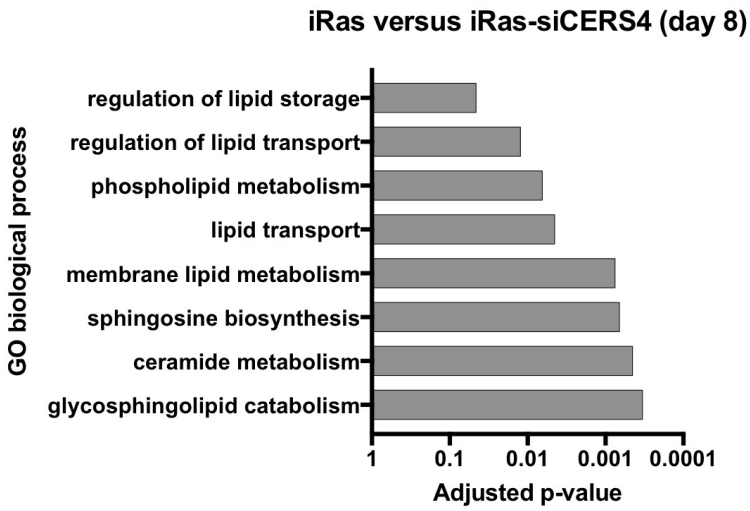

Figure 5.1 Transcriptomics confirmed regulation of lipid and ceramide metabolic programs during OIS

Babelomics 5 'RNA-seq class comparison' and 'Gene Set Enrichment Analysis' tools (Alonso et al., 2015) were used to compare expression of genes in lipid metabolic pathways for the following samples: OIS (iRas) and OIS with targeted CERS4 (iRas-siCERS4). See 2.9 for further details on the methods. Here, the difference in expression of the stated pathways between the two samples is quantified as a significative adjusted p-value

GO = Gene Ontology

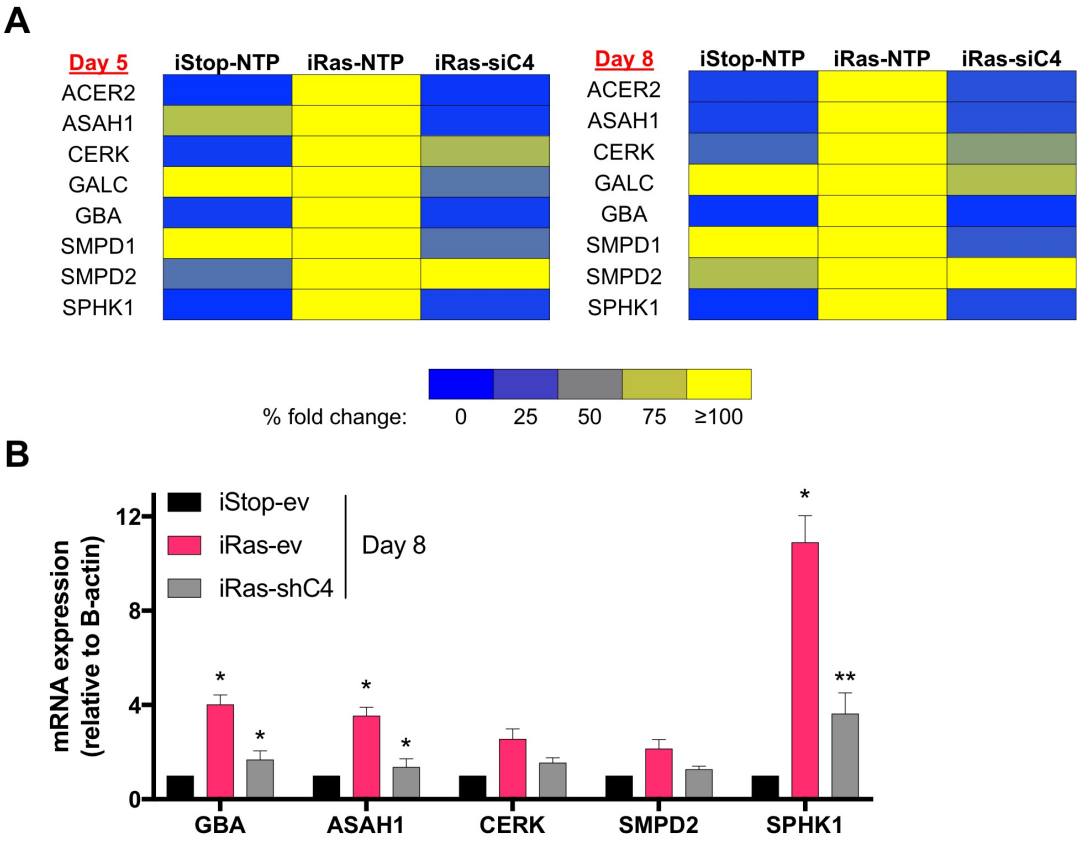

Figure 5.2 Regulation of sphingolipid metabolic transcriptional program by CERS4

(A) *Transcriptomic data analysed using AmpliSeqRNA plugin was subjected to gene expression analysis. The Babelomics 5 'RNA-seq class comparison' tool (Alonso et al., 2015) was used. For this analysis, the normalization method used was TMM and Benjamini and Hochberg multiple-test correction was used to calculate the False Discovery Rate and adjusted p-value (<0.05). Here, the statistic values for 8 ceramide recycling enzymes are plotted as % fold change compared to the OIS control (i.e. iRas with Non-Target).* ***(B)*** *iStop and iRas infected with ev and shC4 were analysed for transcription of ceramide metabolic enzymes at day 8 of 4OHT, and qPCR used to detect mRNA levels of GBA, ASAH1, ERK, SMPD2 and SPHK1. β-actin was used as a housekeeping gene (n=3, ±S.E.M., two-tailed Student's t-test).*

*4OHT = 4-hydroxytamoxifen, ev = pRS-empty vector, shC4 = pRS-shCERS4, * = p≤0.05, ** = p≤0.01.*

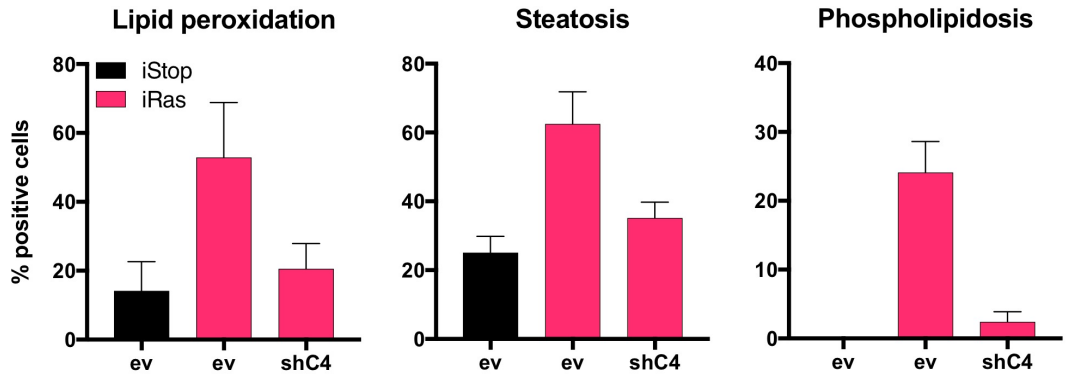

Figure 5.3 Lipid toxicity is activated in OIS

iStop and iRas infected with ev and shC4 were analysed for lipid toxicity at day 5 of 4OHT. See 2.12 for full methods. ***(A)*** *Lipid peroxidation was measured using a Click-iT assay. Briefly, cells were incubated with linoleamide alkyne (LAA) for 2 hours at 37°C. Cells were fixed and incubated with a fluorescent azide for 30 minutes, followed by DAPI. The resulting Click-iT reaction was measured using the FITC filter of the ImageXpress. Positive cells were quantified from images (not shown) and % positive cells calculated (n=1, ±S.D.).* ***(B)*** *Steatosis was detected by incubating fixed cells with a FITC-bound reagent with high affinity for neutral lipid droplets, for 30 minutes, followed by DAPI. Neutral lipids were detected using the FITC filter of the ImageXpress. Positive cells were quantified from images (not shown) and % positive cells calculated (n=1, ±S.D.).* ***(C)*** *Phospholipidosis was detected by incubating cells with a TxRED-bound phospholipid, for 24 hour at 37°C. Cells were fixed and stained with DAPI. Phospholipids were detected using the TxRED filter of the ImageXpress. Positive cells were quantified from images (not shown) and % positive cells calculated (n=1, ±S.D.).*

4OHT = 4-hydroxytamoxifen, ev = pRS-empty vector, shC4 = pRS-shCERS4.

5.1.3 Global lipidomics reveals an OIS-induced rewiring of lipid metabolism

The previous two sections have indicated OIS induces a transcriptional program regulating lipid metabolic gene expression and lipotoxic stress. To gain insight into whether OIS induces changes to the cellular lipidome, global lipidomics was harnessed (in collaboration with UHI). For this analysis, three cell types were used in serum-starved conditions: control (iStop), OIS (iRas), and bypass of senescence (iRas-E6/E7). For the bypass of senescence cell line, HPV proteins E6 and E7 were overexpressed in IMR90-ER:Ras. E6 and E7 are inhibitors of p53 and RB, respectively, and therefore the overexpression of E6/E7 prevents the induction of OIS through p53/RB inhibition. It is important to note here that all cells for lipidomics were cultured in low serum (1% FBS) to keep the baseline of metabolism low. For preliminary evaluation of the samples, a Principle Component Analysis (PCA) was performed. It was clear from the PCA for both positive and negative ion modes that there were clustering of samples depending on variate, i.e. cell type and time point (figure 5.4). It was concluded from the PCA that senescent cells have a distinct lipidome, that was reversed with a bypass of senescence induced by E6/E7 expression.

Next, information about the specific lipid metabolic pathways implicated in OIS was acquired from a multivariate statistical SIMCA analysis. This analysis was performed to identify the lipid subspecies significantly upregulated in OIS compared to control. This data indicated there was a global rewiring of lipid species present during OIS (figure 5.5.A) and it was evident iRas had increased ceramide content (figure 5.5.A, yellow bars). Previously, CERS4 was validated as a lipid metabolic enzyme implicated in OIS and indicated ceramides are associated with OIS. Thus, to determine if ceramides are accumulated in OIS, the global lipidomics dataset was further interrogated to get predictive data for ceramide content. The abundances were normalised against the Total Ion Count of each sample and then normalised to control cells to create a heatmap. OIS caused an accumulation of most ceramides detected and CERS4 specific ceramides 18:0 and 22:0 were fluctuating the most, especially at day 8 (figure 5.5.B). From this data, it was established ceramides are

accumulated in OIS; however, using global lipidomics to quantify specific lipids is not entirely reliable, therefore targeted and quantitative ceramide analysis was next used to develop the global lipidomics observations.

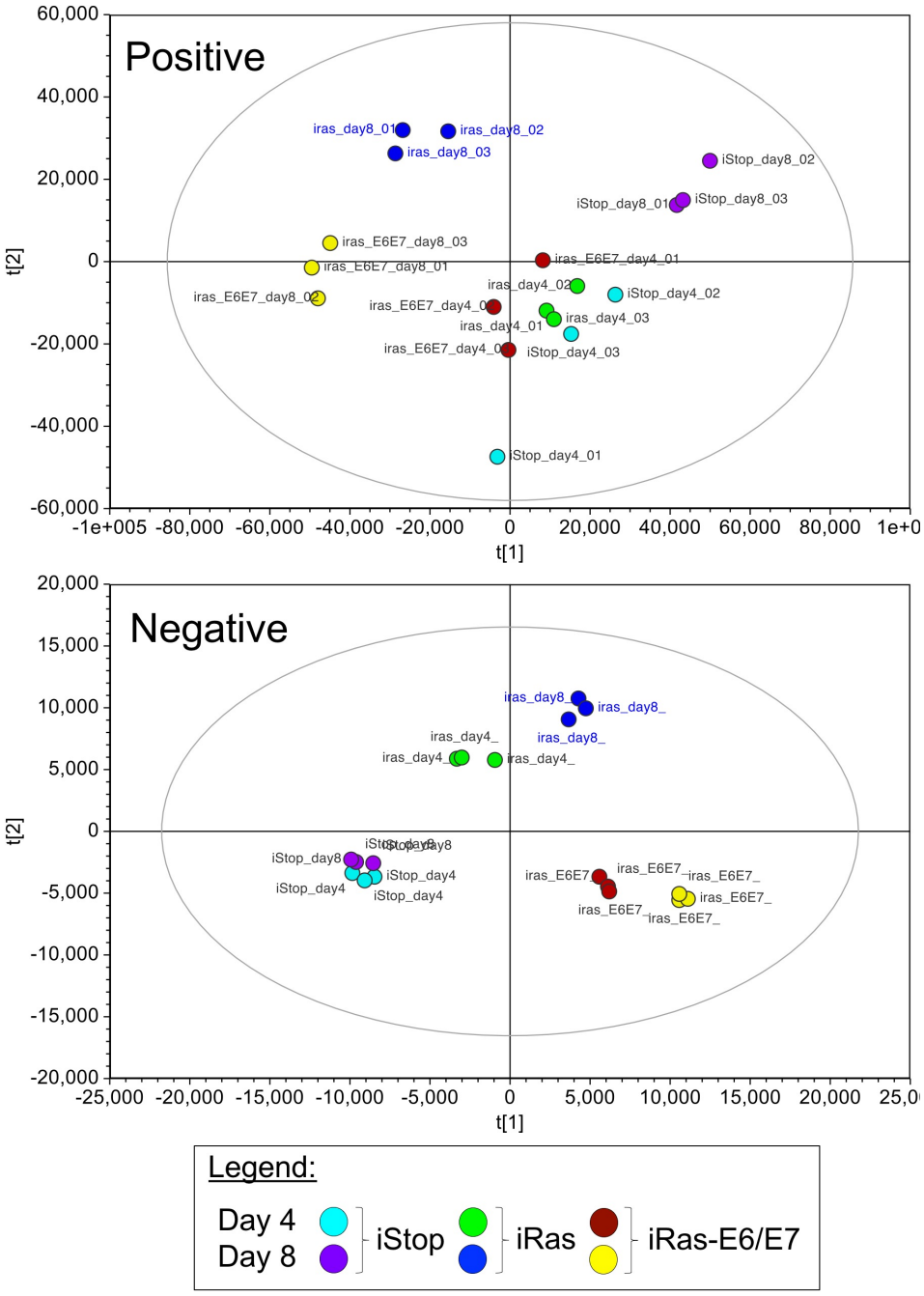

Figure 5.4 Principle Component Analysis for positive and negative modes of the global lipidomics dataset (legend next page)

Figure 5.4 *Samples of iStop, iRas and iRas-E6/E7 were collected at day 4 and 8 of 4OHT treatment. Global lipidomics was performed on these samples by UHI. Cells were solvent extracted according to Folch's method (Folch et al, 1957). The lipids were analysed by LC-MS in positive and negative ion modes using a C18 column and acetonitrile/water/propan-2-ol gradient. All analyses were performed on a Thermo Exactive Orbitrap mass spectrometer coupled to a Thermo Accela 1250 UHPLC system. Here, a Principle Component Analysis was performed, using the raw LC-MS data, to compare the lipidome of each condition (detailed in the legend).*

4OHT = 4-hydroxytamoxifen

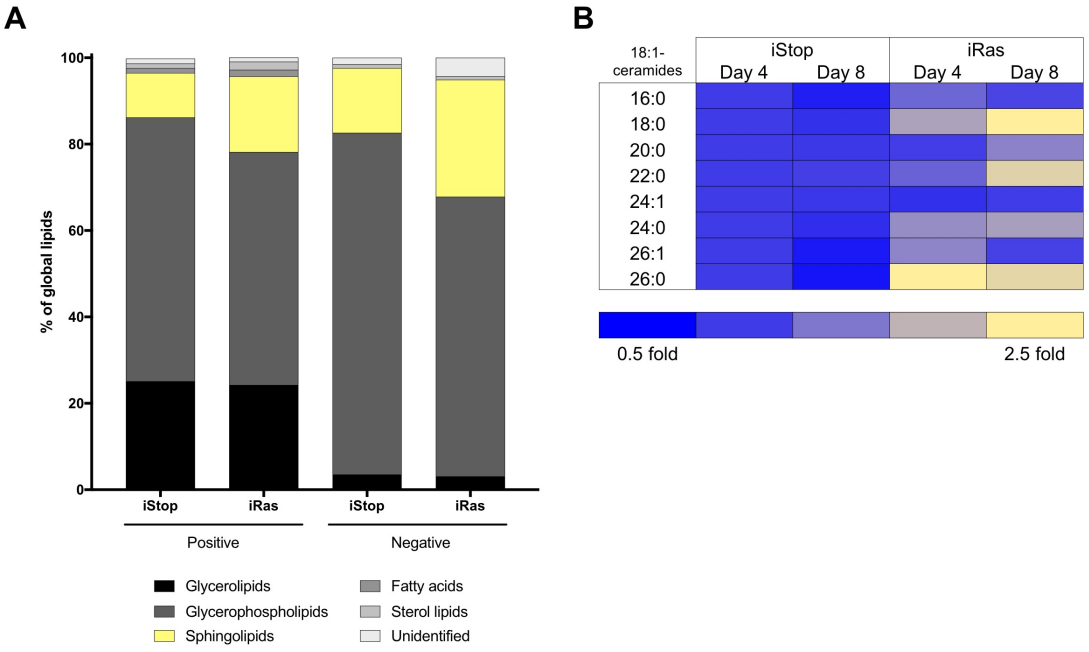

Figure 5.5 OIS induces a rewiring of the lipidome and accumulates ceramide

(A) *Raw LC-MS data for iStop and iRas at day 8 were processed to identify lipid subspecies and subjected to multivariate statistical analysis using SIMCA-P v13.0.2 (Umetrics, Umea, Sweden). This analysis was used to identify the most significantly abundant lipid subspecies present in OIS compared to control. The number of each subspecies was calculated as a percentage of global lipids. The lipid subspecies for both positive and negative ion mode are detailed in the legend.* ***(B)*** *Raw LC-MS data for iStop and iRas at day 4 and 8 were processed to quantify common ceramides, with 18:1-sphingosine backbones. The abundance data is presented as fold change compared to control (iStop, day 4).*

5.1.4 Quantitative lipidomics confirms changes in ceramide content during OIS

Although the global lipidomics provided a good indication of the lipidome alterations OIS induces, identification of specific lipids can be inaccurate due to sub-optimal LC-MS parameters. Therefore, targeted and quantitative analysis of ceramides was performed to confirm: first, ceramides are accumulated in OIS and second, CERS4 is the gene responsible for the activation of ceramide biosynthesis. Control, OIS and CERS4-targeted cells (day 4) were subjected to quantitative ceramide analysis using a triple quadrupole mass spectrometer; internal standards were used to identify and quantify ceramides (in collaboration with UHI). Ceramides with fatty acid lengths of 18:0 and 22:0 were significantly increased during OIS (pink bars, figure 5.6.A). This was likely due to ceramide synthase activity due to the significant rescue when CERS4 was inactivated (grey bars, figure 5.6.A). Other saturated and monounsaturated ceramides with 18/20/22 fatty acid chain lengths with lower abundances were also significantly accumulated during OIS (presented with a smaller y-axis range to observe changes, figure 5.6.B). For this group of ceramides, only 20:0 was significantly rescued with CERS4 knockdown, although 22:1 had a close-to-significance p-value of 0.06 (figure 5.6.B). From the quantitative ceramide analysis, it was concluded that the accumulation of ceramides during OIS was regulated by CERS4 activity.

5.1.5 Summary

In this section, rewiring of lipid metabolism in OIS has been identified by using a combination of global lipidomics and transcriptomics. There were high levels of lipid toxicity in OIS cells and expression of lipid metabolic pathway genes were significantly upregulated during OIS. These observations were dependent on CERS4. Quantitative ceramide analysis confirmed increased CERS4-specific ceramide products (18/20/22 carbon fatty acids) in OIS. Levels of these ceramides were rescued to control levels with CERS4 inactivation. The next aim of this chapter was to determine the mechanism of OIS-related ceramide synthesis.

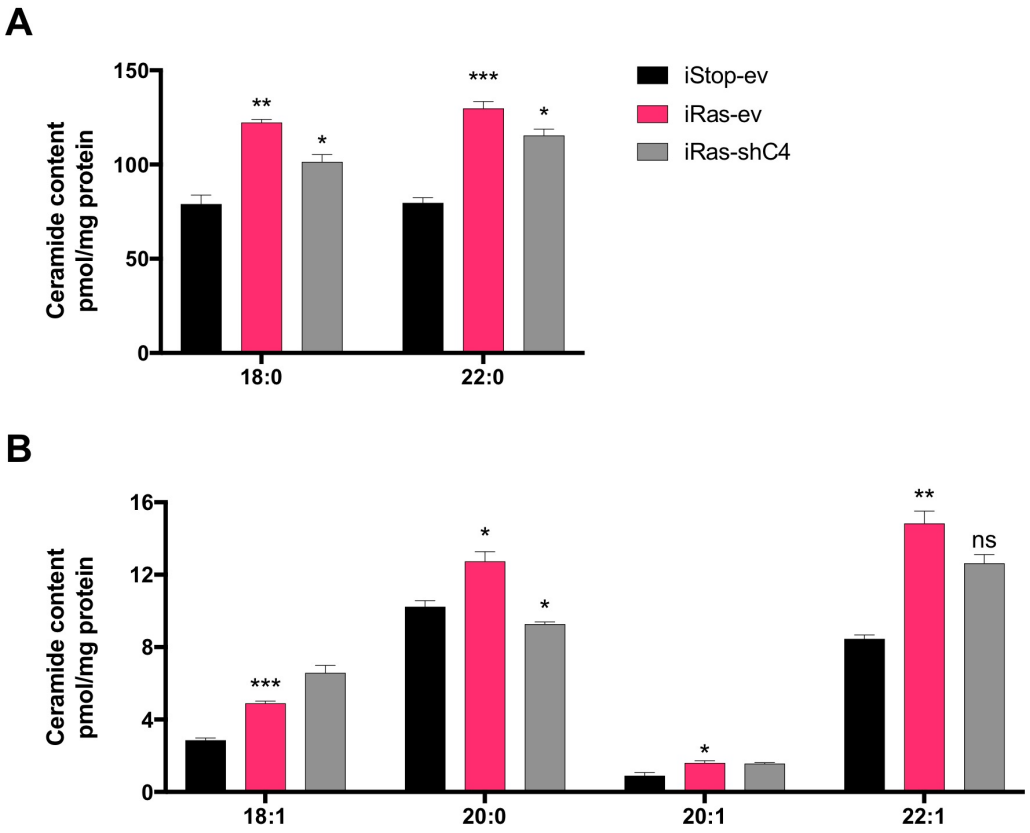

Figure 5.6 CERS4-specific ceramides are accumulated in OIS

Samples of iStop-ev, iRas-ev and iRas-shC4 were collected at day 4 of 4OHT treatment and subjected to quantitative ceramide analysis (UHI). Briefly, cells were solvent extracted according to Folch's method (Folch et al, 1957). Ceramides were isolated by silica solid phase extraction (SPE) chromatography. Ceramides were identified and quantified by LC-MS in positive ion mode using a C8 column and acetonitrile/water/formic acid gradient. All analyses were performed on a Thermo TSQ Quantum Ultra triple quadrupole mass spectrometer equipped with a heated electrospray source (HESI) and coupled to a Thermo Accela 1250 UHPLC system. Here, the concentration of the ceramides was determined by comparison to calibration curves generated with C16:0 and C24:1 standards. The values were normalised to cellular protein content. ***(A)*** *Cellular content of more abundant ceramides: 18:0 and 22:0.* ***(B)*** *Cellular content of less abundant ceramides: 18:1, 20:0, 20:1 and 22:1 (ALL: n=3, ±S.E.M., two-tailed Student's t-test).*

*4OHT = 4-hydroxytamoxifen, ev = pRS-empty vector, shC4 = pRS-shCERS4, * = p≤0.05, ** = p≤0.01, *** = p≤0.001, ns = not significant.*

5.2 *De novo* ceramide synthesis increases during OIS

The *de novo* pathway is one of the main means for cellular ceramide biosynthesis. Stable heavy-isotope labelling is a powerful approach to study the output of metabolic pathways. Therefore, it was decided to analyse the *de novo* synthesis of ceramides in OIS by using a heavy labelled serine molecule (2,3-$^{13}C_2$-serine) as a substrate for the first essential step of ceramide synthesis (figure 5.7). This technique, with accompanying lipid extraction and LC-MS method (described in *2.12*), was designed and optimised with Joy Edwards-Hicks.

As part of the set-up, we optimised the best label time to detect $^{13}C_2$ incorporation into ceramides. All stable heavy-isotope labels can saturate a metabolic pathway if given to cells for a long enough period. Optimising the label time is a balance between not saturating the pathway and being able to observe differences between unlabelled and labelled samples. To optimise the 2,3-$^{13}C_2$-serine label, control and OIS cells (day 4 of 4OHT) were treated for short (6 hours) and long (48 hours) periods with ^{12}C- and $^{13}C_2$-serine. The difference between the %M+2 (i.e. the percentage of $^{13}C_2$ present in total ceramide) for each label was used to determine which treatment time had the largest variance between unlabelled and labelled samples. Figure 5.8 shows the %M+2 for four ceramides (18:0/22:0/24:0/26:0), as a fold change compared to ^{12}C of each sample. It was clear that the 6 hour treatment time resulted in larger changes in %M+2 in labelled samples compared to unlabelled; apart from 24:0-ceramide, which yielded similar %M+2 with 6 and 48 hours treatment. It was likely the 48 hour treatment time was saturating the *de novo* ceramide synthesis pathway. Therefore, further experiments were performed using a 6 hour treatment time of serine.

To determine if the *de novo* synthesis of ceramides is increased in OIS, the optimised labelling was implemented in control, OIS and OIS cells with CERS4 knockdown, at both day 4 and 8 of 4OHT. The %M+2 for unlabelled cells (figures 5.9.A&C) represents the natural abundance of M+2 ceramides (i.e. <10% of naturally abundant ceramides have M+2 masses). The %M+2 for labelled cells indicated OIS induces *de novo* synthesis of all ceramides detected, and this is partially CERS4 dependent (figures 5.9.B&D). This occurred at both day 4 (figure 5.9.B) and 8 (figure 5.9.D) of

4OHT, suggesting ceramide synthesis is vital for induction and maintenance of OIS. In conclusion, by harnessing LC-MS based stable heavy-isotope labelling, the *de novo* pathway has been identified as a mechanism for OIS-related ceramide synthesis. In the next section, the other main route of ceramide synthesis, the recycling pathway, is interrogated to determine if it also contributes to OIS-related ceramide synthesis.

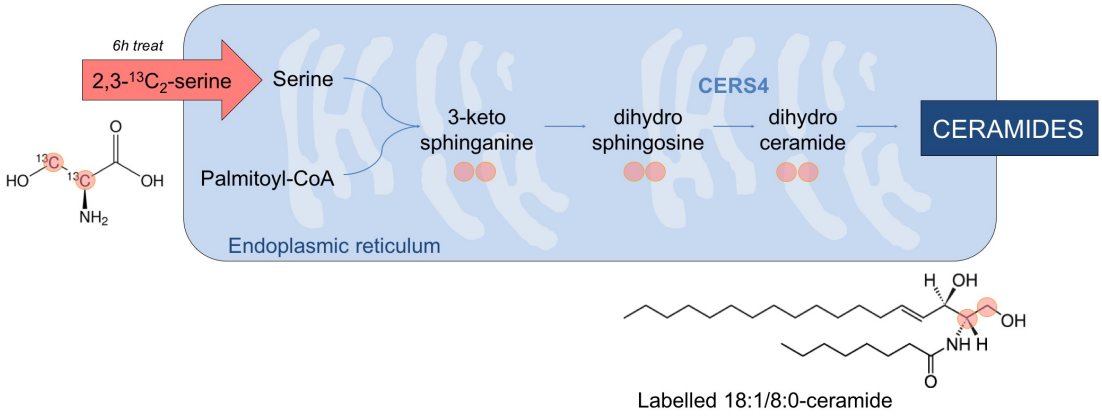

Figure 5.7 Schematic of 2,3-$^{13}C_2$-serine labelling of ceramides

Heavy labelled serine (2,3-$^{13}C_2$-serine) can be used to label the de novo synthesis of ceramides. The two heavy carbons can be traced through the pathway to all ceramide products. CERS4 catalyses one of the last steps in this pathway: the coupling of dihydrosphingosine with a long chain fatty acid to form dihydroceramide. This stable heavy-isotope labelling approach can be used to measure the de novo activity of CERS4.

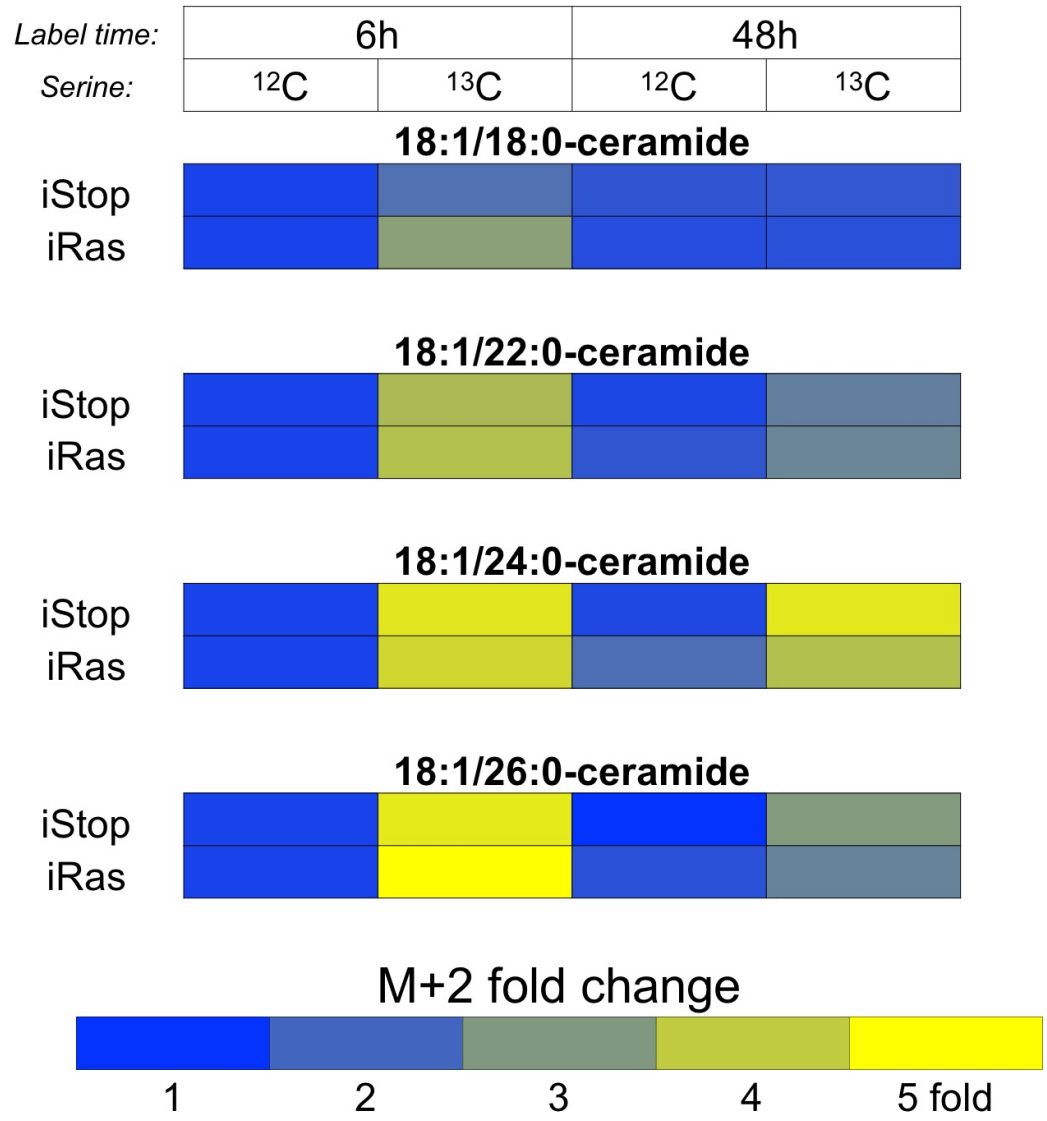

Figure 5.8 Optimisation of the serine label treatment time

iStop and iRas were treated with ^{12}C-serine or $^{13}C_2$-serine for 6 hours or 48 hours on day 4 of 4OHT. Cells were collected and lipids were extracted using a biphasic method based on the Bligh and Dyer method (Bligh and Dyer, 1959). Ceramides were identified and quantified by LC-MS in positive ion mode using a C18 column and acetonitrile/water/formic acid/propan-2-ol gradient. All analyses were performed on a Thermo Q-exactive mass spectrometrer coupled to a Thermo Ultimate BioRS HPLC. The peak areas for M+0 (m/z + no ^{13}C) and M+2 (m/z + two ^{13}C) 18:1-ceramides, 18:0/22:0/24:0/26:0, were extracted using Thermo Xcalibur Quan Browser. The M+2 fold change was calculated compared to each ^{12}C control sample. The legend indicates the colours denoting M+2 fold change. Note: first, compare ^{12}C and ^{13}C columns for each treatment time; second, compare 6h and 48h clusters.

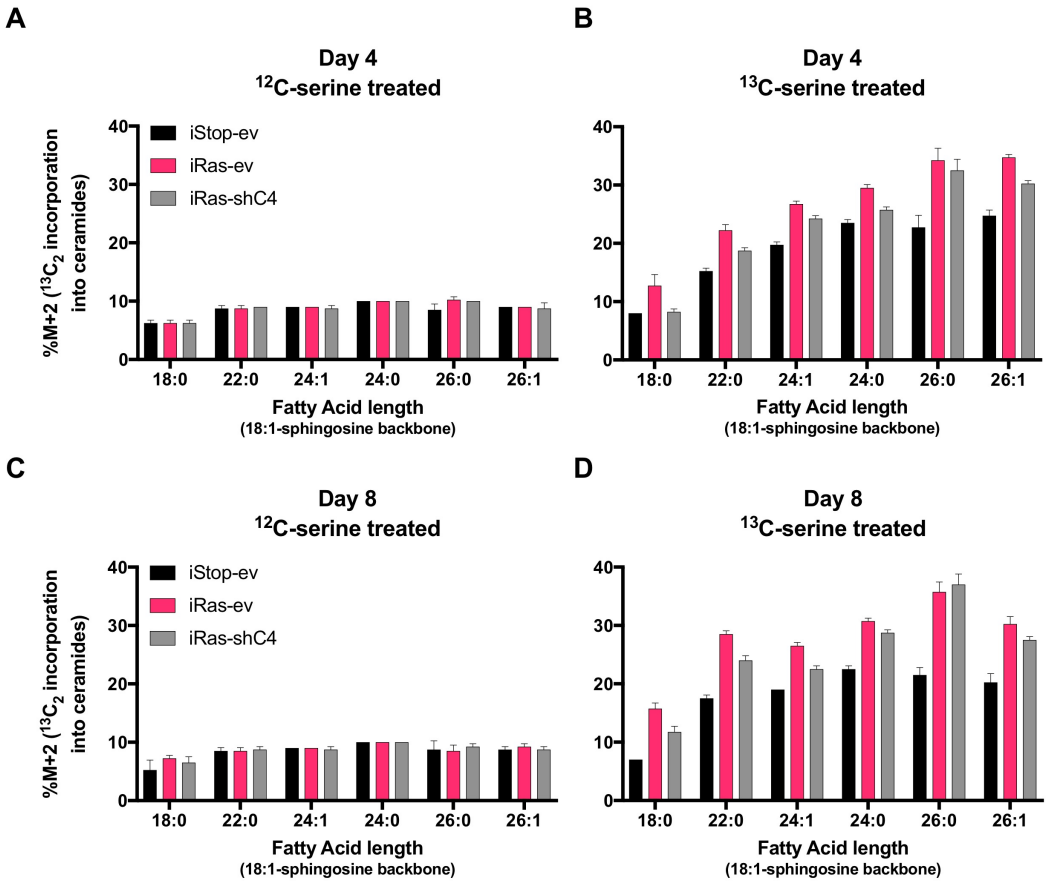

Figure 5.9 OIS induces increased CERS4-dependent *de novo* synthesis of ceramides

iStop-ev, iRas-ev and iRas-shC4 were treated with ^{12}C-serine or $^{13}C_2$-serine for 6 hours on day 4 and 8 of 4OHT. Cells were collected and lipids were extracted using a biphasic method based on the Bligh and Dyer method (Bligh and Dyer, 1959). *Ceramides were identified and quantified by LC-MS in positive ion mode using a C18 column and acetonitrile/water/formic acid/propan-2-ol gradient. All analyses were performed on a Thermo Q-exactive mass spectrometrer coupled to a Thermo Ultimate BioRS HPLC. The peak areas for M+0 (m/z + no ^{13}C) and M+2 (m/z + two ^{13}C) ceramides were extracted using Thermo Xcalibur Quan Browser. The %M+2 incorporation into ceramides was calculated as a percentage of total ceramide: M+0 and M+2.* ***(A)*** *%M+2 of stated ceramides in unlabelled (^{12}C-serine) cells at day 4.* ***(B)*** *%M+2 of stated ceramides in labelled ($^{13}C_2$-serine) cells at day 4.* ***(C)*** *%M+2 of stated ceramides in unlabelled (^{12}C-serine) cells at day 8.* ***(D)*** *%M+2 of stated ceramides in labelled ($^{13}C_2$-serine) cells at day 8 (ALL: n=2, ±S.D.).*

4OHT = 4-hydroxytamoxifen, ev = pRS-empty vector, shC4 = pRS-shCERS4.

5.3 Ceramide synthesis through the recycling pathway is not regulated in OIS

In addition to the *de novo* pathway, cells can synthesise ceramides via the recycling pathway. To confirm if OIS also has upregulation of the ceramide recycling pathway, a 17:1-sphingosine backbone ceramide not usually present in human cells (17:1/8:0-ceramide, see figure 5.10.A for structure) was used as a substrate for recycling enzymes; a similar technique was previously described by Sultan *et al.* (2005). In principle, the 17:1/8:0-ceramide would be broken down into sphingosine and fatty acids, and the 17:1-sphingosine reincorporated into newly synthesised ceramides. This incorporation of 17:1 can then be measured in lipid extracts using LC-MS.

First, an optimisation experiment was performed to determine the best treatment time for IMR90. IMR90 were treated with 17:1/8:0-ceramide or ethanol vehicle for 1, 3, 12 and 24 hours and performed lipid extractions (described in *2.12*). A 17:1/8:0-ceramide standard was analysed on the LC-MS to: (1) gain the retention time to aid identification and (2) ensure the correct product was supplied (figure 5.10.A). 17:1 was incorporated into most ceramides detected, apart from ceramide-20:0 (figure 5.10.B). This could be due to ceramide-20:0 being naturally less abundant (see y-axis values). The incorporation peaked after 3 hours treatment of 17:1/8:0-ceramide, which was particularly clear for 17:1/18:0 and 17:1/22:0 ceramides (figure 5.10.B, panels 1 and 3). To ensure the 17:1/8:0-ceramide treatment was not having a global effect on ceramide recycling, peak areas of 18:1-ceramides were also examined. There was no difference in 18:1-ceramide peak areas between ethanol and 17:1/8:0-ceramide treated (figure 5.10.C), further confirming this technique was specifically measuring 17:1 incorporation and ceramide recycling pathway output.

The optimised 3 hour 17:1/8:0-ceramide treatment was repeated in control, OIS and OIS cells with CERS4 knockdown at day 4 and 8. The %17:1 incorporation into ceramides was calculated as a percentage of total ceramide: 17:1 and 18:1. As expected, %17:1 incorporation in ethanol treated cells was low due to the low natural abundance of 17:1-ceramides in human cells (figures 5.11.A&C). The %17:1 incorporation into cellular 17:1/8:0-ceramide was nearly 100% for all three cell types and two time points (first three bars, figures 5.11.B&D); this was due to saturation

during the treatment time. Looking at the longer 17:1-ceramides, there were no significant changes in 17:1 incorporation (figures 5.11.B&D). As with the optimisation experiment, there was no 17:1 incorporation into ceramide-20:0 (compare ethanol to 17:1/8:0-ceramide treated). This data indicates there is no regulation of ceramide recycling in OIS and CERS4 is not implicated in this pathway.

5.4 Chapter summary

The aim of this chapter was to examine lipid metabolism in OIS and determine the metabolic function of CERS4 in OIS. First, lipid toxicity and expression of genes encoding lipid metabolic enzymes were both upregulated in OIS. Using global lipidomics, a global rewiring of the senescent lipidome was identified. As CERS4 was previously identified as essential for OIS, quantitative lipidomics was used to confirm accumulated ceramide in OIS. This was dependent on CERS4 expression, suggesting CERS4 is functionally responsible for the synthesis of OIS-related ceramide. Next, the *de novo* pathway was identified as the mechanism of OIS-related CERS4-dependent ceramide synthesis, using stable heavy-isotope labelling. By perturbing the recycling pathway with a modified ceramide, it was found OIS does not upregulate this pathway of ceramide synthesis.

In conclusion, increased ceramide content in OIS is regulated by the *de novo* activity of CERS4. This suggests OIS functionally requires ceramide, for an unknown reason. The final chapter focusses on identifying the function of OIS-related ceramide and how it may affect the cell cycle.

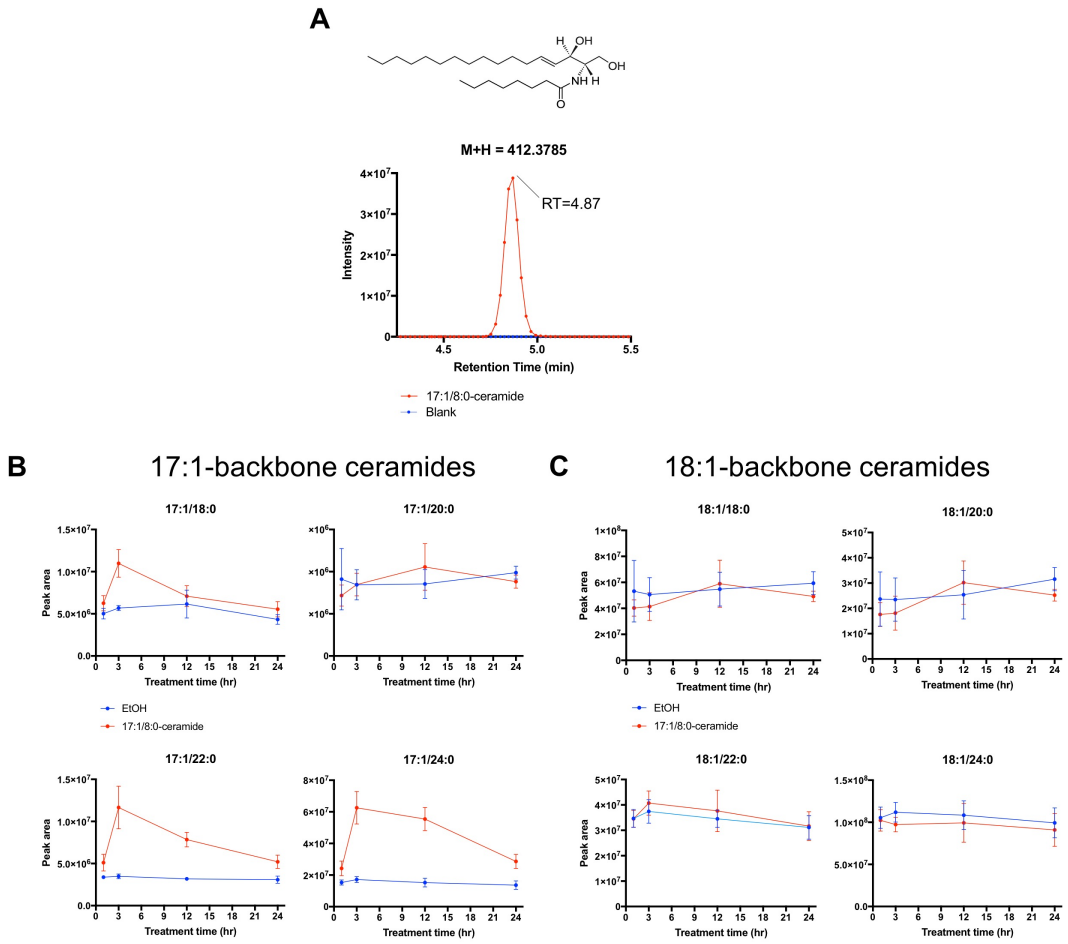

Figure 5.10 17:1/8:0-ceramide can be used to measure ceramide recycling pathway output

(A) *17:1/8:0-ceramide has a sphingosine backbone with one carbon less than 18:1-ceramides, which are more abundant in human cells. The 17:1/8:0-ceramide standard was analysed by LC-MS (method below). Next, IMR90 were treated with EtOH or 17:1/8:0-ceramide for 1, 3, 12 or 24 hours. Cells were collected and lipids were extracted using a biphasic method based on the Bligh and Dyer method* (Bligh and Dyer, 1959). *Ceramides were identified and quantified by LC-MS in positive ion mode using a C18 column and acetonitrile/water/formic acid/propan-2-ol gradient. All analyses were performed on a Thermo Q-exactive mass spectrometrer coupled to a Thermo Ultimate BioRS HPLC. Thermo Xcalibur Quan Browser was used to convert raw data to peak areas for* ***(B)*** *17:1-ceramides and* ***(C)*** *18:1-ceramides (ALL: n=1, ±S.D.).*

RT = retention time, EtOH = ethanol.

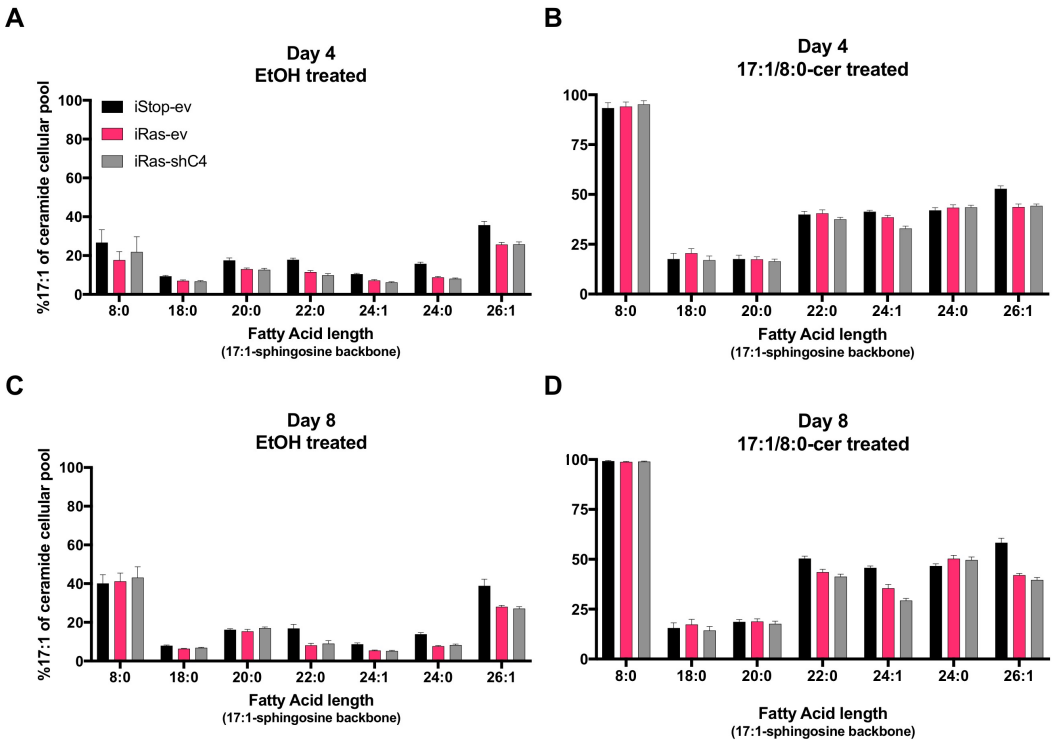

Figure 5.11 Ceramide recycling pathway output is not regulated during OIS

iStop-ev, iRas-ev and iRas-shC4 were treated with EtOH or 17:1/8:0-ceramide for 3 hours on day 4 and 8 of 4OHT. Cells were collected and lipids were extracted using a biphasic method based on the Bligh and Dyer method (Bligh and Dyer, 1959)*. Ceramides were identified and quantified by LC-MS in positive ion mode using a C18 column and acetonitrile/water/formic acid/propan-2-ol gradient. All analyses were performed on a Thermo Q-exactive mass spectrometrer coupled to a Thermo Ultimate BioRS HPLC. The peak areas for 17:1- and 18:1-ceramides were extracted using Thermo Xcalibur Quan Browser. The %17:1 incorporation into ceramides was calculated as a percentage of total ceramide.* ***(A)*** *%17:1 of stated ceramides in unlabelled (EtOH) cells at day 4.* ***(B)*** *%17:1 of stated ceramides in labelled (17:1/8:0-cer) cells at day 4.* ***(C)*** *%17:1 of stated ceramides in unlabelled (EtOH) cells at day 8.* ***(D)*** *%17:1 of stated ceramides in labelled (17:1/8:0-cer) cells at day 8 (ALL: n=3, ±S.E.M.).*

4OHT = 4-hydroxytamoxifen, ev = pRS-empty vector, shC4 = pRS-shCERS4, EtOH = ethanol.

Chapter Six: CERS4 and ceramide activate the PP1/RB axis of cell cycle regulation

In the previous chapter, ceramide accumulation resulting from increased CERS4-driven *de novo* ceramide synthesis was identified as a vital mechanism for OIS. The main aim of this chapter was to uncover the function of OIS-related ceramide, downstream of its synthesis. First, functional rescue experiments with exogenous ceramide were performed, to see if OIS bypass driven by CERS4 knockdown can be reversed. From this data, it was suggested that CERS4 can affect RB phosphorylation state, independent of p53/p21/p16, and further experiments were performed to explore this hypothesis. Using western blotting and qPCR, RB phosphorylation state and downstream effects on E2F target transcription were analysed. Lastly, the relationship between protein phosphatase 1 (PP1), RB and CERS4 was investigated using co-immunoprecipitation. This chapter describes the results that identify CERS4 as a metabolic checkpoint, linking altered ceramide metabolism with OIS.

Dr Andrea Quintanilla optimised and performed the immunoprecipitation experiments for this part of the thesis. Her data has been included as it greatly enhances this story and the work is acknowledged where applicable.

6.1 Ceramide treatment rescues OIS in CERS4-deficient cells

6.1.1 Ceramide reverses proliferation and SA β-gal phenotype of shCERS4-driven OIS bypass

It was previously shown, using LC-MS based techniques, CERS4 knockdown reduces the functional activity of the enzyme. Next, experiments were performed to examine if the function of CERS4 in OIS can be rescued, using ceramide. Exogenous 18:1/8:0-ceramide (henceforth C8-cer) was used because ceramides with shorter fatty acid chains are more cell permeable than longer ceramides. Control, OIS and OIS with CERS4 knockdown were treated every 24 hours with 2μM C8-cer or ethanol alongside 4OHT. Proliferation and SA β-gal markers were measured to observe the

effect of ceramide on the OIS phenotype. BrdU incorporation at day 6 showed a significant decrease in proliferation with ceramide treatment, in cells targeted for CERS4 knockdown, from 50% to 35% (figure 6.1.A). There was also a significant increase in SA β-gal activity, from 7% to 82% (p=0.011), after 8 days of 4OHT and C8-cer treatment (figure 6.1.B). Together this data suggests ceramide treatment can partially rescue CERS4-mediated effects in OIS. It was previously shown ceramides can induce senescence in a different human diploid fibroblast cell line (Venable *et al.*, 1995), indicating why ceramide causes a small decrease in proliferation and increase in SA β-gal activity control cells. However, these changes were not comparable to those occurring with CERS4 knockdown, further suggesting ceramide treatment is truly rescuing the OIS bypass.

6.1.2 Ceramide rescue in CERS4 deficient cells is independent of p53/p21 and p16

Thus far, it was clear ceramide and CERS4 have a functional role in OIS. To delineate the functional mechanism of both in OIS, it was hypothesised ceramide could be vital for tumour suppressor activation in OIS, as previously shown for CERS4. Therefore, the expression of tumour suppressor proteins p53, $p21^{CIP1}$ and $p16^{INK4a}$ were analysed in the rescue experiment, using immunofluorescence and western blotting. As expected, expression of p53, $p21^{CIP1}$ and $p16^{INK4a}$ was significantly increased in OIS at day 6 (first pink bar, figure 6.2.A-C), and significantly rescued with CERS4 knockdown (first grey bar, figure 6.2.A-C). In shCERS4-driven OIS bypass, p53, $p21^{CIP1}$ and $p16^{INK4a}$ were expressed similarly between ethanol and ceramide treatment (compare grey bars, figure 6.2.A-C; and compare lanes 5 & 6, figure 6.2.D). In contrast, the expression levels of p53, $p21^{CIP1}$ and $p16^{INK4a}$ decreased in OIS with ceramide treatment (compare lanes 3 & 4, figure 6.2.D; and compare pink bars, figure 6.2.A). Overall, this data suggests CERS4 can regulate the expression of tumour suppressors as an indirect consequence of regulating cellular senescence.

6.1.3 Summary

In this section, it has been shown exogenous ceramide treatment can rescue the effects of CERS4 knockdown (i.e. OIS-bypass), by promoting a proliferation arrest and SA β-gal activity. However, this proliferation arrest did not correspond with increased expression of tumour suppressors p53, $p21^{CIP1}$ and $p16^{INK4a}$. Together, this data implicates CERS4 and ceramide in a tumour suppressor-independent mechanism in OIS. However, the effect of ceramide treatment on intracellular levels of ceramide was not analysed. To ultimately validate the rescue experiments and understand the discrepancy between the effect of ceramide treatment on $p21^{CIP1}$ and p53 expression in OIS and CERS4-depleted cells (figure 6.2.D), measurement of cellular ceramide content using mass spectrometry is required; this is further discussed in *7.4.2*. The next section examines another potential functional mechanism for CERS4 and ceramide in OIS, focussing on the cell cycle regulator RB.

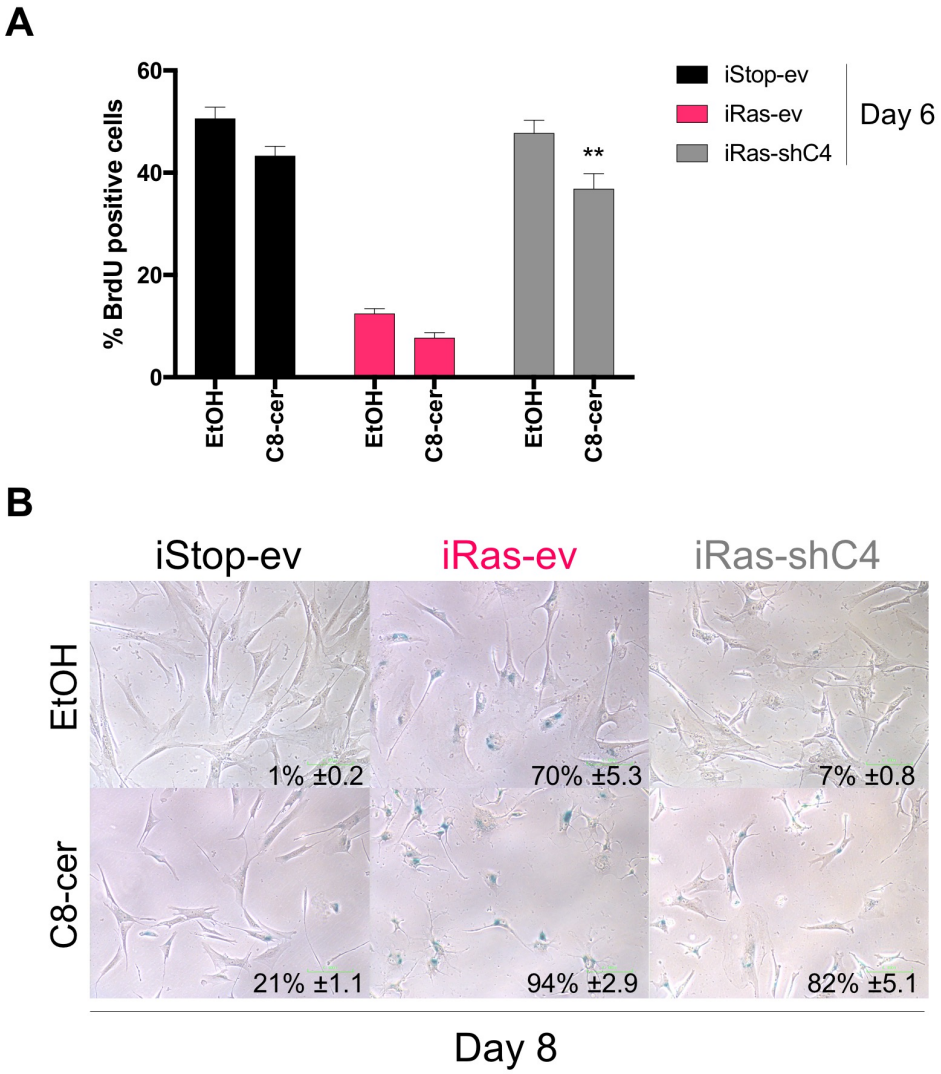

Figure 6.1 Long-term ceramide treatment partially reverses bypass of senescence driven by CERS4 inactivation

iStop and iRas were infected with empty vector (ev) and a stable shRNA targeting CERS4 expression (shC4). Cells were subjected to daily 2μM 18:1/8:0-ceramide treatment from day 0 of 4OHT, and analysed at day 6 and 8. ***(A)*** *At day 6, cells were subjected to a 17h BrdU pulse, fixed and stained for BrdU incorporation using immunofluorescence. BrdU positive cells were quantified and % positive cells calculated (n=3, ±S.E.M., two-tailed Student's t-test).* ***(B)*** *At day 8, cells were fixed and stained for SA β-galactosidase activity. SA β-gal positive cells were quantified from images and % positive cells calculated (bottom right) (n=3, ±S.E.M.).*

*4OHT = 4-hydroxytamoxifen, BrdU = bromodeoxyuridine, ev = pRS-empty vector, shC4 = pRS-shCERS4, EtOH = ethanol, C8-cer = 18:1/8:0-ceramide, ** = p≤0.01.*

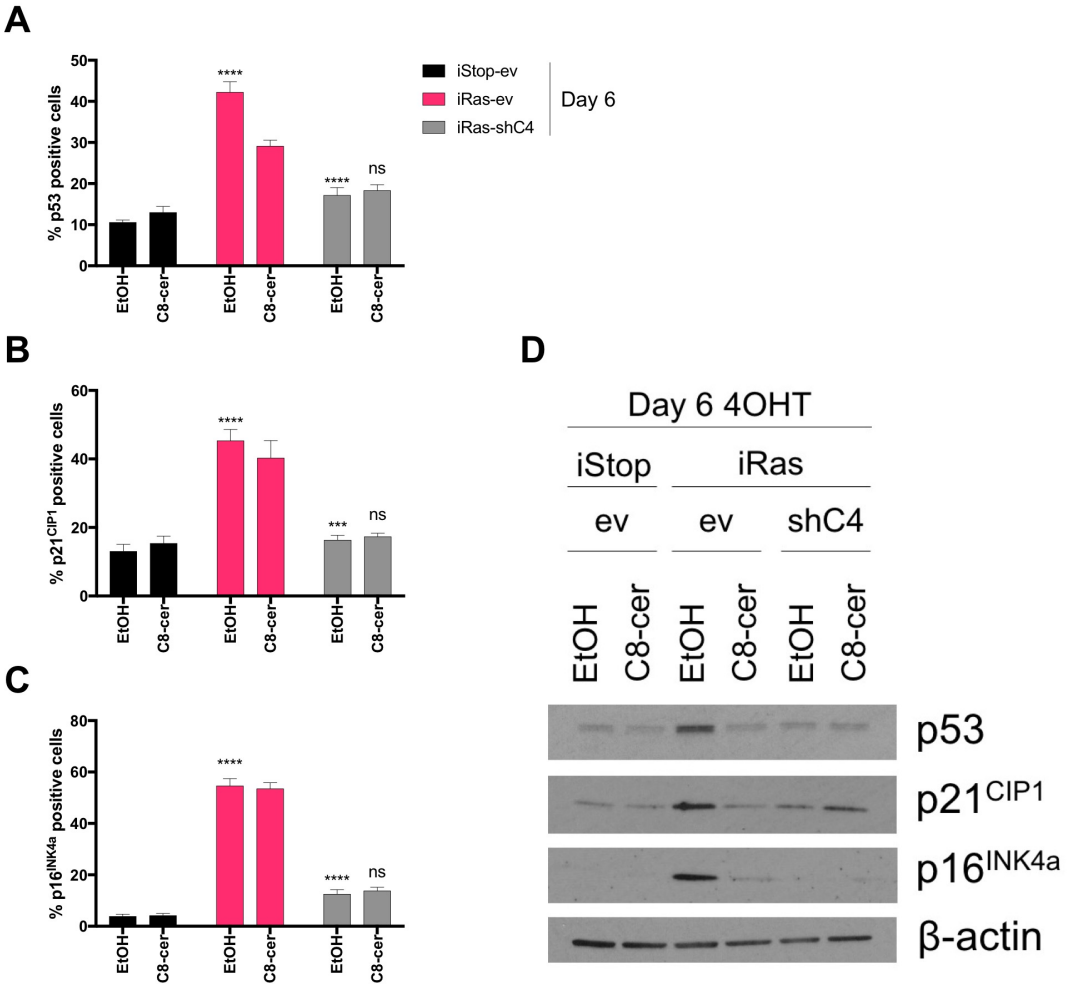

Figure 6.2 Tumour suppressor proteins expression levels are not altered in CERS4-deficient cells after ceramide treatment

iStop and iRas were infected with empty vector (ev) and a stable shRNA targeting CERS4 expression (shC4). Cells were subjected to daily 2μM 18:1/8:0-ceramide treatment from day 0 of 4OHT, and analysed for tumour suppressor protein expression. Cells were subjected to immunofluorescence staining for ***(A)*** *p53* ***(B)*** *$p21^{CIP1}$ and* ***(C)*** *$p16^{INK4a}$. Positive cells were quantified and % positive cells calculated (ALL: n=3, ±S.E.M., two-tailed Student's t-test).* ***(D)*** *Cell pellets were collected and lysed on day 6, and subjected to western blotting to detect $p16^{INK4a}$, $p21^{CIP1}$ and p53. Briefly, 20μg cell lysate was separated on 10-20% Tris-Glycine gels and subjected to western blotting of stated proteins. β-actin was used as a loading control. (representative of 2 independent experiments).*

*4OHT = 4-hydroxytamoxifen, ev = pRS-empty vector, shC4 = pRS-shCERS4, EtOH = ethanol, C8-cer = 18:1/8:0-ceramide, *** = p≤0.001, **** = p≤0.0001, ns = not significant.*

6.2 CERS4 is required for RB activation in OIS

6.2.1 CERS4 regulates expression of E2F target genes

The previous section showed the expression of tumour suppressors was not necessary for CERS4 function in OIS. As described in *1.1.2.3*, retinoblastoma protein (RB) is also implicated in the cell cycle; RB acts as a checkpoint to regulate the expression of E2F target genes, such as cyclin-dependent kinases (CDKs). In proliferating cells, phosphorylated RB is inactivated and frees E2F transcription factors to initiate the transcription of genes essential for cell cycle progression (figure 1.2). In non-proliferating cells, hypophosphorylated RB is activated and prevents transcription of E2F target genes. Therefore, expression of E2F target genes can be used as a readout for RB activity and are an indicator of cell cycle progression (Dick and Rubin, 2013).

To examine if CERS4 regulates RB activity, the transcriptomics dataset (described in *4.3*) was utilised to determine gene expression of RB/E2F targets. A Gene Set Enrichment Analysis (GSEA) comparing CERS4 knockdown to OIS was performed by Dr Tamir Chandra (figure 6.3.A). For this analysis, a gene set annotated as targets of RB in senescence (designated here as RB_TARGETS_SENESCENCE, described by Chicas *et al.*, 2010) was compared to all genes identified in the transcriptomics analysis (~15000). The grey bars (bottom panel, figure 6.3.A) represent all genes ranked by expression and the black lines (middle panel, figure 6.3.A) represent the genes annotated in RB_TARGETS_SENESCENCE. The black lines are accumulated in the left side of the graph, which suggests these genes are highly regulated between the two conditions. The green line (top panel, figure 6.3.A) represents an enrichment score for RB_TARGETS_SENESCENCE. The large left peak indicates there is enrichment of RB targets in CERS4 knockdown compared to OIS. To validate the GSEA observations, the expression of well-characterised RB/E2F target genes was measured by qPCR. These genes included cell cycle regulators CDK1/2 and DNA replication genes CDC6/7, PCNA, ORC1 and MCM2. As expected, OIS decreases expression of all E2F target genes, apart from CDK2, compared to proliferating control (compare black and pink bars, figure 6.3.B). The knockdown of CERS4 in OIS resulted in significant increased expression of all E2F target genes (grey bars, figure 6.3.B). This data suggests CERS4 can affect the expression of E2F target

genes and therefore RB activity. However, this observation could be an independent downstream effect of shCERS4-driven OIS-bypass, eluding the actual mechanism that links CERS4 and ceramide to cell cycle regulation. Therefore, the next aim was to interrogate RB phosphorylation after CERS4 inactivation and rescue with ceramide.

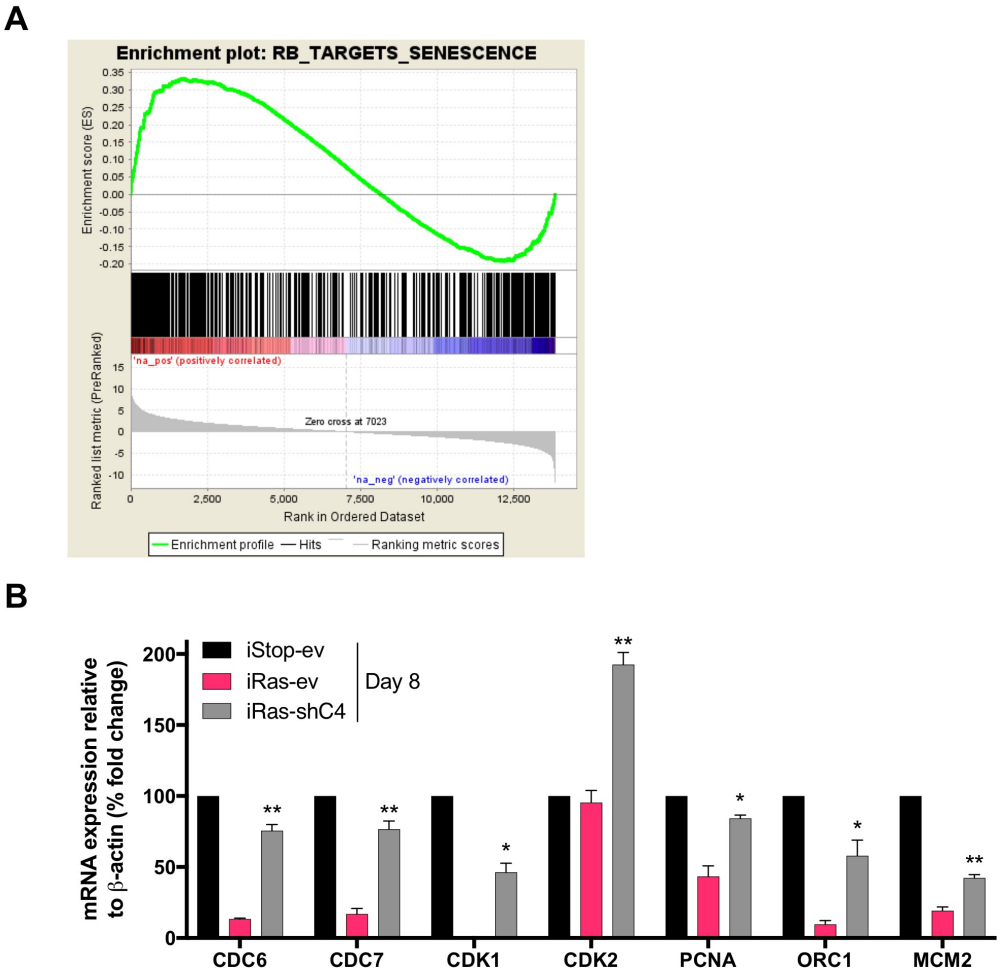

Figure 6.3 Transcriptome data indicates CERS4 regulates RB/E2F activity

(A) *Dr Tamir Chandra performed a GSEA on the transcriptomic dataset, to analyse the enrichment of RB/E2F target genes compared to the total number of genes (~15000).* ***(B)*** *For validation of GSEA in (A), iStop and iRas infected with ev and shC4 were analysed for transcription of E2F target genes at day 8 of 4OHT. qPCR was used to detect mRNA levels of stated genes. β-actin was used as a housekeeping gene (n=3, ±S.E.M., two-tailed Student's t-test).*

** = p≤0.05, ** = p≤0.01.*

6.2.2 CERS4 regulates RB phosphorylation in OIS and replicative senescence

As discussed previously, RB has a key role in cell cycle regulation and can interact with many other cell cycle proteins, including other tumour suppressors. CERS4 knockdown had a significant negative effect on expression of p53, $p21^{CIP1}$ and $p16^{INK4a}$, although ceramide treatment did not rescue this phenotype (figure 6.2). The transcriptomic data in the previous section indicated RB activity is regulated by CERS4, so the next aim was to analyse the phosphorylation state of RB, in cells with CERS4 knockdown. This phosphorylation state was measured by western blot for total RB; a low percentage gel was used to observe separation of RB (~110kDa) from pRB (110-116kDa). Total RB was measured for the following experiments as RB has many different phosphorylation sites (Rubin, 2013) and it was impractical and expensive to test each specific phosphorylated RB.

First, in control cells and iRas with no 4OHT, RB is mostly phosphorylated (lanes 1-3, figure 6.4.A). Upon 8 days of 4OHT treatment, iRas cells hypophosphorylate and activate RB (lane 4, figure 6.4.A), correlating with the decreased expression of RB/E2F targets (pink bars, figure 6.3.B). CERS4 knockdown results in similar phosphorylation of RB to controls (lane 5, figure 6.4.A), correlating with the increased expression of RB/E2F targets (grey bars, figure 6.3.B). In addition, RB phosphorylation state during shCERS4-driven delayed replicative senescence was measured. In was clear at passage 24, where the population doublings between empty vector and shCERS4 were most different (figure 4.7.B), depleting CERS4 resulted in phosphorylated RB (compare lanes 1 & 2, figure 6.4.B). This indicated the control cells were starting to senesce whilst cells with CERS4 targeted were delaying senescence.

Together, this data indicates CERS4 does regulate RB activity and this corresponds with regulation of RB/E2F target expression during senescence. Next, RB phosphorylation state after ceramide treatment was examined to functionally link CERS4 and ceramide to RB activation in senescence.

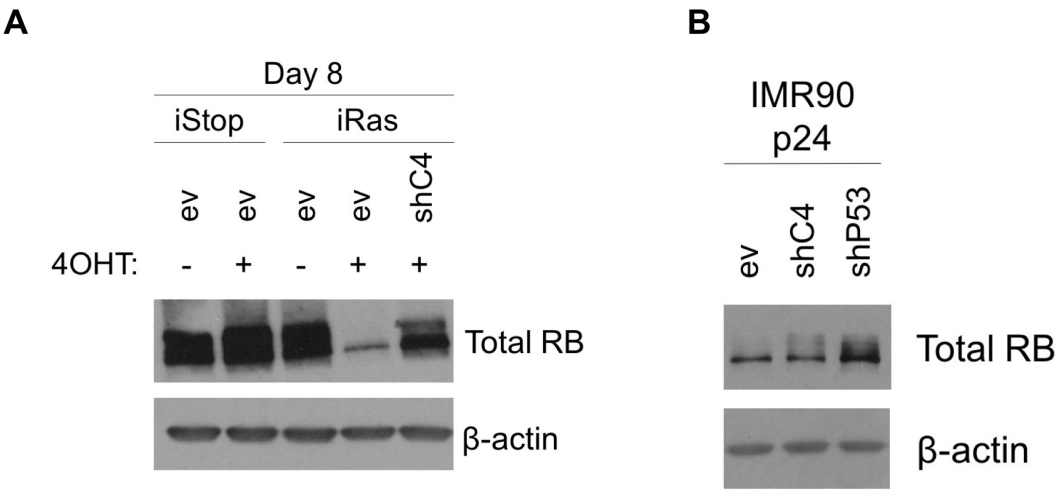

Figure 6.4 CERS4 inactivation mediates RB phosphorylation in OIS

For detecting total RB by western blot, cell pellets were collected and lysed on stated days of 4OHT treatment. For both (A) and (B), cell lysates were separated on 6% Tris-Glycine gels. Proteins were transferred onto a nitrocellulose membrane and blocked with 5% milk. Antibody for total RB (BD Biosciences, 554136) was incubated on the membranes and ECL used to visualize the bands. β-actin was used as a loading control and a 100-130kDa molecular weight marker was used for band identification purposes. ***(A)*** *iStop and iRas were infected with empty vector (ev) and a stable shRNA targeting CERS4 expression (shC4). On day 8 of 4OHT, cell lysates were subjected to western blotting of total RB, as described above (20μg cell lysate). Representative of three independent experiments.* ***(B)*** *IMR90 infected with empty vector (ev) and stable shRNAs targeting CERS4 (shC4) and p53 (shP53) expression were serially passaged. At passage 24, cells were pelleted and subjected to western blotting of total RB, as described above (15μg cell lysate). Representative of three independent experiments.*

4OHT = 4-hydroxytamoxifen, ev = pRS-empty vector, shC4 = pRS-shCERS4.

6.2.3 Ceramide reverses CERS4-driven RB phosphorylation state

Although data thus far indicates CERS4 has a role for RB hypophosphorylation in senescence, the rescue experiment with exogenous ceramide (described in *6.1*) was repeated to confirm the functional mechanism CERS4 has in OIS. First, cells transiently targeted for CERS4 inactivation were treated for 24 hours with 2μM C24-cer or DMSO on day 4 of 4OHT. C24-cer was used to see if longer chain ceramides, more specific to CERS4 activity, could have the same effect as short chain ceramides (i.e. C8-cer used in figure 6.2.D). Initially, the previous observation that CERS4 can regulate RB phosphorylation in OIS was confirmed when comparing the DMSO treated cells (compare lanes 1/3/5, figure 6.5.A). Also, C24-ceramide treatment rescued RB phosphorylation in CERS4 knockdown cells (compare lanes 5 and 6, figure 6.5.A).

Next, RB phosphorylation was analysed in ceramide-treated passage 24 cells derived from those in figure 6.4.B. Cells were re-seeded and treated for 24 hours with 2μM C8-cer or ethanol. C8-cer (short-chain ceramide) was used for all subsequent experiments because titration and effects were more reproducible, possibly due to increased cell-permeability, compared to long-chain ceramide. Ethanol treated cells showed the same RB phosphorylation as the previous experiment (compare lanes 1-2, figure 6.4.B to lanes 1/3/5 figure 6.5.B). C8-ceramide treatment did not have any effect on RB phosphorylation state in the three cell types tested (compare EtOH to C8-cer, figure 6.5.B). This suggests CERS4 and ceramide do not function via RB to regulate replicative senescence.

RB phosphorylation data from figure 6.4.A were recapitulated in separate experiments examined at day 6 of 4OHT: control and CERS4 knockdown cells have phosphorylated RB (lanes 1/5, figure 6.6); OIS cells have hypophosphorylated RB (lane 3, figure 6.6). These cells were also subjected to daily treatment of 2μM C8-cer or ethanol. Ceramide treatment with CERS4 knockdown appeared to cause dephosphorylation of RB (compare lanes 5 & 6, figure 6.6.A). This effect was much clearer in a replicate experiment (figure 6.6.B).

In conclusion, this section has confirmed CERS4 is functionally required for RB hypophosphorylation during OIS but not replicative senescence. This suggests the requirement of CERS4 to function in senescence is dependent on the initial trigger.

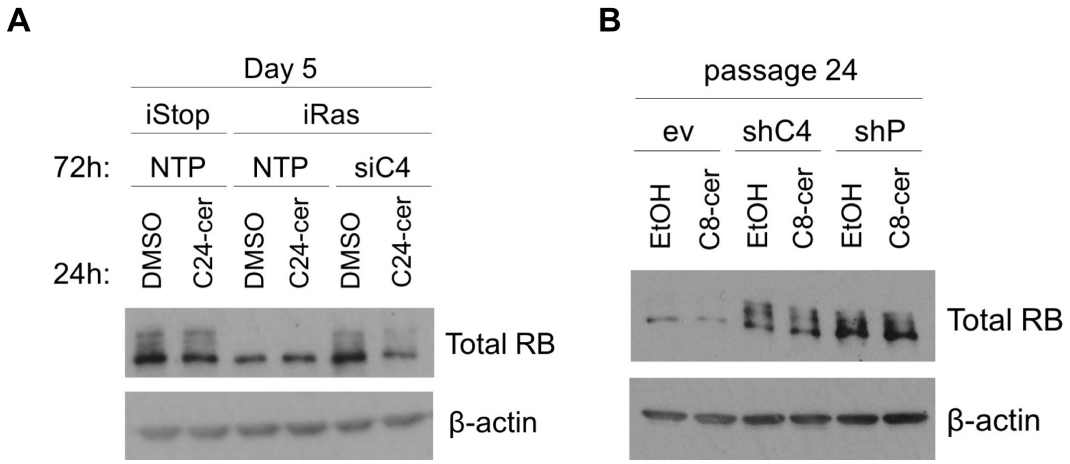

Figure 6.5 Short-term ceramide can reverse RB phosphorylation state in OIS cells but not replicative senescent cells

For detecting total RB by western blot, cell pellets were collected and lysed on stated days of 4OHT treatment. For both (A) and (B), cell lysates were separated on 6% Tris-Glycine gels. Proteins were transferred onto a nitrocellulose membrane and blocked with 5% milk. Antibody for total RB (BD Biosciences, 554136) was incubated on the membranes and ECL used to visualize the bands. β-actin was used as a loading control and a 100-130kDa molecular weight marker was used for band identification purposes. ***(A)*** *iStop and iRas were subjected to reverse transfection with Non-Target and siCERS4 on day 2 of 4OHT and 24h 18:1/24:0-ceramide treatment on day 4. On day 5 of 4OHT, cell lysates were subjected to western blotting of total RB, as described above (15μg cell lysate). Representative of 1 experiment.* ***(B)*** *IMR90 infected with empty vector (ev) and stable shRNAs targeting CERS4 (shC4) and TP53 (shTP53) expression were serially passaged. At passage 24, cells were re-seeded, cultured for 48 hours and treated with 2μM 18:1/8:0-ceramide for 24 hours. Cells were then pelleted and subjected to western blotting of total RB, as described above (10μg cell lysate). Representative of three independent experiments.*

4OHT = 4-hydroxytamoxifen, NTP = Non-Target pool, siC4 = siCERS4, ev = pRS-empty vector, shC4 = pRS-shCERS4, shP = pRS-shTP53, EtOH = ethanol, C8-cer = 18:1/8:0-ceramide, C24-cer = 18:1/24:0-ceramide.

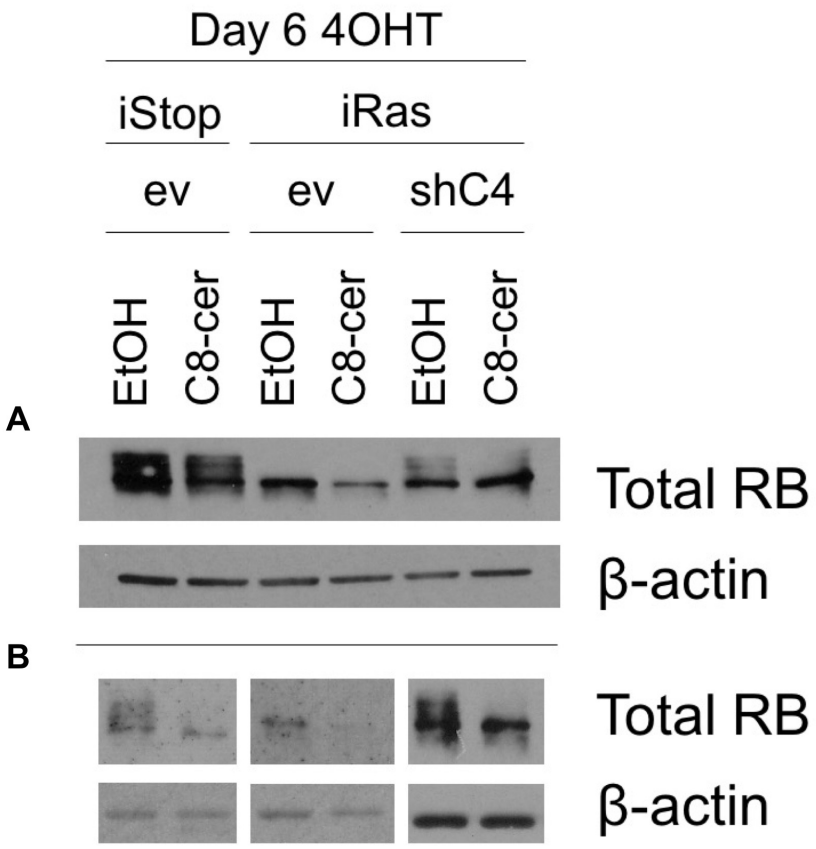

Figure 6.6 Long-term ceramide reverses RB phosphorylation state in CERS4-driven OIS bypass

iStop and iRas were infected with empty vector (ev) and a stable shRNA targeting CERS4 expression (shC4). Cells were subjected to daily 2μM 18:1/8:0-ceramide treatment from day 0 of 4OHT, and analysed for total RB expression by western blot. Briefly, 20μg cell lysate was separated on a 6% Tris-Glycine gel. Proteins were transferred onto a nitrocellulose membrane and blocked with 5% milk. Antibody for total RB (BD Biosciences, 554136) was incubated on the membranes and ECL used to visualize the bands. β-actin was used as a loading control and a 100-130kDa molecular weight marker was used for band identification purposes. This was repeated as three independent experiments; two are presented here: ***(A)*** *First replicate experiment (20μg cell lysate).* ***(B)*** *Second replicate experiment (10μg cell lysate).*

4OHT = 4-hydroxytamoxifen, ev = pRS-empty vector, shC4 = pRS-shCERS4, EtOH = ethanol, C8-cer = 18:1/8:0-ceramide.

6.2.4 Summary

Here, it was confirmed that CERS4 is required for RB hypophosphorylation and subsequent E2F inhibition in OIS and replicative senescence. Using stable and transient knockdown of CERS4, transcriptomics was used to interrogate RB/E2F target gene expression and RB phosphorylation state was extensively examined by western blotting for total RB. Lastly, ceramide rescue experiments confirmed CERS4 is functionally required for RB hypophosphorylation during OIS but not replicative senescence. In the final section, it was aimed to identify the mechanism by which CERS4 regulates RB. As it was suggested in *6.1*, CERS4 and ceramides likely function in OIS independently of tumour suppressors p53/p21 and p16, therefore hypotheses were explored involving interactions with other regulators of RB.

6.3 CERS4 drives PP1-dependent activation of RB

From the previous two sections, it was hypothesised CERS4 is functionally linked to OIS via RB phosphorylation and subsequent E2F target transcription. From the literature, it was found ceramide is an activator of protein phosphatases (PPs) (Chalfant *et al.*, 1999). PPs are regulators of RB and therefore provided a possible link between CERS4 and ceramides and cell cycle regulation. Considering this, the following hypothesis was assumed (illustrated in figure 6.7): senescence induced by oncogenic Ras^{G12V} promotes CERS4-mediated *de novo* ceramide biosynthesis and results in accumulated ceramide. OIS-related ceramide can activate PP to hypophosphorylate RB. RB is then able to bind and inhibit E2F, resulting in no transcription and expression of cell cycle proteins. It was preliminarily hypothesised PP1 being the specific protein phosphatase involved due to previous studies examining RB-PP1 binding (Hirschi *et al.*, 2010; Choy *et al.*, 2014). Furthermore, PP1 has been implicated in a mouse model of *ras*-induced senescence (Castro *et al.*, 2008). To initially address this hypothesis, co-immunoprecipitation (IP) experiments were performed to determine if PP1 and RB can bind during OIS, and if CERS4 is required for this interaction. These experiments were performed by Dr Andrea Quintanilla. To initially test the possible interaction of RB and PP1 in OIS, IP

conditions for RB and PP1 were optimised using control and OIS cells at day 8 of 4OHT (figure 6.8.A). As a positive control, a western blot for total RB was tested to show RB was being pulled down efficiently (top blot, figure 6.8.A). A western blot for PP1 revealed a band in OIS cells, indicating binding of RB and PP1 specifically during OIS (bottom blot, compare lanes 3 & 4, figure 6.8.A). On these blots the arrow denotes non-specific IgGs. Next, to analyse the role of CERS4 in RB-PP1 binding, the IPs were repeated with cells targeted for CERS4 knockdown. Again, this IP showed OIS-specific RB and PP1 binding and this was dependent on CERS4 expression (middle blot, compare lanes 8 & 9, figure 6.8.B). This data links CERS4 to PP1 that binds RB and regulates RBs E2F inhibitory function, specifically in OIS. This is robust evidence supporting the hypothesis that CERS4 can regulate the activation of PP1 and RB in OIS. Although, the rescue experiment with ceramide must be performed to confirm this function of CERS4 in OIS.

6.4 Chapter summary

The aim of this chapter was to identify the function of CERS4 and ceramide in OIS. Firstly, it was shown exogenous ceramide can rescue shCERS4-driven OIS bypass and is thus a functional metabolite in OIS. However, ceramide did not rescue $p16^{INK4a}$, $p21^{CIP1}$ and p53 expression, suggesting a functional mechanism independent of tumour suppressors. Exploring other potential mechanisms, it was found targeting CERS4 in OIS restored E2F target gene expression (a downstream readout for RB activity) and resulted in an accumulation of phosphorylated RB, in OIS and replicative senescence. Ceramide treatment rescued sh/siCERS4-mediated RB phosphorylation in OIS bypass, further indicating its functional role for OIS. Finally, co-immunoprecipitation confirmed CERS4-dependent RB-PP1 binding in OIS, physically connecting the mediators of cell cycle control in OIS. In conclusion, these preliminary results identify CERS4 as an essential metabolic checkpoint for the cell cycle arrest in OIS. Ceramide is known to activate protein phosphatases that regulate the hypophosphorylation of RB, therefore further experiments are required to assess the essentiality of ceramide for the binding of RB-PP1 and resulting activation of RB.

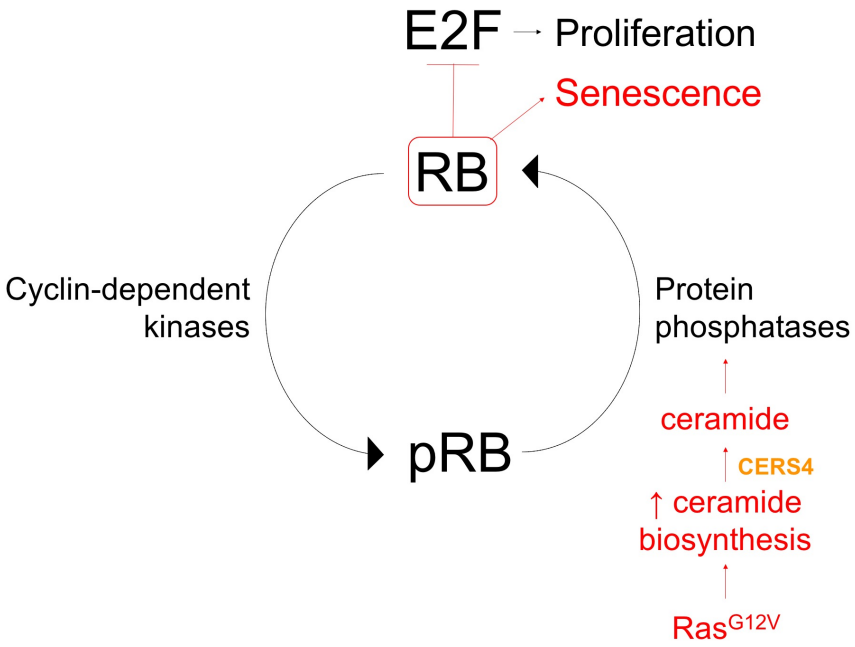

Figure 6.7 Schematic summarising the hypothesis that links CERS4 and ceramide to the PP1/RB axis

CERS4-mediated de novo ceramide biosynthesis is upregulated in senescence induced by oncogenic Ras^{G12V}. Accumulated OIS-related ceramide activates protein phosphatases to remove phosphates from inactivated RB, yielding hypophosphorylated RB. RB is then able to bind and inhibit E2F, resulting in no transcription and expression of cell cycle proteins. This process is results in the induction and maintenance of senescence. The red text and arrows indicate the hypothesis.

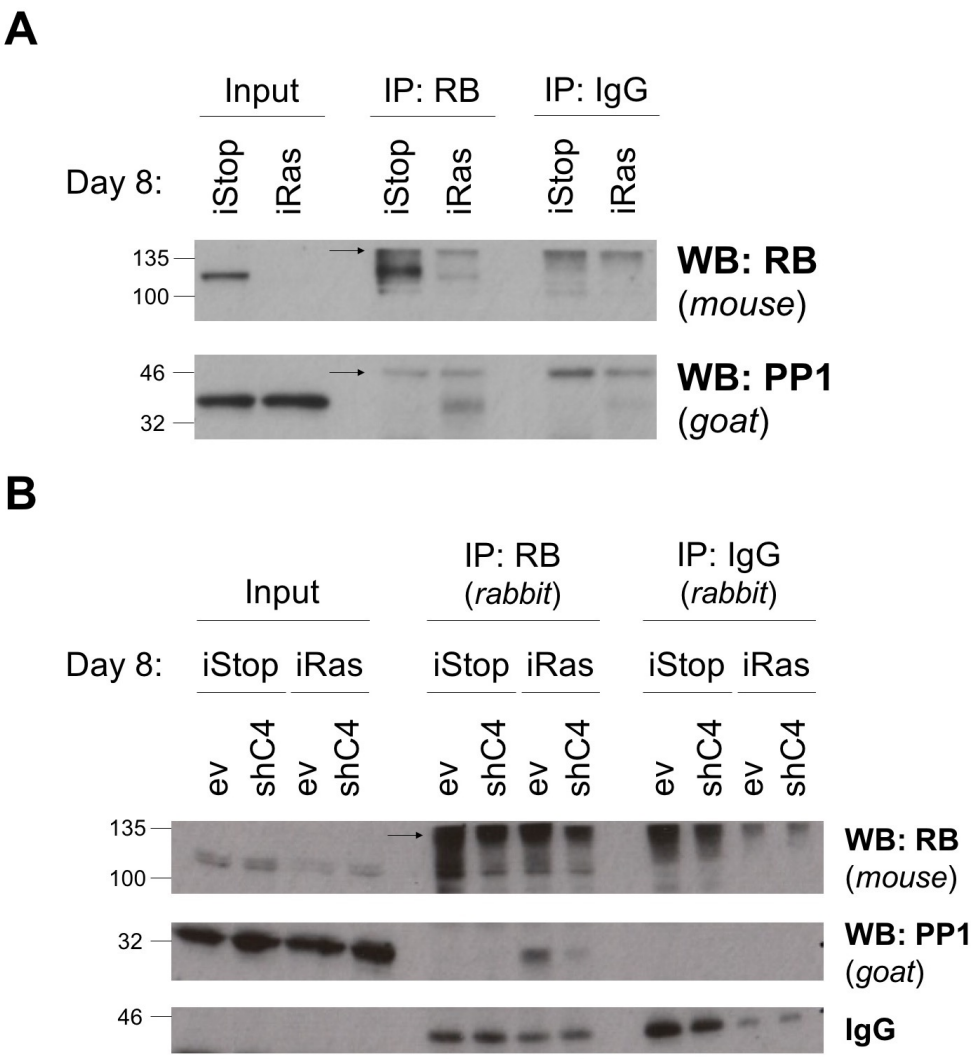

Figure 6.8 IP:RB indicates RB and PP1 binding in OIS is CERS4 dependent

Cells were subjected to immunoprecipitation of RB. Briefly, cells were lysed on ice and pelleted. Supernatant was collected and some lysate reserved for an input control. IP Dynabeads Protein G (Invitrogen, 10003) were equilibrated in lysis buffer and either RB antibody (sc-50) or IgG control (sc-2027) for 1-2 hours. The remaining lysate was incubated with the equilibrated beads for 4-6 hours. The beads were collected using a magnet and washed in lysis buffer. After a final wash, proteins were eluted from beads using SDS loading buffer (see 2.7 for further detail). Collected samples (i.e. input and IP) were analysed for total RB and PP1 expression by western blot, as described previously (PP1 antibody = sc-6108). ***(A)*** *Optimisation of IP.* ***(B)*** *IP repeated with CERS4-deficient cells, in control and OIS cells.*

4OHT = 4-hydroxytamoxifen, ev = pRS-empty vector, shC4 = pRS-shCERS4, WB = western blot, IP = immunoprecipitation, arrows = IgGs.

Chapter Seven: Discussion

7.1 Summary of results

As discussed in *1.2.3*, senescent cells undergo many metabolic alterations that are implicated in cancer progression; therefore, the main focus of this thesis was to identify new metabolic regulators of OIS. High-content siRNA screening coupled with BrdU immunofluorescence, as a proliferation readout, was used to initially identify possible metabolic regulators of OIS; the use of loss-of-function siRNA screening is discussed below (*7.2*). The original primary screen, where 553 genes were targeted with siRNA (see Appendix 1), identified 16 genes bypassing senescence when knocked-down (figure 3.6 & table 3.1 for summary). 11 genes were implicated at day 5, an 'early' OIS time point; 2 genes were implicated at day 10, a 'late' OIS time point; and 3 genes were implicated at both time points. Subsequently, the 16 genes were validated in a secondary siRNA screen. This involved deconvoluting the pooled siRNAs from the primary screen and setting a validation threshold of: genes with two or more siRNAs bypassing OIS. In addition to BrdU incorporation, $p16^{INK4a}$ and $p21^{CIP1}$ expression was also assessed for more robust validation. 14 of the 16 hits were validated by BrdU incorporation, and a further 4 and 5 hits showed an effect on $p16^{INK4a}$ and $p21^{CIP1}$ expression, respectively (table 3.3 for summary). Functional annotation of the validated hits indicated a significant enrichment of genes involved in lipid metabolism, including the top hit ceramide synthase 4 (CERS4).

From chapter 3, it was concluded that lipid metabolism was implicated in regulating OIS. As current literature had not extensively studied lipid metabolism in OIS, this provided an attractive focus for the remainder of this thesis. In particular, the next aim was to thoroughly validate the top screen hit CERS4 as a regulator of OIS. In addition to the siRNA, shRNA stably targeting CERS4 expression was generated and used to identify the essentiality of CERS4 for a number of senescence markers; gene targeting techniques are a topic of discussion below (*7.3*). Bypass of OIS mediated by CERS4 knockdown increased proliferation, reduced SA β-galactosidase activity and reduced expression of tumour suppressors ($p16^{INK4a}$, $p15^{INK4b}$, $p21^{CIP1}$ and p53)

and the SASP. A transcriptomic dataset was utilised for mRNA expression analysis. In addition, CERS4 was implicated in replicative senescence, as knockdown partially delayed senescence in serially passaged IMR90. Furthermore, $p16^{INK4a}$ but not $p53/p21^{CIP1}$ expression was affected in this model of senescence; this result is discussed in further detail below (*7.7.2*). Finally, it was hypothesised CERS4 functions in OIS to increase ceramide synthesis; therefore, this environment was recapitulated using pharmacological inhibitors of enzymes that modify ceramide. Inhibition of three enzymes resulted in a senescence-like cell cycle arrest in IMR90, indicating accumulated ceramide is required for senescence induction.

Chapter 4 identified CERS4 as an essential lipid metabolic regulator in OIS, suggesting ceramide synthesis is mechanistically implicated in OIS. The next aim of the thesis was to analyse lipid metabolism in OIS and determine if CERS4 and ceramides are functionally implicated. First, the transcriptomics dataset was used to identify any lipid metabolic gene sets enriched during OIS. Indeed, a transcriptional regulatory program for many lipid metabolic pathways was identified. In addition, CERS4 knockdown resulted in significant transcriptional downregulation of ceramide metabolic pathways; these surprising observations are further discussed below (*7.6*). Next, LC-MS based global lipidomics identified a rewiring of lipid metabolites present in OIS and specifically, ceramides were accumulated. These results were validated using targeted and quantitative ceramide analysis; CERS4-specific ceramides (18-22 carbon length fatty acids) were accumulated in OIS and reduced after CERS4 knockdown. Labelling studies were then used to identify the mechanism by which OIS-related ceramide is produced. Using stable heavy-isotope of serine (2,3-$^{13}C_2$-serine), an increase in flux through the *de novo* synthesis of ceramides pathway was identified in OIS. A modified ceramide substrate (17:1/8:0-ceramide) was used to demonstrate the activity of the recycling pathway was not increased in OIS and thus was ruled out as a mechanism for OIS-related ceramide synthesis. The results from chapter 5 concluded that OIS has increased ceramide content that is regulated by the *de novo* activity of CERS4; discussion below focusses on ceramide synthases in ceramide metabolism and what other metabolic experiments to perform in the future (*7.4*).

The focus of the final chapter was to determine the function of OIS-related ceramide in OIS, and how CERS4 may be mechanistically linked to the cell cycle arrest. Firstly, to show that ceramide is a functional metabolite in OIS, rescue experiments were performed using exogenous ceramide treatment to reverse OIS bypass driven by CERS4 knockdown. From these experiments, it was found ceramide could not rescue the expression of $p16^{INK4a}$, $p21^{CIP1}$ and p53, suggesting their regulation by CERS4 is likely a consequence of its actual function in OIS (discussed in *7.7.1*). Therefore, different downstream mechanisms of CERS4 in OIS were explored. The transcriptomics dataset revealed a CERS4-dependent regulation of RB targets (E2F-driven cell cycle genes) in OIS. Furthermore, RB hypophosphorylation in OIS was driven by CERS4 and exogenous ceramide rescued this observation. As alluded previously, CERS4 functions independently of $p16^{INK4a}$, $p21^{CIP1}$ and p53, so interactions with other regulators of RB were explored. It has been previously described that protein phosphatase 1 (PP1) initiates RB hypophosphorylation through physical binding (Hirschi *et al.*, 2010) and can be activated by ceramides (Chalfant *et al.*, 1999). Therefore, it was hypothesised that OIS-related ceramide activates PP1 to hypophosphorylate RB and initiate cell cycle arrest through E2F inhibition. To test this hypothesis, co-immunoprecipitation was used to show in RB-PP1 binding was CERS4-dependent in OIS. Although preliminary, this data connects CERS4 to mediators of the cell cycle and suggests CERS4 functions as a metabolic checkpoint, through RB in OIS; this data is further discussed below and future work is proposed to validate these findings (*7.8*). In addition, other potential roles in senescence for increased ceramide metabolism and CERS activity are discussed in *7.5*.

Figure 7.1 provides a graphical summary of results described here. The remainder of this chapter will thoroughly discuss strengths and weaknesses of the data and techniques used, future work and the broader implications of these results for human health and disease.

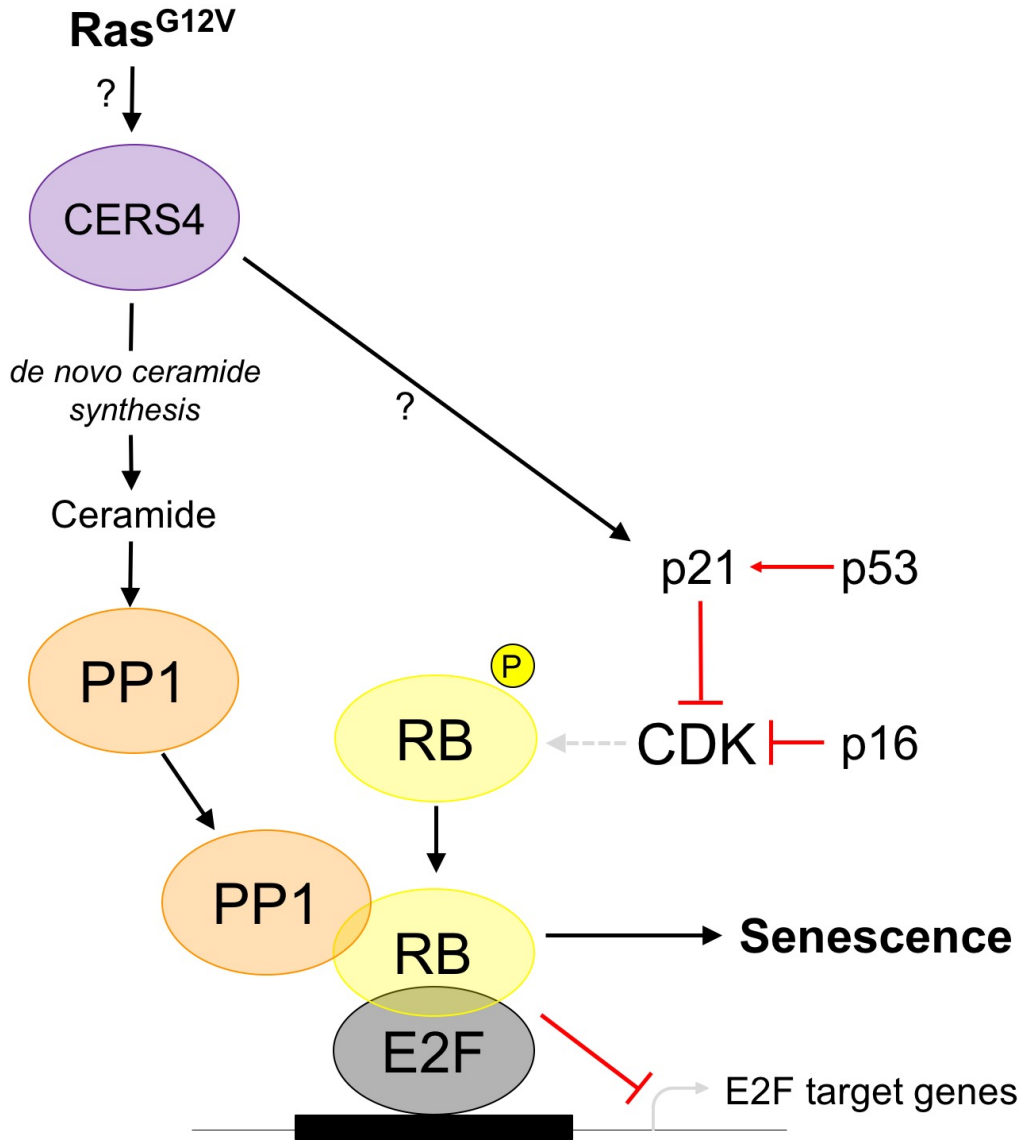

Figure 7.1 Summary of thesis results

The main finding of this thesis was the identification of CERS4 as a metabolic regulator of OIS. Validation studies indicated CERS4 could regulate the four major markers of senescence: proliferation, SA β-gal, tumour suppressor expression and SASP expression. Mass spectrometry techniques were used to identify the de novo synthesis of ceramides as the mechanism for OIS-related ceramide production. Ceramide can activate PP1 to physically bind and hypophosphorylate RB. The resulting inhibition of E2F blocks downstream transcription of E2F target genes involved in the cell cycle and induces senescence. This mechanism revealed CERS4 regulation of tumour suppressors is a consequence of its role as a metabolic checkpoint.

Red lines indicate inhibitory functions. Grey arrows indicate inhibited pathways. Black arrows indicate active pathways. Question marks indicate unknown mechanisms of activation.

7.2 Screening approaches

RNAi is an established technique for the identification of novel regulators of senescence, as described in *1.3.3*. The primary siRNA screen performed in this thesis used BrdU incorporation as the phenotypic readout of OIS, measured using immunofluorescence (*3.1*). To minimize human error and make the screen as reliable as possible, automation was utilised; for example, a liquidator (Mettler Toledo) was used for all liquid-handling steps, to minimize pipetting errors. In addition, to ensure both siRNA transfection and BrdU staining were reliable each plate of the siRNA screen was performed in triplicate. Indeed, replicates of each plate at day 5 had a Spearman's rank correlation coefficient of >0.8 (figure 3.2.C&D). This is a measure of the strength of the relationship between replicates. A value between 0 and 1 represents a positive correlation, however the closer to 0 the value, the worse the correlation. Therefore, a correlation of >0.8 for the day 5 replicates indicated good reproducibility. To adjust for screen-wide inconsistencies, such as edge effects, plate normalisation was implemented (figure 3.2.A & 3.4.A). The selected normalisation method used the plate median as a constant comparison for all data within that plate (Pelz, Gilsdorf and Boutros, 2010). Another student in the lab, Priya Hari, has previously shown the 96-well plates used in a HCS format have minimal edge-effects. Although it was clear from the original distribution boxplots that there were only small screen-wide changes (pink boxes, figure 3.2.A & 3.4.A), normalisation was still used to ensure accurate data analysis. Overall, this screening platform was a reliable method for assessing 'early' OIS-bypass. Of the original 16 genes identified in the primary screen, 14 were validated in the secondary screen (table 3.3). Three genes (CERS4, GCLC and LPCAT4) were validated by BrdU, $p16^{INK4a}$ and $p21^{CIP1}$ expression, indicating these genes are likely to be essential for OIS.

Although for day 5 the screen yielded excellent results that were validated, the day 10 data had a number of issues. First, the Z' Factors indicated poor separation between negative and positive controls (figure 3.4.B). This may be explained by the nature of established OIS (10 days of 4OHT), which is harder to bypass. The positive control targeting p53 struggled to overcome the stable cell cycle arrest, explaining the poor Z' Factor. Second, the day 10 screen data had variable correlations (0.4-0.8)

between replicates (figure 3.4.C). As mentioned above, the Spearman's rank correlation coefficient was used to gain information about the reproducibility between replicates. Although plate 7 had a good correlation of 0.8, the remainder had mediocre correlations. This poor reproducibility could be explained by reduced dynamic range; only a small population of cells are bypassing OIS, increasing chances for variability. To overcome variability and ensure potential hits were not discarded, an alternative data analysis was performed (*3.1.3*). Using the 'individual plates' Web CellHTS2 analysis, CERS4 was also identified as the top hit at day 10 (figure 3.5). Four other genes were also identified using this method of data analysis, reinforcing the decision to use this screening protocol. Although there was variation, choosing the correct data analysis meant the data could still be used to gain significant hits. For future screens of OIS regulators, alternative experimental design should be considered; for example, utilising a double siRNA transfection protocol. This could pick up different regulators, with functions in OIS implicated after the standard 72 hour transfection period.

CERS4 was chosen for follow-up studies due to a strong Z-score representing OIS-bypass at both day 5 and 10, and the clear involvement of lipid metabolism in OIS. However, there were a number of other genes that could be of interest for further examination. For example, GCLC, another hit validated by all three secondary screen readouts, encodes the first rate-limiting enzyme of glutathione synthesis. Glutathione has previously has been shown to have a vital function in OIS-related oxidative stress (Zheng *et al.*, 2015). Additionally, LPCAT4, encoding an enzyme involved in glycerolipid synthesis, may contribute to a different avenue of OIS-related lipid metabolism. Finally, functional annotation analysis (*3.2.3*) also found 'proteolysis' pathways (GO terms: 0030162 & 0008610) significantly enriched in the validated genes list (data not shown). This is of particular interest due to the importance of proteostasis for OIS, as described in *1.2.3.2*. Further validation and mechanistic studies concerning these screen hits could expand current knowledge of protein homeostasis in OIS.

This is the first RNAi screen described that specifically targets metabolic factors in OIS. Using siRNA in this targeted metabolic screen allowed the regulation of

expression levels, rather than complete ablation of genes. Although this method will not be optimum for targeting all metabolic factors, a commendable number of hits was yielded (~3% of starting number of genes targeted). As described above, some genes identified in the primary screen are broadly implicated in metabolic processes known to be altered in senescence. However, this is the first functional characterisation of an individual metabolic gene identified by RNAi screening. Genome-wide screens have been performed on different cellular models of senescence (Bishop *et al.*, 2010; Kaplon *et al.*, 2014), however metabolic factors have not been identified from these screens. This could be due to difficulty recapitulating results in different senescence contexts using different RNAi techniques; Kaplon *et al.* (2014) used shRNAs in $BRAF^{V600E}$-induced senescent human diploid fibroblasts, whilst Bishop *et al.* (2010) used siRNA in replicative senescent human epithelial cells. Furthermore, known metabolic regulators of OIS were targeted in the primary siRNA screen but were not identified as hits. For example, Kaplon *et al.* (2013) identified pyruvate dehydrogenase (PDH) as vital for regulating increased TCA cycle metabolism in OIS. PDH had a Z-score of -0.99 in the day 5 primary screen (data not shown); this Z-score is within non-significant variation of the screen median, suggesting targeting PDH for loss-of-function by siRNA does not affect Ras-mediated senescence. The discrepancies between this thesis and the Kaplon *et al.* study could be explained by inefficient siRNA knockdown of PDH enzymatic activity or again, the different cellular systems used to model OIS. As described throughout *1.1*, genetic context of senescence can have substantial contribution to the resulting cellular phenotype, including rewiring of metabolism. Ras^{G12V}-induced senescence could present with highly altered lipid metabolism rather than glucose metabolism (as seen with $BRAF^{V600E}$) and this was echoed by the enrichment of lipid metabolic genes identified in the screen (table 3.2).

7.3 Targeting CERS4 expression

As described in *1.3.1*, RNAi is a powerful method for targeting the expression of genes. The use of siRNAs in the screening was a robust technique for initial identification of OIS regulators, as discussed in *7.2*. However, siRNAs are notorious

at inducing off-target effects, whereby partially complementary non-target genes are inadvertently targeted (Jackson and Linsley, 2010). For this work, several tactics were used to reduce off-target effects and validate results gained using siRNA. First, all siRNAs were chemically modified with a 2'-*O*-methyl ribosyl at position 2 of the sequence (Jackson *et al.*, 2006), to reduce off-target effects (commercially referred to as ON-TARGET*plus* siRNA (Dharmacon)). Second, the siRNA reverse transfection protocol was optimised by Priya Hari, for a different screening project. Priya optimized conditions such as the siRNA concentration, transfection reagent and time, and cell density; if these factors are not correctly optimized, results using siRNA can be unreliable and inconsistent. In addition, siRNAs were introduced in IMR90s using a lipid-mediated transfection protocol; this could interact with siRNA targeting CERS4 to bias lipid metabolism in OIS. Therefore, for validation purposes it was essential to test other ways of targeting CERS4 expression (e.g. shRNA). An shRNA was generated that stably expressed the siCERS4_1 sequence (figure 4.2). An additional shRNA expressing the target sequence from siCERS4_4 was generated and showed an OIS-bypass effect measured by proliferation (data not shown); however, this was not as striking as the first shRNA and it was decided to proceed with one shRNA for further characterisation. Future attempts to knockout CERS4, using CRISPR, could provide further verification of CERS4s function in OIS, in addition to being more amenable for *in vivo* experiments (this is further discussed in *7.9*).

The primary siRNA screen used pooled siRNAs, that were composed of 4 individual sequences targeting the same gene. For the secondary screen, the pooled siRNAs were deconvoluted and the effects of the individual siRNAs were assessed. With CERS4, there were discrepancies between the effect of individual siRNAs on BrdU incorporation (figure 3.10), $p16^{INK4a}$ expression (figure 3.12) and $p21^{CIP1}$ expression (figure 3.13). Although CERS4 function in OIS was found to be independent of $p16^{INK4a}$ and $p21^{CIP1}$ (chapter 6 and figure 6.2), this discrepancy warrants further discussion due to its implications in siRNA techniques. siCERS4_1 was validated by all three readouts, whilst the other three siRNAs were only validated by BrdU incorporation. This was likely due to the intensity of the effect on proliferation. siCERS4_1 caused a large increase in BrdU incorporation similar to positive control

siTP53, meaning this correlated with significantly decreased tumour suppressor expression. The other three siRNAs caused a smaller (but significant) increase in BrdU incorporation, with small effects, if any, on tumour suppressor expression. This observation was likely due to the efficiencies of different siRNAs on targeting CERS4 expression. Indeed, mRNA knockdown of the individual siRNAs correlated with the effect on BrdU incorporation (compare figure 4.1.A to figure 3.10). siCERS4_2 had the least BrdU incorporation and CERS4 mRNA knockdown. Accordingly, siCERS4_2 did not affect CERS4 mRNA expression but still influenced OIS. Generally, the optimal time for siRNA knockdown is 72 hours post-transfection, therefore mRNA levels were measured at this time point. The optimal transfection time for siCERS4_2 may be shorter and by the time mRNA is measured, CERS4 expression is normal but the effect on proliferation remains. To address this issue, CERS4 mRNA expression can be assessed at multiple time points post-transfection of siCERS4_2. Alternatively, the siRNA could be affecting CERS4 translation without affecting transcription.

7.4 Ceramide synthesis in OIS

7.4.1 Ceramide synthase expression and activity

The key result from this thesis was the identification of ceramide synthase 4 (CERS4) as a regulator of OIS. It was essential to validate this finding, by investigating the expression and activity of CERS4 in OIS. First, CERS4 mRNA expression levels were measured by qPCR, to gain information about knockdown efficiencies and expression in OIS. As shown in figures 4.1.A and 4.2.A, both si and shRNA knockdown of CERS4 at day 5 and 8 of OIS were very efficient at reducing CERS4 mRNA levels. Unexpectedly, CERS4 expression in OIS was reduced ~50% compared to proliferating control, at day 5 and 8 of OIS (figure 4.1.A & 4.2.A, respectively). Protein levels of CERS4 could not be measured by four different antibodies, tested using western blotting and immunofluorescence methods (figure 2.5). Western blot optimisation was pushed to the technique's limits: up to 80μg of lysate was loaded onto SDS-PAGEs and up to 2 hour exposure times were

performed, and no CERS4 was detected. Although this may be due to poor antibody efficiency, it could also be explained by low endogenous levels of CERS4. When measuring CERS4 mRNA levels, the Ct values were high (~30 cycles for OIS samples, data not shown). This implies the starting amount of CERS4 transcript available for translation is low, and therefore protein levels are low. Another explanation may be that CERS4 is under strict transcriptional regulation, that is not inferred by the experiment timings used in this work. This idea is further discussed in *7.6*.

Although there is a 50% decrease in CERS4 mRNA expression, there is increased CERS4 activity in OIS; CERS4-specific ceramides with 18-22 fatty acid chains are accumulated (figure 5.6) due to increased *de novo* synthesis activity of CERS4 (figure 5.9.B&D). This large discrepancy between expression and activity could be due to several reasons. OIS cells could overcome the transcriptional deregulation of CERS4, which occurs as part of the global transcriptional regulation of lipid metabolism, by allosterically activating the remaining CERS4 enzyme. Allosteric activation involves the binding of a regulatory molecule at a site separate from the enzymatic active site. Allosteric activation alters the protein dynamics of the enzyme, resulting in conformational changes that enhance the enzymatic activity. This could account for faster enzyme kinetics and capacity of a single molecule of CERS4. To understand the enzyme kinetics, *in vitro* enzymology could be performed using recombinant CERS4 and ceramide substrate. In addition, the expression of CERS4 could be increased early on in OIS (not measured here) and be still active when ceramide content was measured (day 5), perhaps due to a long half-life. Finally, sub-cellular ceramide metabolism is highly compartmentalised (Hannun and Obeid, 2011). CERS4 expression in OIS could be occurring in a different sub-cellular location that is not indicated from whole cell lysis. To address this issue, CERS4 expression can be analysed in different cell fractions (e.g. nuclear, cytoplasmic, endoplasmic reticulum/Golgi, vesicles).

Mass spec experiments measuring ceramide content and *de novo* flux revealed small but significant changes compared to the control. This effect could be explained by the fact CERS4 is one isoform out of a family of six ceramide synthases. Although

OIS preferentially requires 18/20/22-ceramides, the synthesis of ceramides other than CERS4-specific products is also upregulated (figure 5.9.B&D). Additionally, there was a global rewiring of the lipidome in OIS (figure 5.5). This metabolic data suggests that OIS can alter the activity of all ceramide synthases, but specifically requires CERS4 to mediate this lipidomic rewiring. Furthermore, the OIS-bypass caused by targeting CERS4 is a striking outcome of small changes in the ceramide content. This indicates a delicate balance in lipid metabolism, initiated and mediated by CERS4, is required for robust OIS. Further interrogation of lipid metabolism through an OIS time course could provide further understanding of how CERS4 mediates lipid rewiring, and how this may be connected to other OIS phenotypes, such as SA β-gal.

The increase in *de novo* synthesis of ceramides in this OIS model could be related to recent work showing increased *de novo* serine synthesis in Kras-driven pancreatic and intestinal cancers in mice (Maddocks *et al.*, 2017). Although the downstream mechanisms of ceramide in OIS have been deconvoluted in this thesis, and are further discussed below, upstream mechanisms have not been explored. The increased synthesis of serine in response to oncogenic Ras could be connected to ceramides, as serine is required for the first rate-limiting step of *de novo* ceramide synthesis (figure 1.3). In the Ras-induced senescence model used by Maddocks *et al.* (2017) the increased ceramide content could feedback to increase *de novo* synthesis of serine; this could be initially measured by expression analysis of SSP enzymes followed by $^{13}C_6$-glucose labelling of serine and measurement of $^{13}C_6$ incorporation into ceramides.

7.4.2 Functional *in vitro* experiments perturbing ceramides

A number of experiments were performed in this thesis that perturbed ceramide metabolism and measured the outcome on senescence phenotype. First, pharmacological inhibition of ceramide metabolic enzymes ASAH1, CERK and SPHK1 resulted in a senescence-like cell cycle arrest in parental IMR90 (figure 4.9). It was hypothesised inhibition of enzymes that metabolise ceramide results in accumulation of unmodified ceramide and induce senescence. However, the effect on ceramide levels post-treatment with the inhibitors was not determined. Although the

inhibitors have been confirmed in other biological systems (Graf *et al.*, 2008; Draper *et al.*, 2011; Gao *et al.*, 2012), lipidomics must be performed to confirm levels of ceramide post-inhibition in IMR90 and validate the findings in section *4.5*. In addition, the inhibitors were tested in the OIS system, however, even low doses resulted in cellular stress and death. This suggests ceramide metabolism is indeed a highly regulated process in OIS and imbalance results in catastrophic stress.

Secondly, exogenous ceramide treatment was able to rescue the effects of CERS4 knockdown in OIS, resulting in decreased proliferation and increased SA β-gal (figure 6.1). The effect of high concentration (2μM) ceramide treatment on intracellular levels of ceramide was not measured. Therefore, it is unknown if the results from the rescue experiments are truly due to ceramide entering the cell and compensating for lack of CERS4 activity. To address this issue, mass spectrometry should be used to measure ceramide levels in all of the experiments using exogenous ceramide. It is important to note that it is unknown how cell-permeable ceramide is. This issue was overcome partly by using C8-ceramide – the shorter the fatty acid chain the more likely the ceramide will pass through the cell membrane. Future work recapitulating these experiments with CERS4-specific ceramides (C18-20) would be more relevant and an additional vehicle to encourage cellular uptake of ceramide could be used. Finally, there was no rescue of tumour suppressor expression in CERS4-depleted cells treated with ceramide. This suggests CERS4 is mechanistically independent of tumour suppressors. To confirm this, ceramide treatment or CERS4 overexpression on OIS cells with p53, $p21^{CIP1}$ or $p16^{INK4a}$ knockdown should have no effect on OIS-bypass.

7.4.3 Approaches to measure ceramide synthesis

As described in *1.2.1*, LC-MS is an accurate method to measure metabolites in many different biological scenarios. For this thesis, lipids were extracted from cultured cells under several different conditions. It was vital to optimise the LC-MS methods to gain as much information as possible from the lipidomics experiments (figures 5.8 & 5.10). Once optimised, all ceramides were identified by the presence of a fragment at 264.2682 m/z and retention time. Overall, the LC-MS approaches used in this thesis provided accurate readouts of ceramide metabolism. In addition, this is a novel

description of ceramide synthesis interrogation in human cells, using a combination of 2,3-$^{13}C_2$-serine and 17:1/8:0-ceramide to measure *de novo* and recycling ceramide synthesis, respectively. For future work, deconvoluting the links between glucose and lipid metabolism could provide further insight into OIS metabolism rewiring. As described in *1.2.3.1*, a metabolic switch from glycolysis to the TCA cycle occurs in OIS, controlled by PDH activity (Kaplon *et al.*, 2013). This could be linked to increased ceramide synthesis through citrate and acyl-CoA; this hypothesis could be examined using a glucose with suitably labelled carbon(s) to trace from the TCA cycle to ceramides. Furthermore, the accumulation of ceramides could be related to increased glucose consumption and subsequent proteoxic response observed in therapy-induced senescence by Dörr *et al.* (2013). Finally, the role of RB as a mediator of glucose metabolism in OIS (Takebayashi *et al.*, 2015) may also be linked to ceramide metabolism, and warrants further investigation.

In addition to LC-MS approaches, imaging methods to examine the sub-cellular compartmentalisation of ceramide synthesis in OIS could be used to reveal mechanistic information about how senescent cells physically accommodate rewired ceramide metabolism. This proved to be important for the characterization of the TASSC in OIS, described by Narita *et al.* (2011) (*1.2.3.2*). The *de novo* synthesis of ceramides occurs in the endoplasmic reticulum, whilst the recycling pathway occurs mostly in the lysosomes (Hannun and Obeid, 2008). One would expect, due to increased lysosomal content in senescence (Kurz *et al.*, 2000), that the recycling pathway is activated; however, this is not the case, as proven with 17:1/8:0-ceramide labelling (figure 5.11). Moreover, the function of lysosomal SA β-galactosidase activity is unknown and could be linked to ceramide metabolism through complex galacto-sphingolipids. Thus, understanding the compartmentalisation of lipid metabolism, particularly ceramides, could answer long-standing questions in the senescence research field. However, lipids are much smaller than proteins and could be technically difficult to image without probes that do not disrupt the local environment (Schultz *et al.*, 2010). The recent advance in imaging-mass spectrometry (iMS) technologies may avoid such technical issues. iMS resolves m/z of molecular species to ion maps of an *in situ* biological sample (Harkewicz and

Dennis, 2011). iMS is generally used on tissues, particularly in clinical settings, but there is scope for the technique to identify sub-cellular locations of metabolites.

7.5 Role of ceramide and ceramide synthases in senescence

It has been concluded from this thesis that CERS4-synthesised ceramide acts in a metabolic checkpoint to activate PP1-mediated RB dephosphorylation and initiate cell cycle arrest. This mechanism correlates with current mechanistic knowledge regarding ceramides and senescence (*1.2.4.3*). However, an additional hypothesis not considered here is the role ceramide plays in cell membranes. Senescent cells are generally very enlarged and have increased vesicle content (Serrano *et al.*, 1997). Therefore, increased ceramide content, and altered lipidome as a whole, could be linked to the considerable production of lipid bilayers for cellular membranes during senescence. As reported by Atilla-Gokcumen *et al.* (2014), atomic force microscopy can be used to determine mechanical properties of cell membranes. This approach could be used to examine the effect of CERS4 depletion on the cell membrane of bypassed cells, compared to both proliferating and senescent cells. In addition, if a working CERS4 antibody is available, co-staining with vesicular proteins could be used asses the role CERS4 plays in vesicle formation. This could also determine if there is a physical link between subcellular location of CERS4-driven ceramide synthesis and sites where cellular membranes are required.

Ceramides have previously been implicated in replicative senescence and aging-related pathologies. Current knowledge also indicates cancer cells downregulate ceramide biosynthesis by overexpressing ceramide metabolic enzymes (*1.2.4*). However, this work is the first indication that ceramide accumulation is a characteristic of OIS. This thesis also presents CERS4 as a key mediator of OIS, and correlates with the cancer attenuation effect of CERS4-synthesised ceramide reported by Gencer *et al.* (2017). Although *in vivo* data is lacking (*7.9* for further discussion), this thesis identifies a promising novel metabolic pathway, regulated by many different genes, to further investigate for cancer therapeutic development. Furthermore, this work has preliminarily identified other genes encoding metabolic

proteins (table 3.3), that may provide additional novel OIS mechanisms to explore for cancer therapeutic potential.

As described in *1.2.4.4*, there has been some research in combining traditional cancer chemotherapy with increasing ceramide levels. This can be achieved by either activating ceramide synthesis enzymes or inhibiting ceramide metabolic enzymes or introducing exogenous ceramide. These approaches have shown to increase sensitivity of cancer cells *in vitro* to chemotherapy-induced apoptosis. The work from this thesis suggests there is a balance of ceramide metabolism that is differentially altered in senescence and cancer. In theory, this metabolic balance could be targeted pharmacologically to induce senescence in tumours, in combination with induction of senescent cell apoptosis and clearance. This approach is similar to the synthetic lethal metabolic targeting of senescent cells in an *in vivo* cancer model, performed by Dörr *et al.* (2013). For example, NVP-231 is an inhibitor of ceramide kinase and results in accumulated unmodified ceramide (although this has not been proven by mass spectrometry, *7.4.2*). In principle, NVP-231 could be used to induce senescence of cancer cells, as already shown for human cell *in vitro* (Pastukhov *et al.*, 2014). The senescent lesion can be subsequently targeted for apoptosis and clearance by the immune system. In conclusion, this scientific evidence presented in this thesis warrants further work analysing the effect of targeting ceramide metabolism for cancer therapy.

7.6 Transcriptional regulation of lipid metabolism in OIS

It is evident that senescence causes unique gene expression patterns, that are regulated by SAHFs (*1.1.2.4*); however, the global transcriptional regulation of lipid metabolism observed in this thesis is remarkable (figure 5.1). Transcriptomics revealed OIS modifies transcription of many different lipid metabolic pathways, including transport, storage and synthesis. Moreover, targeting CERS4 expression significantly reversed this global modification of lipid metabolic pathways, not just ceramide-related pathways (figures 5.1 & 5.2). Although, further qPCR validation of specific lipid metabolic genes is required; it can be concluded from this data that OIS

induces a tightly regulated lipid metabolic gene transcriptional program and CERS4 is an essential mediator of this regulation. Furthermore, CERS4 has a homeobox domain (Holland, Booth and Bruford, 2007), that have well-known transcriptional regulatory activity through DNA-binding. This suggests how CERS4 may be linked to the regulation of lipid metabolic gene expression in OIS. This function of CERS4 is discussed further in *7.7.2*, in terms of p16 transcription.

Throughout this thesis, CERS4 has been associated with both the initiation and maintenance of OIS. To confirm this, it would be important to analyse both the transcriptome and lipidome in a time course of OIS, using comprehensive sequencing and mass spectrometry technologies. This could be performed initially *in vitro* using the IMR90-ER:Ras 4OHT-inducible system. Subsequently, an *in vivo* panel of normal, senescent and cancerous tissues (such as the PanINs described in *7.9*) could be utilised to gain data more relevant to humans. A time course would yield vital information about the regulation of the transcription of CERS4 and related genes, in parallel with their activity. This information should be carefully considered if lipid metabolism in OIS becomes a potential target for cancer therapy, to ensure the optimum effectiveness.

7.7 Regulation of tumour suppressors by CERS4

7.7.1 CERS4 function in OIS is independent of $p16^{INK4a}$, $p21^{CIP1}$ and p53

It was evident from the secondary siRNA screen that CERS4 can regulate the expression of $p16^{INK4a}$ and $p21^{CIP1}$ (figure 3.12 & 3.13). Further validation of these observations was performed in chapter 4; additionally, CERS4 regulates p53 protein/mRNA expression and CDKN2B ($p15^{INK4b}$) expression (figure 4.3 & 4.4). The identification of the mechanism that links CERS4 and OIS-related ceramide to the cell cycle revealed CERS4-driven regulation of tumour suppressors is a consequence of its actual function in OIS. Initially, rescue experiments indicated that ceramide, as a functional metabolite of CERS4, can reverse proliferation and SA β-gal activity (figure 6.1) but not tumour suppressor protein expression (figure 6.2). CERS4 was then implicated in the PP1-RB axis of cell cycle regulation (as discussed

in *7.8*). There could be a number of reasons why and how CERS4 inadvertently regulates tumour suppressors in OIS. For example, it is evident that CERS4 is a central mediator of the OIS transcriptional program, thus could regulate tumour suppressor expression through this function. Additionally, there may be a positive feedback mechanism occurring; whereby, $p21^{CIP1}$ and p53 are activated through the DDR and $p16^{INK4a}$ through oncogenic stress. Their expression is reinforced by CERS4 (by an unknown mechanism) to ensure the inhibition of CDKs and continual hypophosphorylation of RB. Additionally, as CERS4 is essential for the expression of the SASP (*4.3*), it could be mediating an autocrine program contributing to senescence maintenance (described in *1.1.2.6*). To test this hypothesis, an interaction experiment could identify novel binding partners of CERS4 and suggest implicated signalling pathways. Further to this, CERS4 could be regulating tumour suppressor signalling through its product ceramide, which is a well-established signalling molecule (Hannun and Obeid, 2008). Overall, in response to oncogene activation, CERS4 can indirectly regulate tumour suppressor expression to maintain the cell cycle arrest. This suggests a complex mechanism that links altered metabolism to well-characterised OIS programs.

7.7.2 CERS4 regulation of $p16^{INK4a}$ in replicative senescence

As described in *1.1.4.2*, $p16^{INK4a}$ is a functional biomarker for aged tissues and is triggered independently of telomere shortening (Herbig *et al.*, 2004). Therefore, $p16^{INK4a}$ expression must be controlled through an alternative mechanism; specifically, the *INK4A* locus (encoding $p16^{INK4a}$) is transcriptionally regulated through histone modifications and polycomb proteins. In this thesis, targeting CERS4 expression in IMR90s partially delayed replicative senescence (figure 4.7) and resulted in repressed $p16^{INK4a}$ expression (figure 4.8). Due to this works focus on OIS and cancer, the regulation of $p16^{INK4a}$ by CERS4 in replicative senescence was not examined further. Here, several follow up experiments are hypothesized to ascertain the relationship between CERS4 and $p16^{INK4a}$. First, it would be interesting to analyse the effect of targeting CERS4 on CDKN2A mRNA expression during replicative senescence. It would be expected that due to the complete reduction in $p16^{INK4a}$ protein after CERS4 knockdown, that the transcription of its gene is also

repressed. Second, to understand the mechanism of repressed $p16^{INK4a}$ with CERS4 knockdown in replicative senescence, the function of the homeobox domain of CERS4 should be assessed (introduced in *7.6*). As stated above, the *INK4A* locus is normally repressed through polycomb proteins, which themselves are recruited through homeobox proteins (HOX) (Martin *et al.*, 2013). Chromatin immunoprecipitation experiments could be performed to determine (1) if the CERS4 through its homeobox domain can bind to *INK4A* promoter DNA and (2) whether this functions to inhibit HOX recruitment of polycomb proteins, resulting in transcriptional activation of the *INK4A* locus. Although identified in the replicative senescence model, $p16^{INK4a}$ is also regulated by CERS4 during OIS (figure 4.3), albeit due to its PP1-activating function. Therefore, understanding the molecular mechanisms behind CERS4 regulation of $p16^{INK4a}$ expression could have implications for both aging and cancer biology.

7.8 CERS4 regulation of PP1-RB-E2F axis

It was originally hypothesised that CERS4 could drive RB-PP1 binding using previously published evidence; first, ceramides can activate protein phosphatases (Chalfant *et al.*, 1999) and second, RB has a docking site for PP1 that inhibits CDK binding and facilitates RB hypophosphorylation (Hirschi *et al.*, 2010). Therefore, to link these two facts, co-immunoprecipitation was used to show in RB-PP1 can bind in OIS in a CERS4-dependent manner (figure 6.8). Although ceramides have already been implicated in replicative senescence and cell cycle control (*1.2.4*), this is the first proposed functional mechanism of specifically *de novo* synthesised ceramide in OIS, (summarised in figure 7.1). To verify the role of PP1 in OIS, the ceramide rescue experiment (described in *6.1*) could be repeated in the presence or absence of PP1. If ceramide is indeed activating PP1 to hypophosphorylate RB in OIS, one would expect reducing PP1 expression will prevent ceramide from reversing shCERS4-driven OIS-bypass. This would also further confirm the tumour suppressors are not implicated in CERS4s checkpoint function. Next, repeating the RB-PP1 co-immunoprecipitation with ceramide rescue is an essential experiment to demonstrate CERS4 is functionally required for this interaction. Additionally, PP1-

activated RB hypophosphorylation results in the inactivation of E2F-driven transcription in OIS, as indicated by mRNA expression of E2F target genes (figure 6.3). For further mechanistic insight of CERS4s role as a metabolic checkpoint, it is vital to determine its necessity for RB-PP1-E2F binding using more complex immunoprecipitations. Furthermore, it must be determined which E2F transcription factors are implicated in this cell cycle checkpoint. All these experiments must be performed with the ceramide rescue for confirmation of CERS4s function. Finally, the CDK-driven phosphorylation of RB can occur at multiple different sites and different phospho-sites can modulate the function of RB (Dick and Rubin, 2013; Rubin, 2013). Therefore, identifying the sites at which RB is phosphorylated in OIS-bypass driven by CERS4 knockdown could reveal further insight to the overlapping checkpoint functions of RB and CERS4.

7.9 *In vivo* research

The *in vitro* experiments performed in this thesis were necessary for the identification and validation of CERS4 as a novel regulator of OIS. Importantly, this work has also identified the mechanistic function of CERS4 in OIS. However, as with all biological processes, OIS can present differently *in vivo* (described throughout *1.1*), therefore it is essential to determine if this work can be replicated in a relevant cancer *in vivo* model. Additionally, cultured cells do not represent the complex environment of a pre-cancerous lesion. Overall, the use of *in vivo* models will confirm if this work is relevant for human health and disease, and if ceramide metabolism is a candidate target for therapy. Until this work is recapitulated *in vivo*, thoughts of how CERS4 and ceramide metabolism may be implicated in human cancers are wholly speculative.

An initial *in vivo* readout could be used to analyse ceramide metabolism in sections of mouse and human senescent tissues. One well-established *in vivo* model of OIS is the pancreatic intraepithelial neoplasms (PanINs) that are a precursor for invasive ductal adenocarcinoma of the pancreas (PDAC) (Caldwell *et al.*, 2012; Distler *et al.*, 2014). Both mouse and human tissue panels that progress from normal tissue to

senescent PanIN to cancerous PDAC are available for immuno-staining, and have been exploited for several OIS studies (Acosta *et al.*, 2013; Hoare *et al.*, 2016). Unfortunately, CERS4 is a poorly characterised gene/protein, thus suitable human and mouse antibodies are required for future expression analysis. In addition, CERS4 appears to have low expression in OIS (figure 4.1.A) but its activity is increased (chapter 5). Even if a decent antibody was produced for CERS4 there may not be any detectable changes in expression in the PanIN model. Therefore, the use of more complex *in vivo* models may be prudent, for measurement of metabolic activity.

As described in *1.1.3.2*, there are many oncogenes recognised to induce senescence, in addition to a specific senescence associated with tumour suppressor loss (PICS). It is essential to determine if results from this thesis, that used Ras-induced senescence, can be recapitulated in other models of OIS. The mechanisms of OIS are highly dependent on genetic context and this must be understood and considered before developing therapies targeting ceramide metabolism in cancer. It would be particularly interesting to study the role of ceramide metabolism in OIS and obesity-related cancers, due to the obvious imbalance in lipid metabolism that occurs in obese tissues. Finally, ceramides also function in human skin physiology (Meckfessel and Brandt, 2014), thus recapitulating results in a BRAF-induced senescence model of melanocytic nevi (Michaloglou *et al.*, 2005) could have implications for melanoma tumourigenesis.

Furthermore, this thesis has identified increased ceramide content through the *de novo* synthesis pathway in OIS (figures 5.6 & 5.9). As described in *1.2.4* (figure 1.3), the *de novo* synthesis of ceramides involves a series of reactions catalysed by four enzymes; some of these enzymes have many isoforms, like the ceramide synthases. Thus, to fully understand the role of ceramide synthesis in OIS, it may be beneficial to analyse different *de novo* ceramide synthetic enzymes. For initial analysis of other *de novo* ceramide synthesis enzymes, the cBioPortal open access platform for cancer genomics data (Cerami *et al.*, 2012; Gao *et al.*, 2013) was used to explore genomic alterations in human cancers. KDSR was found to be deleted in 19.3% and 8.2% cases of human pancreatic and prostate cancers, respectively (data not shown). This could be of interest to OIS research for two reasons; first, these two tissues are

widely implicated to induce senescence in response to pre-cancerous growth. Second, KDSR is encoded by the q21 locus of chromosome 18, closeby to tumour suppressor SMAD4 (NCBI, 2004). This may imply *de novo* synthesis of ceramides is genetically deregulated alongside mutated SMAD4, providing the two hits required for pancreatic and prostate cancer to progress. KDSR is a single isoform enzyme, therefore depleting KDSR levels may result in more striking effects in ceramide metabolism and subsequent OIS phenotype than targeting CERS4. KDSR was included in the primary screen and had a Z-score of 0.15 at day 5 (data not shown); KDSR was possibly not a screen hit due to siRNA inefficiencies. These observations suggest using cBioPortal to support *in vitro* experiments can reveal alternative and more intuitive approaches to investigate metabolic pathways.

Finally, CERS4 is implicated in replicative senescence (figure 4.7-4.8), therefore it may be of interest to perform *in vivo* analysis on aged tissues, such as the BubR1 progeroid mouse model (Baker *et al.*, 2008). Using the INK-ATTAC mouse (Baker *et al.*, 2011) to combine ablation of p16 and CERS4, may provide further insight into the role CERS4 plays for p16 regulation in replicative senescence, as discussed in *7.7.2*.

7.10 Final conclusions

Oncogene-induced senescence is a stable cell cycle arrest, employed to protect cells from cancer. Although recently OIS has been an intriguing topic for cancer therapeutic research, more insight to the mechanisms that control OIS is required. Metabolism of senescent cells is highly altered and metabolic regulators could be attractive targets for novel cancer therapies. This thesis aimed to identify novel metabolic regulators of OIS and determine the upstream/downstream mechanisms that link the identified factors to cell cycle arrest. This thesis has identified and validated CERS4 as a regulator of OIS and found increased *de novo* synthesis activity of CERS4, correlating with accumulated ceramides in OIS. CERS4 is mechanistically linked to cell cycle via the PP1-RB-E2F axis. CERS4 is also required for replicative senescence, suggesting this lipid metabolic checkpoint is

implicated in aging-related diseases, in addition to cancer. Future work must focus on confirming the function of CERS4 and ceramides in OIS using models more relevant to humans, so the therapeutic benefit of targeting lipid metabolism can be established.

References

Abraham, R. T. (2002) 'Checkpoint signalling: focusing on 53BP1', *Nat Cell Biol*. Nature Publishing Group, 4(12), pp. E277–E279.

Acosta, J. C. *et al.* (2008) 'Chemokine Signaling via the CXCR2 Receptor Reinforces Senescence', *Cell*, 133(6), pp. 1006–1018. doi: http://dx.doi.org/10.1016/j.cell.2008.03.038.

Acosta, J. C. *et al.* (2013) 'A complex secretory program orchestrated by the inflammasome controls paracrine senescence.', *Nature cell biology*. Nature Publishing Group, 15(8), pp. 978–90. doi: 10.1038/ncb2784.

Acosta, J. C. and Gil, J. (2012) 'Senescence: a new weapon for cancer therapy', *Trends Cell Biol*, 22(4), pp. 211–219. doi: 10.1016/j.tcb.2011.11.006.

Adams, P. D. (2007) 'Remodeling of chromatin structure in senescent cells and its potential impact on tumor suppression and aging', *Gene*, 397(1–2), pp. 84–93. doi: 10.1016/j.gene.2007.04.020.

Agger, K. *et al.* (2009) 'The H3K27me3 demethylase JMJD3 contributes to the activation of the INK4A–ARF locus in response to oncogene- and stress-induced senescence', *Genes & Development*. Cold Spring Harbor Laboratory Press, 23(10), pp. 1171–1176. doi: 10.1101/gad.510809.

Aguayo-Mazzucato, C. *et al.* (2017) 'β Cell Aging Markers Have Heterogeneous Distribution and Are Induced by Insulin Resistance', *Cell Metabolism*. Elsevier, 25(4), p. 898–910.e5. doi: 10.1016/j.cmet.2017.03.015.

Aird, K. M. *et al.* (2013) 'Suppression of Nucleotide Metabolism Underlies the Establishment and Maintenance of Oncogene-Induced Senescence', *Cell Reports*, 3(4), pp. 1252–1265. doi: 10.1016/j.celrep.2013.03.004.

Aird, K. M. *et al.* (2015) 'ATM Couples Replication Stress and Metabolic Reprogramming during Cellular Senescence', *Cell Reports*, 11(6), pp. 893–901. doi: http://dx.doi.org/10.1016/j.celrep.2015.04.014.

Alimonti, A. *et al.* (2010) 'A novel type of cellular senescence that can be enhanced in mouse models and human tumor xenografts to suppress prostate tumorigenesis', *The Journal of Clinical Investigation*. American Society for Clinical Investigation, 120(3), pp. 681–693. doi: 10.1172/JCI40535.

Alonso, R. *et al.* (2015) 'Babelomics 5.0: functional interpretation for new generations of genomic data', *Nucleic Acids Research*. Oxford University Press, 43(Web Server issue), pp. W117–W121. doi: 10.1093/nar/gkv384.

Altman, B. J., Stine, Z. E. and Dang, C. V (2016) 'From Krebs to clinic: glutamine metabolism to cancer therapy', *Nat Rev Cancer*. Nature Publishing Group, a division

of Macmillan Publishers Limited. All Rights Reserved., 16(10), pp. 619–634.

Anastasiou, D. *et al.* (2012) 'Pyruvate kinase M2 activators promote tetramer formation and suppress tumorigenesis', *Nat Chem Biol*. Nature Publishing Group, a division of Macmillan Publishers Limited. All Rights Reserved., 8(10), pp. 839–847.

Ashrafi, K. *et al.* (2003) 'Genome-wide RNAi analysis of Caenorhabditis elegans fat regulatory genes', *Nature*, 421(6920), pp. 268–272.

Atilla-Gokcumen, G. E. E. *et al.* (2014) 'Dividing Cells Regulate Their Lipid Composition and Localization', *Cell*, 156(3), pp. 428–439. doi: 10.1016/j.cell.2013.12.015.

Baar, M. P. *et al.* (2017) 'Targeted Apoptosis of Senescent Cells Restores Tissue Homeostasis in Response to Chemotoxicity and Aging', *Cell*. Elsevier, 169(1), p. 132–147.e16. doi: 10.1016/j.cell.2017.02.031.

Baker, D. J. *et al.* (2008) 'Opposing roles for p16Ink4a and p19Arf in senescence and ageing caused by BubR1 insufficiency', *Nat Cell Biol*. Nature Publishing Group, 10(7), pp. 825–836.

Baker, D. J. *et al.* (2011) 'Clearance of p16Ink4a-positive senescent cells delays ageing-associated disorders', *Nature*. 2011/11/04, 479(7372), pp. 232–236. doi: 10.1038/nature10600.

Baker, D. J. *et al.* (2016) 'Naturally occurring p16 Ink4a -positive cells shorten healthy lifespan', *Nature*. Nature Publishing Group, 530(7589), pp. 1–5. doi: 10.1038/nature16932.

Barradas, M. *et al.* (2009) 'Histone demethylase JMJD3 contributes to epigenetic control of INK4a/ARF by oncogenic RAS', *Genes & Development*. Cold Spring Harbor Laboratory Press, 23(10), pp. 1177–1182. doi: 10.1101/gad.511109.

Bartkova, J. *et al.* (2006) 'Oncogene-induced senescence is part of the tumorigenesis barrier imposed by DNA damage checkpoints', *Nature*, 444(7119), pp. 633–637.

Bekker-Jensen, S. *et al.* (2006) 'Spatial organization of the mammalian genome surveillance machinery in response to DNA strand breaks', *The Journal of Cell Biology*. The Rockefeller University Press, 173(2), pp. 195–206. doi: 10.1083/jcb.200510130.

Ben-Porath, I. and Weinberg, R. A. (2005) 'The signals and pathways activating cellular senescence', *The International Journal of Biochemistry & Cell Biology*, 37(5), pp. 961–976. doi: http://dx.doi.org/10.1016/j.biocel.2004.10.013.

Bennecke, M. *et al.* (2010) 'Ink4a/Arf and Oncogene-Induced Senescence Prevent Tumor Progression during Alternative Colorectal Tumorigenesis', *Cancer Cell*, 18(2), pp. 135–146. doi: https://doi.org/10.1016/j.ccr.2010.06.013.

Bensaad, K. *et al.* (2006) 'TIGAR, a p53-Inducible Regulator of Glycolysis and

Apoptosis', *Cell*, 126(1), pp. 107–120. doi: http://dx.doi.org/10.1016/j.cell.2006.05.036.

Berns, K. *et al.* (2004) 'A large-scale RNAi screen in human cells identifies new components of the p53 pathway', *Nature*, 428(6981), pp. 431–437.

Bernstein, E. *et al.* (2001) 'Role for a bidentate ribonuclease in the initiation step of RNA interference', *Nature*, 409(6818), pp. 363–366.

Berry, D. C. *et al.* (2017) 'Cellular Aging Contributes to Failure of Cold-Induced Beige Adipocyte Formation in Old Mice and Humans', *Cell Metabolism*. Elsevier, 25(1), pp. 166–181. doi: 10.1016/j.cmet.2016.10.023.

Besancenot, R. *et al.* (2010) 'A Senescence-Like Cell-Cycle Arrest Occurs During Megakaryocytic Maturation: Implications for Physiological and Pathological Megakaryocytic Proliferation', *PLOS Biology*. Public Library of Science, 8(9), p. e1000476.

Bhutia, Y. D. *et al.* (2015) 'Amino Acid Transporters in Cancer and Their Relevance to "Glutamine Addiction": Novel Targets for the Design of a New Class of Anticancer Drugs', *Cancer Research*, 75(9), p. 1782 LP-1788.

Birmingham, A. *et al.* (2006) '3' UTR seed matches, but not overall identity, are associated with RNAi off-targets.', *Nature methods*, 3(3), pp. 199–204. doi: 10.1038/nmeth854.

Bishop, C. L. *et al.* (2010) 'Primary Cilium-Dependent and -Independent Hedgehog Signaling Inhibits p16INK4A', *Molecular Cell*, 40(4), pp. 533–547. doi: http://dx.doi.org/10.1016/j.molcel.2010.10.027.

Bittles, A. H. and Harper, N. (1984) 'Increased glycolysis in ageing cultured human diploid fibroblasts', *Bioscience Reports*, 4(9), p. 751 LP-756.

Blackburn, E. H. (1991) 'Structure and function of telomeres', *Nature*, 350(6319), pp. 569–573.

Bligh, E. G. and Dyer, W. J. (1959) 'A rapid method of total lipid extraction and purification', *Canadian Journal of Biochemistry and Physiology*. NRC Research Press, 37(8), pp. 911–917. doi: 10.1139/o59-099.

Bobbin, M. L. and Rossi, J. J. (2016) 'RNA Interference (RNAi)-Based Therapeutics: Delivering on the Promise?', *Annual Review of Pharmacology and Toxicology*. Annual Reviews, 56(1), pp. 103–122. doi: 10.1146/annurev-pharmtox-010715-103633.

Bodnar, A. G. *et al.* (1998) 'Extension of Life-Span by Introduction of Telomerase into Normal Human Cells', *Science*, 279(5349), p. 349 LP-352.

Boutros, M. *et al.* (2004) 'Genome-Wide RNAi Analysis of Growth and Viability in Drosophila Cells', *Science*, 303(5659), pp. 832–835. doi: 10.1126/science.1091266.

Brummelkamp, T. R., Bernards, R. and Agami, R. (2002a) 'A System for Stable Expression of Short Interfering RNAs in Mammalian Cells', *Science*, 296(5567), p. 550 LP-553.

Brummelkamp, T. R., Bernards, R. and Agami, R. (2002b) 'Stable suppression of tumorigenicity by virus-mediated RNA interference', *Cancer Cell*, 2(3), pp. 243–247. doi: http://dx.doi.org/10.1016/S1535-6108(02)00122-8.

Brunelli, L. *et al.* (2014) 'Capturing the metabolomic diversity of KRAS mutants in non-small-cell lung cancer cells', *Oncotarget*. Impact Journals LLC, 5(13), pp. 4722–4731.

Buscemi, G. *et al.* (2004) 'Activation of ATM and Chk2 kinases in relation to the amount of DNA strand breaks', *Oncogene*. Nature Publishing Group, 23(46), pp. 7691–7700.

Cabot, M. C. *et al.* (1999) 'SDZ PSC 833, the cyclosporine A analogue and multidrug resistance modulator, activates ceramide synthesis and increases vinblastine sensitivity in drug-sensitive and drug-resistant cancer cells.', *Cancer research*. United States, 59(4), pp. 880–885.

Cairns, R. A. and Mak, T. W. (2016) 'The current state of cancer metabolism', *Nat Rev Cancer*. Nature Publishing Group, a division of Macmillan Publishers Limited. All Rights Reserved., 16(10), pp. 613–614.

Caldwell, M. E. *et al.* (2012) 'Cellular features of senescence during the evolution of human and murine ductal pancreatic cancer', *Oncogene*. 2011/08/24, 31(12), pp. 1599–1608. doi: 10.1038/onc.2011.350.

Capparelli, C. *et al.* (2012) 'CDK inhibitors (p16/p19/p21) induce senescence and autophagy in cancer-associated fibroblasts, "fueling" tumor growth via paracrine interactions, without an increase in neo-angiogenesis', *Cell Cycle*. Taylor & Francis, 11(19), pp. 3599–3610. doi: 10.4161/cc.21884.

Carragher, L. A. S. *et al.* (2010) '(V600E)Braf induces gastrointestinal crypt senescence and promotes tumour progression through enhanced CpG methylation of p16(INK4a)', *EMBO Molecular Medicine*. Berlin: WILEY-VCH Verlag, 2(11), pp. 458–471. doi: 10.1002/emmm.201000099.

Carrel, A. and Ebeling, A. H. (1921) 'Age and multiplication of fibroblasts', *The Journal of Experimental Medicine*. The Rockefeller University Press, 34(6), pp. 599–623.

Castro, M. E. *et al.* (2008) 'PPP1CA contributes to the senescence program induced by oncogenic Ras', *Carcinogenesis*, 29(3), pp. 491–499. doi: 10.1093/carcin/bgm246.

Catalano, A. *et al.* (2004) '5- Lipoxygenase regulates senescence- like growth arrest by promoting ROS- dependent p53 activation', *The EMBO Journal*, 24(1), p. 170 LP-179.

Caudy, A. A. *et al.* (2003) 'A micrococcal nuclease homologue in RNAi effector complexes', *Nature*, 425(6956), pp. 411–414.

Causeret, C. *et al.* (2000) 'Further characterization of rat dihydroceramide desaturase: Tissue distribution, subcellular localization, and substrate specificity', *Lipids*, 35(10), pp. 1117–1125. doi: 10.1007/s11745-000-0627-6.

Celeste, A. *et al.* (2002) 'Genomic Instability in Mice Lacking Histone H2AX', *Science (New York, N.Y.)*, 296(5569), pp. 922–927. doi: 10.1126/science.1069398.

Cerami, E. *et al.* (2012) 'The cBio Cancer Genomics Portal: An Open Platform for Exploring Multidimensional Cancer Genomics Data', *Cancer Discovery*, 2(5), p. 401 LP-404.

Chalfant, C. E. *et al.* (1999) 'Long Chain Ceramides Activate Protein Phosphatase-1 and Protein Phosphatase-2A: Activation is stereospecific and regulated by phosphatidic acid', *Journal of Biological Chemistry*, 274(29), pp. 20313–20317. doi: 10.1074/jbc.274.29.20313.

Chang, B.-D. *et al.* (1999) 'A Senescence-like Phenotype Distinguishes Tumor Cells That Undergo Terminal Proliferation Arrest after Exposure to Anticancer Agents', *Cancer Research*, 59(15), p. 3761 LP-3767.

Chen, Z. *et al.* (2005) 'Crucial role of p53-dependent cellular senescence in suppression of Pten-deficient tumorigenesis', *Nature*. Nature Publishing Group, 436(7051), pp. 725–730.

Cheung, E. C., Ludwig, R. L. and Vousden, K. H. (2012) 'Mitochondrial localization of TIGAR under hypoxia stimulates HK2 and lowers ROS and cell death', *Proceedings of the National Academy of Sciences of the United States of America*. National Academy of Sciences, 109(50), pp. 20491–20496. doi: 10.1073/pnas.1206530109.

Chicas, A. *et al.* (2010) 'Dissecting the Unique Role of the Retinoblastoma Tumor Suppressor during Cellular Senescence', *Cancer Cell*. Elsevier, 17(4), pp. 376–387. doi: 10.1016/j.ccr.2010.01.023.

Chien, Y. *et al.* (2011) 'Control of the senescence-associated secretory phenotype by NF-κB promotes senescence and enhances chemosensitivity', *Genes & Development*. Cold Spring Harbor Laboratory Press, 25(20), pp. 2125–2136. doi: 10.1101/gad.17276711.

Childs, B. G. *et al.* (2016) 'Senescent intimal foam cells are deleterious at all stages of atherosclerosis', *Science*, 354(6311), p. 472 LP-477.

Childs, B. G. *et al.* (2017) 'Senescent cells: an emerging target for diseases of ageing', *Nat Rev Drug Discov*. Nature Publishing Group, a division of Macmillan Publishers Limited. All Rights Reserved., advance on.

Chokkathukalam, A. *et al.* (2014) 'Stable isotope-labeling studies in metabolomics:

new insights into structure and dynamics of metabolic networks', *Bioanalysis*, 6(4), pp. 511–524. doi: 10.4155/bio.13.348.

Choy, M. S. *et al.* (2014) 'Understanding the antagonism of retinoblastoma protein dephosphorylation by PNUTS provides insights into the PP1 regulatory code', *Proceedings of the National Academy of Sciences*, 111(11), pp. 4097–4102. doi: 10.1073/pnas.1317395111.

Christofk, H. R., Vander Heiden, M. G., Wu, N., *et al.* (2008) 'Pyruvate kinase M2 is a phosphotyrosine-binding protein', *Nature*. Nature Publishing Group, 452(7184), pp. 181–186.

Christofk, H. R., Vander Heiden, M. G., Harris, M. H., *et al.* (2008) 'The M2 splice isoform of pyruvate kinase is important for cancer metabolism and tumour growth', *Nature*. Nature Publishing Group, 452(7184), pp. 230–233.

Christophorou, M. A. *et al.* (2006) 'The pathological response to DNA damage does not contribute to p53-mediated tumour suppression', *Nature*, 443(7108), pp. 214–217.

Chuprin, A. *et al.* (2013) 'Cell fusion induced by ERVWE1 or measles virus causes cellular senescence', *Genes & Development*, 27(21), pp. 2356–2366. doi: 10.1101/gad.227512.113.

Clements, M. E. *et al.* (2013) 'Increased Cellular Senescence and Vascular Rarefaction Exacerbate the Progression of Kidney Fibrosis in Aged Mice Following Transient Ischemic Injury', *PLoS ONE*. Edited by J.-C. Dussaule. San Francisco, USA: Public Library of Science, 8(8), p. e70464. doi: 10.1371/journal.pone.0070464.

Coet, T. *et al.* (1998) 'New perspectives on the function of myelin galactolipids', *Trends in Neurosciences*. Elsevier, 21(3), pp. 126–130. doi: 10.1016/S0166-2236(97)01178-8.

Collado, M. *et al.* (2005) 'Tumour biology: senescence in premalignant tumours', *Nature*. 2005/08/05, 436(7051), p. 642. doi: 10.1038/436642a.

Commisso, C. *et al.* (2013) 'Macropinocytosis of protein is an amino acid supply route in Ras-transformed cells', *Nature*, 497(7451), pp. 633–637. doi: 10.1038/nature12138.

Cooke, H. J. and Smith, B. A. (1986) 'Variability at the Telomeres of the Human X/Y Pseudoautosomal Region', *Cold Spring Harbor Symposia on Quantitative Biology*, 51, pp. 213–219. doi: 10.1101/SQB.1986.051.01.026.

Cooper, G. M. (1982) 'Cellular transforming genes', *Science*, 217(4562), p. 801 LP-806.

Coppé, J.-P. *et al.* (2006) 'Secretion of Vascular Endothelial Growth Factor by Primary Human Fibroblasts at Senescence', *Journal of Biological Chemistry*, 281(40), pp. 29568–29574. doi: 10.1074/jbc.M603307200.

Coppé, J.-P. *et al.* (2008) 'Senescence-Associated Secretory Phenotypes Reveal Cell-Nonautonomous Functions of Oncogenic RAS and the p53 Tumor Suppressor', *PLOS Biology*. Public Library of Science, 6(12), p. e301.

Corpe, C. P. *et al.* (2013) 'Intestinal Dehydroascorbic Acid (DHA) Transport Mediated by the Facilitative Sugar Transporters, GLUT2 and GLUT8', *The Journal of Biological Chemistry*. 9650 Rockville Pike, Bethesda, MD 20814, U.S.A.: American Society for Biochemistry and Molecular Biology, 288(13), pp. 9092–9101. doi: 10.1074/jbc.M112.436790.

Correia-Melo, C. *et al.* (2016) 'Mitochondria are required for pro-ageing features of the senescent phenotype', *The EMBO Journal*, 35(7), pp. 724–742. doi: 10.15252/embj.201592862.

Courtois-Cox, S. *et al.* (2006) 'A negative feedback signaling network underlies oncogene-induced senescence', *Cancer Cell*, 10(6), pp. 459–472. doi: http://dx.doi.org/10.1016/j.ccr.2006.10.003.

d'Adda di Fagagna, F. (2008) 'Living on a break: cellular senescence as a DNA-damage response', *Nat Rev Cancer*. Nature Publishing Group, 8(7), pp. 512–522.

D'mello, N. P. *et al.* (1994) 'Cloning and characterization of LAG1, a longevity-assurance gene in yeast.', *Journal of Biological Chemistry* , 269(22), pp. 15451–15459.

Dbaibo, G. S. *et al.* (1995) 'Retinoblastoma gene product as a downstream target for a ceramide-dependent pathway of growth arrest.', *Proceedings of the National Academy of Sciences of the United States of America*, 92(5), pp. 1347–1351.

Dbaibo, G. S. *et al.* (2001) 'Ceramide generation by two distinct pathways in tumor necrosis factor α-induced cell death', *FEBS Letters*, 503(1), pp. 7–12. doi: 10.1016/S0014-5793(01)02625-4.

DeBerardinis, R. J. *et al.* (2007) 'Beyond aerobic glycolysis: Transformed cells can engage in glutamine metabolism that exceeds the requirement for protein and nucleotide synthesis', *Proceedings of the National Academy of Sciences*, 104(49), pp. 19345–19350. doi: 10.1073/pnas.0709747104.

Demaria, M. *et al.* (2014) 'An essential role for senescent cells in optimal wound healing through secretion of PDGF-AA', *Developmental Cell*, 31(6), pp. 722–733. doi: 10.1016/j.devcel.2014.11.012.

Deschênes-Simard, X. *et al.* (2013) 'Tumor suppressor activity of the ERK/MAPK pathway by promoting selective protein degradation', *Genes & Development*. Cold Spring Harbor Laboratory Press, 27(8), pp. 900–915. doi: 10.1101/gad.203984.112.

Dick, F. A. and Rubin, S. M. (2013) 'Molecular mechanisms underlying RB protein function', *Nature reviews. Molecular cell biology*, 14(5), pp. 297–306. doi: 10.1038/nrm3567.

Dimri, G. P. *et al.* (1995) 'A biomarker that identifies senescent human cells in culture and in aging skin in vivo', *Proc Natl Acad Sci U S A*. 1995/09/26, 92(20), pp. 9363–9367.

Dirac, A. M. G. and Bernards, R. (2003) 'Reversal of senescence in mouse fibroblasts through lentiviral suppression of p53', *Journal of Biological Chemistry*, 278(14), pp. 11731–11734. doi: 10.1074/jbc.C300023200.

Distler, M. *et al.* (2014) 'Precursor lesions for sporadic pancreatic cancer: PanIN, IPMN, and MCN', *Biomed Res Int*. 2014/05/02, 2014, p. 474905. doi: 10.1155/2014/474905.

Dörr, J. R. *et al.* (2013) 'Synthetic lethal metabolic targeting of cellular senescence in cancer therapy', *Nature*, 501(7467), pp. 421–425. doi: 10.1038/nature12437.

Draper, J. M. *et al.* (2011) 'Discovery and Evaluation of Inhibitors of Human Ceramidase', *Molecular cancer therapeutics*, 10(11), pp. 2052–2061. doi: 10.1158/1535-7163.MCT-11-0365.

Ducker, G. S. *et al.* (2016) 'Reversal of cytosolic one-carbon flux compensates for loss of mitochondrial folate pathway', *Cell metabolism*, 23(6), pp. 1140–1153. doi: 10.1016/j.cmet.2016.04.016.

Dykxhoorn, D. M., Novina, C. D. and Sharp, P. A. (2003) 'Killing the messenger: short RNAs that silence gene expression', *Nat Rev Mol Cell Biol*. Nature Publishing Group, 4(6), pp. 457–467.

Efeyan, A. *et al.* (2007) 'Induction of p53-Dependent Senescence by the MDM2 Antagonist Nutlin-3a in Mouse Cells of Fibroblast Origin', *Cancer Research*, 67(15), p. 7350 LP-7357.

Efeyan, A. and Serrano, M. (2007) 'p53: Guardian of the Genome and Policeman of the Oncogenes', *Cell Cycle*. Taylor & Francis, 6(9), pp. 1006–1010. doi: 10.4161/cc.6.9.4211.

Eggert, T. *et al.* (2016) 'Distinct Functions of Senescence-Associated Immune Responses in Liver Tumor Surveillance and Tumor Progression', *Cancer Cell*, 30(4), pp. 533–547. doi: https://doi.org/10.1016/j.ccell.2016.09.003.

Elbashir, S. M. *et al.* (2001) 'Duplexes of 21-nucleotide RNAs mediate RNA interference in cultured mammalian cells', *Nature*, 411(6836), pp. 494–498.

Fagagna, F. d'Adda di *et al.* (2003) 'A DNA damage checkpoint response in telomere-initiated senescence', *Nature*. Macmillian Magazines Ltd., 426(6963), pp. 194–198.

Farber, S. *et al.* (1948) 'Temporary Remissions in Acute Leukemia in Children Produced by Folic Acid Antagonist, 4-Aminopteroyl-Glutamic Acid (Aminopterin)', *New England Journal of Medicine*. Massachusetts Medical Society, 238(23), pp. 787–793. doi: 10.1056/NEJM194806032382301.

Fendt, S.-M. *et al.* (2013) 'Metformin Decreases Glucose Oxidation and Increases the Dependency of Prostate Cancer Cells on Reductive Glutamine Metabolism', *Cancer Research*, 73(14), p. 4429 LP-4438.

Feng, J. *et al.* (1995) 'The RNA component of human telomerase', *Science*, 269(5228), p. 1236 LP-1241.

Feng, L.-X. *et al.* (2014) 'Synergistic Enhancement of Cancer Therapy Using a Combination of Ceramide and Docetaxel', *International Journal of Molecular Sciences*. Molecular Diversity Preservation International (MDPI), 15(3), pp. 4201–4220. doi: 10.3390/ijms15034201.

Finn, R. S. *et al.* (2015) 'The cyclin-dependent kinase 4/6 inhibitor palbociclib in combination with letrozole versus letrozole alone as first-line treatment of oestrogen receptor-positive, HER2-negative, advanced breast cancer (PALOMA-1/TRIO-18): a randomised phase 2 study', *The Lancet Oncology*, 16(1), pp. 25–35. doi: http://dx.doi.org/10.1016/S1470-2045(14)71159-3.

Fire, A. *et al.* (1998) 'Potent and specific genetic interference by double-stranded RNA in Caenorhabditis elegans', *Nature*, 391(6669), pp. 806–811.

Flores, I. *et al.* (2008) 'The longest telomeres: a general signature of adult stem cell compartments', *Genes & Development*. Cold Spring Harbor Laboratory Press, 22(5), pp. 654–667. doi: 10.1101/gad.451008.

Folch, J., Lees, M. and Sloane Stanley, G. H. (1957) 'A simple method for the isolation and purification of total lipides from animal tissues.', *The Journal of biological chemistry*, 226(1), pp. 497–509. doi: 10.1371/journal.pone.0020510.

Fuchs, Y. and Steller, H. (2011) 'Programmed Cell Death in Animal Development and Disease', *Cell*, 147(4), pp. 742–758. doi: 10.1016/j.cell.2011.10.033.

Fumagalli, M. *et al.* (2012) 'Telomeric DNA damage is irreparable and causes persistent DNA-damage-response activation', *Nat Cell Biol*. Nature Publishing Group, a division of Macmillan Publishers Limited. All Rights Reserved., 14(4), pp. 355–365.

Futerman, A. H. and Hannun, Y. A. (2004) 'The complex life of simple sphingolipids', *EMBO reports*, 5(8), p. 777 LP-782.

Fyrst, H. and Saba, J. D. (2010) 'An update on sphingosine-1-phosphate and other sphingolipid mediators', *Nat Chem Biol*. Nature Publishing Group, a division of Macmillan Publishers Limited. All Rights Reserved., 6(7), pp. 489–497.

Gaglio, D. *et al.* (2011) 'Oncogenic K-Ras decouples glucose and glutamine metabolism to support cancer cell growth', *Molecular Systems Biology*. Nature Publishing Group, 7, p. 523. doi: 10.1038/msb.2011.56.

Galadari, S. *et al.* (2006) 'Identification of a novel amidase motif in neutral ceramidase', *Biochemical Journal*. Portland Press Ltd., 393(Pt 3), pp. 687–695. doi:

10.1042/BJ20050682.

Galluzzi, L. *et al.* (2015) 'Autophagy in malignant transformation and cancer progression', *The EMBO Journal*, 34(7), p. 856 LP-880.

Gamerdinger, M. *et al.* (2009) 'Protein quality control during aging involves recruitment of the macroautophagy pathway by BAG3', *The EMBO Journal*. Nature Publishing Group, 28(7), pp. 889–901. doi: 10.1038/emboj.2009.29.

Gao, J. *et al.* (2013) 'Integrative Analysis of Complex Cancer Genomics and Clinical Profiles Using the cBioPortal', *Science signaling*, 6(269), p. pl1-pl1. doi: 10.1126/scisignal.2004088.

Gao, P. *et al.* (2009) 'c-Myc suppression of miR-23a/b enhances mitochondrial glutaminase expression and glutamine metabolism', *Nature*. Macmillan Publishers Limited. All rights reserved, 458(7239), pp. 762–765.

Gao, P. *et al.* (2012) 'Characterization of Isoenzyme-Selective Inhibitors of Human Sphingosine Kinases', *PLoS ONE*. Edited by K. Takabe. San Francisco, USA: Public Library of Science, 7(9), p. e44543. doi: 10.1371/journal.pone.0044543.

Gasparri, F. *et al.* (2004) 'Quantification of the Proliferation Index of Human Dermal Fibroblast Cultures with the ArrayScan™ High-Content Screening Reader', *Journal of Biomolecular Screening*. SAGE Publications Inc STM, 9(3), pp. 232–243. doi: 10.1177/1087057103262836.

Gencer, S. *et al.* (2017) 'TGF-β receptor I/II trafficking and signaling at primary cilia are inhibited by ceramide to attenuate cell migration and tumor metastasis', *Science Signaling*, 10(502).

Gerland, L.-M. *et al.* (2003) 'Association of increased autophagic inclusions labeled for β-galactosidase with fibroblastic aging', *Experimental Gerontology*, 38(8), pp. 887–895. doi: http://dx.doi.org/10.1016/S0531-5565(03)00132-3.

Gonzalez-Covarrubias, V. (2013) 'Lipidomics in longevity and healthy aging', *Biogerontology*, 14(6), pp. 663–672. doi: 10.1007/s10522-013-9450-7.

Gorgoulis, V. G. *et al.* (2005) 'Activation of the DNA damage checkpoint and genomic instability in human precancerous lesions', *Nature*. Macmillian Magazines Ltd., 434(7035), pp. 907–913.

Gorgoulis, V. G. and Halazonetis, T. D. (2010) 'Oncogene-induced senescence: the bright and dark side of the response', *Current Opinion in Cell Biology*, 22(6), pp. 816–827. doi: http://dx.doi.org/10.1016/j.ceb.2010.07.013.

Graf, C. *et al.* (2008) 'Targeting Ceramide Metabolism with a Potent and Specific Ceramide Kinase Inhibitor', *Molecular Pharmacology*, 74(4), p. 925 LP-932.

Greider, C. W. and Blackburn, E. H. (1985) 'Identification of a specific telomere terminal transferase activity in tetrahymena extracts', *Cell*, 43(2), pp. 405–413. doi:

http://dx.doi.org/10.1016/0092-8674(85)90170-9.

Griffith, J. D. *et al.* (1999) 'Mammalian Telomeres End in a Large Duplex Loop', *Cell*, 97(4), pp. 503–514. doi: http://dx.doi.org/10.1016/S0092-8674(00)80760-6.

Gross, M. I. *et al.* (2014) 'Antitumor Activity of the Glutaminase Inhibitor CB-839 in Triple-Negative Breast Cancer', *Molecular Cancer Therapeutics*, 13(4), p. 890 LP-901.

Guillou, S. *et al.* (2011) 'The moisturizing effect of a wheat extract food supplement on women's skin: a randomized, double-blind placebo-controlled trial', *International Journal of Cosmetic Science*. Blackwell Publishing Ltd, 33(2), pp. 138–143. doi: 10.1111/j.1468-2494.2010.00600.x.

Gulbins, E. and Kolesnick, R. (2003) 'Raft ceramide in molecular medicine', *Oncogene*. Nature Publishing Group, 22, p. 7070.

Haimovitz-Friedman, A. *et al.* (1994) 'Ionizing radiation acts on cellular membranes to generate ceramide and initiate apoptosis', *The Journal of Experimental Medicine*. The Rockefeller University Press, 180(2), pp. 525–535.

Haley, B. and Zamore, P. D. (2004) 'Kinetic analysis of the RNAi enzyme complex', *Nat Struct Mol Biol*, 11(7), pp. 599–606.

Hamilton, A. J. and Baulcombe, D. C. (1999) 'A Species of Small Antisense RNA in Posttranscriptional Gene Silencing in Plants', *Science*, 286(5441), p. 950 LP-952.

Hammond, S. M. *et al.* (2000) 'An RNA-directed nuclease mediates post-transcriptional gene silencing in Drosophila cells', *Nature*, 404(6775), pp. 293–296.

Hammond, S. M. *et al.* (2001) 'Argonaute2, a Link Between Genetic and Biochemical Analyses of RNAi', *Science*, 293(5532), p. 1146 LP-1150.

Hannun, Y. A. and Obeid, L. M. (2008) 'Principles of bioactive lipid signalling: lessons from sphingolipids', *Nat Rev Mol Cell Biol*. Nature Publishing Group, 9(2), pp. 139–150.

Hannun, Y. A. and Obeid, L. M. (2011) 'Many Ceramides', *Journal of Biological Chemistry*, 286(32), pp. 27855–27862. doi: 10.1074/jbc.R111.254359.

Harkewicz, R. and Dennis, E. A. (2011) 'Applications of Mass Spectrometry to Lipids and Membranes', *Annual review of biochemistry*, 80, pp. 301–325. doi: 10.1146/annurev-biochem-060409-092612.

Harley, C. B., Futcher, A. B. and Greider, C. W. (1990) 'Telomeres shorten during ageing of human fibroblasts', *Nature*, 345(6274), pp. 458–460.

Harman, D. (1972) 'The Biologic Clock: The Mitochondria?', *Journal of the American Geriatrics Society*. Blackwell Publishing Ltd, 20(4), pp. 145–147. doi: 10.1111/j.1532-5415.1972.tb00787.x.

Harvey, J. (1964) ‘An Unidentified Virus which causes the Rapid Production of Tumours in Mice’, *Nature*, 204(4963), pp. 1104–1105.

Hashimoto, M. *et al.* (2016) ‘Elimination of p19ARF-expressing cells enhances pulmonary function in mice’, *JCI Insight*. The American Society for Clinical Investigation, 1(12). doi: 10.1172/jci.insight.87732.

Hay, N. (2016) ‘Reprogramming glucose metabolism in cancer: can it be exploited for cancer therapy?’, *Nature reviews. Cancer*, 16(10), pp. 635–649. doi: 10.1038/nrc.2016.77.

Hayflick, L. (1965) ‘The limited in vitro lifetime of human diploid cell strains’, *Experimental Cell Research*, 37(3), pp. 614–636. doi: http://dx.doi.org/10.1016/0014-4827(65)90211-9.

Hayflick, L. and Moorhead, P. S. (1961) ‘The serial cultivation of human diploid cell strains’, *Experimental Cell Research*, 25(3), pp. 585–621. doi: http://dx.doi.org/10.1016/0014-4827(61)90192-6.

Hecker, L. *et al.* (2014) ‘Reversal of Persistent Fibrosis in Aging by Targeting Nox4-Nrf2 Redox Imbalance’, *Science translational medicine*, 6(231), p. 231ra47-231ra47. doi: 10.1126/scitranslmed.3008182.

Vander Heiden, M. G., Cantley, L. C. and Thompson, C. B. (2009) ‘Understanding the Warburg Effect: The Metabolic Requirements of Cell Proliferation’, *Science*. 2009/05/23, 324(5930), pp. 1029–1033. doi: 10.1126/science.1160809.

Herbig, U. *et al.* (2004) ‘Telomere Shortening Triggers Senescence of Human Cells through a Pathway Involving ATM, p53, and p21CIP1, but Not p16INK4a’, *Molecular Cell*. Elsevier, 14(4), pp. 501–513. doi: 10.1016/S1097-2765(04)00256-4.

Herbig, U. *et al.* (2006) ‘Cellular Senescence in Aging Primates’, *Science*, 311(5765), p. 1257 LP-1257.

Herranz, N. *et al.* (2015) ‘mTOR regulates MAPKAPK2 translation to control the senescence-associated secretory phenotype’, *Nat Cell Biol*. Nature Publishing Group, 17(9), pp. 1205–1217.

Hirschi, A. *et al.* (2010) ‘An overlapping kinase and phosphatase docking site regulates activity of the retinoblastoma protein’, *Nat Struct Mol Biol*. Nature Publishing Group, a division of Macmillan Publishers Limited. All Rights Reserved., 17(99), pp. 1051–1057.

Hoare, M. *et al.* (2016) ‘NOTCH1 mediates a switch between two distinct secretomes during senescence’, *Nature cell biology*, 18(9), pp. 979–992. doi: 10.1038/ncb3397.

Holland, P. W. H., Booth, H. A. F. and Bruford, E. A. (2007) ‘Classification and nomenclature of all human homeobox genes’, *BMC Biology*. BioMed Central, 5, p. 47. doi: 10.1186/1741-7007-5-47.

Huang, D. W., Sherman, B. T. and Lempicki, R. A. (2008) 'Systematic and integrative analysis of large gene lists using DAVID bioinformatics resources', *Nat. Protocols*. Nature Publishing Group, 4(1), pp. 44–57.

Hubackova, S. *et al.* (2012) 'IL1- and TGFβ-Nox4 signaling, oxidative stress and DNA damage response are shared features of replicative, oncogene-induced, and drug-induced paracrine "Bystander senescence"', *Aging (Albany NY)*. Impact Journals LLC, 4(12), pp. 932–951.

Iannello, A. *et al.* (2013) 'p53-dependent chemokine production by senescent tumor cells supports NKG2D-dependent tumor elimination by natural killer cells', *The Journal of Experimental Medicine*. The Rockefeller University Press, 210(10), pp. 2057–2069. doi: 10.1084/jem.20130783.

Inman, S. (2015) *FDA Approves Palbociclib for Metastatic Breast Cancer*, *onclive.com*. Available at: http://www.onclive.com/web-exclusives/fda-approves-palbociclib-for-metastatic-breast-cancer (Accessed: 18 July 2017).

Jackson, A. L. *et al.* (2006) 'Position-specific chemical modification of siRNAs reduces "off-target" transcript silencing', *RNA*. Cold Spring Harbor Laboratory Press, 12(7), pp. 1197–1205. doi: 10.1261/rna.30706.

Jackson, A. L. and Linsley, P. S. (2010) 'Recognizing and avoiding siRNA off-target effects for target identification and therapeutic application', *Nat Rev Drug Discov*. Nature Publishing Group, 9(1), pp. 57–67.

Jacobs, J. J. L. *et al.* (1999) 'The oncogene and Polycomb-group gene bmi-1 regulates cell proliferation and senescence through the ink4a locus', *Nature*, 397(6715), pp. 164–168.

Jacque, N. *et al.* (2015) 'Targeting glutaminolysis has antileukemic activity in acute myeloid leukemia and synergizes with BCL-2 inhibition', *Blood*, 126(11), p. 1346 LP-1356.

Jain, M. *et al.* (2012) 'Metabolite Profiling Identifies a Key Role for Glycine in Rapid Cancer Cell Proliferation', *Science (New York, N.Y.)*, 336(6084), pp. 1040–1044. doi: 10.1126/science.1218595.

Janzen, V. *et al.* (2006) 'Stem-cell ageing modified by the cyclin-dependent kinase inhibitor p16INK4a', *Nature*, 443(7110), pp. 421–426.

Jen, K.-Y. and Cheung, V. G. (2005) 'Identification of Novel p53 Target Genes in Ionizing Radiation Response', *Cancer Research*, 65(17), p. 7666 LP-7673.

Jensen, J.-M. *et al.* (2005) 'Acid and neutral sphingomyelinase, ceramide synthase, and acid ceramidase activities in cutaneous aging', *Experimental Dermatology*. Munksgaard International Publishers, 14(8), pp. 609–618. doi: 10.1111/j.0906-6705.2005.00342.x.

Jeon, O. H. *et al.* (2017) 'Local clearance of senescent cells attenuates the

development of post-traumatic osteoarthritis and creates a pro-regenerative environment', *Nat Med*. Nature Publishing Group, a division of Macmillan Publishers Limited. All Rights Reserved., 23(6), pp. 775–781.

Jeyapalan, J. C. *et al.* (2007) 'Accumulation of Senescent Cells in Mitotic Tissue of Aging Primates', *Mechanisms of ageing and development*, 128(1), pp. 36–44. doi: 10.1016/j.mad.2006.11.008.

Jiang, J. C. *et al.* (1998) 'Homologs of the Yeast Longevity Gene LAG1 in Caenorhabditis elegans and Human', *Genome Research* , 8(12), pp. 1259–1272. doi: 10.1101/gr.8.12.1259.

Jiang, P. *et al.* (2013) 'Reciprocal regulation of p53 and malic enzymes modulates metabolism and senescence', *Nature*, 493(7434), pp. 689–693. doi: 10.1038/nature11776.

Jing, H. *et al.* (2011) 'Opposing roles of NF-κB in anti-cancer treatment outcome unveiled by cross-species investigations', *Genes & Development*. Cold Spring Harbor Laboratory Press, 25(20), pp. 2137–2146. doi: 10.1101/gad.17620611.

Johnson, C. H., Ivanisevic, J. and Siuzdak, G. (2016) 'Metabolomics: beyond biomarkers and towards mechanisms', *Nat Rev Mol Cell Biol*. Nature Publishing Group, a division of Macmillan Publishers Limited. All Rights Reserved., 17(7), pp. 451–459.

Jun, J.-I. and Lau, L. F. (2010) 'The Matricellular Protein CCN1/CYR61 Induces Fibroblast Senescence and Restricts Fibrosis in Cutaneous Wound Healing', *Nature cell biology*, 12(7), pp. 676–685. doi: 10.1038/ncb2070.

Kamijo, T. *et al.* (1997) 'Tumor Suppression at the Mouse INK4a Locus Mediated by the Alternative Reading Frame Product p19 ARF', *Cell*, 91(5), pp. 649–659. doi: http://dx.doi.org/10.1016/S0092-8674(00)80452-3.

Kamphorst, J. J. *et al.* (2015) 'Human pancreatic cancer tumors are nutrient poor and tumor cells actively scavenge extracellular protein', *Cancer research*, 75(3), pp. 544–553. doi: 10.1158/0008-5472.CAN-14-2211.

Kang, C. *et al.* (2015) 'The DNA damage response induces inflammation and senescence by inhibiting autophagy of GATA4', *Science*, 349(6255).

Kang, T.-W. *et al.* (2011) 'Senescence surveillance of pre-malignant hepatocytes limits liver cancer development', *Nature*. Nature Publishing Group, 479(7374), pp. 547–551. doi: 10.1038/nature10599.

Kaplon, J. *et al.* (2013) 'A key role for mitochondrial gatekeeper pyruvate dehydrogenase in oncogene-induced senescence', *Nature*, 498 VN-(7452), pp. 109–112. doi: 10.1038/nature12154.

Kaplon, J. *et al.* (2014) 'Near-genomewide RNAi screening for regulators of BRAFV600E-induced senescence identifies RASEF, a gene epigenetically silenced

in melanoma', *Pigment Cell & Melanoma Research*, 27(4), pp. 640–652. doi: 10.1111/pcmr.12248.

Kell, D. B. and Oliver, S. G. (2016) 'The metabolome 18 years on: a concept comes of age', *Metabolomics*, 12(9), p. 148. doi: 10.1007/s11306-016-1108-4.

Kelloff, G. J. *et al.* (2005) 'Progress and Promise of FDG-PET Imaging for Cancer Patient Management and Oncologic Drug Development', *Clinical Cancer Research*, 11(8), p. 2785 LP-2808.

Kihara, A. and Igarashi, Y. (2004) 'FVT-1 Is a Mammalian 3-Ketodihydrosphingosine Reductase with an Active Site That Faces the Cytosolic Side of the Endoplasmic Reticulum Membrane', *Journal of Biological Chemistry*, 279(47), pp. 49243–49250. doi: 10.1074/jbc.M405915200.

Kim, D. *et al.* (2015) 'SHMT2 drives glioma cell survival in ischaemia but imposes a dependence on glycine clearance', *Nature*. Nature Publishing Group, a division of Macmillan Publishers Limited. All Rights Reserved., 520(7547), pp. 363–367.

Kim, D.-H. *et al.* (2005) 'Synthetic dsRNA Dicer substrates enhance RNAi potency and efficacy', *Nat Biotech*. Nature Publishing Group, 23(2), pp. 222–226.

Kim, K.-H. *et al.* (2013) 'Matricellular Protein CCN1 Promotes Regression of Liver Fibrosis through Induction of Cellular Senescence in Hepatic Myofibroblasts', *Molecular and Cellular Biology*. 1752 N St., N.W., Washington, DC: American Society for Microbiology, 33(10), pp. 2078–2090. doi: 10.1128/MCB.00049-13.

Kim, S.-T. *et al.* (1999) 'Substrate Specificities and Identification of Putative Substrates of ATM Kinase Family Members', *Journal of Biological Chemistry*, 274(53), pp. 37538–37543. doi: 10.1074/jbc.274.53.37538.

Kim, W. H. *et al.* (2000) 'Induction of p53-independent p21 during ceramide-induced G1 arrest in human hepatocarcinoma cells', *Biochemistry and Cell Biology*, 78(2), pp. 127–135.

Kitatani, K., Idkowiak-Baldys, J. and Hannun, Y. A. (2008) 'The sphingolipid salvage pathway in ceramide metabolism and signaling', *Cellular Signalling*, 20(6), pp. 1010–1018. doi: http://dx.doi.org/10.1016/j.cellsig.2007.12.006.

Knapp, P. *et al.* (2017) 'Plasma and ovarian tissue sphingolipids profiling in patients with advanced ovarian cancer', *Gynecologic Oncology*, 147(1), pp. 139–144. doi: https://doi.org/10.1016/j.ygyno.2017.07.143.

Kohno, M. *et al.* (2006) 'Intracellular Role for Sphingosine Kinase 1 in Intestinal Adenoma Cell Proliferation', *Molecular and Cellular Biology*, 26(19), pp. 7211–7223. doi: 10.1128/MCB.02341-05.

Kondoh, H. *et al.* (2005) 'Glycolytic Enzymes Can Modulate Cellular Life Span', *Cancer Research*, 65(1), pp. 177–185.

Kong, X. *et al.* (2012) 'Interleukin-22 Induces Hepatic Stellate Cell Senescence and Restricts Liver Fibrosis', *Hepatology (Baltimore, Md.)*, 56(3), pp. 1150–1159. doi: 10.1002/hep.25744.

Krebs, H. A. (1935) 'Metabolism of amino-acids: The synthesis of glutamine from glutamic acid and ammonia, and the enzymic hydrolysis of glutamine in animal tissues', *Biochemical Journal*, 29(8), pp. 1951–1969.

Krishnamurthy, J. *et al.* (2004) 'Ink4a/Arf expression is a biomarker of aging', *Journal of Clinical Investigation*. American Society for Clinical Investigation, 114(9), pp. 1299–1307. doi: 10.1172/JCI200422475.

Krishnamurthy, J. *et al.* (2006) 'p16INK4a induces an age-dependent decline in islet regenerative potential', *Nature*, 443(7110), pp. 453–457. doi: 10.1038/nature05092.

Krizhanovsky, V. *et al.* (2008) 'Senescence of activated stellate cells limits liver fibrosis', *Cell*, 134(4), pp. 657–667. doi: 10.1016/j.cell.2008.06.049.

Kroesen, B.-J. *et al.* (2001) 'Induction of Apoptosis through B-cell Receptor Cross-linking Occurs via de Novo Generated C16-Ceramide and Involves Mitochondria ', *Journal of Biological Chemistry* , 276(17), pp. 13606–13614. doi: 10.1074/jbc.M009517200.

Krtolica, A. *et al.* (2001) 'Senescent fibroblasts promote epithelial cell growth and tumorigenesis: A link between cancer and aging', *Proceedings of the National Academy of Sciences of the United States of America*. The National Academy of Sciences, 98(21), pp. 12072–12077. doi: 10.1073/pnas.211053698.

Kuilman, T. *et al.* (2008) 'Oncogene-Induced Senescence Relayed by an Interleukin-Dependent Inflammatory Network', *Cell*. Elsevier, 133(6), pp. 1019–1031. doi: 10.1016/j.cell.2008.03.039.

Kujjo, L. L. *et al.* (2013) 'Ceramide and its transport protein (CERT) contribute to deterioration of mitochondrial structure and function in aging oocytes', *Mechanisms of Ageing and Development*, 134(1), pp. 43–52. doi: https://doi.org/10.1016/j.mad.2012.12.001.

Kurz, D. J. *et al.* (2000) 'Senescence-associated β-galactosidase reflects an increase in lysosomal mass during replicative ageing of human endothelial cells', *Journal of Cell Science*, 113(20), p. 3613 LP-3622.

Laberge, R.-M. *et al.* (2015) 'MTOR regulates the pro-tumorigenic senescence-associated secretory phenotype by promoting IL1A translation', *Nat Cell Biol*. Nature Publishing Group, 17(8), pp. 1049–1061.

Labuschagne, C. F. *et al.* (2014) 'Serine, but Not Glycine, Supports One-Carbon Metabolism and Proliferation of Cancer Cells', *Cell Reports*, 7(4), pp. 1248–1258. doi: http://dx.doi.org/10.1016/j.celrep.2014.04.045.

Laviad, E. L. *et al.* (2008) 'Characterization of Ceramide Synthase 2: Tissue

distribution, substrate specificity, and inhibition by sphingosine 1-phosphate', *Journal of Biological Chemistry*, 283(9), pp. 5677–5684. doi: 10.1074/jbc.M707386200.

Lee, B. Y. *et al.* (2006) 'Senescence-associated β-galactosidase is lysosomal β-galactosidase', *Aging Cell*. Blackwell Science Ltd, 5(2), pp. 187–195. doi: 10.1111/j.1474-9726.2006.00199.x.

Lee, J. Y., Bielawska, A. E. and Obeid, L. M. (2000) 'Regulation of Cyclin-Dependent Kinase 2 Activity by Ceramide', *Experimental Cell Research*, 261(2), pp. 303–311. doi: http://dx.doi.org/10.1006/excr.2000.5028.

Lee, W.-N. P. *et al.* (1998) 'Mass isotopomer study of the nonoxidative pathways of the pentose cycle with [1,2-13C2]glucose', *American Journal of Physiology - Endocrinology And Metabolism*, 274(5), p. E843 LP-E851.

Lenain, C. *et al.* (2015) 'Autophagy-mediated degradation of nuclear envelope proteins during oncogene-induced senescence', *Carcinogenesis*, 36(11), pp. 1263–1274.

Di Leonardo, A. *et al.* (1994) 'DNA damage triggers a prolonged p53-dependent G1 arrest and long-term induction of Cip1 in normal human fibroblasts.', *Genes & Development*, 8(21), pp. 2540–2551. doi: 10.1101/gad.8.21.2540.

Leung, R. K. and Whittaker, P. A. (2005) 'RNA interference: from gene silencing to gene-specific therapeutics', *Pharmacol Ther*. 2005/05/24, 107(2), pp. 222–239. doi: 10.1016/j.pharmthera.2005.03.004.

Levy, M. and Futerman, A. H. (2010) 'Mammalian Ceramide Synthases', *IUBMB life*, 62(5), pp. 347–356. doi: 10.1002/iub.319.

Li, F. and Zhang, N. (2015) 'Ceramide: Therapeutic Potential in Combination Therapy for Cancer Treatment.', *Current drug metabolism*. Netherlands, 17(1), pp. 37–51.

Lindsey, J. *et al.* (1991) 'In vivo loss of telomeric repeats with age in humans', *Mutation Research/DNAging*, 256(1), pp. 45–48. doi: http://dx.doi.org/10.1016/0921-8734(91)90032-7.

Linn, S. C. *et al.* (2001) 'Regulation of de novo sphingolipid biosynthesis and the toxic consequences of its disruption', *Biochemical Society Transactions*, 29(6), p. 831 LP-835.

Liton, P. B. *et al.* (2005) 'Cellular senescence in the glaucomatous outflow pathway', *Experimental gerontology*, 40(8–9), pp. 745–748. doi: 10.1016/j.exger.2005.06.005.

Liu, J. *et al.* (2012) 'Accelerated senescence of renal tubular epithelial cells is associated with disease progression of patients with immunoglobulin A (IgA) nephropathy', *Translational Research*, 159(6), pp. 454–463. doi: http://dx.doi.org/10.1016/j.trsl.2011.11.008.

Liu, X. *et al.* (2010) 'Targeting of survivin by nanoliposomal ceramide induces complete remission in a rat model of NK-LGL leukemia', *Blood*, 116(20), p. 4192 LP-4201.

Liu, Y. *et al.* (2012) 'A Small-Molecule Inhibitor of Glucose Transporter 1 Downregulates Glycolysis, Induces Cell-Cycle Arrest, and Inhibits Cancer Cell Growth In Vitro and <em>In Vivo</em&gt';, *Molecular Cancer Therapeutics*, 11(8), p. 1672 LP-1682.

Llanos, S. *et al.* (2016) 'Stabilization of p21 by mTORC1/4E-BP1 predicts clinical outcome of head and neck cancers', *Nature Communications*. Nature Publishing Group, 7, p. 10438. doi: 10.1038/ncomms10438.

Lou, Z. *et al.* (2003) 'MDC1 is coupled to activated CHK2 in mammalian DNA damage response pathways', *Nature*, 421(6926), pp. 957–961.

Lv, X. *et al.* (2013) 'Rupatadine Protects against Pulmonary Fibrosis by Attenuating PAF-Mediated Senescence in Rodents', *PLOS ONE*. Public Library of Science, 8(7), p. e68631.

Maddocks, O. D. K. *et al.* (2013) 'Serine starvation induces stress and p53-dependent metabolic remodelling in cancer cells.', *Nature*. Nature Publishing Group, 493(7433), pp. 542–6. doi: 10.1038/nature11743.

Maddocks, O. D. K. *et al.* (2016) 'Serine Metabolism Supports the Methionine Cycle and DNA/RNA Methylation through De Novo ATP Synthesis in Cancer Cells', *Molecular Cell*, 61(2), pp. 210–221. doi: http://dx.doi.org/10.1016/j.molcel.2015.12.014.

Maddocks, O. D. K. *et al.* (2017) 'Modulating the therapeutic response of tumours to dietary serine and glycine starvation', *Nature*. Macmillan Publishers Limited, part of Springer Nature. All rights reserved., 544(7650), pp. 372–376.

Malone, R. W., Felgner, P. L. and Verma, I. M. (1989) 'Cationic liposome-mediated RNA transfection.', *Proceedings of the National Academy of Sciences of the United States of America*, 86(16), pp. 6077–6081.

Manche, L. *et al.* (1992) 'Interactions between double-stranded RNA regulators and the protein kinase DAI.', *Molecular and Cellular Biology*, 12(11), pp. 5238–5248.

Mann, D. M., McKeown-Longo, P. J. and Millis, A. J. (1988) 'Binding of soluble fibronectin and its subsequent incorporation into the extracellular matrix by early and late passage human skin fibroblasts.', *Journal of Biological Chemistry*, 263(6), pp. 2756–2760.

Markowski, D. N. *et al.* (2013) 'HMGA2 expression in white adipose tissue linking cellular senescence with diabetes', *Genes & Nutrition*. Berlin/Heidelberg: Springer Berlin Heidelberg, 8(5), pp. 449–456. doi: 10.1007/s12263-013-0354-6.

Martin, J. A. and Buckwalter, J. A. (2003) 'The Role of Chondrocyte Senescence in

the Pathogenesis of Osteoarthritis and in Limiting Cartilage Repair', *JBJS*, 85(suppl_2).

Martin, N. *et al.* (2013) 'Interplay between Homeobox proteins and Polycomb repressive complexes in p16(INK4a) regulation', *The EMBO Journal*. Nature Publishing Group, 32(7), pp. 982–995. doi: 10.1038/emboj.2013.37.

Mashimo, T. *et al.* (2014) 'Acetate Is a Bioenergetic Substrate for Human Glioblastoma and Brain Metastases', *Cell*, 159(7), pp. 1603–1614. doi: http://dx.doi.org/10.1016/j.cell.2014.11.025.

McClintock, B. (1941) 'The Stability of Broken Ends of Chromosomes in Zea Mays', *Genetics*, 26(2), pp. 234–282.

McManus, M. T. *et al.* (2002) 'Gene silencing using micro-RNA designed hairpins.', *RNA*, 8(6), pp. 842–850.

Meckfessel, M. H. and Brandt, S. (2014) 'The structure, function, and importance of ceramides in skin and their use as therapeutic agents in skin-care products', *Journal of the American Academy of Dermatology*, 71(1), pp. 177–184. doi: http://dx.doi.org/10.1016/j.jaad.2014.01.891.

van Meer, G., Voelker, D. R. and Feigenson, G. W. (2008) 'Membrane lipids: where they are and how they behave', *Nat Rev Mol Cell Biol*. Nature Publishing Group, 9(2), pp. 112–124.

Meiser, J. *et al.* (2016) 'Serine one-carbon catabolism with formate overflow', *Science Advances*. American Association for the Advancement of Science, 2(10), p. e1601273. doi: 10.1126/sciadv.1601273.

Mencarelli, C. and Martinez–Martinez, P. (2013) 'Ceramide function in the brain: when a slight tilt is enough', *Cellular and Molecular Life Sciences*, 70(2), pp. 181–203. doi: 10.1007/s00018-012-1038-x.

Messner, M. C. and Cabot, M. C. (2010) 'Glucosylceramide in Humans BT - Sphingolipids as Signaling and Regulatory Molecules', in Chalfant, C. and Poeta, M. Del (eds). New York, NY: Springer New York, pp. 156–164. doi: 10.1007/978-1-4419-6741-1_11.

Metallo, C. M. *et al.* (2012) 'Reductive glutamine metabolism by IDH1 mediates lipogenesis under hypoxia', *Nature*. Nature Publishing Group, a division of Macmillan Publishers Limited. All Rights Reserved., 481(7381), pp. 380–384.

Metallo, C. M. and Vander Heiden, M. G. (2013) 'Understanding Metabolic Regulation and Its Influence on Cell Physiology', *Molecular Cell*. Elsevier, 49(3), pp. 388–398. doi: 10.1016/j.molcel.2013.01.018.

Metallo, C. M., Walther, J. L. and Stephanopoulos, G. (2009) 'Evaluation of (13)C isotopic tracers for metabolic flux analysis in mammalian cells', *Journal of biotechnology*, 144(3), pp. 167–174. doi: 10.1016/j.jbiotec.2009.07.010.

Di Micco, R. *et al.* (2006) 'Oncogene-induced senescence is a DNA damage response triggered by DNA hyper-replication.', *Nature*, 444(7119), pp. 638–642. doi: 10.1038/nature05327.

Michaloglou, C. *et al.* (2005) 'BRAFE600-associated senescence-like cell cycle arrest of human naevi', *Nature*. Nature Publishing Group, 436(7051), pp. 720–724.

Michaud, K. *et al.* (2010) 'Pharmacologic inhibition of cdk4/6 arrests the growth of glioblastoma multiforme intracranial xenografts', *Cancer research*, 70(8), pp. 3228–3238. doi: 10.1158/0008-5472.CAN-09-4559.

Mikirova, N. *et al.* (2012) 'Effect of high-dose intravenous vitamin C on inflammation in cancer patients', *Journal of Translational Medicine*. BioMed Central, 10, p. 189. doi: 10.1186/1479-5876-10-189.

Millis, A. J. T. *et al.* (1989) 'Collagenase production by early and late passage cultures of human fibroblasts', *Experimental Gerontology*, 24(5), pp. 559–575. doi: http://dx.doi.org/10.1016/0531-5565(89)90060-0.

Minamino, T. *et al.* (2009) 'A crucial role for adipose tissue p53 in the regulation of insulin resistance', *Nat Med*. Nature Publishing Group, 15(9), pp. 1082–1087.

Di Mitri, D. *et al.* (2014) 'Tumour-infiltrating Gr-1+ myeloid cells antagonize senescence in cancer', *Nature*. Nature Publishing Group, a division of Macmillan Publishers Limited. All Rights Reserved., 515(7525), pp. 134–137.

Mitsutake, S. *et al.* (2004) 'Ceramide Kinase Is a Mediator of Calcium-dependent Degranulation in Mast Cells', *Journal of Biological Chemistry* , 279(17), pp. 17570–17577. doi: 10.1074/jbc.M312885200.

Mizutani, Y., Kihara, A. and Igarashi, Y. (2005) 'Mammalian Lass6 and its related family members regulate synthesis of specific ceramides', *Biochemical Journal*. Portland Press Ltd., 390(Pt 1), pp. 263–271. doi: 10.1042/BJ20050291.

Mizutani, Y., Kihara, A. and Igarashi, Y. (2006) 'LASS3 (longevity assurance homologue 3) is a mainly testis-specific (dihydro)ceramide synthase with relatively broad substrate specificity', *Biochemical Journal*, 398(3), p. 531 LP-538.

Molofsky, A. V *et al.* (2006) 'Increasing p16INK4a expression decreases forebrain progenitors and neurogenesis during ageing', *Nature*, 443(7110), pp. 448–452.

Morad, S. A. F. and Cabot, M. C. (2013) 'Ceramide-orchestrated signalling in cancer cells', *Nat Rev Cancer*. Nature Publishing Group, a division of Macmillan Publishers Limited. All Rights Reserved., 13(1), pp. 51–65.

Moreadith, R. W. and Lehninger, A. L. (1984) 'The pathways of glutamate and glutamine oxidation by tumor cell mitochondria. Role of mitochondrial NAD(P)+-dependent malic enzyme.', *Journal of Biological Chemistry*, 259(10), pp. 6215–6221.

Mosteiro, L. *et al.* (2016) 'Tissue damage and senescence provide critical signals for cellular reprogramming in vivo', *Science*, 354(6315).

Mullarky, E. *et al.* (2016) 'Identification of a small molecule inhibitor of 3-phosphoglycerate dehydrogenase to target serine biosynthesis in cancers', *Proceedings of the National Academy of Sciences*, 113(7), pp. 1778–1783. doi: 10.1073/pnas.1521548113.

Mullen, A. R. *et al.* (2012) 'Reductive carboxylation supports growth in tumour cells with defective mitochondria', *Nature*. Nature Publishing Group, a division of Macmillan Publishers Limited. All Rights Reserved., 481(7381), pp. 385–388.

Muñoz-Espín, D. *et al.* (2013) 'Programmed cell senescence during mammalian embryonic development.', *Cell*, 155(5), pp. 1104–18. doi: 10.1016/j.cell.2013.10.019.

Muñoz-Espín, D. and Serrano, M. (2014) 'Cellular senescence: from physiology to pathology.', *Nature reviews. Molecular cell biology*, 15(7), pp. 482–96. doi: 10.1038/nrm3823.

Narendra, D. *et al.* (2008) 'Parkin is recruited selectively to impaired mitochondria and promotes their autophagy', *The Journal of Cell Biology*. The Rockefeller University Press, 183(5), pp. 795–803. doi: 10.1083/jcb.200809125.

Narita, M. *et al.* (2003) 'Rb-Mediated Heterochromatin Formation and Silencing of E2F Target Genes during Cellular Senescence', *Cell*, 113(6), pp. 703–716. doi: http://dx.doi.org/10.1016/S0092-8674(03)00401-X.

Narita, M. *et al.* (2006) 'A Novel Role for High-Mobility Group A Proteins in Cellular Senescence and Heterochromatin Formation', *Cell*. Elsevier, 126(3), pp. 503–514. doi: 10.1016/j.cell.2006.05.052.

Narita, M. *et al.* (2011) 'Spatial Coupling of mTOR and Autophagy Augments Secretory Phenotypes', *Science*, 332(6032), pp. 966–970.

NCBI (2004) *Gene*. Available at: https://www.ncbi.nlm.nih.gov/gene/ (Accessed: 28 August 2017).

Neumann, B. *et al.* (2006) 'High-throughput RNAi screening by time-lapse imaging of live human cells', *Nat Meth*, 3(5), pp. 385–390.

Neumann, E. *et al.* (1982) 'Gene transfer into mouse lyoma cells by electroporation in high electric fields.', *The EMBO Journal*, 1(7), pp. 841–845.

Newman, A. C. and Maddocks, O. D. K. (2017) 'One-carbon metabolism in cancer', *Br J Cancer*. The Author(s), pp. 1499–1504.

Noureddine, H. *et al.* (2011) 'Pulmonary artery smooth muscle cell senescence is a pathogenic mechanism for pulmonary hypertension in chronic lung disease', *Circulation Research*. Lippincott Williams & Wilkins, 109(5), pp. 543–553. doi:

10.1161/CIRCRESAHA.111.241299.

Nykänen, A., Haley, B. and Zamore, P. D. (2001) 'ATP Requirements and Small Interfering RNA Structure in the RNA Interference Pathway', *Cell*, 107(3), pp. 309–321. doi: http://dx.doi.org/10.1016/S0092-8674(01)00547-5.

Ogretmen, B. *et al.* (2001) 'Role of Ceramide in Mediating the Inhibition of Telomerase Activity in A549 Human Lung Adenocarcinoma Cells', *Journal of Biological Chemistry*, 276(27), pp. 24901–24910. doi: 10.1074/jbc.M100314200.

Ogretmen, B. and Hannun, Y. A. (2004) 'Biologically active sphingolipids in cancer pathogenesis and treatment', *Nature Reviews Cancer*. Nature Publishing Group, 4, p. 604.

Ohuchida, K. *et al.* (2004) 'Radiation to Stromal Fibroblasts Increases Invasiveness of Pancreatic Cancer Cells through Tumor-Stromal Interactions', *Cancer Research*, 64(9), p. 3215 LP-3222.

Okazumi, S. *et al.* (1992) 'Evaluation of Liver Tumors Using fluorine- 18-Fluorodeoxyglucose PET: Characterization of Tumor and Assessment of Effect of Treatment', *Journal of Nuclear Medicine*, 33(3), pp. 333–339.

Olovnikov, A. M. (1973) 'A theory of marginotomy', *Journal of Theoretical Biology*, 41(1), pp. 181–190. doi: http://dx.doi.org/10.1016/0022-5193(73)90198-7.

Pacold, M. E. *et al.* (2016) 'A PHGDH inhibitor reveals coordination of serine synthesis and one-carbon unit fate', *Nat Chem Biol*. Nature Publishing Group, a division of Macmillan Publishers Limited. All Rights Reserved., 12(6), pp. 452–458.

Paddison, P. J. *et al.* (2002) 'Short hairpin RNAs (shRNAs) induce sequence-specific silencing in mammalian cells', *Genes & Development*. Cold Spring Harbor Laboratory Press, 16(8), pp. 948–958. doi: 10.1101/gad.981002.

Paddison, P. J. *et al.* (2004) 'A resource for large-scale RNA-interference-based screens in mammals', *Nature*, 428(6981), pp. 427–431.

Palm, W. and de Lange, T. (2008) 'How Shelterin Protects Mammalian Telomeres', *Annual Review of Genetics*. Annual Reviews, 42(1), pp. 301–334. doi: 10.1146/annurev.genet.41.110306.130350.

Parada, L. F. *et al.* (1982) 'Human EJ bladder carcinoma oncogene is homologue of Harvey sarcoma virus ras gene', *Nature*, 297(5866), pp. 474–478.

Parenti, G., Andria, G. and Ballabio, A. (2015) 'Lysosomal Storage Diseases: From Pathophysiology to Therapy', *Annual Review of Medicine*. Annual Reviews, 66(1), pp. 471–486. doi: 10.1146/annurev-med-122313-085916.

Parrinello, S. *et al.* (2005) 'Stromal-epithelial interactions in aging and cancer: senescent fibroblasts alter epithelial cell differentiation', *Journal of cell science*, 118(Pt 3), pp. 485–496. doi: 10.1242/jcs.01635.

Passos, J. F., von Zglinicki, T. and Kirkwood, T. B. L. (2007) 'Mitochondria and ageing: winning and losing in the numbers game', *BioEssays*. Wiley Subscription Services, Inc., A Wiley Company, 29(9), pp. 908–917. doi: 10.1002/bies.20634.

Pastukhov, O. *et al.* (2014) 'The ceramide kinase inhibitor NVP-231 inhibits breast and lung cancer cell proliferation by inducing M phase arrest and subsequent cell death', *British Journal of Pharmacology*. Oxford, UK: BlackWell Publishing Ltd, 171(24), pp. 5829–5844. doi: 10.1111/bph.12886.

Patel, D. *et al.* (2016) 'Aspartate Rescues S-phase Arrest Caused by Suppression of Glutamine Utilization in KRas-driven Cancer Cells', *Journal of Biological Chemistry*, 291(17), pp. 9322–9329. doi: 10.1074/jbc.M115.710145.

Patel, P. L. *et al.* (2016) 'Derepression of hTERT gene expression promotes escape from oncogene-induced cellular senescence', *Proceedings of the National Academy of Sciences*, 113(34), pp. E5024–E5033. doi: 10.1073/pnas.1602379113.

Patra, K. C. *et al.* (2013) 'Hexokinase 2 is required for tumor initiation and maintenance and its systemic deletion is therapeutic in mouse models of cancer', *Cancer cell*, 24(2), pp. 213–228. doi: 10.1016/j.ccr.2013.06.014.

Patra, K. C. and Hay, N. (2013) 'Hexokinase 2 as oncotarget', *Oncotarget*. Impact Journals LLC, 4(11), pp. 1862–1863.

Patschan, S. *et al.* (2008) 'Lipid mediators of autophagy in stress-induced premature senescence of endothelial cells', *American Journal of Physiology - Heart and Circulatory Physiology*, 294(3), p. H1119 LP-H1129.

Patti, G. J., Yanes, O. and Siuzdak, G. (2012) 'Innovation: Metabolomics: the apogee of the omics trilogy', *Nat Rev Mol Cell Biol*. Nature Publishing Group, a division of Macmillan Publishers Limited. All Rights Reserved., 13(4), pp. 263–269.

Pelz, O., Gilsdorf, M. and Boutros, M. (2010) 'web cellHTS2: a web-application for the analysis of high-throughput screening data', *BMC Bioinformatics*, 11, p. 185. doi: 10.1186/1471-2105-11-185.

Pewzner-Jung, Y., Ben-Dor, S. and Futerman, A. H. (2006) 'When Do Lasses (Longevity Assurance Genes) Become CerS (Ceramide Synthases)?: INSIGHTS INTO THE REGULATION OF CERAMIDE SYNTHESIS ', *Journal of Biological Chemistry* , 281(35), pp. 25001–25005. doi: 10.1074/jbc.R600010200.

Pollard, P. J. *et al.* (2005) 'Accumulation of Krebs cycle intermediates and over-expression of HIF1α in tumours which result from germline FH and SDH mutations', *Human Molecular Genetics*, 14(15), pp. 2231–2239.

Pollari, S. *et al.* (2011) 'Enhanced serine production by bone metastatic breast cancer cells stimulates osteoclastogenesis', *Breast Cancer Research and Treatment*, 125(2), pp. 421–430. doi: 10.1007/s10549-010-0848-5.

Possemato, R. *et al.* (2011) 'Functional genomics reveal that the serine synthesis

pathway is essential in breast cancer', *Nature*. Nature Publishing Group, a division of Macmillan Publishers Limited. All Rights Reserved., 476(7360), pp. 346–350.

Prior, I. A., Lewis, P. D. and Mattos, C. (2012) 'A comprehensive survey of Ras mutations in cancer', *Cancer Research*, 72(10), pp. 2457–2467. doi: 10.1158/0008-5472.CAN-11-2612.

Pruschy, M. *et al.* (1999) 'Ceramide triggers p53-dependent apoptosis in genetically defined fibrosarcoma tumour cells', *British Journal of Cancer*. Nature Publishing Group, 80(5–6), pp. 693–698. doi: 10.1038/sj.bjc.6690411.

Quijano, C. *et al.* (2012) 'Oncogene-induced senescence results in marked metabolic and bioenergetic alterations', *Cell Cycle*. 2012/03/17, 11(7), pp. 1383–1392. doi: 10.4161/cc.19800.

Rader, J. *et al.* (2013) 'Dual CDK4/CDK6 Inhibition Induces Cell Cycle Arrest and Senescence in Neuroblastoma', *Clinical cancer research : an official journal of the American Association for Cancer Research*, 19(22), p. 10.1158/1078-0432.CCR-13-1675. doi: 10.1158/1078-0432.CCR-13-1675.

Ramstedt, B. and Slotte, J. P. (2002) 'Membrane properties of sphingomyelins', *FEBS Letters*, 531(1), pp. 33–37. doi: 10.1016/S0014-5793(02)03406-3.

Reynolds, A. *et al.* (2006) 'Induction of the interferon response by siRNA is cell type– and duplex length–dependent', *RNA*. Cold Spring Harbor Laboratory Press, 12(6), pp. 988–993. doi: 10.1261/rna.2340906.

Riboni, L. *et al.* (2002) 'Ceramide levels are inversely associated with malignant progression of human glial tumors', *Glia*. Wiley Subscription Services, Inc., A Wiley Company, 39(2), pp. 105–113. doi: 10.1002/glia.10087.

Riebeling, C. *et al.* (2003) 'Two mammalian longevity assurance gene (LAG1) family members, trh1 and trh4, regulate dihydroceramide synthesis using different fatty acyl-CoA donors.', *The Journal of biological chemistry*, 278(44), pp. 43452–9. doi: 10.1074/jbc.M307104200.

Rodier, F. *et al.* (2009) 'Persistent DNA damage signalling triggers senescence-associated inflammatory cytokine secretion', *Nat Cell Biol*. Nature Publishing Group, 11(8), pp. 973–979.

Rogakou, E. P. and Sekeri–Pataryas, K. E. (1999) 'Histone variants of H2A and H3 families are regulated during in vitro aging in the same manner as during differentiation', *Experimental Gerontology*, 34(6), pp. 741–754. doi: http://dx.doi.org/10.1016/S0531-5565(99)00046-7.

Rose, M. *et al.* (1999) 'Dietary glycine prevents the development of liver tumors caused by the peroxisome proliferator WY-14,643', *Carcinogenesis*, 20(11), pp. 2075–2081.

Rubin, A. L. (1990) 'Suppression of Transformation by and Growth Adaptation to

Low Concentrations of Glutamine in NIH-3T3 Cells', *Cancer Research*, 50(9), p. 2832 LP-2839.

Rubin, S. M. (2013) 'Deciphering the retinoblastoma protein phosphorylation code', *Trends in Biochemical Sciences*, 38(1), pp. 12–19. doi: http://dx.doi.org/10.1016/j.tibs.2012.10.007.

Rubinson, D. A. *et al.* (2003) 'A lentivirus-based system to functionally silence genes in primary mammalian cells, stem cells and transgenic mice by RNA interference', *Nat Genet*. Nature Publishing Group, 33(3), pp. 401–406.

Sage, J. *et al.* (2003) 'Acute mutation of retinoblastoma gene function is sufficient for cell cycle re-entry', *Nature*, 424(6945), pp. 223–228.

Salama, R. *et al.* (2014) 'Cellular senescence and its effector programs', *Genes Dev*, 28(2), pp. 99–114. doi: 10.1101/gad.235184.113.

Sanchez, E. L. *et al.* (2015) 'Latent KSHV Infected Endothelial Cells Are Glutamine Addicted and Require Glutaminolysis for Survival', *PLOS Pathogens*. Public Library of Science, 11(7), p. e1005052.

Schafer, M. J. *et al.* (2016) 'Exercise Prevents Diet-Induced Cellular Senescence in Adipose Tissue', *Diabetes*. American Diabetes Association, 65(6), pp. 1606–1615. doi: 10.2337/db15-0291.

Schafer, M. J. *et al.* (2017) 'Cellular senescence mediates fibrotic pulmonary disease', *Nature Communications*. Nature Publishing Group, 8, p. 14532. doi: 10.1038/ncomms14532.

Schiffmann, S. *et al.* (2009) 'Ceramide synthases and ceramide levels are increased in breast cancer tissue', *Carcinogenesis*, 30(5), pp. 745–752.

Schmitt, C. A. *et al.* (2002) 'A Senescence Program Controlled by p53 and p16INK4a Contributes to the Outcome of Cancer Therapy', *Cell*, 109(3), pp. 335–346. doi: http://dx.doi.org/10.1016/S0092-8674(02)00734-1.

Schug, Z. T. *et al.* (2016) 'Acetyl-CoA Synthetase 2 Promotes Acetate Utilization and Maintains Cancer Cell Growth under Metabolic Stress', *Cancer Cell*. Elsevier, 27(1), pp. 57–71. doi: 10.1016/j.ccell.2014.12.002.

Schultz, C. *et al.* (2010) 'Imaging Lipids in Living Cells', *Cold Spring Harbor Protocols*, 2010(7), p. pdb.top83. doi: 10.1101/pdb.top83.

Seelan, R. S. *et al.* (2000) 'Human acid ceramidase is overexpressed but not mutated in prostate cancer', *Genes, Chromosomes and Cancer*. John Wiley & Sons, Inc., 29(2), pp. 137–146. doi: 10.1002/1098-2264(2000)9999:9999<::AID-GCC1018>3.0.CO;2-E.

Serrano, M. *et al.* (1997) 'Oncogenic ras provokes premature cell senescence associated with accumulation of p53 and p16INK4a', *Cell*, 88(5), pp. 593–602.

Shamma, A. *et al.* (2009) 'Rb Regulates DNA Damage Response and Cellular Senescence through E2F-Dependent Suppression of N-Ras Isoprenylation', *Cancer Cell*, 15(4), pp. 255–269. doi: https://doi.org/10.1016/j.ccr.2009.03.001.

Shay, J. W. and Wright, W. E. (2000) 'Hayflick, his limit, and cellular ageing', *Nat Rev Mol Cell Biol*. Macmillan Magazines Ltd., 1(1), pp. 72–76.

Shay, J. W. and Wright, W. E. (2006) 'Telomerase therapeutics for cancer: challenges and new directions', *Nat Rev Drug Discov*, 5(7), pp. 577–584.

Shelton, D. N. *et al.* (1999) 'Microarray analysis of replicative senescence', *Current Biology*, 9(17), pp. 939–945. doi: http://dx.doi.org/10.1016/S0960-9822(99)80420-5.

Simons, K. and Ikonen, E. (1997) 'Functional rafts in cell membranes', *Nature*. Macmillan Magazines Ltd., 387, p. 569.

Singh, K. *et al.* (2012) 'Autophagy-dependent senescence in response to DNA damage and chronic apoptotic stress', *Autophagy*. Taylor & Francis, 8(2), pp. 236–251. doi: 10.4161/auto.8.2.18600.

Siskind, L. J., Kolesnick, R. N. and Colombini, M. (2002) 'Ceramide Channels Increase the Permeability of the Mitochondrial Outer Membrane to Small Proteins', *Journal of Biological Chemistry* , 277(30), pp. 26796–26803. doi: 10.1074/jbc.M200754200.

Sledz, C. A. *et al.* (2003) 'Activation of the interferon system by short-interfering RNAs', *Nat Cell Biol*. Nature Publishing Group, 5(9), pp. 834–839.

Sottile, J. *et al.* (1989) 'Regulation of collagenase and collagenase mRNA production in early- and late-passage human diploid fibroblasts', *Journal of Cellular Physiology*. Wiley Subscription Services, Inc., A Wiley Company, 138(2), pp. 281–290. doi: 10.1002/jcp.1041380209.

Stancevic, B. and Kolesnick, R. (2010) 'Ceramide-rich platforms in transmembrane signaling', *FEBS Letters*, 584(9), pp. 1728–1740. doi: 10.1016/j.febslet.2010.02.026.

van Steensel, B., Smogorzewska, A. and de Lange, T. (1998) 'TRF2 Protects Human Telomeres from End-to-End Fusions', *Cell*. Elsevier, 92(3), pp. 401–413. doi: 10.1016/S0092-8674(00)80932-0.

Stewart, S. A. *et al.* (2003) 'Lentivirus-delivered stable gene silencing by RNAi in primary cells', *RNA*, 9(4), pp. 493–501. doi: 10.1261/rna.2192803.

Storer, M. *et al.* (2013) 'Senescence Is a Developmental Mechanism that Contributes to Embryonic Growth and Patterning', *Cell*. Elsevier, 155(5), pp. 1119–1130. doi: 10.1016/j.cell.2013.10.041.

Struckhoff, A. P., Patel, B. and Beckman, B. S. (2010) 'Inhibition of p53 sensitizes MCF-7 cells to ceramide treatment', *International Journal of Oncology*, 37(1), pp. 21–30. doi: https://doi.org/10.3892/ijo_00000649.

Sultan, I. *et al.* (2005) 'Regulation of the sphingosine-recycling pathway for ceramide generation by oxidative stress, and its role in controlling c-Myc/Max function', *Biochemical Journal*, 393(2), p. 513 LP-521.

Sun, R. C. and Denko, N. C. (2014) 'Hypoxic Regulation of Glutamine Metabolism through HIF1 and SIAH2 Supports Lipid Synthesis that Is Necessary for Tumor Growth', *Cell Metabolism*, 19(2), pp. 285–292. doi: http://dx.doi.org/10.1016/j.cmet.2013.11.022.

Sun, Y. *et al.* (2012) 'Treatment-induced damage to the tumor microenvironment promotes prostate cancer therapy resistance through WNT16B', *Nature medicine*, 18(9), pp. 1359–1368. doi: 10.1038/nm.2890.

Tagaram, H. R. S. *et al.* (2011) 'Nanoliposomal ceramide prevents in vivo growth of hepatocellular carcinoma', *Gut*, 60(5), p. 695 LP-701.

Takebayashi, S. *et al.* (2015) 'Retinoblastoma protein promotes oxidative phosphorylation through upregulation of glycolytic genes in oncogene-induced senescent cells', *Aging Cell*. Chichester, UK: John Wiley & Sons, Ltd, 14(4), pp. 689–697. doi: 10.1111/acel.12351.

Tchkonia, T. *et al.* (2010) 'Fat tissue, aging, and cellular senescence', *Aging Cell*, 9(5), pp. 667–684. doi: 10.1111/j.1474-9726.2010.00608.x.

Thangavel, C. *et al.* (2011) 'Therapeutically activating RB: reestablishing cell cycle control in endocrine therapy-resistant breast cancer', *Endocrine-related cancer*, 18(3), pp. 333–345. doi: 10.1530/ERC-10-0262.

Thomas, S. *et al.* (2004) 'Analysis of lipid rafts in T cells', *Molecular Immunology*, 41(4), pp. 399–409. doi: https://doi.org/10.1016/j.molimm.2004.03.022.

Tomlinson, I. P. M. *et al.* (2002) 'Germline mutations in FH predispose to dominantly inherited uterine fibroids, skin leiomyomata and papillary renal cell cancer', *Nat Genet*, 30(4), pp. 406–410.

Ullah, Z. *et al.* (2009) 'Developmentally programmed endoreduplication in animals', *Cell cycle (Georgetown, Tex.)*, 8(10), pp. 1501–1509.

Vasile, E. *et al.* (2001) 'Differential expression of thymosin β-10 by early passage and senescent vascular endothelium is modulated by VPF/VEGF: evidence for senescent endothelial cells in vivo at sites of atherosclerosis', *The FASEB Journal*, 15(2), pp. 458–466. doi: 10.1096/fj.00-0051com.

Venable, M. E. *et al.* (1995) 'Role of Ceramide in Cellular Senescence', *Journal of Biological Chemistry*, 270(51), pp. 30701–30708. doi: 10.1074/jbc.270.51.30701.

Venkataraman, K. *et al.* (2002) 'Upstream of Growth and Differentiation Factor 1 (uog1), a Mammalian Homolog of the Yeast Longevity Assurance Gene 1 (LAG1), RegulatesN-Stearoyl-sphinganine (C18-(Dihydro)ceramide) Synthesis in a Fumonisin B1-independent Manner in Mammalian Cells ', *Journal of Biological*

Chemistry , 277(38), pp. 35642–35649. doi: 10.1074/jbc.M205211200.

Venneti, S. *et al.* (2015) 'Glutamine-based PET imaging facilitates enhanced metabolic evaluation of gliomas in vivo', *Science translational medicine*, 7(274), p. 274ra17-274ra17. doi: 10.1126/scitranslmed.aaa1009.

Wajapeyee, N. *et al.* (2008) 'Oncogenic BRAF Induces Senescence and Apoptosis through Pathways Mediated by the Secreted Protein IGFBP7', *Cell*, 132(3), pp. 363–374. doi: http://dx.doi.org/10.1016/j.cell.2007.12.032.

Wang, D. *et al.* (2006) 'A mouse model for Glut-1 haploinsufficiency', *Human Molecular Genetics*, 15(7), pp. 1169–1179.

Warburg, O. (1956) 'On the Origin of Cancer Cells', *Science*, 123(3191), p. 309 LP-314.

Warburg, O., Posener, K. and Negelein, E. (1924) 'Uber den Stoffwechsel der Carcinomzelle.', *Biochem Z.*, 152, pp. 319–344.

Watson, J. D. (1972) 'Origin of concatemeric T7 DNA', *Nature - New Biology*. Basingstoke: Stockton Press LTD, 239(94), p. 197-.

Watters, R. J. *et al.* (2012) 'Chapter five - Development and Use of Ceramide Nanoliposomes in Cancer', in Düzgüneş, N. B. T.-M. in E. (ed.) *Nanomedicine*. Academic Press, pp. 89–108. doi: https://doi.org/10.1016/B978-0-12-391860-4.00005-7.

Wei, S., Wei, W. and Sedivy, J. M. (1999) 'Expression of Catalytically Active Telomerase Does Not Prevent Premature Senescence Caused by Overexpression of Oncogenic Ha-Ras in Normal Human Fibroblasts', *Cancer Research*, 59(7), p. 1539 LP-1543.

Wei, W., Hemmer, R. M. and Sedivy, J. M. (2001) 'Role of p14(ARF) in Replicative and Induced Senescence of Human Fibroblasts', *Molecular and Cellular Biology*. American Society for Microbiology, 21(20), pp. 6748–6757. doi: 10.1128/MCB.21.20.6748-6757.2001.

Weinberg, F. *et al.* (2010) 'Mitochondrial metabolism and ROS generation are essential for Kras-mediated tumorigenicity', *Proceedings of the National Academy of Sciences of the United States of America*. National Academy of Sciences, 107(19), pp. 8788–8793. doi: 10.1073/pnas.1003428107.

Weismann, A. *et al.* (1891) *Essays upon heredity and kindred biological problems, by Dr. August Weismann. Ed. by Edward B. Poulton, Selmar Schönland, and Arthur E. Shipley. Authorised translation.* . 2d ed. Oxford,: Clarendon Press,.

Wiemann, S. U. *et al.* (2002) 'Hepatocyte telomere shortening and senescence are general markers of human liver cirrhosis', *The FASEB Journal*, 16(9), pp. 935–942. doi: 10.1096/fj.01-0977com.

Wiley, C. D. *et al.* (2016) 'Mitochondrial Dysfunction Induces Senescence with a Distinct Secretory Phenotype', *Cell Metabolism*. Elsevier, 23(2), pp. 303–314. doi: 10.1016/j.cmet.2015.11.011.

Wilson, R. C. and Doudna, J. A. (2013) 'Molecular Mechanisms of RNA Interference', *Annual Review of Biophysics*. Annual Reviews, 42(1), pp. 217–239. doi: 10.1146/annurev-biophys-083012-130404.

Windmueller, H. G. and Spaeth, A. E. (1974) 'Uptake and Metabolism of Plasma Glutamine by the Small Intestine', *Journal of Biological Chemistry*, 249(16), pp. 5070–5079.

Wise, D. R. *et al.* (2008) 'Myc regulates a transcriptional program that stimulates mitochondrial glutaminolysis and leads to glutamine addiction', *Proceedings of the National Academy of Sciences of the United States of America*. National Academy of Sciences, 105(48), pp. 18782–18787. doi: 10.1073/pnas.0810199105.

Wise, D. R. *et al.* (2011) 'Hypoxia promotes isocitrate dehydrogenase-dependent carboxylation of α-ketoglutarate to citrate to support cell growth and viability', *Proceedings of the National Academy of Sciences*, 108(49), pp. 19611–19616. doi: 10.1073/pnas.1117773108.

Wolff, R. A. *et al.* (1994) 'Role of ceramide-activated protein phosphatase in ceramide-mediated signal transduction.', *Journal of Biological Chemistry*, 269(30), pp. 19605–19609.

Xu, M. *et al.* (2015) 'Targeting senescent cells enhances adipogenesis and metabolic function in old age', *eLife*. Edited by A. Dillin. eLife Sciences Publications, Ltd, 4, p. e12997. doi: 10.7554/eLife.12997.

Xu, R. *et al.* (2006) 'Golgi alkaline ceramidase regulates cell proliferation and survival by controlling levels of sphingosine and S1P', *The FASEB Journal*, 20(11), pp. 1813–1825. doi: 10.1096/fj.05-5689com.

Xue, W. *et al.* (2007) 'Senescence and tumour clearance is triggered by p53 restoration in murine liver carcinomas', *Nature*, 445(7128), pp. 656–660.

Yang, M. and Vousden, K. H. (2016) 'Serine and one-carbon metabolism in cancer', *Nat Rev Cancer*. Nature Publishing Group, a division of Macmillan Publishers Limited. All Rights Reserved., 16(10), pp. 650–662.

Yang, N.-C. and Hu, M.-L. (2005) 'The limitations and validities of senescence associated-β-galactosidase activity as an aging marker for human foreskin fibroblast Hs68 cells', *Experimental Gerontology*, 40(10), pp. 813–819. doi: http://dx.doi.org/10.1016/j.exger.2005.07.011.

Ye, J. *et al.* (2014) 'Serine catabolism regulates mitochondrial redox control during hypoxia', *Cancer discovery*, 4(12), pp. 1406–1417. doi: 10.1158/2159-8290.CD-14-0250.

Yosef, R. *et al.* (2016) 'Directed elimination of senescent cells by inhibition of BCL-W and BCL-XL', *Nature Communications*. Nature Publishing Group, 7, p. 11190. doi: 10.1038/ncomms11190.

Young, A. P. *et al.* (2008) 'VHL loss actuates a HIF-independent senescence programme mediated by Rb and p400', *Nat Cell Biol*. Nature Publishing Group, 10(3), pp. 361–369.

Yun, J. *et al.* (2009) 'Glucose Deprivation Contributes to the Development of KRAS Pathway Mutations in Tumor Cells', *Science*, 325(5947), p. 1555 LP-1559.

Yuneva, M. *et al.* (2007) 'Deficiency in glutamine but not glucose induces MYC-dependent apoptosis in human cells', *The Journal of Cell Biology*. The Rockefeller University Press, 178(1), pp. 93–105. doi: 10.1083/jcb.200703099.

Zeng, G. and Millis, A. J. T. (1994) 'Expression of 72-kDa Gelatinase and TIMP-2 in Early and Late Passage Human Fibroblasts', *Experimental Cell Research*, 213(1), pp. 148–155. doi: http://dx.doi.org/10.1006/excr.1994.1184.

Zhang, J.-H., Chung, T. D. Y. and Oldenburg, K. R. (1999) 'A Simple Statistical Parameter for Use in Evaluation and Validation of High Throughput Screening Assays', *Journal of Biomolecular Screening*. SAGE Publications Inc STM, 4(2), pp. 67–73. doi: 10.1177/108705719900400206.

Zhang, R. *et al.* (2005) 'Formation of MacroH2A-Containing Senescence-Associated Heterochromatin Foci and Senescence Driven by ASF1a and HIRA', *Developmental Cell*, 8(1), pp. 19–30. doi: http://dx.doi.org/10.1016/j.devcel.2004.10.019.

Zhang, R., Chen, W. and Adams, P. D. (2007) 'Molecular Dissection of Formation of Senescence-Associated Heterochromatin Foci', *Molecular and Cellular Biology*. American Society for Microbiology, 27(6), pp. 2343–2358. doi: 10.1128/MCB.02019-06.

Zhang, W. C. *et al.* (2012) 'Glycine Decarboxylase Activity Drives Non-Small Cell Lung Cancer Tumor-Initiating Cells and Tumorigenesis', *Cell*, 148(1–2), pp. 259–272. doi: https://doi.org/10.1016/j.cell.2011.11.050.

Zheng, L. *et al.* (2015) 'Fumarate induces redox-dependent senescence by modifying glutathione metabolism', *Nat Commun*, 6, p. 6001. doi: 10.1038/ncomms7001.

Zhu, F. *et al.* (2013) 'Senescent Cardiac Fibroblast Is Critical for Cardiac Fibrosis after Myocardial Infarction', *PLOS ONE*. Public Library of Science, 8(9), p. e74535.

Zwerschke, W. *et al.* (2003) 'Metabolic analysis of senescent human fibroblasts reveals a role for AMP in cellular senescence', *Biochemical Journal*, 376(2), p. 403 LP-411.

Appendix 1

The table below has information about the 553 genes targeted in the primary siRNA screen, described in *3.1*.

	Gene Symbol	Gene ID		Gene Symbol	Gene ID
1	A4GALT	53947	33	ADH1B	125
2	AASDHPPT	60496	34	ADSL	158
3	ABHD5	51099	35	ADSS	159
4	ACAA2	10449	36	AGER	177
5	ACACA	31	37	AGK	55750
6	ACACB	32	38	AGMO	392636
7	ACAD11	84129	39	AGPAT1	10554
8	ACAD8	27034	40	AGPAT2	10555
9	ACADL	33	41	AGPAT3	56894
10	ACADM	34	42	AGPAT4	56895
11	ACADS	35	43	AGPAT5	55326
12	ACADVL	37	44	AGPAT6	137964
13	ACER1	125981	45	AGPAT9	84803
14	ACER2	340485	46	AGPS	8540
15	ACER3	55331	47	AIFM1	9131
16	ACLY	47	48	AIFM2	84883
17	ACOT8	10005	49	AKR1A1	10327
18	ACOX1	51	50	AKR1B1	231
19	ACOX2	8309	51	AKR1C1	1645
20	ACOX3	83110	52	ALDH1A1	216
21	ACSL1	2180	53	ALDH1A2	8854
22	ACSL3	2181	54	ALDH2	217
23	ACSL4	2182	55	ALDH3A2	224
24	ACSL5	51703	56	ALDH5A1	7915
25	ACSL6	23305	57	ALDH8A1	64577
26	ACSM1	116285	58	ALDOA	226
27	ACSM2A	123876	59	ALDOB	229
28	ACSM2B	348158	60	ALDOC	230
29	ACSM3	6296	61	ALG9	79796
30	ACSS1	84532	62	ALOX12	239
31	ACSS2	55902	63	ALOX12B	242
32	ADCY6	112	64	ALOX15	246

65	ALOX15B	247
66	ALOX5	240
67	AMD1	262
68	AMPD1	270
69	AMPD2	271
70	AMPD3	272
71	APRT	353
72	ARNT	405
73	ARSG	22901
74	ASAH1	427
75	ASAH2	56624
76	ASAH2C	653365
77	ASPH	444
78	ASS1	445
79	ATG3	64422
80	ATG7	10533
81	ATIC	471
82	ATP5G1	516
83	AWAT1	158833
84	AWAT2	158835
85	B3GALNT1	8706
86	B3GALT1	8708
87	B3GALT4	8705
88	B3GNT5	126792
89	B4GALNT1	2583
90	B4GALT1	2683
91	B4GALT6	9331
92	BAD	572
93	BAK1	578
94	BAX	581
95	BCKDHA	593
96	BCL2	596
97	BCL2A1	597
98	BCL2L1	598
99	BCL2L10	10017
100	BCL2L11	10018
101	BCL2L13	23786
102	BCL2L14	79370
103	BCL2L2	599
104	BDH1	622
105	BDH2	56898
106	BID	637
107	BOK	666
108	BPGM	669
109	C14ORF1	11161
110	CAD	790
111	CBR4	84869
112	CDIPT	10423
113	CDS1	1040
114	CDS2	8760
115	CEPT1	10390
116	CERK	64781
117	CERS1	10715
118	CERS2	29956
119	CERS3	204219
120	CERS4	79603
121	CERS5	91012
122	CERS6	253782
123	CH25H	9023
124	CHDH	55349
125	CHKA	1119
126	CHPT1	56994
127	COQ7	10229
128	COQ7	10229
129	COX5A	9377
130	COX7B	1349
131	CRLS1	54675
132	CS	1431
133	CTH	1491
134	CYC1	1537
135	CYCS	54205
136	CYP2S1	29785
137	CYP51A1	1595
138	DEGS1	8560
139	DEGS2	123099
140	DGAT1	8694
141	DGAT2	84649
142	DGAT2L6	347516
143	DGKE	8526
144	DHCR24	1718
145	DHCR7	1717
146	DHFR	1719

147	DHODH	1723
148	DHRS7	51635
149	DLAT	1737
150	DLD	1738
151	DLST	1743
152	DOLK	22845
153	DOLPP1	57171
154	DPAGT1	1798
155	DPM1	8813
156	DPYSL2	1808
157	EBP	10682
158	ECHS1	1892
159	EIF2AK4	440275
160	ELOVL1	64834
161	ELOVL2	54898
162	ELOVL3	83401
163	ELOVL4	6785
164	ELOVL5	60481
165	ELOVL6	79071
166	ELOVL7	79993
167	ENO1	2023
168	ENO2	2026
169	ENO3	2027
170	EPAS1	2034
171	EPT1	85465
172	FA2H	79152
173	FADS1	3992
174	FADS2	9415
175	FADS3	3995
176	FADS6	283985
177	FAH	2184
178	FASN	2194
179	FBP1	2203
180	FBP2	8789
181	FDFT1	2222
182	FDPS	2224
183	FH	2271
184	FIG4	9896
185	FMO2	2327
186	FOXO1	2308
187	FOXO3	2309
188	G6PD	2539
189	GAL3ST1	9514
190	GALC	2581
191	GALNT6	11226
192	GAMT	2593
193	GAPDH	2597
194	GART	2618
195	GBA	2629
196	GBA2	57704
197	GBA3	57733
198	GCLC	2729
199	GGPS1	9453
200	GJA1	2697
201	GK	2710
202	GLA	2717
203	GLB1	2720
204	GLS	2744
205	GLS2	27165
206	GLUD1	2746
207	GLUL	2752
208	GMPR	2766
209	GMPS	8833
210	GNPAT	8443
211	GOT1	2805
212	GOT2	2806
213	GPAM	57678
214	GPAT2	150763
215	GPD1	2819
216	GPD2	2820
217	GPI	2821
218	GPT	2875
219	GPT	2875
220	GPX3	2878
221	GSR	2936
222	GSS	2937
223	GSTA1	2938
224	GSTA2	2939
225	GSTA3	2940
226	GSTA4	2941
227	GSTA5	221357
228	GUCY1A3	2982

229	GUCY1B3	2983	270	LPCAT4	254531
230	GXYLT2	727936	271	LPGAT1	9926
231	HADH	3033	272	LPIN1	23175
232	HADHA	3030	273	LPIN2	9663
233	HADHB	3032	274	LPIN3	64900
234	HDC	3067	275	LPL	4023
235	HEXB	3074	276	LSS	4047
236	HGPRT	5651628	277	LYPLA1	10434
237	HIF1A	3091	278	LYPLA2	11313
238	HK1	3098	279	MAN1C1	57134
239	HK2	3099	280	MAT1A	4143
240	HK3	3101	281	MAT2A	4144
241	HMGCL	3155	282	MAT2B	27430
242	HMGCR	3156	283	MBOAT1	154141
243	HMGCS1	3157	284	MBOAT2	129642
244	HMGCS2	3158	285	MBOAT7	79143
245	HPGDS	27306	286	MCCC2	64087
246	HSD17B4	3295	287	MCL1	4170
247	IDH1	3417	288	MDH1	4190
248	IDH2	3418	289	MDH2	4191
249	IDI1	3422	290	ME1	4199
250	IDI2	91734	291	ME2	4200
251	INPP5E	56623	292	MECR	51102
252	ISYNA1	51477	293	MGLL	11343
253	KDSR	2531	294	MOGAT1	116255
254	KEAP1	9817	295	MOGAT2	80168
255	KYNU	8942	296	MOGAT3	346606
256	LARGE	9215	297	MOXD1	26002
257	LCAT	3931	298	MOXD1	26002
258	LCLAT1	253558	299	MPC1	51660
259	LDHA	3939	300	MPC2	25874
260	LDHB	3945	301	MSMO1	6307
261	LDHC	3948	302	MTHFD1	4522
262	LIAS	11019	303	MTM1	4534
263	LIPC	3990	304	MTMR3	8897
264	LIPE	3991	305	MTOR	2475
265	LIPG	9388	306	MTR	4548
266	LIPT2	387787	307	MVD	4597
267	LPCAT1	79888	308	MYC	4609
268	LPCAT2	54947	309	NAMPT	10135
269	LPCAT3	10162	310	NCEH1	57552

311	NDUFA2	4695
312	NDUFAB1	4706
313	NDUFB6	4712
314	NDUFS8	4728
315	NDUFV2	4729
316	NEU1	4758
317	NFE2L2	4780
318	NMNAT1	64802
319	NMNAT2	25057
320	NMNAT3	349565
321	NQO1	1728
322	NRF1	4899
323	NSDHL	50814
324	NT5E	4907
325	NUAK1	9891
326	OCRL	4952
327	ODC1	4953
328	OGDH	4967
329	OLAH	55301
330	ORMDL1	94101
331	ORMDL2	29095
332	ORMDL3	94103
333	OXSM	54995
334	P4HA1	5033
335	P4HA2	8974
336	PAH	5053
337	PCK1	5105
338	PDE5A	8654
339	PDHA1	5160
340	PDHA2	5161
341	PDHB	5162
342	PDHX	8050
343	PDK1	5163
344	PDK4	5166
345	PDP2	57546
346	PECR	55825
347	PEMT	10400
348	PEX2	5828
349	PFKFB3	5209
350	PFKFB4	5210
351	PFKL	5219
352	PFKM	5213
353	PFKP	5214
354	PGAM1	5223
355	PGAM2	5224
356	PGAM4	441531
357	PGD	5226
358	PGK1	5230
359	PGK2	5232
360	PGLS	25796
361	PGM2L1	283209
362	PGS1	9489
363	PI4K2A	55361
364	PI4KA	5297
365	PI4KB	5298
366	PIK3C2A	5286
367	PIK3C2B	5287
368	PIK3C2G	5288
369	PIK3CA	5290
370	PIK3CB	5291
371	PIK3CD	5293
372	PIK3CG	5294
373	PIK3R1	5295
374	PIKFYVE	200576
375	PIP5K1A	8394
376	PISD	23761
377	PKLR	5313
378	PKM	5315
379	PLA1A	51365
380	PLA2G15	23659
381	PLA2G1B	5319
382	PLA2G4A	5321
383	PLA2G4B	100137049
384	PLA2G4C	8605
385	PLA2G4F	255189
386	PLA2G5	5322
387	PLA2G6	8398
388	PLCB1	23236
389	PLCE1	51196
390	PLD1	5337
391	PLSCR1	5359
392	PLSCR2	57047

393	PLSCR3	57048
394	PLSCR4	57088
395	PNP	4860
396	PNPLA3	80339
397	PNPLA8	50640
398	PPAP2A	8611
399	PPAP2B	8613
400	PPAP2C	8612
401	PPARG	5468
402	PPARGC1A	10891
403	PPAT	5471
404	PPCS	59717
405	PPIF	10105
406	PPME1	
407	PPT1	5538
408	PRKAA1	105787
409	PRKAA2	5563
410	PRKACA	5566
411	PRKAR1A	5573
412	PRPS1	5631
413	PRPS2	5634
414	PSAP	5660
415	PSAPL1	768239
416	PTDSS1	9791
417	PTDSS2	81490
418	PTEN	5728
419	PTGS1	5742
420	PTGS2	5743
421	PTPLA	9200
422	PTPLAD1	51495
423	PTPLAD2	401494
424	PTPLB	201562
425	PYCR2	29920
426	RICTOR	253260
427	RPE	6120
428	RPIA	22934
429	RPS6KB1	6198
430	RPS6KB2	6199
431	RPTOR	57521
432	SACM1L	22908
433	SAMD8	142891
434	SAT1	6303
435	SC4MOL	6307
436	SC5DL	6309
437	SCD	6319
438	SCD5	79966
439	SDHA	6389
440	SDHB	6390
441	SDHC	6391
442	SDHD	6392
443	SERINC1	57515
444	SERINC4	619189
445	SERINC5	256987
446	SGK1	6446
447	SGMS1	25923
448	SGMS2	166929
449	SGPL1	8879
450	SGPP1	81537
451	SGPP2	130367
452	SHMT1	6470
453	SHMT2	6472
454	SIRT1	23411
455	SIRT2	22933
456	SIRT3	23410
457	SIRT4	23409
458	SIRT5	23408
459	SIRT6	51548
460	SIRT7	51547
461	SLC16A1	6566
462	SLC16A3	9123
463	SLC16A6	9120
464	SLC16A7	9194
465	SLC19A1	6573
466	SLC19A2	10560
467	SLC1A3	6507
468	SLC1A4	6509
469	SLC1A5	6510
470	SLC20A1	6574
471	SLC23A2	9962
472	SLC25A1	6576
473	SLC25A11	8402
474	SLC25A13	10165

475	SLC25A14	9016
476	SLC25A15	10166
477	SLC25A20	788
478	SLC25A27	9481
479	SLC25A31	83447
480	SLC25A4	291
481	SLC25A5	292
482	SLC25A6	293
483	SLC26A6	65010
484	SLC27A1	376497
485	SLC27A2	11001
486	SLC2A1	6513
487	SLC2A4	6517
488	SLC38A7	55238
489	SLC38A9	153129
490	SLC52A1	55065
491	SLC5A3	6526
492	SLC5A7	60482
493	SLC6A15	55117
494	SLC6A5	9152
495	SLC6A6	6533
496	SLC6A9	6536
497	SLC7A1	6541
498	SLC7A11	23657
499	SLC7A2	6542
500	SLC7A5	8140
501	SLC7A8	23428
502	SMOX	54498
503	SMPD1	6609
504	SMPD2	6610
505	SMPD3	55512
506	SMPD4	55627
507	SMPDL3A	10924
508	SMPDL3B	27293
509	SMS	6611
510	SOAT1	6646
511	SPHK1	8877
512	SPHK2	56848
513	SPTLC1	10558
514	SPTLC2	9517
515	SPTLC3	55304
516	SQLE	6713
517	SRD5A3	79644
518	SREBF1	6720
519	SREBF2	6721
520	SSSPTA	171546
521	SSSPTB	165679
522	ST3GAL5	8869
523	ST6GALNAC6	30815
524	ST8SIA1	6489
525	ST8SIA3	51046
526	ST8SIA5	29906
527	STK11	6794
528	SUCLA2	8803
529	SUCLG1	8802
530	SUCLG2	8801
531	TAZ	6901
532	TECR	9524
533	TGM2	7052
534	TK1	7083
535	TK2	7084
536	TKT	7086
537	TM7SF2	7108
538	TP53	7157
539	TPI1	7167
540	TSC1	7248
541	TSC2	7249
542	TXN	7295
543	UCP1	7350
544	UCP2	7351
545	UCP3	7352
546	UGCG	7357
547	UGT8	7368
548	UMPS	7372
549	UPP1	7378
550	UPP2	151531
551	UQCRC1	7384
552	VDAC1	7416
553	YY1	7528